Titre: Title:	Numerical and Experimental Seismic Assessment and Retrofit of Steel Tension-Only Double Angle Braced Frames Designed Before the Implementation of Detailing Provisions for Ductile Seismic Response
Auteur: Author:	Yan Jiang
Date:	2013
Type:	Mémoire ou thèse / Dissertation or Thesis
Référence: Citation:	Jiang, Y. (2013). Numerical and Experimental Seismic Assessment and Retrofit of Steel Tension-Only Double Angle Braced Frames Designed Before the Implementation of Detailing Provisions for Ductile Seismic Response [Mémoire de maîtrise, École Polytechnique de Montréal]. PolyPublie. https://publications.polymtl.ca/1135/

UNIVERSITÉ DE MONTRÉAL

NUMERICAL AND EXPERIMENTAL SEISMIC ASSESSMENT AND RETROFIT OF STEEL TENSION-ONLY DOUBLE ANGLE BRACED FRAMES DESIGNED BEFORE THE IMPLEMENTATION OF DETAILING PROVISIONS FOR DUCTILE SEISMIC RESPONSE

YAN JIANG
DÉPARTEMENT DES GÉNIES CIVIL, GÉOLOGIQUE ET DES MINES
ÉCOLE POLYTECHNIQUE DE MONTRÉAL

MÉMOIRE PRÉSENTÉ EN VUE DE L'OBTENTION
DU DIPLÔME DE MA ÎTRISE ÈS SCIENCES APPLIQUÉES
(GÉNIE CIVIL)
AVRIL 2013

UNIVERSITÉ DE MONTRÉAL

~~ÉCOLE POLYTECHNIQUE DE MONTRÉAL~~

Ce mémoire intitulé:

NUMERICAL AND EXPERIMENTAL SEISMIC ASSESSMENT AND RETROFIT OF STEEL TENSION-ONLY DOUBLE ANGLE BRACED FRAMES DESIGNED BEFORE THE IMPLEMENTATION OF DETAILING PROVISIONS FOR DUCTILE SEISMIC RESPONSE

présenté par : JIANG Yan

en vue de l'obtention du diplôme de : Maîtrise ès sciences appliquées

a été dûment accepté par le jury constitué de :

Mme KOBOEVIC Sanda, Ph.D., présidente

M. TREMBLAY Robert, Ph.D., membre et directeur de recherche

Mme TIRCA Lucia, Ph.D., membre et codirectrice de recherche

M. LIGNOS Dimitrios, Ph.D., membre

ACKNOWLEDGEMENTS

Completion of this research project at École Polytechnique of Montréal is inseparable from the help and support of many people, I would like to thank.

First, I want to express my sincere and deepest gratitude to my supervisor Professor Robert Tremblay and co-supervisor Professor Lucia Tirca for their continued encouragement and their expert guidance. Their help and support for this research project will never be forgotten.

I would like to present my special thanks to Professor Ali Davaran for his assistance in the development of the numerical model of the bracing member, and Martin Leclerc who was involved directly on preparation of hybrid test setups. My sincere appreciation also go to Marc Charbonneau, Patrice Bédanger, David EK, Guillaume Cossette, Xavier Willem and Cédric Androuet at the Structures Laboratory of École Polytechnique of Montréal for their invaluable assistance.

I wish to thank the external jury, Professor Sanda Koboevic from École Polytechnique of Montréal and Professor Dimitrios Lignos from Mcgill University to have read and evaluated this Master Thesis.

Funding from the Canadian Seismic Research Network (CSRN) of the Natural Sciences and Engineering Research Council (NSERC) of Canada and the Strategic Network Program of the Fonds Québécois pour la Recherche sur la Nature et les Technologies (FQRNT) is acknowledged.

It was a pleasure to shear this wonderful time with all my colleagues and friends in Polytechnique.

Finally, I would like to thank to my dear wife and parents for their unconditional love, support and trust.

RÉSUMÉ

Au Canada, une proportion importante des bâtiments en acier de faible hauteur ont été conçus et construits avant l'introduction, en 1989, des normes de conception parasismique dans la norme pour la conception des structures en acier. Il est donc probable que l'évaluation de ces structures sur la base des codes en vigueur, révèle des déficiences quant à leur capacité de résister adéquatement aux effets des tremblements de terre. Il est donc nécessaire de développer des méthodes efficaces et facilement applicables pour l'évaluation et la réhabilitation sismiques de ces structures de bâtiments.

Dans cette étude, on se concentre sur l'évaluation et la réhabilitation sismique des contrenventements en acier de type tension-seulement, construits avec des diagonales faites de deux cornières assemblées entre elles, qui ont été largement utilisés au Canada pour la résistance aux charge latérales dans les bâtiments de faible hauteur. Ces structures sont encore populaires aujourd'hui.

Un bâtiment prototype de 4 étages de hauteur avec contenvetements en tension-seulement a été conçu conformément aux codes et critères en vigueur au début des années 1980. La structure est localisée sur un sol ferme à Vancouver, Colombie-Britannique. Les diagonales des contreventements sont formées de cornières assemblées dos-à-dos avec des assemblages boulonnés aux extrémités. L'évaluation de l'un des contreventements a été effectué conformément au Code national du bâtiment du Canada 2010 et à la norme CSA S16-09 pour les structures en acier. Les résultats montrent que certaines des diagonales de contreventement, que tous les assemblages des diagonales de contreventement et que certains des poteaux avaient une résistance insuffisante. Cette déficience était plus marquée pour les assemblages des diagonales compte tenu qu'un calcul par capacité visant à établir un ordonnancement de la plastification et un comportement ductile des diagonales n'avait pas été considéré pour leur conception. Compte tenu de ce constat et de la ductilité limitée associée aux modes de rupture dans les assemblages, on s'est concentré dans ce projet sur l'évaluation du comportement sismique des assemblages des diagonales et au développement et à la validation de méthodes de réhabilitation permettant d'éviter la rupture fragile des assemblages et l'effondrement des structures pouvant en découler.

Un programme d'essais cyclique quasi-statique a été réalisé sur des spécimens à varaie grandeur de diagonales faites de cornières dos-à-dos et de leurs assemblages d'extrémité pour confirmer les

déficiences qui avaient été identifiées par calculs et valider les méthodes de réhabilitation. Comme prévu, les essais ont démontré qu'une ductilité plus élevée pouvait être atteinte dans un système diagonale-assemblage lorsque les déformations inélastiques se développaient principalement dans l'aire brute des diagonales. Malgré qu'elle était limitée, la rupture dans un assemblage des diagonales pouvait cependant offrir un certain niveau de ductilité. La répartition de la sollicitation inélastique entre les diagonales et les assemblages dépend principalement de leur résistance relative et, par conséquent, des propriétés mécaniques de l'acier des composantes. La capacité de prédire le comportement dépend donc fortement de la précision des équations utilisées pour évaluer la résistance associée aux divers états limites et de la connaissance des propriétés réelles des matériaux. Dans la présente étude, par exemple, on a noté que les équations pour déterminer la résistance en traction sur l'aire nette étaient du côté de la sécurité et que la limite élastique de l'acier des diagonales étaient plus faible que la valeur probable utilisée dans les calculs, ce qui a eu comme effet de produire des déformations inélastiques plus importantes dans la diagonale et une ductilité plus élevée que prévues. On a aussi observé que l'écrouissage de l'acier pouvait aussi contribuer à favoriser les déformations inélastiques entre les composantes.

L'adéquation d'une technique de réhabilitation sismique dépend aussi fortement de la capacité de prédire la résistance relative des différents modes de rupture le long du cheminement des efforts. Les essais ont démontré que la stratégie de réhabilitation la plus prometteuse parmi celles qui ont été examinées dans cette étude est celle où on introduit des trous oblongs pour former des fusibles ductiles parallèles dans les goussets d'asssemblage, entre les diagonales et les poutres ou poteaux. Le système offre un comportement inélastique prévisivible qui permet d'augmenter la ductilité de l'assemblage out en controllant les forces induites dans le système.

Les connaissances acquises et les résultats obtenus dans les essais ont permis de développer et de valider un modèle numérique pour la diagonales de contreventement faites de deux cornières assemblées. Le modèle tient compte de l'influence des contraintes résiduelles, des défauts de rectitude et de la stabilité des cornières individuelles et combinées sur le flambement de la diagonale. Le comportement en flexion, les déformations axiales inélastiques et la rupture des diagonales ont aussi été incorporées dans le modèle. Des simulations hybrides ont été réalisées pour vérifier la possibilité de prédire le comportement inélastique des diagonales, incluant la rupture des assemblages et leurs conséquences sur la résistance à l'effondrement des structures. Ce

travail présentait un défi particulier en raison du caractère peu ductile de la rupture des assemblages et du fait qu'il s'agissait d'une première série de simulations hybrides réalisées à l'École Polytechnique avec les applications OpenSees/OpenFresco. Les simulations ont par conséquent été réalisées avec un model simplifié de la structure prototype. Une bonne corrélation a été obtenue entre les simulations purement numériques et les simulations hybrides.

Dans la dernière phase de la recherche, on a réalisé des analyses dynamiques temporelles non linéaires de grande envergure pour évaluer la résistance contre l'effondrement de la structure prototype. Un modèle numérique détaillé a été utilisé à cette fin. Ce modèle comprenait le système de résistance aux charges de gravité, incluant le comportement non-linéaire des assemblages entre les poutres et les poteaux. La structure a été évaluée dans les conditions originale et réhabilitée. Les analyses ont montré que la structure originale devait être réhabilitée pour atteindre les niveaux de fiabilité minimum requis contre les séismes. En dépit des avantages, la technique de réhabilitation avec des trous oblongs percés dans les goussets n'a pas permis n'obtenir le niveau de fiabilité requis.

ABSTRACT

In Canada, a large portion of low-rise steel buildings were designed and built before the implementation of the first provision of seismic design and detailing introduced in steel structure design standard in 1989. It is therefore likely that an assessment of these structures based on current seismic design requirements reveals the deficiencies that may affect the ability of these structures to properly withstand earthquake effects. Hence, an efficient and convenient method to seismically assess and retrofit these buildings is necessary.

This study focuses on the seismic assessment and retrofit of steel tension-only braced frames built with double angle braces, a seismic force resisting system (SFRS) that has been extensively used for low-rise building structures. The system is still popular today. In this study, a 4-storey prototype steel building structure with tension-only braced frame was designed according to the design regulations applicable in the early 1980's. The structure was assumed to be located on a firm ground site in Vancouver, British Columbia. The bracing members were back-to-back double angle sections with bolted end connections. Seismic assessment of one braced frame was performed using the current design requirements and design equations of the National Building Code of Canada 2010 and the CSA S16-09 steel design standard. It was found that some of the bracing members, all bracing member connections and some of the columns had insufficient seismic resistance. The lack of resistance was more significant for the brace connections as no capacity design provisions was applied in the design to ensure hierarchy of yielding and ductile brace response. In view of this situation and the limited ductility typically associated to connection failure, the study then focused on the evaluation of the seismic response of the deficient connections and the development and validation of retrofit strategies to avoid brittle connection failure and building structural collapse.

Physical quasi-static cyclic tests were carried out on full scale double angle braces and brace connections to confirm the deficiencies identified by calculations and investigate the adequacy of the proposed retrofit strategies. As expected, the tests showed that greater ductile performance for brace-connection assemblies could be achieved when inelastic deformations concentrated in the gross area of the bracing members. Although limited, failure in the brace connections still exhibited some degree of ductility. The distribution of inelastic demand between the braces and their connections depend on their relative strength and thereby, on the material strength properties of the components. The ability to predict the system behaviour then heavily relies on the accuracy of the

equations used to evaluate the resistance associated with the various failure modes and the knowledge of the actual material strength properties. In this study, for instance, current code equations for net section rupture were found to be conservative and the yield strength of the bracing members was lower than expected. The combined effect was higher inelastic straining in the bracing members and greater ductility than expected. Strain hardening was also found to favor the distribution of the inelastic demand among the components.

The adequacy of a retrofit scheme is also highly dependent on the ability to predict the relative strength of the various failure modes along the load path. Among the various possible retrofit strategies examined in this study, the one where slotted holes are introduced in the gusset plates to form parallel ductile steel fuses between the bracing members and the beams or columns was found to the most promising. The system has a predictable inelastic response that increases the ductility capacity of the connection while controlling the force demand in the seismic force resisting system.

The knowledge gained and data obtained from the tests was utilized to develop and calibrate numerical models for double angle bracing members and their connections using OpenSees finite element program. The model accounts for residual stress effects, initial out-of-straightness, and stability of the individual and combined angle sections on the buckling response of the braces. The flexural response, inelastic axial deformations, and failure of connections are also included in the model. Hybrid simulations were performed to verify the ability of the model to predict the brace inelastic response including connection failure and its consequences on the braced frame collapse capacity. This task represented a major challenge in view of the limited ductility associated with the failure modes investigated and the fact that this was the first implementation of the OpenSees-OpenFresco platform for hybrid simulation at École Polytechnique of Montréal. The simulations were therefore realized using a simplified model of the prototype braced frame. Good correlations could be obtained between hybrid and purely numerical simulations.

In the last phase of the research, extensive nonlinear time history dynamic analysis was performed to assess the collapse capacity of the prototype braced frame. A detailed numerical model was used that included the tributary gravity system and the nonlinear response of the beam-to-column connections. The structure was evaluated in the original and retrofitted conditions. The analysis showed that the structure as originally designed needed to be retrofitted to achieve the minimum level of safety against earthquakes. In spite of its advantages, the proposed retrofit strategy with

slotted holes in the gusset plates was not found to develop sufficient ductility to reach the minimum safety level.

TABLE OF CONTENTS

LIST OF FIGURES

LIST OF TABLES

LIST OF SYMBOLS

A	Ground acceleration ratio in NBCC 1980.
A_{cn}	Net cross-section area of the connected leg at the critical cross-section (mm^2).
A_g	Gross area (mm^2).
A_{gv}	Gross area in shear for block failure (mm^2).
A_n	Net area (mm^2).
A_{ne}	Effective net area (mm^2).
A_o	Gross cross-section area of the outstanding leg (mm^2).
B_r	Factored bearing resistance of a member or component (kN).
$C_{f\text{-}10}$	Factored compressive design force in columns in 2010 design (kN).
$C_{f\text{-}10p}$	Probable compressive design force in columns (kN).
$C_{f\text{-}80}$	Factored compressive design force in columns in 1980 design (kN).
$C_{r\text{-}10}$	Factored buckling strength of columns using equation provided in CSA S16-09 (kN).
$C_{r\text{-}80}$	Factored buckling strength of columns using equation provided in CSA S16-M78 (kN).
$C_{u\text{-}10}$	Expected buckling load of columns (kN).
C'_u	Post-buckling compressive resistance (kN).
d	Nominal bolt diameter (mm).
e	Distance from center of hole to an edge in bolted connections (mm).
F	Foundation factor or soil condition factor.
F_x	Seismic force at every level (kN).
F_t	Additional force concentrated at the top of the structure (kN).

F_u Specified minimum tensile strength (MPa).

F_{sm} Modification factor used to adjust scaling factor (S_f) in incremental analysis.

F_y Specified minimum yield stress or yield strength (MPa).

g Transverse spacing between fastener gauge lines (mm).

h_n Total building height (m).

h_s Storey height (m).

h_{sm} Inter-storey drift in percentage.

I Importance factor of the structure.

K Numerical coefficient that reflects the material and type of construction, damping, ductility and/or energy-absorptive capacity of the structure in NBCC 1970, 1975, 1980 and 1985.

KL Effective length (mm).

L Brace length (mm).

M_w Seismic moment magnitude

n Number of bolts.

R Force modification factor that reflects the capability of a structure to dissipate energy through inelastic behaviour in NBCC 1990 and 1995.

R_d Seismic force reduction factor accounting for system ductility.

R_o Seismic force reduction factor accounting for system overstrength.

R_t Ratio of expected tensile strength to the specified minimum tensile strength, F_u.

R_y Ratio of expected yield strength to the specified minimum yield strength, F_y

r_x Radius of gyration of a single-angle member about its geometric axis parallel to the connected leg (mm).

r_y Radius of gyration of a member about its weak axis (mm).

$r_{y'}$ Radius of gyration of a member about its minor principal axis (mm).

S	Seismic response factor in NBCC 1980.
S_f	Scaling factor used to scale historical earthquakes to respective NBCC uniform hazard spectrum.
s	Centre-to-centre longitudinal spacing (pitch) of any two successive fastener holes (mm).
T_{emp}	Structural fundamental period based on NBCC formula (s).
$T_{f\text{-}10}$	Factored tensile force in braces in 2010 design (kN).
$T_{f\text{-}10p}$	Probable tensile force in braces (kN).
$T_{f\text{-}80}$	Factored tensile force in braces in 1980 design (kN).
$T_{r\text{-}10}$	Factored tensile resistance of braces using equation provided in CSA S16-09 (kN).
$T_{r\text{-}80}$	Factored tensile resistance of braces using equation provided in CSA S16-M78 (kN).
$T_{r\text{-}c\text{-}10}$	Factored tensile resistance of brace connections using equation provided in CSA S16-09 (kN).
$T_{r\text{-}c\text{-}80}$	Factored tensile resistance of brace connections using equation provided in CSA S16-M78 (kN).
T_u	Probable tensile resistance of braces (kN).
$T_{u\text{-}c\text{-}10}$	Probable tensile resistance of brace connections (kN).
t_g	Thickness of gusset plate (mm).
V	Seismic base shear based on the NBCC 2010 equivalent static force procedure (kN)
V_c	Column shear limitation (kN).
V_d	Elastic seismic base shear coming from the response spectrum analyses, Ve, multiplied by I_e/R_dR_o (kN).
V_{design}	The seismic base shear was used to design existing structure in 1980(kN).
V_e	Elastic seismic base shear coming from the response spectrum analysis (kN).

$V_{P-\Delta}$ Storey shear produced by the overturning moment of the gravity load (kN).

V_r Factored shear resistance of a member or component (kN).

W Structure seismic weight (kN).

W_e Whitmore's effective gusset plate width (mm).

δ Brace and brace connections axial deformation or controlling axial displacement (mm).

δ_b Net brace axial deformation (mm).

δ_c Brace connections axial deformation (mm).

$\delta_{lat.}$ Brace lateral deformation (mm).

δ_o Brace initial out-of-straightness (mm).

μ_T Period-based ductility.

LIST OF APPENDICES

INTRODUCTION

Background

In Canada, the National Building Code of Canada (NBCC) provides seismic loading and analysis requirements for building structures, whereas special seismic design and detailing provisions for steel structures are prescribed in the CSA S16 steel structure design standard. Since the introduction of the first seismic design provisions in NBCC 1941, 13 different versions of NBCC were published (Mitchell et al., 2010). The current edition of NBCC was released in 2010 (NRCC, 2010). The concepts and methods that are given in the NBCC for the seismic analysis and design of seismic force resisting systems, employed in building structures, have consistently improved during the last 70 years. The knowledge gained on seismic hazard and structural seismic response evolved markedly. In particular, the methods for the calculation of the minimum seismic design loading have been improved significantly. Although 13 different versions of CSA S16 steel structure design standard corresponding to each version of the NBCC were available to designers during the same period of time, the first ductile seismic design and detailing provisions given in CSA S16 were only implemented in 1989, which means that CSA S16 did not contain any rule to ensure ductility levels consistent with the NBCC loading prior to 1989. Since then, new research findings and lessons learned from the recent past earthquakes have been continually updated in the CSA S16 provisions (Tremblay, 2011).

Seismic deficiencies and lack of lateral resistance and/or ductility are expected for steel structures designed and built before the 1990s and their performance is uncertain in case of a severe earthquake. Accurate seismic assessment of steel structures built before 1989 needs to be carried out to identify potential seismic deficiencies and their possible consequences. In order to prevent severe damage that can lead to structural failure or collapse, the results of such an assessment can then be used to decide on the necessity of seismic retrofitting.

Limited information is available for the seismic evaluation and retrofit of steel structures. In addition, different assessment results can be obtained when different assessment methods are used. Moreover, there is no standard to evaluate these results. The first time when requirements for seismic retrofit of existing structures were addressed in the NBCC was given in Commentary “L” of NBCC 2010. In that commentary, it is recommended that buildings that have been designed for

an earthquake load, V_{design}, less than 0.6 times the minimum earthquake load specified in NBCC 2010 must be seismically upgraded.

Nowadays, seismic analysis and strength verification is typically performed automatically using computer programs such as ETABS (CSI 2009). Response spectrum analysis performed in the elastic range is now preferred to the equivalent static force procedure to evaluate earthquake effects on structures. By employing automatic computations, an engineer can rapidly determine the seismic design forces in the structure. The OpenSees finite element program (Mazzoni, 2006) has been developed to predict the inelastic seismic structure response through nonlinear time history analysis. The program can also be used to examine the consequences of identified deficiencies. The accuracy of OpenSees structural models can be validated and verified using the hybrid simulation technology where the OpenSees finite element analysis model and the OpenFresco middleware (Schellenberg et al., 2006) are combined. In this technology, critical structural components are physically tested in the laboratory while performing the seismic analysis of the whole structure.

Once it is determined that an existing structure needs to be retrofitted, different retrofit strategies must be established and compared to evaluate costs, retrofitting time, and the seismic performance after the retrofit has been implemented. Generally, retrofit strategies can be divided into two major categories: conventional retrofit technologies and innovative retrofit technologies. While the conventional retrofit technologies typically involves strengthening of structure, the second group often calls for the addition of energy dissipating devices. Normally, the cost of a conventional retrofit method is lower than that of adding energy dissipation devices; however, the ductility performance is better enhanced when energy dissipating devices are considered in design. Extensive seismic upgrade projects have been performed by using innovative retrofit technologies. However, due to its appealing lower costs, there is a need to develop more conventional retrofit technologies that can help achieving an improved seismic response. The performance of such retrofitted structures can be evaluated using OpenSees models or hybrid testing.

A large number of existing structures were built before the 1990s. Among these structures, many are low-rise steel structures such as commercial buildings, factories, hospitals and schools. These structures are typically less than five storeys in height. Steel braced frames are very popular SFRSs for these structures. In these braced frames, built-up double angle braces were commonly used as

brace sections. One reason for this preference is the ease of connections of angle braces to either single vertical gusset plates or connecting plates. Due to the shape of the cross-section of double angles, their tensile strength is higher than their compression resistance. Thus, theses braces have been very commonly used in tension-only braced frames. In existing steel braced frames, failure of brace connections that were designed without details to ensure a ductile performance is considered as one of the most critical deficiencies.

Finite element models of built-up double angle sections and their connections have not been created yet in the OpenSees framework. Hence, the development and calibration of an accurate model is necessary to predict the inelastic seismic response of double angle braces and their connections in OpenSees. OpenSees models have already been used extensively in recent years by researchers (Aguero et al., 2006; Uriz et al. 2008; Tremblay et al., 2009; Castonguay, 2009; Chen 2011), but the capability of accurately predicting structural collapse due to failure of brace connections has not been validated yet. Hybrid simulation using OpenSees and OpenFresco has already been used for braced frame analysis (Yang et al., 2006; Schellenberg et al, 2008). However, no test program has been devoted to the evaluation of deficient existing structures or the validation of retrofit strategies.

Objectives

The principal objective of this project is to perform the seismic assessment and retrofit of a steel concentrically braced frame (CBF) for a low-rise existing structure that was built prior to 1989. The study should examine seismic deficiencies related to the braces and their connections. Conventional retrofit technologies should be proposed and their feasibility verified. The project should also serve to the development of knowledge on the assessment of seismic deficiencies for existing steel building and the evaluation of the seismic performance of retrofitted buildings. More specifically, this project will focus on the following objectives:

- Identify potential seismic deficiencies for braced frames built with double angle braces.
- Propose possible seismic retrofit strategies.
- Develop an OpenSees model to predict the seismic response of built-up double angle brace members and their connections.
- Calibrate the built-up double angle braces and brace connections model using cyclic quasi-static tests.

- Use the hybrid simulation technique with the OpenFresco platform to verify the OpenSees model.
- Use the calibrated OpenSees model to carry nonlinear time history analysis of an existing deficient structure to examine its capacity against collapse in the as-built and retrofitted conditions.

Methodology

To attain these objectives, this project can be divided into four main parts: an assessment part, an OpenSees model development and calibration part, a hybrid simulation part, and a final detailed seismic performance assessment part.

In the design standard assessment part, a braced frame using built-up double angle braces for a prototype low-rise steel building is designed using a version of the NBCC and CSA S16 standard in force prior to 1990. This existing structure is evaluated by using the latest code design provisions. For this purpose, an ETABS model is created to perform response spectrum analysis to determine the seismic demand and find out potential seismic deficiencies. Possible conventional retrofit strategies are proposed to address the identified deficiencies.

In the OpenSees model development and calibration part, a model is developed for the built-up double angle braces. A quasi-static test program is performed on double angle braces with their connections to generate sufficient data for the calibration of the brace model. All tests are carried out on the bracing member of the first-storey of the prototype building. In the quasi-static cyclic tests, double angle braces with the original connections and retrofitted connections are tested.

In the hybrid simulation part of this project, the double angle braces model is used to develop a simplified model of the entire braced frame that will be used to predict the behaviour of existing structure under seismic events. Two models are developed: one with the original braced frame and one with the retrofitted structure. For the hybrid simulation, a full-scale brace specimen with its connections is tested in the laboratory. The rest of the braced frame is reproduced with the numerical model. OpenFresco commands are introduced in the numerical model to ensure communication with the laboratory loading equipment. A total of four hybrid tests were carried out to verify the OpenSees model predictions.

In the last part of the project, extensive nonlinear dynamic analysis of the prototype structure are performed to evaluate the consequences of the existing structure deficiencies and assess the benefits resulting from the implementation of the proposed retrofit strategy. The structure models were expanded to also include the gravity frame. Nonlinear beam-column connections were considered in the models. Two series of analysis are performed for the existing structure: one assuming the calculated resistances of the brace connections and one assuming the measured resistances of the brace connections. A third model is also developed that includes two of the retrofit strategies that have been proposed and studied experimentally. Incremental dynamic analysis was carried out in all cases to develop fragility curves. The adequacy of the structure performance was determined using the FEMA P695 approach (FEMA 2009).

Organization of thesis

The thesis includes seven chapters:

- Chapter 1 consists of literature review, including a comparison of the NBCC versions from 1970 to 2010.
- Chapter 2 presents the design and assessment of the prototype building, together with the proposed retrofit methods.
- Chapter 3 describes the coupon tests and the quasi-static tests performed on the double angle braces and their connections. Testing of the proposed retrofit strategies is also described in this chapter.
- Chapter 4 presents the development of the OpenSees model of the built-up double angle braces and their connections. The model calibration is also presented in this chapter.
- Chapter 5 describes the tension-only braced frame modelling in OpenSees. The hybrid test program is presented in this chapter. The test results are also presented and discussed. Difficulties faced in braced frame numerical model analysis and the hybrid simulations are also introduced.
- Chapter 6 presents the detailed seismic assessment of the building structure using nonlinear dynamic analysis. An expanded braced frame model is introduced. This model is used to carry out incremental time history analysis under twenty selected ground motions to evaluate the collapse capacity of the structure for three different conditions. The results of this assessment work are presented and discussed.

- Chapter 7 concludes the research project. Recommendations for existing building assessment, retrofitting strategies, and model analysis are given. Possible future work is also discussed.

CHAPTER 1: LITERATURE REVIEW

The literature review of this research project includes four parts. The first part referrers to literature review for seismic assessment of existing building assessment according to the National Building Code of Canada and the CSA S16 standard for steel structures. The second part addresses previous research work performed on the behaviour of double angle braces and their connections under earthquake loads. The third part is assigned to previous modelling studies conducted on double angle braces, braces connections, and braced frames. The last part reports on hybrid simulation technique used in seismic structural engineering.

1.1 NBCC Seismic Loads

A study providing a summary of the evolution of seismic design in Canada was presented by Mitchell el al. (2010). In particular, the seismic base shear values have evolved significantly over the last 70 years due to changes in the approach taken for determining seismic hazards and seismic hazard maps. The design philosophy had also changed from working stress design to ultimate strength design, with the introduction of load factors and capacity reduction factors, and then to limit states design, with load factors resistance factors. This paper discussed important parameters that affect the seismic base shear such as the building period, structure type factor, soil factor, and ductility factor.

To illustrate the code changes, the seismic design base shears determined from different versions of the National Building Code of Canada for the 2- and 10-storey reinforced concrete frame structures located in Montreal and Vancouver are compared in Figure 1.1. The ductile design concept was first introduced in NBCC 1970, and structures designed prior to 1970 were considered as conventional structures. Seismic resistant systems designed with ductility factor R = 2 and 3 in seismic design provisions after 1990 were referred to nominally ductile systems. In the figure, it is clear that design shear forces were too small compared with current design force levels for conventional structures built before 2005, especially for low-rise buildings in Montreal.

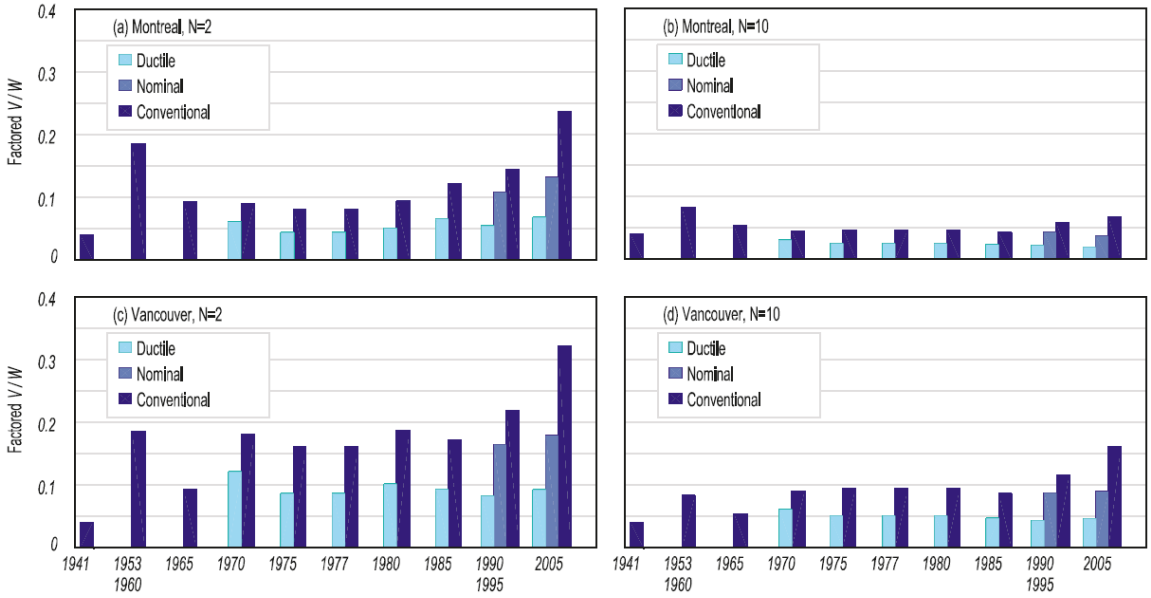

Figure 1.1: Comparisons of ‘‘factored’’ design base shears for concrete moment resisting frame structures in Montreal and Vancouver. Note that values of V/W before 1965 were based on working stress design and hence were multiplied by 2 for comparison (a) two-storey frame (Montreal), (b) ten-storey frame (Montreal), (c) two-storey frame (Vancouver), and (d) ten-storey frame (Vancouver) (Mitchell et al., 2010)

Additional base shear comparisons were performed as part of this project for the selection of a prototype building for the study. The comparison focuses on the seismic design provisions of NBCC 1970 to NBCC 2010. Although the first seismic design provisions were introduced in NBCC 1941, the first truly probabilistic seismic map developed by Milne and Davenport in 1969 was only adopted in NBCC 1970.

The spectra were calculated for two cities in the eastern part of Canada (Montreal and Ottawa), and for two cities (Vancouver and Victoria) near the western coast. The calculations were performed for a prototype structure assumed to be a commercial building built on very dense soil or soft rock. The lateral loads were assumed to be resisted by tension-only steel braced frames, which is considered as a conventional construction category (CC type) structure in NBCC 2005 and 2010. The importance factor and the foundation factor for this structure were considered as 1.0. Ductility factor *K* in NBCC 1970 to 1985 was set equal to 1.3. The ductility factor *R* used was 1.5 in NBCC 1990 to 2010 for Type CC structures. Figure 1.2 shows the comparison between the spectra for the four aforementioned cities. Generally, all seismic design provisions give similar design base shears for medium- to high-rise buildings that have the fundamental period longer than 1.0s. The

differences in design base shears for these structures are smaller for cities in eastern Canada than for the cities in the west. For low-rise structures that have periods less than 1.0 s, the design base shears exhibit large differences among the different seismic design provisions. Similar design base shears were obtained for NBCC 1970 to NBCC 1980, but those values are the lowest. Starting with NBCC 1985 when an updated seismic map was included, the design base shear began to increase. For example, design base shear from NBCC 1990 and NBCC 1995 increased about twice when compared to the lowest illustrated values. Then, it increased about 4 to 5 times when comparing to NBCC 2005 and 2010. Although the exact changes for certain buildings may not be as high because other modifications were also implemented in NBCC, such as the equations for the building periods. This comparison of different design spectra provides a general idea about the variations in design base shears over the last 5 decades. The results clearly show that low- and medium-rise building structures will very likely require major retrofit action, while the situation is more critical for structures designed and built prior to 1989.

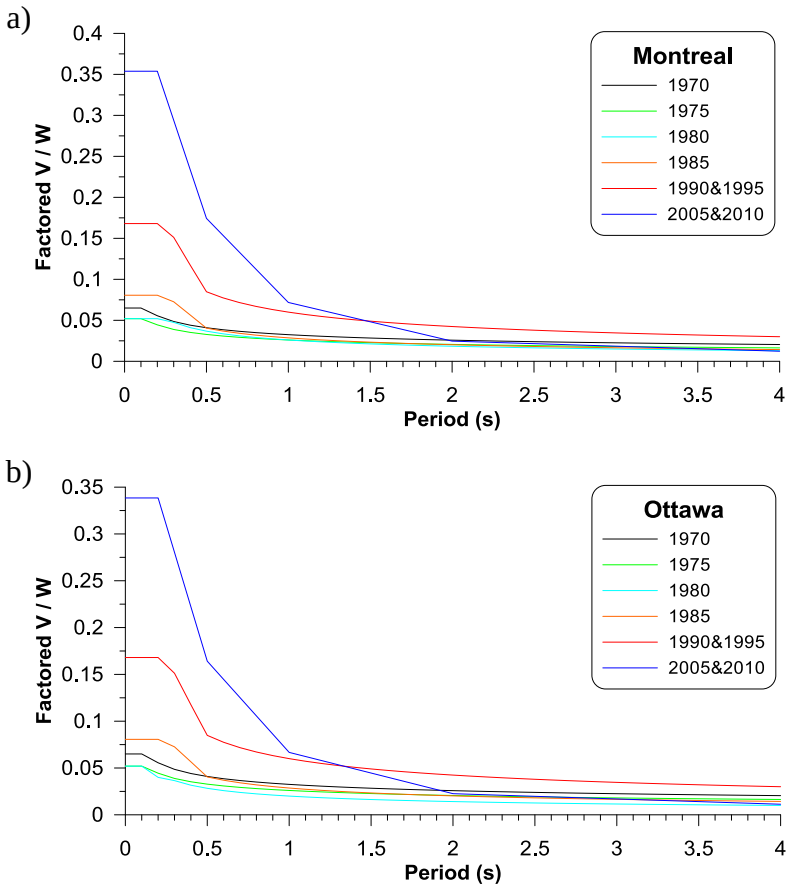

Figure 1.2: Spectrum analysis results: a)Montreal; b)Ottawa; c)Vancouver; d)Victoria

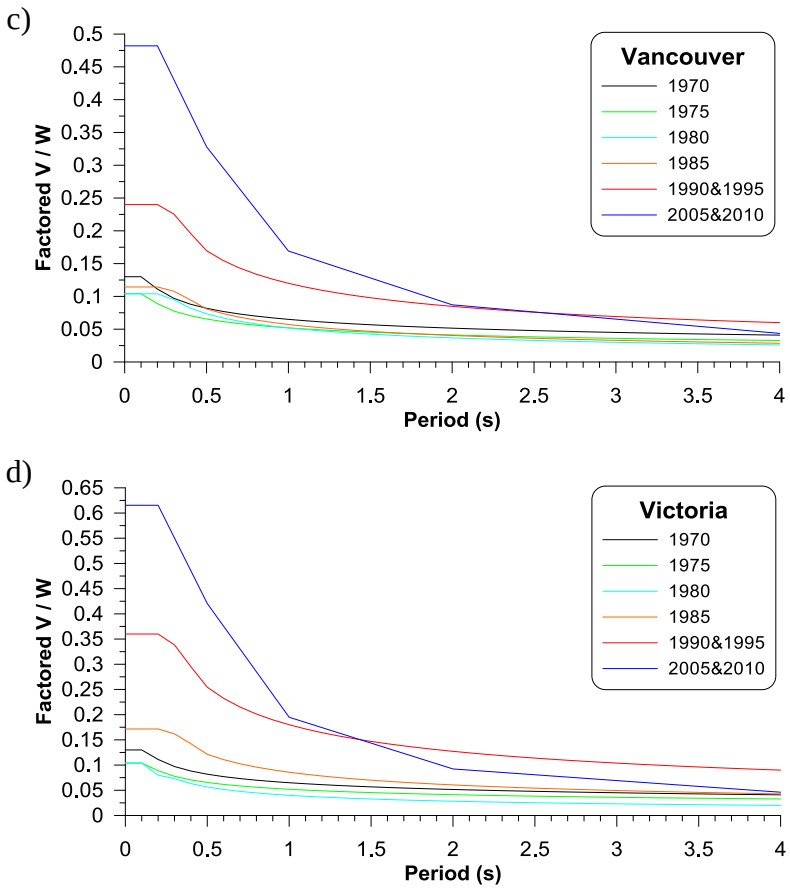

Figure 1.2: Spectrum analysis results: a) Montreal; b) Ottawa; c) Vancouver; d) Victoria (Continued)

Based on this survey, it appears that the assessment of the seismic performance of a low-rise building that was built in 1980 would be most interesting because NBCC 1980 required nearly the smallest design base shear among the editions released between 1970 and 1985.

It is important to mention that dynamic analysis was permitted to be used as an alternative procedure to determine the seismic design forces in the 1975 NBCC. Since then, because computers became used in structural analysis, dynamic analysis was gradually adopted by structural engineers.

1.2 Seismic design and detailing provisions in CSA S16

In Canada, the design of steel structures is performed in accordance with the CSA S16 design standards. Seismic design and detailing provisions in CSA S16 were only implemented in 1989. Since then, they have been continually updated to reflect new research findings and lessons learned in recent past earthquakes (Tremblay, 2011).

Prior to 1989, there were no special design and detailing provisions in S16 to ensure ductile seismic response. For instance, all members and connections were designed for the same load combinations and a brittle failure mode (e.g., tension rupture on net section) could be the governing failure mode along the seismic load path of the structure. In 1989, capacity design provisions were introduced in CSA S16 to establish a strength hierarchy along the seismic load paths such that inelastic demand will develop in ductile elements capable of accommodating the anticipated inelastic deformations and sufficient resistance are provided to non-ductile elements in order to assure their elastic response.

For a given seismic force resisting system, the ductile (yielding) elements are identified in CSA S16 and special detailing requirements are prescribed so that they can withstand the inelastic deformations without premature fracture. For the remaining, non-ductile (capacity protected) elements, the seismic induced forces are increased to the level corresponding to the probable resistance of the ductile elements. For instance, in steel braced frames, the bracing members are selected to be the ductile elements. Brace connections, columns, beams and other connections along the seismic load path must be designed to resist seismic loads required to develop the probable resistance of the braces. Thus, the seismic force resisting systems should have a ductility consistent with the seismic loads that are specified in the NBCC such that a ductile and stable inelastic response can be safely achieved under the design level earthquake. This project focuses on braced frames with double angle steel bracing members and bolted connections. The inelastic seismic responses of this type of bracing members is reviewed in the following sections, together with the design equations that are used for brace bolted connections. These aspects are of particular importance when performing the seismic design or seismic assessment of these braced frames.

1.3 Built-up double angle braces

Angle braces, either single angle brace or built-up double angle braces, have been and still are very popular for steel concentrically braced frames. For instance, in the AISC design guideline on connections published in the early 1980's (AISC, 1984), almost all illustrated bracing members are made of angle sections. One reason may be the facility of connections fabrication and installation for angle braces. This characteristic of the angle braces led to an extensive usage of angle braces in the construction field.

1.3.1 Cyclic-inelastic behaviour of double angle bracing members

The behaviour of double angle braces with bolted or welded connections was investigated by Astaneh-Asl and Goel (1984, 1985). In their cyclic tests, in-plane and out-of-plane brace buckling was observed. In both cases, it was found that the buckling load decreases significantly after the angle brace has buckled. After buckling, the compressive resistance continues to decrease gradually in the following loading cycles. In tension, braces can develop their full probable yield tensile resistances based on the gross-section yielding, provided that their connections have sufficient resistance.

From the observations made in the out-of-plane buckling tests, the authors proposed that the gusset plates be designed with a smaller flexural strength and stiffness compared to the double angle brace members such that ductile rotation takes place in the gusset plates upon brace buckling. With this design, three plastic hinges formed in the braces: one at the brace mid-span and both in the gusset plates. In the tests conducted by Astaneh-Asl and Goel (1984), the gusset plates generally showed poor ductility and early fractures, due to undesirable constraint which prevented plastic hinge free rotation at the ends during post buckling stage. As shown in Figure 1.3, they recommended to leave a minimum free distance of twice the thickness of the gusset plate between the end of the double angle brace and the corner of gusset plate to ensure the free formation of plastic hinges.

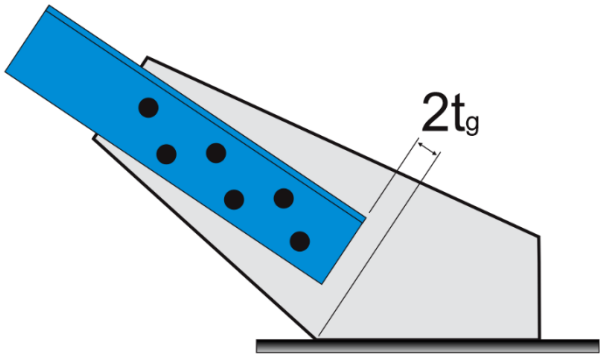

Figure 1.3: Free length of gusset plate

The deformed shape of double angle braces with long legs back-to-back is nearly a half-sine curve resulting in effective length factor of approximately 1.0. It was indicated that flexural yielding in the gusset plates occurred before that in the angles brace because the combined effect of bending and axial load in the post-buckling region. Local buckling was observed at the outstanding legs of

angles, on the concave side and in the central plastic zone of the buckled brace. Local buckling of the outstanding legs appeared to be strongly related to the b/t ratio of the legs. Local buckling of angle braces may lead to fracture on the gross section at the location of local buckling. Compression yielding or local buckling did not exhibited at the connected legs of the angles.

1.3.2 Factored compressive strength of double angle members

In CSA S16-09 (CSA 2009), Equations 1.1 is used to calculate the factored compressive (buckling) strength, C_r, of double angle bracing members.

$$C_r = \phi \mathrm{A} F_y (1 + \lambda^{2n})^{-1/n} \ , with: \lambda = \sqrt{\frac{F_y}{F_e}}, n = 1.34 \tag{1.1}$$

In this equation, ϕ is the resistance factor (ϕ = 0.9), A is the brace cross-section, F_y is the steel yield strength, λ is the slenderness parameter and F_e is the lesser of F_{ex} (in-plane flexural elastic buckling stress) and F_{eyz} (out-of-plane flexural-torsional elastic buckling stress):

$$F_{ex} = \frac{\pi^2 E}{\left(\frac{K_x L_x}{r_x}\right)^2} \tag{1.2}$$

and:

$$F_{eyz} = \frac{F_{ey} + F_{ez}}{2\Omega}\left[1 - \sqrt{1 - \frac{4 F_{ey} F_{ez} \Omega}{\left(F_{ey} + F_{ez}\right)^2}}\right] \tag{1.3}$$

where:

$$F_{ey} = \frac{\pi^2 E}{\left(\frac{KL}{r}\right)^2_{ye}}; \tag{1.4}$$

$$F_{ez} = \left[\frac{\pi^2 E C_w}{(K_z L_z)^2} + GJ\right]\frac{1}{A\overline{r_o}^2} \tag{1.5}$$

$$\Omega = 1 - \left[\frac{y_o^2}{\overline{r_o}^2}\right] \tag{1.6}$$

$$\overline{r_o}^2 = r_x^2 + r_y^2 + y_o^2 \tag{1.7}$$

In these expressions, E is the Young's modulus of elasticity of steel (E = 200 000 MPa), KL is the effective length, F_{ey} and F_{ez} are the out-of-plane flexural and torsional elastic buckling stresses, respectively, r_x and r_y are the radius of gyration for in-plane and out-of-plane flexural buckling, and y_o is the in-plane distance between the shear center and the center of gravity (see Figure 1.4). All the above properties are for the double angle cross-section and the equations account for overall

brace buckling. For in-plane buckling, buckling of the individual angles forming the built-up double angle brace may occur about the angle minor axis. In CSA S16, this is accounted for by using an effective brace slenderness $(KL/r)_{ye}$:

$$\left(\frac{KL}{r}\right)_{ye} = \sqrt{\left(\frac{KL}{r}\right)_{y}^{2} + \left(\frac{KL}{r}\right)_{o}^{2}} \tag{1.8}$$

where $(KL/r)_o$ is the slenderness of the individual angle determined with the effective buckling length between the stitches connecting the two angles, $(KL)_o$, and the radius of gyration of the angle section about its minor axis. In CSA S16, an effective length $(KL)_o = 0.65L$ is specified for welded stitches or stitches with pre-tensioned bolts. For snug tight bolts, $(KL)_o = L$ is recommended.

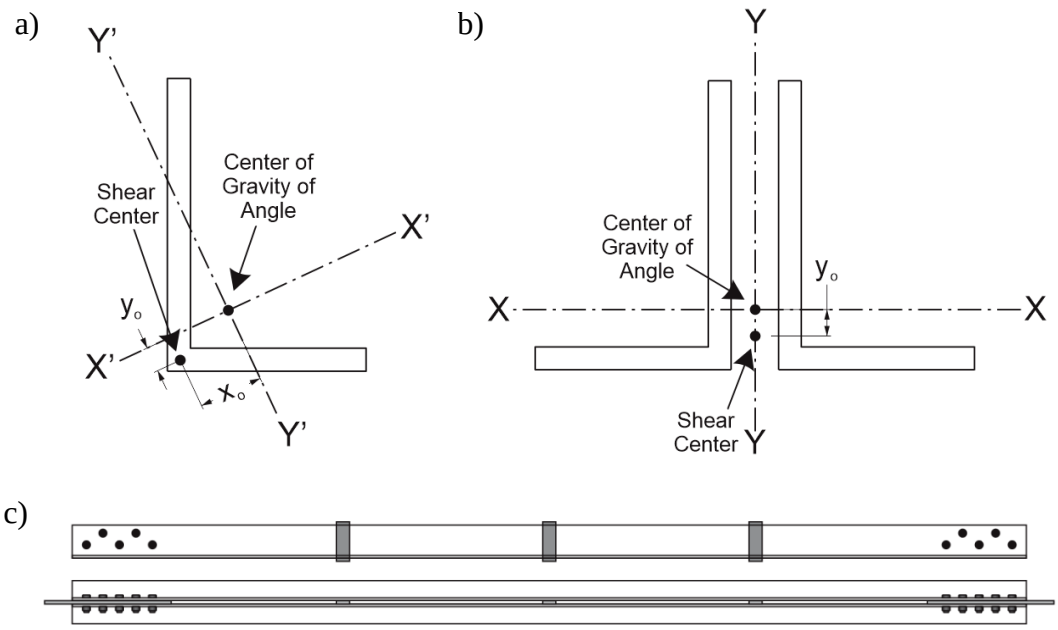

Figure 1.4: Properties of angle cross-sections and build-up brace: a) single angle; b) double angle; c) double angle brace

1.3.3 Residual stress distribution

Residual stress in an angle section can reduce its buckling strength. In order to develop a more accurate numerical model for angles, residual stress distribution of angles need to be included in the numerical model. The residual stress pattern in hot-rolled steel angles was studied by Adluri and Madugula (1995). Residual stresses were measured in nine equal-leg and six unequal-leg steel angle sizes. It was observed that the maximum residual stress level in steel angles is usually less

than one quarter of the steel yield strength. In addition, residual stress patterns in the two legs of angles are rarely similar. The residual stress distributions from twenty-five angle sections are presented in Figure 1.5: the measured residual stresses, the average stress distribution curve and the assumed distribution curve are shown. The assumed symmetric linearly varying distribution of residual stresses is recommended.

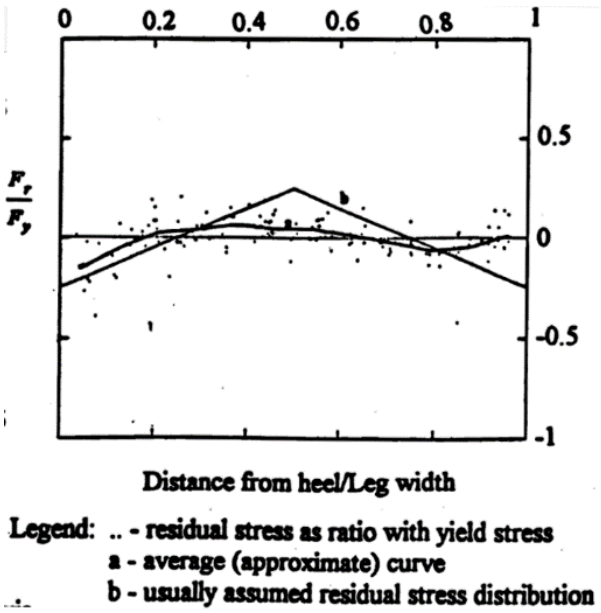

Figure 1.5: Residual stress level along the legs of hot-rolled steel angles (Adluri and Madugula, 1995)

1.3.4 Influence of stitch connections

Welded or bolted stitches are used to connect two separate angles in double angle sections. The number of stitches along the brace length, or the spacing between stitches, can influence the overall compressive strength and energy dissipation capacity of double angle braces. A smaller stitch spacing results in higher normalized cyclic peak compression loads but the effect of stitch spacing on energy dissipation is not obvious; larger compression loads results in higher energy dissipation but may also lead to earlier brace fracture when local buckling dominates the brace buckling strength (Aslani and Goel, 1991).

For double angle braces that are likely to buckle out-of-plane, longitudinal shear forces must be transferred by the stitches upon buckling of the brace (Astaneh-Asl et al., 1985). These forces may cause failure of the stitch connections. Once a stitch fractured, the buckling length of the individual

angles increase, which leads to a decrease of the overall buckling strength of the double angle brace member. Hence, welding in welded stitches or bolts in bolted stitches need to be strong enough to transfer the anticipated shear forces. For braced frames for which inelastic brace response is expected, minimum design forces are specified for the stitches in CSA S16.

1.3.5 Current seismic detailing requirements for double angle braces

Limits are specified for the angle legs' width-thickness (b/t) ratios and the brace slenderness ratio in order to prevent local buckling of the angle sections and ensure proper overall performance of double angle braces for braced frames designed for ductile inelastic response. In the current CSA S16-09 steel design standard, the maximum slenderness ratio is limited to 200 for bracing members. For the b/t ratio, the limit is $145/\sqrt{F_y}$ for braces with slenderness less than or equal to 100. For a brace slenderness of 200, the limit is increased to $170/\sqrt{F_y}$ and linear interpolation is permitted for intermediate brace slenderness values. For double angle braces buckling out-of-plane, the limit is relaxed to $200/\sqrt{F_y}$ for the back-to-back vertical legs. The limit need not be less than $170/\sqrt{F_y}$ in low-seismicity regions. No such provisions existed for the seismic design of angle braces before 1989.

1.4 Brace connection

1.4.1 Connection design forces

Before the capacity design concept was introduced in CSA S16-89 (CSA 1989), the design of braces and their connections were based on the same design forces. In the 1989 edition of CSA S16, the new seismic provisions for braced frames exhibiting ductile response required that the brace connections be designed for the probable tensile capacity of brace, which was then specified as AF_y. In CSA S16-01 (CSA 2001), this force was modified to AR_yF_y where R_y is a factor that accounts for the possibility that the actual yield strength of steel exceeds the nominal yield strength used in design. It was also required that the connections be designed for a compression load equal to the probable compressive resistance. In 2009, the probable resistances of braces acting in tension and compression were designated as T_u and C_u, respectively:

$$T_u = AR_yF_y \tag{1.9}$$

$$C_u = 1.2AR_yF_y(1+\lambda^{2n})^{-1/n} \leq T_u \ , with: \lambda = \sqrt{\frac{R_yF_y}{F_e}} \quad (1.10)$$

After buckling of the brace under cyclic loading, the brace post-buckling compressive resistance, C'_u, can be estimated from:

$$C'_u = 0.2AR_yF_y \leq C_r/\phi \ , with\ \lambda = \lambda_y \quad (1.11)$$

Capacity design is not required for steel braced frames of the conventional construction category (Type CC seismic force resisting system) designed with a ductility-related force modification factor of 1.5. However, since 2001, CSA S16 requires that the design forces for the connections of primary members along the seismic load path be increased by 1.5 if the governing failure mode is not ductile. This provision applies in regions of moderate and high seismicity, i.e., where the short-period spectral acceleration ratio, $I_EF_aS_a(0.2)$, exceeds 0.45. Unfortunately, no quantitative limit has yet been introduced in CSA S16 to determine whether the amplification factor must be applied or not.

Since capacity design or the 1.5 amplification factor were not mandatory for the design of brace connections before 1989, it is very likely that brace connections in braced frames designed before that time do not meet current strength requirements and, therefore, may be prone to non-ductile failure modes.

1.4.2 Connection failure modes

In bolted connections for double angle braces, there are seven potential failure modes. They are tension rupture on the net area of the angle brace or gusset plate, bearing failure on the angle brace or the gusset plate, block shear failure of the angle or the gusset plate, and bolt shear failure. A sketch of the three failure modes for the angle brace is shown in Figure 1.6. The same three failure modes can also occur in the gusset plate. In addition to these failure modes, bolt shear failure is a possibility that must be considered.

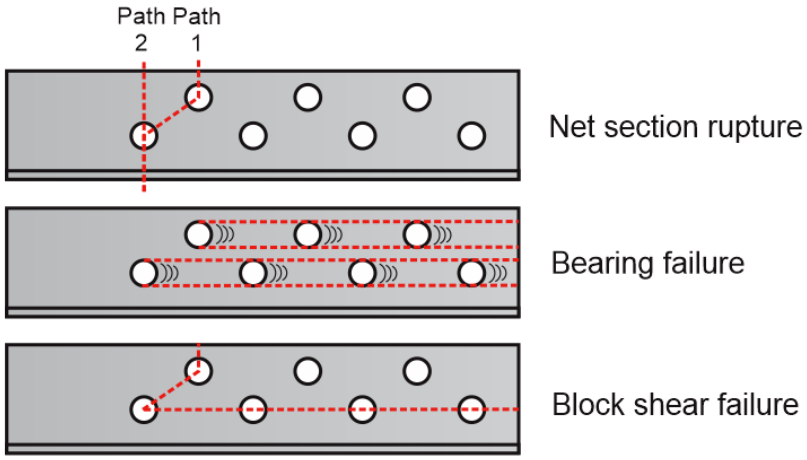

Figure 1.6: Possible failure modes in angles with bolted end connections

In these mentioned bolted connection failure modes, net rupture failure and block shear failure are discussed in the following sections because shear lag effect wasn't counted in net section tensile capacity calculation, moreover, block shear failure mechanism was not introduced prior to 1989.

Five different connection designs for back-to-back double angle braces corresponding to five different connection failure mechanisms were tested under monotonic tension loading to investigate the ductility behaviour of each connection failure mode (Castonguay and Tremblay, 2010). Welded and bolted connections were investigated. The specimens were designed and fabricated according to the latest steel structure design provisions. Load-displacement curves for the various failure modes observed are shown in Figure 1.7. The weld failure was the least ductile with an average deformation of 9.4 mm. Conversely, bearing failure resulted in the most ductile performance with an average deformation of all specimens of approximately 30 mm. Other failure modes exhibited intermediate ductility levels. Average deformations of 20.1 mm, 16.2 mm, and 19.7 mm were respectively recorded for the specimens with tension rupture on the net section, bolt shear failure and block shear failure. Note that the deformations are the sum of the deformations that developed at both specimen ends but inelastic deformations and failure occurred at one end only.

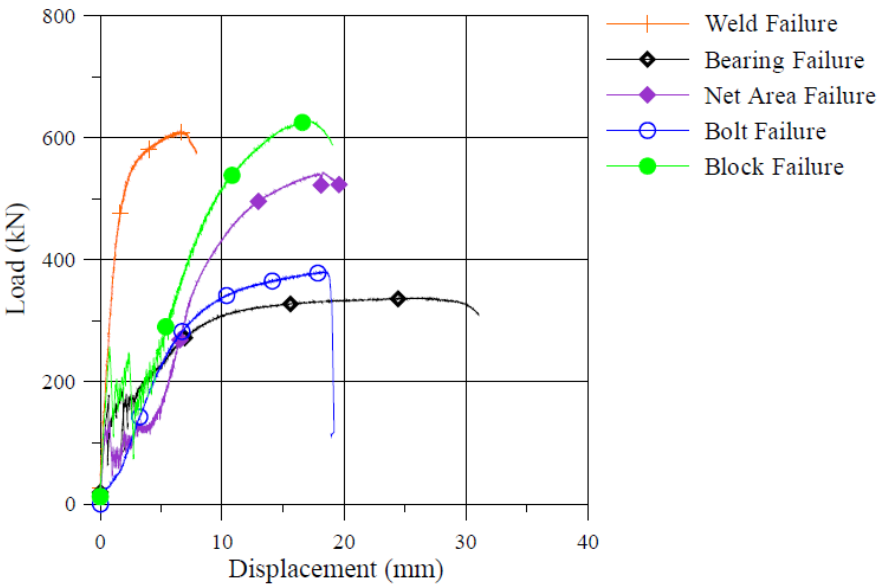

Figure 1.7: Load-displacement curve of each failure mechanism (Castonguay, 2009)

In addition, a study on existing concentrically braced frame connections was carried out by Hartley and Rogers (2011). A total of 12 brace-to-column or brace-to-beam connections were extracted from a structure that was being demolished. The structure served as primarily support for equipment or storage facilities. The dates of construction vary from the 1960s to 1980s. The existing connections were installed appropriately into a load frame to proceed with monotonic tension tests. The failure modes of the specimens varied significantly from specimen to specimen. The calculations of the predicted strengths were good indicators of the observed failure mode. A common failure was the shear fracture of bolts through the threads. This failure mode was the most brittle one. Block shear and net section tension fracture of the braces were also observed. The former provided the highest amount of ductility, followed by specimens in which the brace first yielded, then fractured through the net section. For some specimens, higher than anticipated material properties for the braces resulted in bolt shear fracture due to longer thread length and lower grade of older bolts. This aspect needs to be carefully considered by engineers or researchers involved in the evaluation or retrofitting existing structures.

1.4.3 Failure in tension on net section

In CSA S16.1-M78 (CSA 1978), Equations 1.12 to 1.14 were used to calculate the factored tension resistance (T_r) of bolted connected elements.

$$T_r = \phi A_n F_y, if: A_n F_u \geq A_g F_y \tag{1.12}$$

$$T_r = \phi A_n F_u \left(\frac{A_n}{A_g}\right), if: A_n F_u < A_g F_y \tag{1.13}$$

$$T_r \leq \phi 0.85 A_n F_u \tag{1.14}$$

where A_g and A_n are the gross and net cross-section areas of the member at the connection, F_y and F_u are respectively the material yield and tensile strengths and ϕ is the resistance factor (ϕ = 0.9). If yielding on the gross section occurs before tension fracture on net area ($A_nF_u \geq A_gF_y$), the resistance is based on yielding of the net section. When net section fracture governs, the resistance is reduced by the ratio A_n/A_g to account for the limited available ductility. In either case, T_r shall not exceed $\phi 0.85A_nF_u$. The factor 0.85 is included to increase the reliability index for this brittle failure mode. In addition, upper limits on A_n/A_g were specified according to different F_y/F_u ratios. For CSA-G40.21-300W steel as commonly used in the 1980's, F_y = 300 MPa and F_u = 450 MPa, and A_n cannot exceed $0.85A_g$. At that time, shear lag effects due to uniform stress distribution in bolted angle connections was not introduced.

Shear lag in bolted single and double angle tension members was investigated by Wu and Kulak (1993). Tensile tests were carried out on 24 angle specimens with 20 individual configurations. Among them, 11 specimens were single angle members and the rest were double angle members. The angles were fabricated using CSA-G40.21-M Grade 300W steel. All the specimens were from the same stock angles. The length of the members varied from 1786 mm to 2036 mm. All specimens were connected through only one leg and in all connections, the holes were punched along a single line.

In their analysis, it was found that the average stress reaches the steel ultimate tensile stress at fractured section of the connected leg. However, at failure, the average stress of the outstanding leg was close to the steel yield strength for the connections with four or more bolts per line. For connections with three or less bolts, the average stress in the non-connected leg was smaller than the steel yield strength. The authors suggested to use one-half of the yield strength for this case. Based on the analysis of the test results, Equation 1.15 was proposed to predict the net section strength of single or double angle members in tension.

$$P_u = F_u A_{cn} + \beta F_y A_o \tag{1.15}$$

Where P_u is the expected net section strength, A_{cn} is net cross-section area of the connected leg at the critical cross-section, A_o is the gross cross-section area of the outstanding leg, β is 1.0 for connections with four or more fasteners per line, and 0.5 for connections with less than four fasteners per line. The net section efficiency is defined as:

$$U = \frac{A_{cn} + \beta \frac{F_y}{F_u} A_o}{A_n} \tag{1.16}$$

In a format consistent with CSA S16.1-M89, the factored resistance of the net section (T_r) is given by:

$$T_r = 0.85\phi(F_u A_{cn} + \beta F_y A_o) \tag{1.17}$$

where ϕ is the resistance factor (ϕ = 0.9), and 0.85 is used to increase the safety index. This equation can be further simplified to:

$$T_r = 0.85\phi F_u A_{ne}\,, with\ A_{ne} = U A_n \tag{1.18}$$

In this expression, A_n is the net cross-section area of the entire brace at the critical cross-section. The factor U is 0.8 for connections with more than three fasteners per line and 0.6 for connections with three or less fasteners per line. In CSA S16-09, the factors 0.85 and ϕ are combined together to obtained ϕ_u= 0.75, which is an even smaller value.

In Figure 1.8, the net section strength of tested angle connections by Wu and Kulak, as well as by other researchers, are compared to the proposed equation. The proposed equation can predict very well the net section strength of angle brace connections. Test results from the three tests performed by Castonguay (2009) on net section failure mechanisms are also compared to the equation prediction. The difference is only 6%. However, the equation may be too conservative for angle connections in actual braced frames. There are two reasons for this. Firstly, all test data have been obtained from monotonic tensile tests, and the performance of angle connections under cyclic loading is not well studied. Secondly, the bolts in the tests were arranged along a single line. The performance of connections with staggered (zig-zag) bolt pattern is unknown.

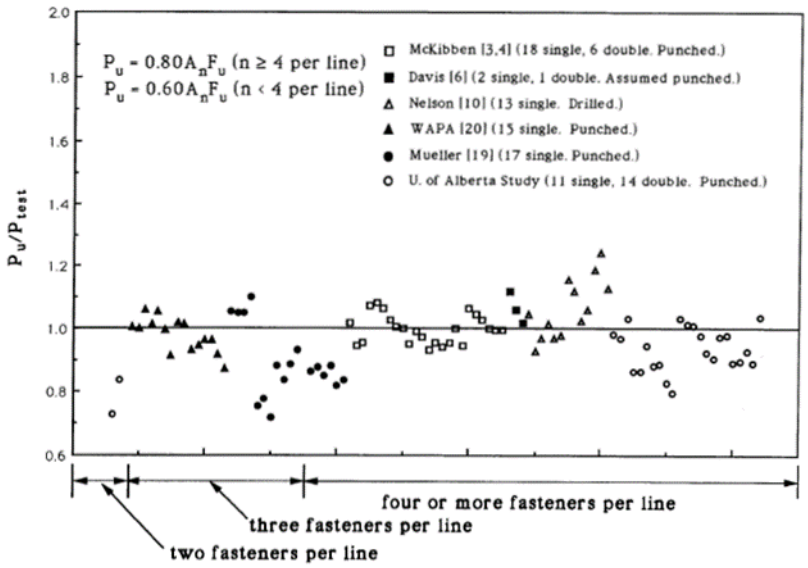

Figure 1.8: Evaluation of proposed net section strength equation (Wu and Kulak, 1993)

The axial deformation of tested angle braces was also investigated by Wu and Kulak (1993). It was found that specimens with longer connection (more bolts in line) have better ductility performance. Figure 1.9 shows the overall axial deformation of the same size of single angle braces with different number of bolts in connections. The specimen with the shortest connection (2 bolts in line) has the lowest ductility performance. The ductility performance of specimens with connections that have 6 bolts is the best because by increasing the number of bolts the shear lag effect reduces and it results in more uniform stress distribution and more extended yielding before fracture on net section occurs.

Although the curves in this figure represent the overall brace elongations, the majority of the deformations for the 2-bolt connection can be considered as developing in the connection because, unlike the curves for the 4- and 6-bolt connection, strain hardening of the steel in the angle has not initiated for this specimen. When excluding the elastic deformation of the net length of brace member and assuming equal deformations in both end connections, one can estimate the deformation for each 2-bolt connection to be about 6mm at failure. The length of each connection was 152 mm.

Similar deformations of bolted connections at the net section failure of single angle bolted connections were obtained in tests performed by Castonguay (2009). In that case, the connection length was 225 mm and the average deformation for a connection that failed at the net section was

9 mm. The ratio between the connection length and the connection deformation at failure from both research projects are very close: 3.95% for Kulak and Wu (1993) and 4% for Castonguay (2009).

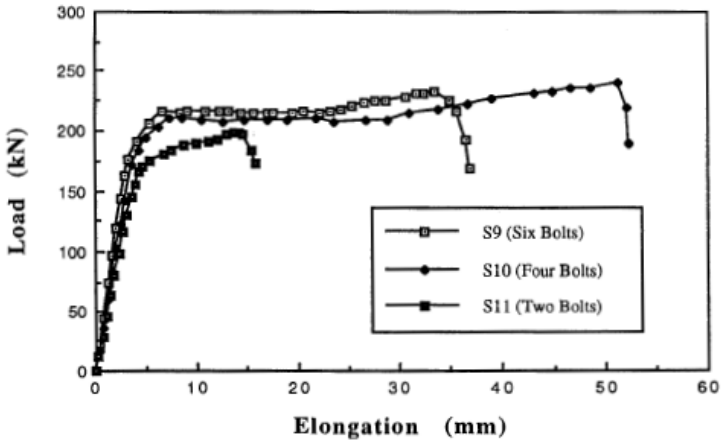

Figure 1.9: Load *vs* overall brace elongation (Wu and Kulak, 1993)

1.4.4 Block Shear failure

A sketch of a block shear failure is shown in Figure 1.6, and the block shear failure in angle brace connection with bolts arranged in one line is shown in Figure 1.10. As illustrated, failure occurs both in tension and shear along two distinct failure planes.

Figure 1.10: Block shear failure (Castonguay, 2009)

The first provisions for block shear failure were introduced in CSA S16.1-94 (CSA 1994). They were based on the assumption that the ultimate tensile strength and the ultimate shear strength are

reached simultaneously along both failure planes. Equation 1.19 was provided to calculate the capacity of connection against block shear failure.

$$\phi P_u = 0.85\phi(F_u A_{nt} + 0.6F_u A_{nv}) \quad (1.19)$$

In this equation, P_u is the nominal block shear capacity, A_{nt} is the net area of the failure plane subjected to tension, A_{nv} is the net area along the shear failure plane, and ϕ= 0.9. The shear strength of the material is taken as 0.6 times the ultimate tensile strength.

Kulak and Grondin (2001) studied and summarized a large amount of experiment tests for block shear failure. They recommended that the block shear resistance to be taken as the sum of the tensile resistance on the net section and the shear yield resistance on the gross shear area. This change was proposed because fracture on the tension area occurred before facture on the shear area was observed in many tests. The recommended equation is Equation 1.20 for gusset plates and angles. This equation was adopted in CSA S16-01 (CSA 2001). In addition, Equation 1.21 was also adopted in CSA S16-01 to limit the capacity of the shear planes to that corresponding to the rupture strength on the net shear area. Although no observed failure mode supported this limitation, it provided a sufficient level of safety. Hence, the capacity of gusset plates was to be taken as the lesser of:

$$T_r + V_r = \phi A_{nt} F_u + 0.60\phi A_{gv} F_y \quad (1.20)$$

$$T_r + V_r = \phi A_{nt} F_u + 0.60\phi A_{nv} F_u \quad (1.21)$$

where A_{gv} is the gross area in shear for block failure.

Based on experimental and numerical analysis investigations, Huns et al. (2002) recommended using Equation 1.22 to calculate the block shear resistance for gusset plates. This equation is identical to the equation proposed by Franchuk et al. (2002) for block failure resistance on coped beams.

$$P_r = \phi R_t A_{nt} F_u + \phi \frac{1}{\sqrt{3}} A_{gv} \frac{(F_y + F_u)}{2} \quad (1.22)$$

where ϕ is taken as 1.0 and R_t is taken as 1.0 for gusset plates.

A modified version of Equation 1.22 was adopted in CSA S16-09 (CSA 2009) to calculate block shear resistance of different sections:

$$T_r = \phi_u \left[U_t A_n F_u + 0.6 A_{gv} \frac{(F_y + F_u)}{2} \right] \quad (1.23)$$

In this equation, the U_t factor depends on the section types: U_t = 0.6 for angles connected by one leg and U_t = 1.0 for gusset plates. The factor, ϕ_u = 0.75.

As shown in Figure 1.7, the ductility performance of connections failing by block shear is similar to that of connections failing in tension at the net section.

1.4.5 Summary of angle brace connections

Angle braces connected with one leg in CBF buildings designed prior to 1989 are very likely to be deficient because: 1) capacity design concept was not applied yet for the design of the connections; 2) shear lag effects were not included in the equation to calculate the tensile capacity on the net section; and 3) block shear failure mode was not considered in design.

1.5 OpenSees modelling

OpenSees software framework is an open system for earthquake engineering simulation (McKenna and Fenves, 2004). It utilizes finite element method to develop applications to simulate the behaviour and performance of structural and geotechnical systems in seismic event. Various modelling, analysis, output and database commands are available for developing accurate OpenSees applications.

1.5.1 Steel bracing member modelling

OpenSees is a suitable finite element program for simulating the hysteretic behaviour of steel braces. A large-displacement buckling formulation with fiber sections incorporated in OpenSees has already been used to reproduce the inelastic cyclic response of steel bracing members (Uriz and Mahin, 2004). Another study has been performed to investigate the possibility of modelling the seismic inelastic cyclic response of steel bracing member made of rectangular and square steel tubes using the OpenSees program (Aguerro et al., 2006). In that study, the Giuffré-Menegotto-Pinto hysteretic material (*Steel02*) with fiber discretization of the cross section and a co-rotational transformation were implemented to model the inelastic and nonlinear geometric behaviour of tubular steel bracing members. The Giuffré-Menegotto-Pinto material accounts for both isotropic and kinematic strain hardening. Numerical models of braces with various slenderness ratios and

boundary conditions were calibrated and validated against experimental test results to determine the values of the parameters for the Giuffré-Menegotto-Pinto material (F_y, E, b, R_0 and a_1 to a_4). The influence of the number of elements, integration points and fibers was also investigated. Typical results and bracing models with different slenderness ratios are shown in Figure 1.11. In order to find out the relationship between accuracy and complexity in the bracing model, a sensitivity analysis was also carried out. In the sensitivity analysis, differences between a reference and various combinations of number of elements, integration points, and fibers were compared. It provided useful data for numerical model simplification.

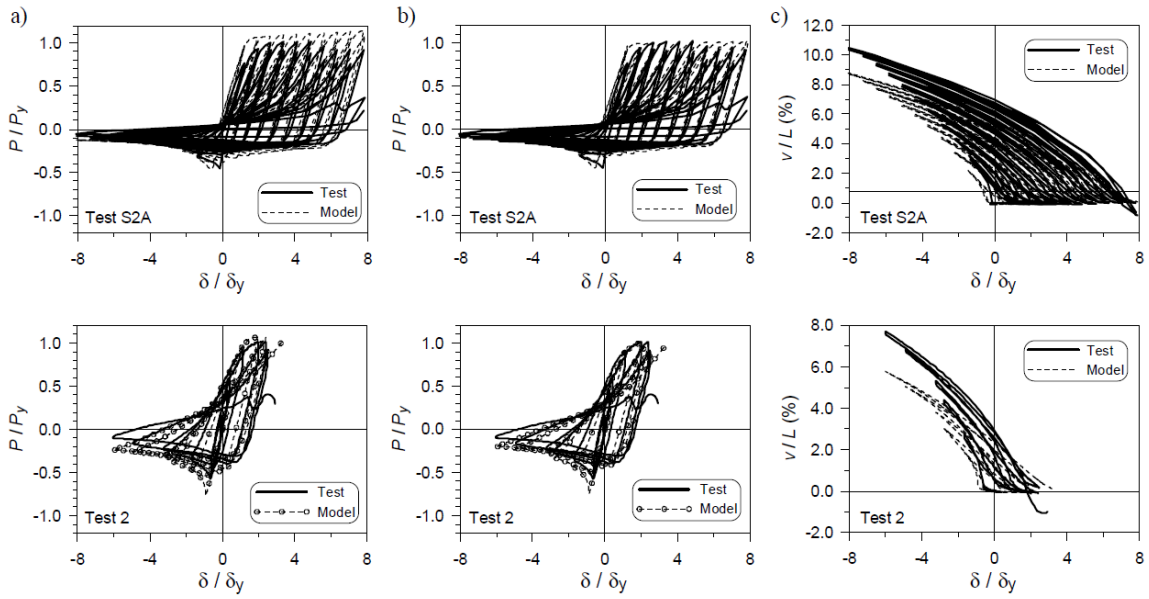

Figure 1.11: Comparison between test and pin-ended model with length KL: a) Hysteretic response with R_0= 25, a_1= a_3= 0.00001, and a_2= a_4= 0.00002; b) Hysteretic response with R_0= 25 and $a_1$to a_4= 0.0; c) Out-of-plane response at brace mid-length with R_0 = 20 and a_1 to a_4 = 0.0 (Aguerro et al. 2006)

Although results from model prediction and experimental test were slightly different, OpenSees showed the ability to simulate the inelastic and nonlinear of bracing member under cyclic loading. During the last years, several researchers have used this type of model for investigating the seismic response of steel braced frames with tubular bracing members (Izvernari et al., 2007; Uriz et al., 2008; Tremblay 2008; Chen 2011; Hsiao et al., 2012; Salawdeh and Goggins, 2013). In their study, Izvernari et al. (2007) also modelled W-shape bracing members using a similar technique. Lamarche and Tremblay (2009) introduced the capability of specifying residual stresses in the fiber

cross-section models in OpenSees. No such model has been developed yet for double angle bracing members.

1.5.2 Modelling the hysteretic behaviour of brace connection

The Pinching4 material is an uniaxial material available in OpenSees that can be used to represent a "pinched" load-deformation response and exhibits degradation under cyclic loading (McKenna et al., 2004). In Figure 1.12, the Pinching4 material was selected to model the axial cyclic behaviour and failure phenomena of the brace to gusset plate connections (Castonguay, 2009). The figure presents the envelope response where V_s is the connection slip force and R_oC_f is the connection ultimate load. The parameters in the Pinching4 material for this connection model were calibrated by using connection experimental test results. Zero value was applied to those parameters representing cyclic degradation in Pinching4 material.

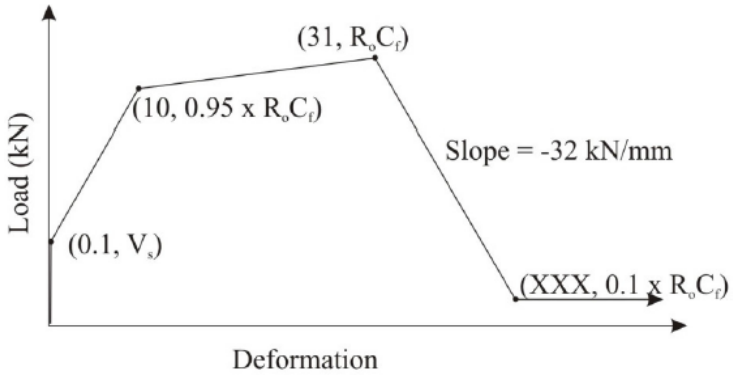

Figure 1.12: Pinching4 material used for incremental analyses of brace connections (Castonguay, 2009)

A comparison between the results from the numerical model and experimental data is shown in Figure 1.13. Good match was obtained, which indicated that the Pinching4 material has the capability to simulate the stiffness and strength reduction in brace connections.

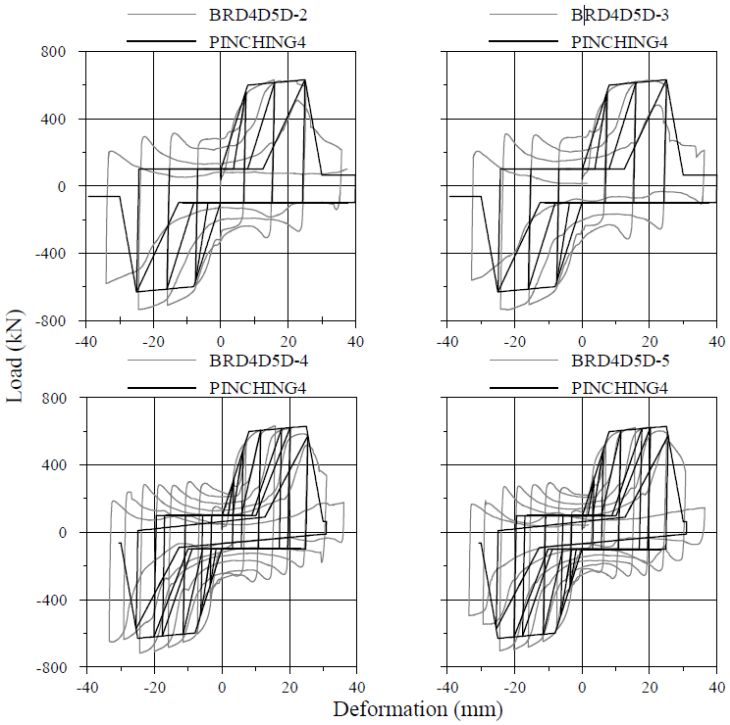

Figure 1.13: Calibrating of Pinching4 to cyclic results (Castonguay, 2009)

1.6 Hybrid simulation in structural seismic engineering

Hybrid simulation testing method is an innovated experimental method that can be used in structural seismic engineering. The structure model combined both numerical and physical components of the structure and is analyzed step-by-step to compute the response under a seismic ground motion. The numerical and physical parts in the hybrid simulation are interacting with each other at all time during the test. The physical part in the simulation is subjected to the demand determined from the structure response, and that response is influenced by the measured behaviour of the physical component being tested. Unlike quasi-static cyclic testing, the physical specimen may be under or over tested depending on the demand being computed for the structure. The test setup and program for hybrid testing are similar to the one required for quasi-static tests. It is much simpler, however, than the setup and program that are necessary in shaking table tests. This simplified test procedure implies low cost, efficient test setup and program, while helping researchers and engineers to save time. In addition, the most important reason to use hybrid tests in structural seismic engineering is the accuracy and reliability of results simulation. Two hybrid simulations that were studied using OpenSees finite element program and OpenFresco middleware hybrid simulation technique are introduced in this section.

1.6.1 Hybrid simulation of structural collapse

Several researchers used hybrid simulation technology to study the behaviour of structures beyond collapse. Wang et al. (2012) simulated the behaviour upon collapse of a one-half scale moment-resisting frame performed on a distributed hybrid test framework. Schellenberg et al. (2008) investigated the seismic response of a one-storey portal frame with two ductile columns up to structural collapse using OpenSees and OpenFresco hybrid simulation technique at the University of California at Berkeley. In their hybrid test program, a numerically modeled elastic beam was connected to two physical columns that were installed in the test setup at the NEES laboratory at Berkeley. The hybrid model and the test setup are shown in Figure 1.14. Two cases were considered for the gravity loads (with and without applying gravity load to the portal frame). The test was conducted to evaluate the influence of the gravity loads on the structure response under a seismic event. Based on the hybrid simulation results shown in Figure 1.15, it was observed that gravity loading can change significantly the seismic behaviour of a portal frame because of second-order effects.

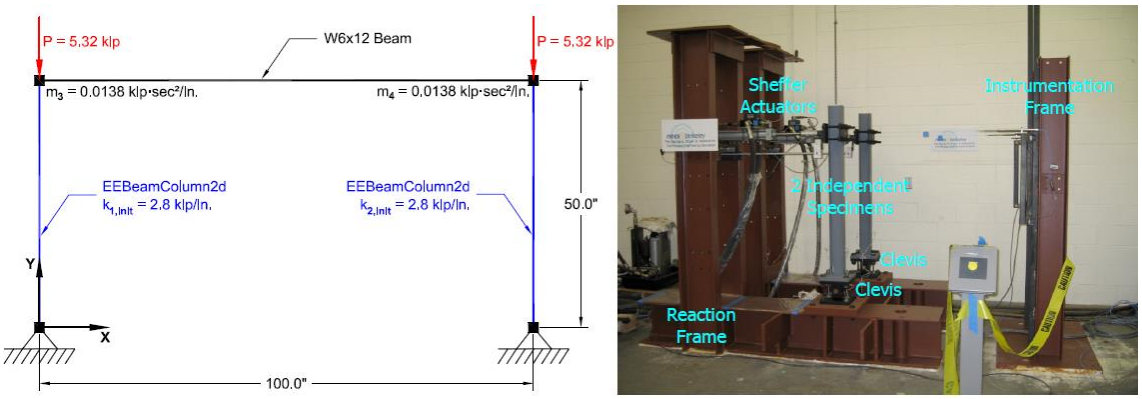

Figure 1.14: Hybrid model and experimental setup (Schellenberg et al., 2008)

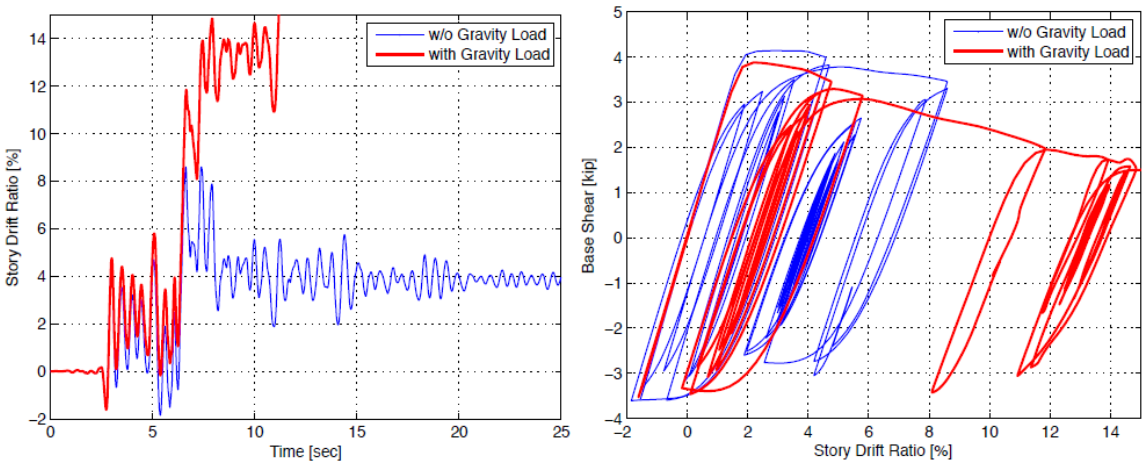

Figure 1.15: Comparison of storey-drift time-histories and total storey hysteretic-loops (Schellenberg et al., 2008)

Schellenberg et al. revealed that correctly accounting for second-order effects in hybrid models is crucial to properly simulate the structural collapse under seismic loading. In addition, the hybrid simulation technique using OpenSees and OpenFresco was demonstrated and validated and was found to be adequate for the prediction of the collapse mechanism of a one-storey portal frame under a rare strong earthquake.

1.6.2 Hybrid simulation evaluation of innovative steel braced framing system

Yang et al. (2006) implemented the hybrid simulation method to evaluate the seismic performance of the suspended zipper braced steel frame system. Before the hybrid simulation, a quasi-static test was conducted to calibrate the OpenSees chevron braced frame model that was used in the hybrid test. The hybrid simulation model is shown in Figure 1.16. It is a one-bay, three-storey, and two-dimensional suspended zipper frame. The chevron braced frame at the first floor is the physical component in the simulation because it was expected that most of the nonlinear response would occur based on the numerical model analysis. The remaining components of the structure were modelled numerically in OpenSees. The results of the hybrid simulation were compared with the results from pure numerical OpenSees model simulation. Excellent match of the results from both simulation techniques can be seen in Figure 1.17. This hybrid simulation of a suspended zipper braced frame indicates that the hybrid simulation method implemented in OpenSees and Openfresco can be used to study the seismic performance of complex structural systems.

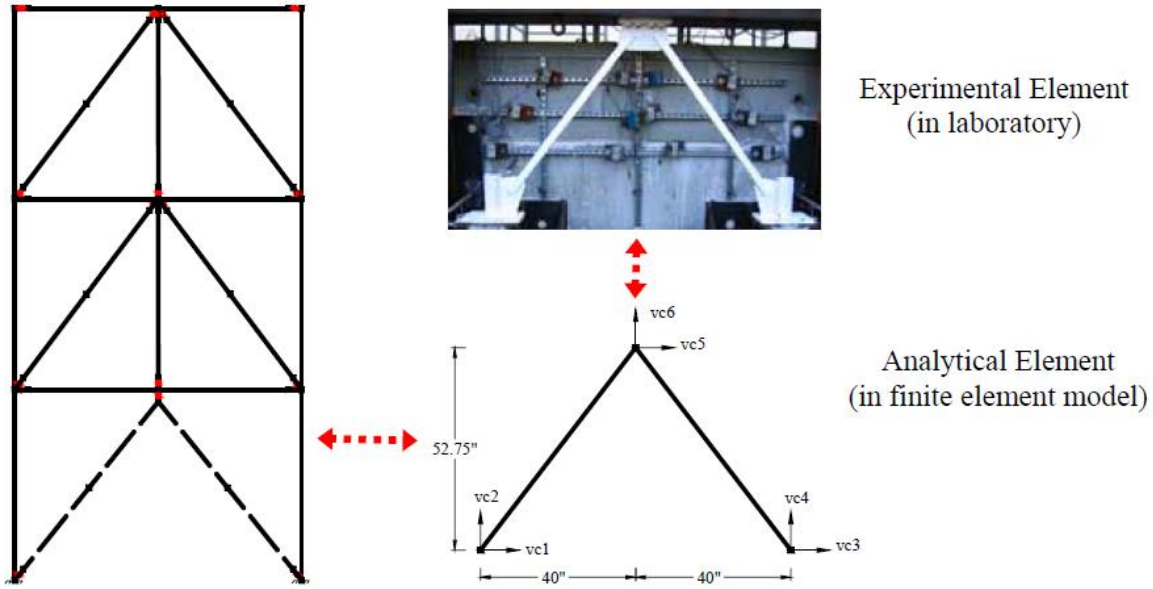

Figure 1.16: Hybrid simulation model (Yang et al., 2009)

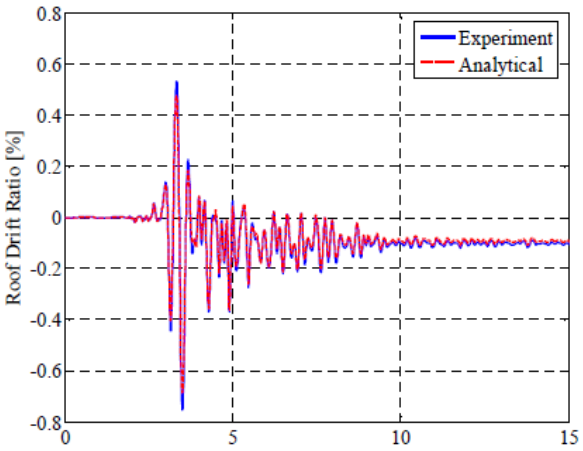

Figure 1.17: Comparison of roof drift (Yang et al., 2009)

1.7 Summary

Several quasi-static cyclic test programs have been performed on double angle braces or braced frames with double angle braces but no tests were performed to investigate the cyclic performance of the braces with deficient brace connections designed prior to the implementation of seismic design provisions in design codes. The OpenSees platform has been found to be an excellent tool for modelling the cyclic inelastic response of tubular and W-shaped steel members, but the program has not been used to predict the response of single angle or built-up double angle bracing members, including brace connection failure. Hybrid simulation has been successfully applied to complex

steel structures, but the technique has not been used yet to assess the seismic response of seismically deficient braced frame structures. The seismic assessment of deficient steel braced frames using nonlinear time history analysis in OpenSees has not been carried out yet.

CHAPTER 2: BUILDING DESIGN AND ASSESSMENT

In this chapter, the prototype building investigated in this study is described. The design of the seismic force resisting system according to NBCC 1980 and CSA S16.1-M78 is presented. The adequacy of the seismic force resisting system is then evaluated using the seismic loads from the 2010 NBCC and the design provisions of CSA S16-09. Retrofit strategies are proposed at the end of the chapter.

2.1 Design of the prototype building

2.1.1 Selection of the prototype building

A fictitious four-storey prototype commercial office building was selected for the study. The structure is located in Vancouver, British Columbia, and is designed in accordance with the 1980 NBCC and CSA S16.1-M78 standard. The site condition at the building location is assumed to be very dense soil or soft rock. A low-rise building was retained because these structures are very common in urban areas and the changes in seismic loads over the years were more pronounced for these buildings, as observed in Section 2.1. From the survey in Section 2.1, NBCC 1980 was selected as the design seismic loads started to increase significantly after this code edition. Furthermore, ductile design and detailing provisions were implemented only in 1989 in the CSA S16 standard. Hence, structures designed in accordance with CSA S16.1-M78 are likely to present several deficiencies. A site in western Canada (Vancouver) was adopted because the seismic loads increased significantly between 1980 and today in that part of the country and Vancouver is the largest city in western Canada where the likelihood of having low- and medium-rise steel buildings is the highest.

2.1.2 Building geometry and seismic force resisting system

A plan view of the structure is shown in Figure 2.1. The typical storey height of this building is 4 m, and the floor plan dimensions are 24 m by 24 m. The seismic force resisting system (SFRS) in both directions of the structure is tension-only braced frames with built-up double angle braces. This construction system was selected because it was common in the 1980's. The brace frame located on Axis 4, between Axis B and D, is selected for the following analysis.

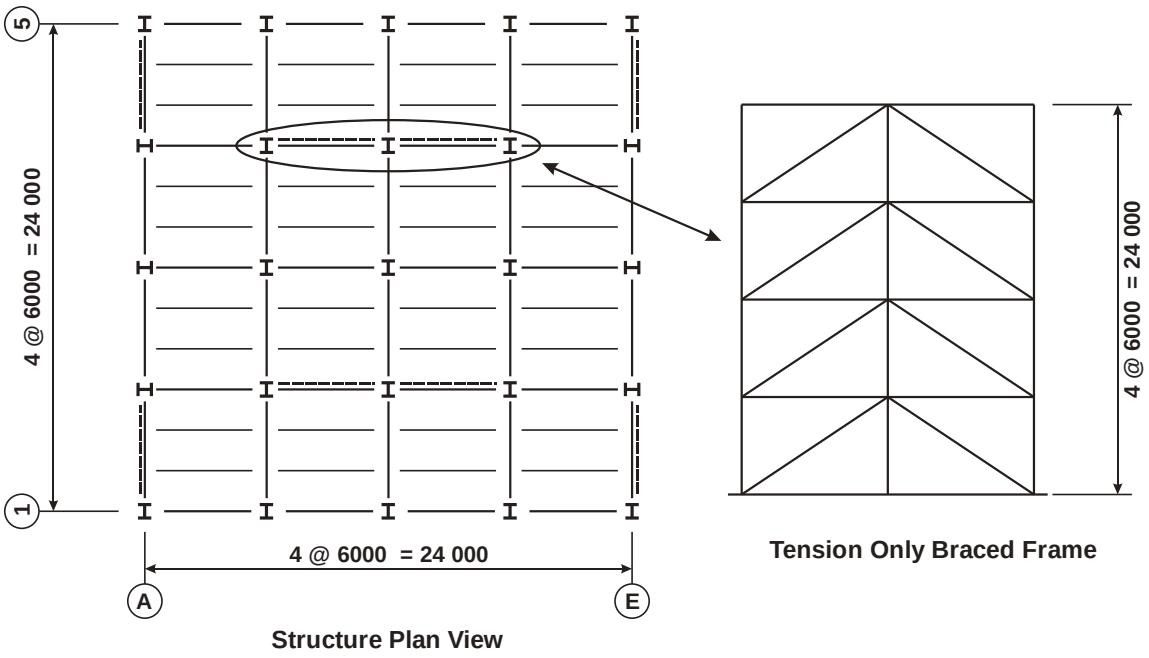

Figure 2.1: Plan view of the structure located at Vancouver

2.1.3 Minimum specified gravity loads (NBCC 1980)

According to NBCC 1980, Part 4: seismic design provisions and the NBCC supplement 1980 climate data, the minimum specified uniformly distributed gravity loads for the structure design are given in Table 2.1. The roof and floors were made of a 63 mm thick concrete slab composite with a 38 mm steel deck supported on regularly spaced steel beams, as was done in the 1980's. The slabs at the roof and floor levels act as rigid diaphragms. P-delta effects, notional loads, and in-plane torsion effects were not considered in the calculations to simplify the design process at the beginning because they are considered to be ignorable in such a regular low-rise structure. The impact of these assumptions is discussed later.

Table 2.1: Minimum specified gravity loads

Roof Level		
Dead Load	3.0 kPa	Roofing on composite 38+63 mm deck slab with ceiling/mechanical systems
Snow Load	1.52 kPa	Flat roof
Typical Floor		
Dead Load	3.0 kPa	Floor composite 38+63 mm deck slab system plus partitions & ceiling/mechanical systems
Partitions	1.0 kPa	
Live Load	2.4 kPa	Office occupancy
Exterior Wall	1.0 kPa	Typical value

2.1.4 Seismic loads (NBCC 1980)

In the NBCC 1980 seismic design provisions, the minimum lateral seismic force was calculated using Equation 2.1. The design base shear is related to the ground acceleration ratio (*A*), the seismic response factor (*S*), the structure factor (*K*), the importance factor (*I*), the soil condition factor (*F*), and the structure seismic weight (*W*).

$$V = A \times S \times K \times I \times F \times W \tag{2.1}$$

The acceleration ratio is obtained from the seismic zone map shown in Figure 2.2. This seismic zone map is the same as in the NBCC 1970. The acceleration ratio is equal to 0.08g for Vancouver, as shown on the map. The seismic response factor depends on the structure fundamental period. Equation 2.2 is used to evaluate the structure period. In the equation, the period is related to the structure total building, h_n, and the structure dimension *D* in the direction being considered. The building height is 16 m and its dimension is 24 m, which gives a period of is 0.294s. The corresponding seismic response factor is equal to 0.922, as computed using Equation 2.3. Herein, *K* is a numerical coefficient that reflects the material and type of construction, damping, ductility and/or energy-absorptive capacity of the structure. The coefficient *K* for steel tension-only braced frame corresponds to Case 6 in the commentary J of the NBCC supplement 1980 and it is equals to 1.3. The importance factor is 1.0 for commercial buildings and the foundation factor *F* is equal to 1.0 for the assumed site type. The seismic weight is the sum of 100% of the dead load plus 25% of the roof snow load. The total structure seismic weight *W* is equal to 5102kN per frame, which includes 1070 kN for the roof and 1344 kN for typical floors.

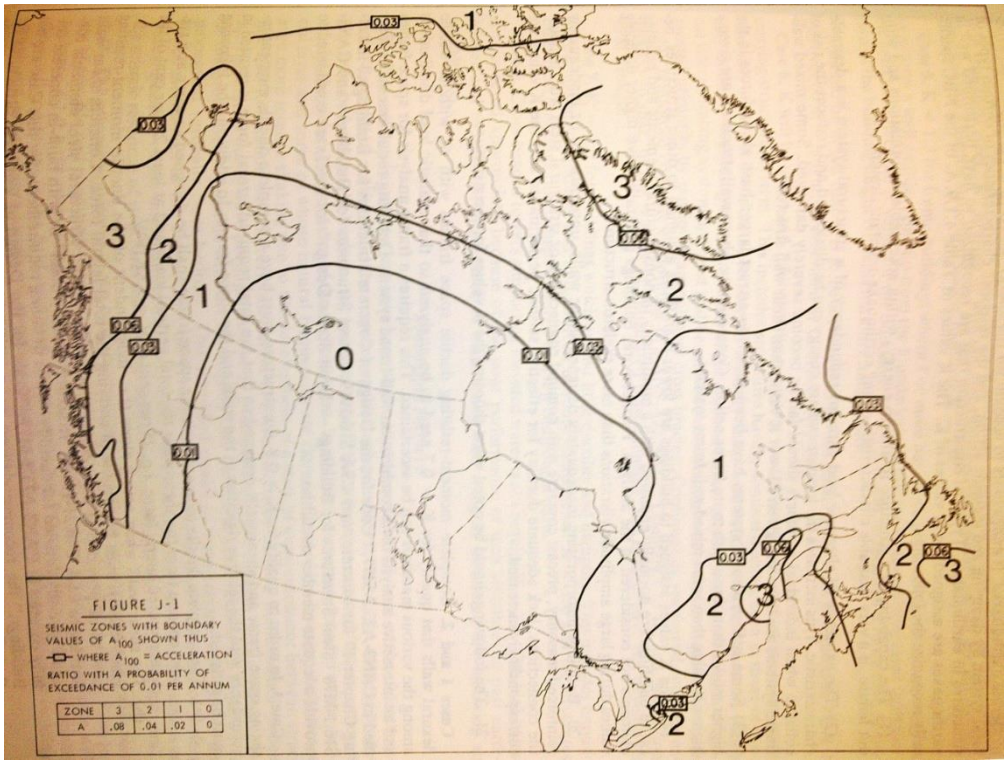

Figure 2.2: Seismic zone map (NBCC 1980 supplement)

$$T = 0.09 \times \frac{h_n}{\sqrt{D}} \tag{2.2}$$

$$S = \frac{0.5}{\sqrt{T}} \leq 1.0 \tag{2.3}$$

Substituting all the factors into Equation 2.1 gives a minimum design base shear V equal to 489 kN. This value is multiplied by the factor 1.5 to obtain the factored design lateral load. Thus, the factored lateral earthquake load used for design is 734 kN.

The factored design base shear is distributed to each storey using Equation 2.4. In this equation, F_x is the seismic force at every level and F_t is an additional force concentrated at the top of the structure. The ratio of the total building height equal to 16 m and the dimension of the braced frame in the direction being considered, D_s, equal to 12 m does not exceed 3. Hence, the force F_t is considered to be zero. Had the ratio been higher than 3.0, F_t would have been determined using Equation 2.5.

$$F_x = (V - F_t)\frac{W_x h_x}{\sum_{i=1}^{n} W_i h_i} \tag{2.4}$$

$$F_t = 0.004V\left(\frac{h_n}{D_s}\right)^2 \leq 0.15V, if\ \frac{h_n}{D_s} > 3 \tag{2.5}$$

The factored lateral seismic loads obtained from the base shear distribution and applied to the braced frame on line 4 are given in Figure 2.3, together with the resulting axial forces in the braces and the columns. These forces were determined without considering P-Delta and in-plane accidental torsional effects. The magnitude of these two effects is examined later. Hence, the seismic loads were equally distributed to the two braced frames on column lines 2 and 4.

According to NBCC 1980, three load combinations must be considered: 1.25*DL* + 1.5*E*, 1.25*DL* + 1.5*LL*, and 1.25*DL* + 0.7 x (1.25*E* + 1.5*LL*) , in which *DL* means the dead load, *LL* means the live load, and *E* means the seismic load. The design forces for the center column of the brace frame correspond to the sum of the vertical projection of the brace design forces plus the tributary gravity loads from the load combination 1.25*DL* + 1.5*E*. For the exterior columns, maximum compression forces is obtained from the load combination 1.25*DL* + 1.5*LL* (braces only induce tension in the exterior columns). The critical (design) forces used for the design of the columns are indicated in red in Figure 2.3.

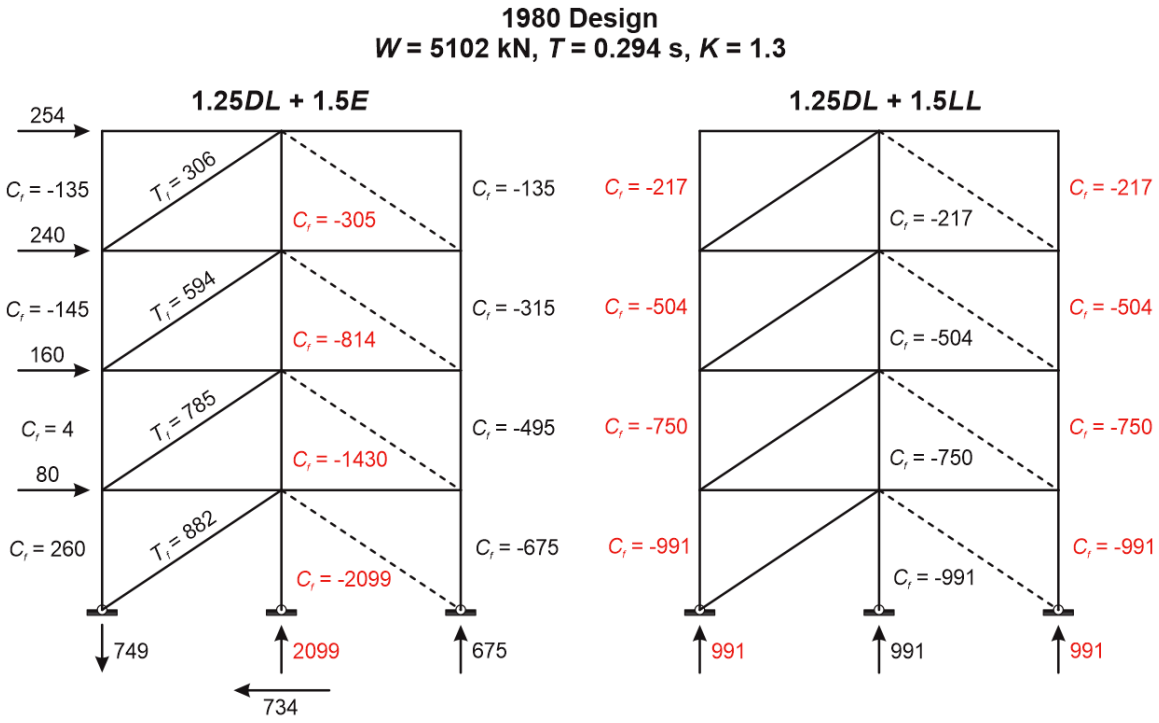

Figure 2.3: NBCC 1980 design factored member forces in the tension-only braced frame on line 4

2.1.5 Brace frame member design

In the 1980's, CSA G40.20-300Wsteel with a nominal yield strength of 300 MPa was the most popular steel for building structures. Hence, all members are designed using this steel grade.

The selected built-up double angle brace sections are given in Table 2.2. The braces were designed to resist the entire storey shear in tension considering tension yielding on the brace gross cross-section as well as various possible failure modes of the braces at their end connections. The factored tensile resistance based on gross-section yielding is given in Table 2.2. In the table, "80" is used in the symbol for the factored tensile resistance, $T_{r\text{-}80}$, to refer to the "1980 design". Details on brace connections and the associated brace factored resistances are given in Section 2.1.6. The factored resistance for gross section yielding is given by:

$$T_r \leq \phi 0.9 A_g F_y \tag{2.6}$$

The compressive resistances of these braces were small and neglected in design (tension-only design). In CSA S16.1-M78, the slenderness ratio of tension members must not exceed 300. The slenderness ratios of the selected braces are also given in the table. According to CSA S16, the slenderness ratio for members that only resist loads in tension shall be taken as the ratio of the unbraced length to the corresponding radius of gyration (L/r). For built-up double angle sections, the unbraced length may have two different values because of the section configuration. Built-up double angle braces are made up of two identical single angle sections with vertical legs back-to-back as shown in Figure 2.4. A number of stitch connectors are welded or bolted between the two back-to-back legs to reduce the slenderness of the individual angles. Even for double angle braces that are designed to resist only tensile forces, at least one stitch connector is needed at mid-span of double angle braces to keep the two pieces together during shipping. Thus, an unbraced length equal to the length between the brace end and the stitch connector is used for the individual angle while the overall brace length is used to verify the slenderness about each of the two orthogonal axes of the composite section. The largest slenderness ratios among these three values is considered and checked against the limit of 300.

Table 2.2: Brace section and demand-to-capacity (stress) ratios

Level	Brace Section	# of stitch	$0.5L / r_{y'}$	L / r_x	L / r_y	$T_{r\text{-}80}$(kN)	$T_{f\text{-}80} / T_{r\text{-}80}$
4	2L-76X51X6.4	1	**295**	267	285	413	0.74
3	2L-102X76X7.9	1	197	**200**	196	729	0.75
2	2L-102X89X9.5	1	175	**203**	155	934	0.84
1	2L-127X76X9.5	1	195	159	**207**	999	0.88

The columns are assumed to be tiered in two-storey segments. In CSA S16.1-M78, the factored compressive resistance of W-shape column sections is calculated with Equation 2.7. The column sections were also selected from Class 1, 2 or 3 sections. At the first-storey, an effective length *KL* = 3750 mm was assumed for column design, i.e., 4000 mm minus the thickness of the slab (100 mm) and a 150 mm for the vertical distance between the top of the beams and the center of the beam-to-column joints. For the other storeys, a column length *KL* = 4000 mm was used. The column design results are shown in Table 2.3.

$$
\begin{aligned}
&\text{(a) } 0 \le \lambda \le 0.15 \quad C_r = \phi A F_y \\
&\text{(b) } 0.15 < \lambda \le 1.0 \quad C_r = \phi A F_y (1.035 - 0.202\lambda - 0.222\lambda^2) \\
&\text{(c) } 1.0 < \lambda \le 2.0 \quad C_r = \phi A F_y (-0.111 + 0.636\lambda^{-1} + 0.087\lambda^{-2}) \\
&\text{(d) } 2.0 < \lambda \le 3.6 \quad C_r = \phi A F_y (0.009 + 0.877\lambda^{-2}) \\
&\text{(e) } 3.6 < \lambda \quad\quad C_r = \phi A F_y \lambda^{-2} = \phi A \left[\frac{1970000}{(KL/r)^2}\right]
\end{aligned}
\tag{2.7}
$$

where $\lambda = \frac{KL}{r}\sqrt{\frac{F_y}{\pi^2 E}}$

Table 2.3: Column sections and demand-to-capacity ratios

Level	Center Column	$C_{r\text{-}80}$ (kN)	Class	$C_{f\text{-}80} / C_{r\text{-}80}$	Side Column	$C_{r\text{-}80}$ (kN)	Class	$C_{f\text{-}80} / C_{r\text{-}80}$
4&3	W200X52	1146	1	0.71	W200X36	586	1	0.86
2&1	W310X79	2092	1	1.00	W200X52	1146	1	0.86

Beam design results are shown in Table 2.4. For class 1 and 2 W-shape sections, the beam strength and stability under combined axial forces and bending moments about strong (x-x) axis are checked

using Equations 2.8 to 2.10. To determine factor compression force and bending moment on beams in each equation, different load combinations were used. In Equation 2.8, maximum bending moment is obtained from combination 1.25*DL* + 1.5*LL*. In Equation 2.9 and Equation 2.10, combination 1.25*DL* + 1.5*E* and 1.25*DL* + 0.7 x (1.25*E* + 1.5*LL*) are used to consider axial loads on beams. The controlling M_f and C_f and corresponding demand-to-capacity ratios are also given for each limit state in the table. In the calculations, the beams were assumed to be supported laterally by the composite steel deck over the full beam length. Hence, the flexural resistance M_{rx} is taken equal to $\phi Z_x F_y$. In Equation 2.10, C_{rx} is determined using Equation 2.7 for strong axis buckling with KL_x = 6000 mm. The parameter ω_x is equal to 1.0.

$$\frac{M_{fx}}{M_{rx}} \leq 1.0 \tag{2.8}$$

$$\frac{C_f}{C_r} + \frac{0.85M_{fx}}{M_{rx}} \leq 1.0, where\ C_r = \phi A F_y \tag{2.9}$$

$$\frac{C_f}{C_{rx}} + \frac{\omega_x M_{fx}}{M_{rx}\left(1-\frac{C_f}{C_{ex}}\right)} \leq 1.0 \tag{2.10}$$

Table 2.4: Beam section and demand-to-capacity ratios

Level	Beam Section	Class	Eq. 3.8		Eq. 3.9			Eq. 3.10		
			M_f	ratio	M_f	C_f	ratio	M_f	C_f	ratio
4	W310X28	2	54	0.49	48	178	0.56	48	178	0.69
3	W360X39	1	77	0.43	68	347	0.58	68	347	0.70
2	W410X39	1	77	0.39	45	655	0.68	45	655	0.79
1	W360X45	1	77	0.36	45	735	0.66	45	735	0.78

*Unit for M_f is kN·m. Unit for C_f is kN

2.1.6 Design of brace connections

The detail of the brace connection at level 1 is shown in Figure 2.4. A photo of the brace specimen used to examine experimentally the brace connection at that level is shown in Figure 2.5. As shown, the brace connection pattern looks like a “sandwich” with the gusset plate located between the two vertical legs of the double angle brace. The connection was built with A325 grade bolts, ¾" (19.1 mm) in diameter; this bolt grade and size were widely used in bolted connections in the 1980's.

Bolt holes were assumed to be drilled. The same detail was used at every level and specific information of the connections designed at each level are given in Table 2.5. A staggered bolt arrangement was used when more than three bolts were needed in a connection. This was the case at all levels except at the top level where the bolts were arranged along a single straight line. Requirements for the location of the bolt holes can be found in section 21 of CSA S16.1-M78. The pitch distance (*s*) must be not less than 3 bolt diameters. Minimum edge distance (*e*) to a sheared edge and a rolled edge are 32 and 25 mm, respectively, for ¾" bolts. The minimum end distance is the same as the minimum edge distance for more than two bolts in a line parallel to the loading direction. An end distance of 45 mm (1¾") was used for all brace connections. No requirement for gauge distance (*g*) is mentioned in S16.1, but the gauge distance plus the edge distances must be less than the width of the angle legs. Design forces for the connections are the same as those considered for the design of the braces. The Whitmore theory was considered to determine the effective gusset plate width (W_e), and the gusset plate thickness (t_g) could then be determined to resist the design forces.

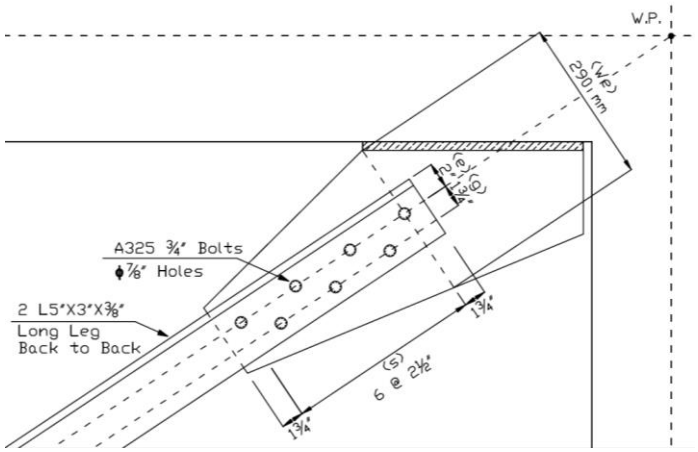

Figure 2.4: Brace connection at level 1

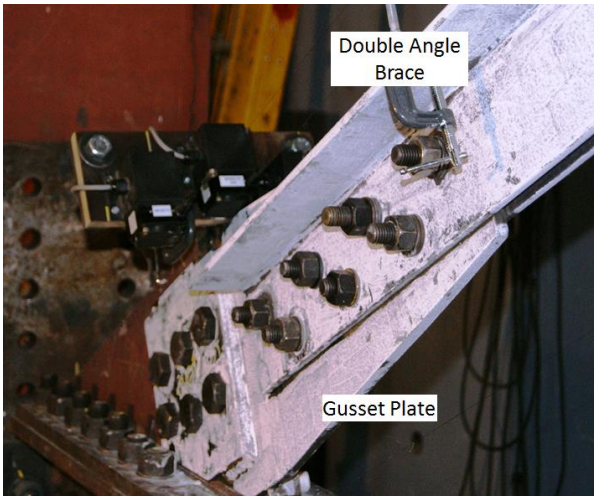

Figure 2.5: Connection pattern for double angle brace at level 1

Table 2.5: Brace connection design

Level	# of bolts	Type	e (mm)	g (mm)	s (mm)	w_e (mm)	t_g (mm)
4	3	Single line	45	N/A	57	140	9.5
3	5	Staggered	38	32	57	230	11.1
2	6	Staggered	38	32	64	230	12.7
1	7	Staggered	51	45	64	290	12.7

Five different failure modes were examined with CSA S16.1-M78 for the connections: tension rupture on the net section of the brace (Equations 2.12 to 2.14), tension rupture on the net section of the gusset plate (Equations 2.12 to 2.14), shear failure of the bolts (Equation 2.11), bearing failure of the braces and bearing failure of the gusset plates (Equation 2.12). The equations used to determine tension rupture on net section are explained in Section 1.4.3. The factored shear resistance of the bolts is obtained from Equation 2.11, in which ϕ is equal to 0.67. The ultimate tensile stress (F_u) for A325 bolt is 825MPa. The bearing resistance in bearing-type connections is calculated using Equation 2.12.

$$V_r = 0.60\phi \mathrm{nm} A_b F_u \tag{2.11}$$

$$B_r = \phi \mathrm{tne} F_u \leq 3\phi t d n F_u \tag{2.12}$$

where n is the number of bolts, m is the number of shear planes, A_b is the cross section area of bolts and e is the end distance. The failure modes and demand-to-capacity ratios for each connection are

also given in Table 2.6. As shown, net section rupture controlled at all levels except at level 2 where bolt shear failure governed.

Table 2.6: Connections' demand-to-capacity ratios

Failure mode	1st floor		2nd floor		3rd floor		4th floor	
	$T_{r\text{-}c\text{-}80}$ (kN)	$T_{f\text{-}80}$ / $T_{r\text{-}c\text{-}80}$	$T_{r\text{-}c\text{-}80}$(kN)	$T_{f\text{-}80}$/ $T_{r\text{-}c\text{-}80}$	$T_{r\text{-}c\text{-}80}$(kN)	$T_{f\text{-}80}$ / $T_{r\text{-}c\text{-}80}$	$T_{r\text{-}c\text{-}80}$(kN)	$T_{f\text{-}80}$ / $T_{r\text{-}c\text{-}80}$
Net rupture of angle	893	**0.99**	828	0.95	641	**0.93**	342	**0.90**
Bearing failure of angle	1782	0.49	1528	0.51	1059	0.56	515	0.59
Bolt shear failure	926	0.95	794	**0.99**	662	0.90	397	0.77
Net rupture of gusset plate	924	0.95	838	0.94	733	0.81	358	0.85
Bearing failure of gusset plate	1191	0.74	1021	0.77	745	0.80	383	0.80

2.1.7 Influence of torsional and P-delta effects.

For simplicity, the effect of accidental in-plane torsion and P-delta effects were ignored in the design. This assumption is verified in this section.

According to NBCC 1980, an additional eccentricity equal to 5% of the structure dimension perpendicular to the direction of loading must be considered to evaluate torsional effects. Equation 2.13 is used to calculate these torsional effects. This is a simplified approach that assumes independent torsional response at every level. In this equation, V_{Ti} is the additional storey shear due to accidental torsion resisted in frame i, T is the accidental torsional moment at level x (storey shear V multiplied by 5% of the building dimension, L= 24 m $(T = 1.2V)$), k_i and k_j are the horizontal shear stiffness for each braced frame and d is the distance from each braced frame to the shear center. For the braced frame on line 2 and 4, k_i = 1.0 (relative value), d_i = 6 m, and the stiffness and the distance of the braced frames on lines A and E are 1.0 and 12 m, respectively, which gives V_{Ti} = 0.006 V at every level.

$$V_{Ti} = T\frac{K_i d_i}{\sum K_j d_j^2} \tag{2.13}$$

Equation 2.14 is recommended in CSA S16.1-M78 to calculate the additional storey shear at each storey due to P-delta effects. In this equation, the subscript *x* refers to the level number, Σ*P* is the total factored gravity load carried by the columns at the level, h_x is the storey height, and *Δ* are the lateral displacements under seismic loads. The latter were obtained from analysis of the structure under the seismic loads. The governing gravity load combination 1.25*DL* + 1.5*LL* is used to obtain the value.

$$V_x' = \frac{\sum P_x}{h_x}(\Delta_{x+1} - \Delta_x) \tag{2.14}$$

Accidental torsional effects and P-delta effects on storey shear forces are shown in Table 2.7. Torsion and P-delta effects introduced between 5.4% and 7.3% extra design loads to the braces, which is relatively small. Thus, neglecting these effects is deemed acceptable to simplify the design process, and this is probably what engineers would have done in the 1980s. Hence, these effects were omitted in the design of the prototype building.

Table 2.7: Brace design force comparison

Without Torsion and P-Delta effects (kN)	Additional torsional effect (kN)	P-Delta effect (kN)	With Torsion and P-Delta effects (kN)	Difference (%)
254	5	4	268	5.4
494	10	10	524	6.1
654	13	17	697	6.6
734	15	24	787	7.3

2.2 Seismic assessment according to NBCC 2010 and CSA S16-09

In this section, the braced frame designed using NBCC 1980 and CSA S16.1-M78 is evaluated using the design provisions of NBCC 2010 and CSA S16.1-09 to identify possible seismic deficiencies in existing braced frames.

2.2.1 Seismic loads and analysis

In the NBCC 2010, the equivalent base shear is calculated using Equation 2.15.

$$V = \frac{S(T_a) \times M_v \times I_E}{R_d R_o} \times W \quad (2.15)$$

In this equation, $S(T_a)$is introduced as the design spectral acceleration , which replaces the seismic zone factor A in the NBCC 1980. For each city in Canada, four S_a values are specified at periods of 0.2, 0.5, 1.0 and 2.0 s: $S_a(0.2)$, $S_a(0.5)$, $S_a(1.0)$, and $S_a(2.0)$. For Vancouver, these values are 0.94, 0.64, 0.33, 0.17. These values are multiplied by the site coefficients factors, F_a and F_v, specified for the site class to obtain the design, $S(T)$. For site class C as considered in this study, $F_a = F_v = 1.0$ and $S(T) = S_a(T)$.

For a specific building with a period T, the value of $S_a(T)$can be calculated using linear interpolation between these four values. A numerical model of the structure was created using the ETABS computer program (CSI, 2009) to carry out a dynamic (model response spectrum) analysis. The entire model is shown in Figure 2.6a. To emulate the tension-only behaviour of the braces in ETABS, only one brace bay out of the two braced bays was implemented in the model, as shown in Figure 2.6b, assuming that the braces in the other bay would be in compression.

a)

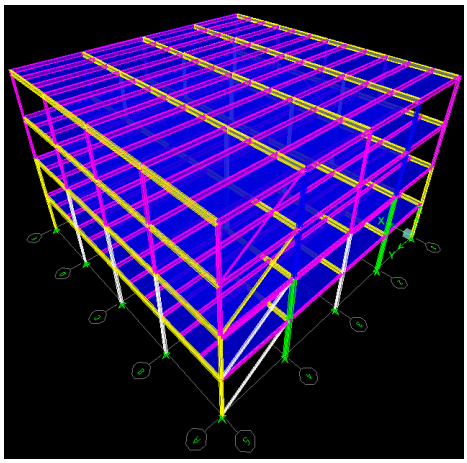

Figure 2.6: ETABS model: a) 3D view of the structure model; b) Model of the tension-only braced frame on line 4

b)

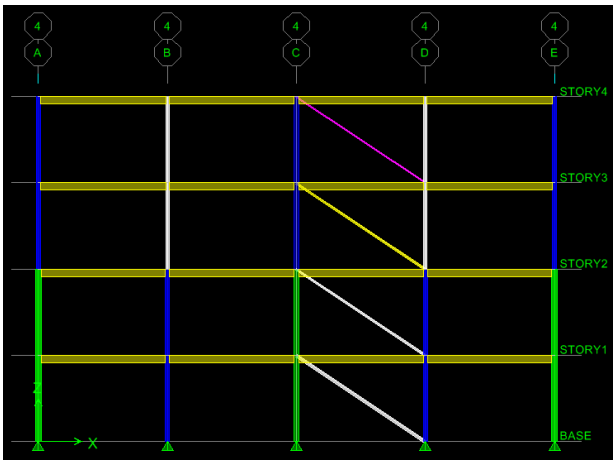

Figure 2.6: ETABS model: a) 3D view of the structure model; b) Model of the tension-only braced frame on line 4 (continued)

In the direction of interest, the computed 1st mode period of the structure is 0.919s. In NBCC 2010, the period for the calculation of the seismic loads, T_a, must not exceed two times the period value computed with the empirical equation, T_{emp}. For steel braced frames, the period T_{emp} is obtained from Equation 2.16. As shown, T_{emp} is equal to 0.4 s for the building studied, and the upper limit for T_a is therefore equal to 0.8 s, which is shorter than the computed period. Thus, the fundamental lateral period T_a = 0.8s is used in the calculations. Using linear interpolation, the resulting value of S(0.8 s) is 0.454:

$$T_{emp} = 0.025 \times h_n = 0.0025 \times 16 = 0.4\ s \tag{2.16}$$

$$S(T_a) = S(0.8) = 0.454 \tag{2.17}$$

For $T_a \leq 1.0$, the higher mode factor M_v in Equation 2.15 is equal to 1.0. The importance factor I_E is also equal to 1.0, as was the case for the importance factor in 1980. In NBCC 2010, two changes affected the calculation of the structure seismic weight, W, compared to NBCC 1980. First, in NBCC 2010, it is permitted to limit the weight of the partition walls to 0.5 kPa when determining the structure seismic weight W (instead of 1.0 kPa in NBCC 1980). Second, the design roof snow load was changed from 2.16 kPa in NBCC 1980 to 2.24 kPa in NBCC 2010. This resulted in a total seismic weight W = 4678 kN, a value which is 8% smaller than the NBCC 1980 value (1078 kN at top floor, 1200 kN at typical floors).

The tension-only braced frames used in the prototype building were designed without consideration of any special seismic design and detailing requirements. Therefore, they are considered as steel seismic force resisting systems of the Conventional Construction category (Type CC). For this category, the ductility-related force modification factor R_d is equal to 1.5 and the corresponding overstrength related force modification factor R_o = 1.3. Using these and previous values, the design earthquake load V can be determined:

$$V = \frac{0.454 \times 1.0 \times 1.0}{1.5 \times 1.3} \times 4678kN = 1089kN \tag{2.18}$$

In NBCC 2010, the seismic load for steel braced frames must not be less than the value determined at a period of 2.0 s (V_{min}) but need not exceed 2/3 the value computed at a period of 0.2 s (V_{max}). These two limits did not govern the design:

$$V_{min} = \frac{S(2.0) \times M_v \times I_E}{R_d R_o} \times W = \frac{0.17 \times 1.0 \times 1.0}{1.5 \times 1.3} \times 4678kN = 408kN \tag{2.19}$$

$$V_{max} = \frac{\frac{2}{3} \times S(0.2) \times I_E}{R_d R_o} \times W = \frac{\frac{2}{3} \times 0.94 \times 1.0}{1.5 \times 1.3} \times 4678kN = 1503kN \tag{2.20}$$

When performing a dynamic (response spectrum) analysis in NBCC 2010, the results of the analysis are scaled by the ratio between the base shear V and the larger of V and the base shear V_d. The latter is equal to the base shear from the analysis, V_{ed}, divided by I_E/R_dR_o. For structures that do not exhibit torsional irregularity conditions requiring dynamic analysis, the scaling can be performed with respect to 0.8 V instead of V, which represents a potential reduction of up to 20% in seismic effects.

In NBCC 2010, a structure is said to be torsional irregular if the ratio between the maximum and average storey drifts at any level is larger than 1.7. This calculation is performed by applying static seismic loads at a distance equal to 10% of the building dimension perpendicular to the loading direction away from the center of mass. For the prototype structure, the analysis shows that this ratio varies between 1.15 and 1.17, and the structure does not have torsional irregularity. In that case, scaling can be performed using 0.8 V.

From the model response spectrum analysis, the elastic base shear V_{ed}= 1456 kN and V_d = 747 kN. This design base shear is less than 80% V = 0.8 x 1089 = 871 kN. This base shear of 871 kN is 19% higher compared to the factored design base shear used in 1980 (734 kN).

Axial forces on members were obtained from response spectrum analysis directly. In response spectrum analysis, additional torsion effect was considered through adding static torsional moments equal to the storey shear applied at a 10% (2.4 m) eccentricity at each floor. P-delta effect was ignored because it was less than 10%. Then they were scaled corresponding to the 0.8 *V* design base shear. Braces, columns, and connections design forces are show in Figure 2.7. For the center column of the braced frame, the governing load combination for the verification of the column section changed from 1.25*DL* + 1.5*E*inNBCC 1980 to 1.0*DL* + 1.0*E* + 0.5*LL* + 0.25*SL* in NBCC 2010 (*SL* is the roof snow load). For the side columns, the load combination is changed to 1.25*DL*+1.5*LL*+0.5*SL*.

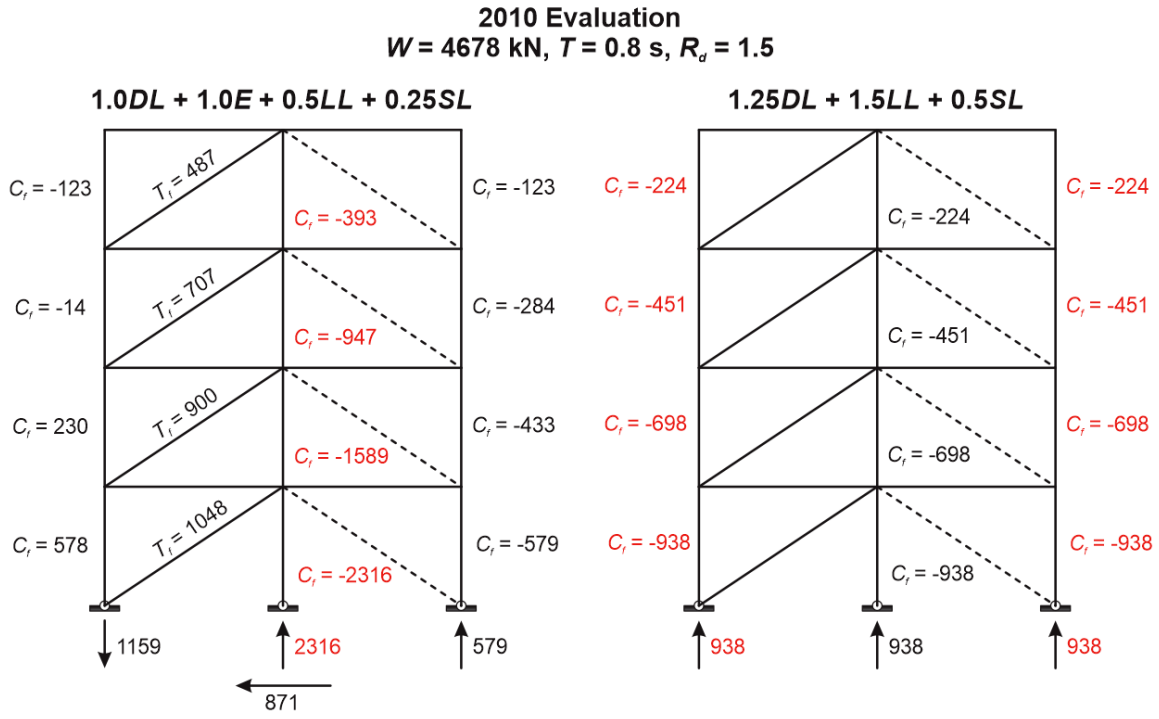

Figure 2.7: Design factored member forces based on NBCC 2010

2.2.2 Verification of member resistances

The way to calculate the brace gross section yield capacity in CSA S16-09 is the same as in CSA S16.1-M78. Hence, the brace yielding resistance has not changed in 2010 and the values in Table 2.2 still apply, whereas the brace design forces have increased by approximately 20% at every level. The design forces and resistances are summarized in Table 2.8. As shown, the resistance of the braces at the first and top floors is insufficient. However, this deficiency is not considered as

critical as it corresponds to a ductile failure mode (gross section yielding) and should not result in a premature member failure that may lead to collapse of the structure. Nevertheless, it may result in excessive inelastic deformation demand, and this aspect will be examined through nonlinear time history analysis in Chapter 6.

Table 2.8: Brace demand-to-capacity ratios

Level	Brace Section	$T_{r\text{-}10}$ (kN)	$T_{f\text{-}10}/\ T_{r\text{-}10}$
4	2L76X51X6.4	413	1.18
3	2L102X76X7.9	729	0.97
2	2L102X89X9.5	934	0.96
1	2L127X76X9.5	999	1.05

Assessment results for the columns are shown in Table 2.9. Compared to S16.1-M78, the equation used to calculate the factored axial compressive resistance has been modified in CSA S16-09. The new equation is given in Equation 2.21. The change is minimal, however, the column buckling resistance is almost the same as the resistances that were obtained from Equation 2.7 and that are given in Table 2.3. All the columns have found to have sufficient resistance except the center column at the ground level. For this column segment, the axial compressive resistance is 11% lower than the factored design force. This problem cannot be ignored. Unless the forces can be reduced, column strengthening will need to be performed as part of the retrofit of the structure.

Table 2.9: Column demand-to-capacity ratios

Floor	Center Column	$C_{r\text{-}10}$(kN)	$C_{f\text{-}10}$ / $C_{r\text{-}10}$	Side Column	$C_{r\text{-}10}$(kN)	$C_{f\text{-}10}$ / $C_{r\text{-}10}$
4&3	W200X52	1117	0.85	W200X36	594	0.76
2& 1	W310X79	2081	1.11	W200X52	1117	0.84

$$C_r = \phi A F_y (1 + \lambda^{2n})^{-1/n},\ \lambda = \sqrt{\frac{F_y}{F_e}}, F_e = \frac{\pi^2 E}{\left(\frac{KL}{r}\right)^2} \tag{2.21}$$

Beam members are verified as beam-column elements. In CSA S16-09, the interaction equation used to check member strength and stability under axial compression force and bending for class 1 and class 2 W-shape sections has been changed. The new interaction equation for bending about strong axis is given in Equation 2.22. The same equation is used to verify the capacity of the

member for cross-sectional strength, overall member strength and lateral torsional buckling strength. The latter is not verified for the beams as they are considered as laterally supported by the floor slabs. In the interaction equation, C_r is determined using Equation 2.21 with KL = 0 and 6000 mm for cross-sectional strength and overall member strength, respectively. For both limit states, $M_r = \phi Z_x F_y$. For cross-sectional strength, U_{1x} = 1.0. For overall member strength, U_{1x} is obtained from Equation 2.23, where ω_{1x} = 1.0 for uniformly distributed load and $C_{ex} = AF_{ex}$ (see Equation 2.21). The results of the interaction equation for both limit states are given in Table 2.10. All beams are found to be adequate.

$$\frac{C_f}{C_r} + \frac{0.85U_{1x}M_{fx}}{M_{rx}} \leq 1.0 \tag{2.22}$$

$$U_1 = \left[\frac{\omega_1}{1-\frac{C_f}{C_e}}\right] \tag{2.23}$$

Table 2.10: Beam demand-to-capacity ratios

Floor	Beam Section	M_f (kN·m)	C_f (kN)	Cross-sectional Strength	Overall member Strength
4	W310X28	31	405	0.69	0.84
3	W360X39	42	588	0.66	0.77
2	W410X39	42	740	0.75	0.86
1	W360X45	42	871	0.76	0.89

2.2.3 Verification of brace connection resistances

In CSA S16-09, a new connection failure mode, the block shear failure mode, has been introduced and shear lag effects are now considered when verifying rupture on net section and. As discussed in Section 2.4.4., block shear failure may happen in the connection region of the brace or in the gusset plate. The resistance against this failure mode can be calculated using Equation 2.23. The first part in the brackets of the equation is the tension resistance whereas the second part is associated to shear resistance. In addition, a modification factor U_t is applied to tension rupture failure mode.

For the net section failure mode, the shear lag concept has been introduced in CSA S16-09 and the effective net cross section area (A_{ne}) must be used instead of the net cross section area (A_n) to

calculate the brace tensile resistance capacity at the connection, as described in Section 2.4.3. The equation for the bolt shear failure mode is almost the same as in S16.1-M78. However, the resistance factor for this failure mode has been increased from 0.67 to 0.8. The equation for the bearing failure mode has been modified from Equation 2.24 in S16.1-M78 to Equations 2.25 in S16-09. For the bearing failure mode, the resistance factor has also been changed from 0.67 to 0.8. This modification increased the resistance capacity of bearing failure mode. For the selected Vancouver site, the short-period spectral acceleration ratios $I_E F_a S_a(0.2)$ is equal to 0.94 and therefore exceeds 0.45. Hence, connections design forces for Type CC braced frames, $T_{f\text{-}10}$, must be amplified by 1.5 if the governing connection failure mode is non ductile. In absence of specific information on the required and available ductility levels for connections, that 1.5 factor was applied in the seismic assessment. However, the so amplified brace connection forces need not exceed the brace probable tensile strength, $T_u = AR_yF_y$, where A is the brace gross cross-section and R_yF_y is the probable steel yield strength. In CSA S16-09, R_yF_y = 385 MPa for G40.21-300W steel. For all braces, T_u was less than 1.5 $T_{f\text{-}10}$ and $T_{fc\text{-}10} = T_u$.

$$B_r = \phi tneF_u \leq 3\phi tdnF_u \tag{2.24}$$

$$B_r = 3\phi_{br}tdnF_u \tag{2.25}$$

The results of the assessment are presented in Table 2.11 for all failure modes. As shown, tension rupture on net section is the critical failure mode at every level and the factored resistances of the connections as designed according to the 1980's codes are only 43% to 63% of the current design factored forces. Premature failure of the brace connections at anyone of the building level would likely result in a severe reduction of the storey shear capacity which could lead to soft-storey response and, eventually, collapse of the structure at that level.

Table 2.11: Connection failure modes and demand-to-capacity ratios

	1st floor		2nd floor		3rd floor		4th floor	
$T_{fc\text{-}10}$ (kN)	1425		1332		1040		589	
Failure mode	$T_{r\text{-}c\text{-}10}$ (kN)	$T_{fc\text{-}10}$ / $T_{r\text{-}c\text{-}10}$	$T_{r\text{-}c\text{-}10}$ (kN)	$T_{fc\text{-}10}$/ $T_{r\text{-}c\text{-}10}$	$T_{r\text{-}c\text{-}10}$ (kN)	$T_{fc\text{-}10}$ / $T_{r\text{-}c\text{-}10}$	$T_{r\text{-}c\text{-}10}$ (kN)	$T_{fc\text{-}10}$ / $T_{r\text{-}c\text{-}10}$
Net section rupture of angle	891	**1.60**	826	**1.61**	639	**1.63**	255	**2.30**
Block shear failure of angles	1617	0.88	1366	0.98	899	1.16	430	1.37
Bearing failure of angles	2744	0.52	2352	0.57	1633	0.64	784	0.75
Bolt shear failure	1106	1.29	948	1.41	790	1.32	474	1.24
Net rupture of gusset plate	1155	1.23	897	1.48	785	1.32	384	1.53
Block shear failure of gusset plate	1885	0.76	1692	0.79	1115	0.93	544	1.08
Bearing failure of gusset plate	1829	0.78	1568	0.85	1143	0.91	588	1.00

In Table 2.11, the results show that all connections would still have insufficient factored resistance even if the 1.5 amplification factor was not applied to the design forces. Note that the use of a single factor of 1.5 to all "non-ductile" failure modes may not be rigorous because some connection failure modes may provide some degree of ductility whereas others such as bolt shear failure may only provide limited ductility, sometimes close to zero. In CSAS16.1-M78, a design requirement played a role similar to the 1.5 factor: when net section rupture was critical, the tension resistance associated to this failure mode had to be divided by $\frac{A_g}{A_n}$ to account for the limited available ductility. The correction factor depended on the net section ratio, which was an indicator for the potential for reduced ductility. Tension rupture on net section controls in all connections of the braced frames and this failure mode may exhibit some ductility because failure is generally preceded by yielding on net section. However, no sufficient data is available on the ductility capacity *vs.* demand to determine if the 1.5 amplification factor is fully applicable for this failure mode for the connections as designed.

2.2.4 Summary of seismic assessment based on factored resistance

This assessment was performed by applying the design procedure currently prescribed in NBCC 2010 and CSA S16-09 for Type CC concentrically steel braced frames. The results indicate that the bracing members at two levels may not have sufficient tension resistance based on gross-section yielding. This deficiency is not critical because this failure mode is ductile. All beams and columns are found to have sufficient resistance except for the central column at level 1. Although the overstress is limited for that column (8%), this deficiency is associated to a non-ductile (buckling) failure mode and the column would need to be strengthened. All brace connections are found to have insufficient resistance and the expected failure mode is rupture on net section, a limit state that may not have sufficient ductility to accommodate the inelastic demand. Brace connection failure may result in total loss of storey shear resistance, which may have catastrophic consequences.

2.3 Seismic assessment based on probable resistances

In order to more realistically predict the seismic performance of the braced frame studied, a second assessment is performed assuming that the bracing members will reach their probable resistance and that the other elements of the structure possess their probable resistances. This way, the most likely failure scenarios can be identified such that realistic consequences can be predicted.

2.3.1 Brace forces

The calculation of the brace probable resistances, T_u and C_u, was performed as specified in CSA S16-09 and described in Section 2.4.1. For angles and plates made of G40.21 steel, the probable steel yield strength, R_yF_y, was taken equal to 385 MPa according to CSA S16-09 requirement. The probable ultimate tensile stress is not specified in CSA S16-09. The probable tensile and compressive capacities of double angle braces are given in Figure 2.8. If no failure occurs in the other elements of the existing structure, i.e., inelastic response was concentrated in the double angle braces dissipating energy while the other members remained elastic, the corresponding base shear could reach 1312 kN, which is 178% of the base shear used to design the structure in the 1980's. This may cause problems at the structure anchorage system and the foundations. These aspects are not considered here. Only the other structural components of the frame are examined.

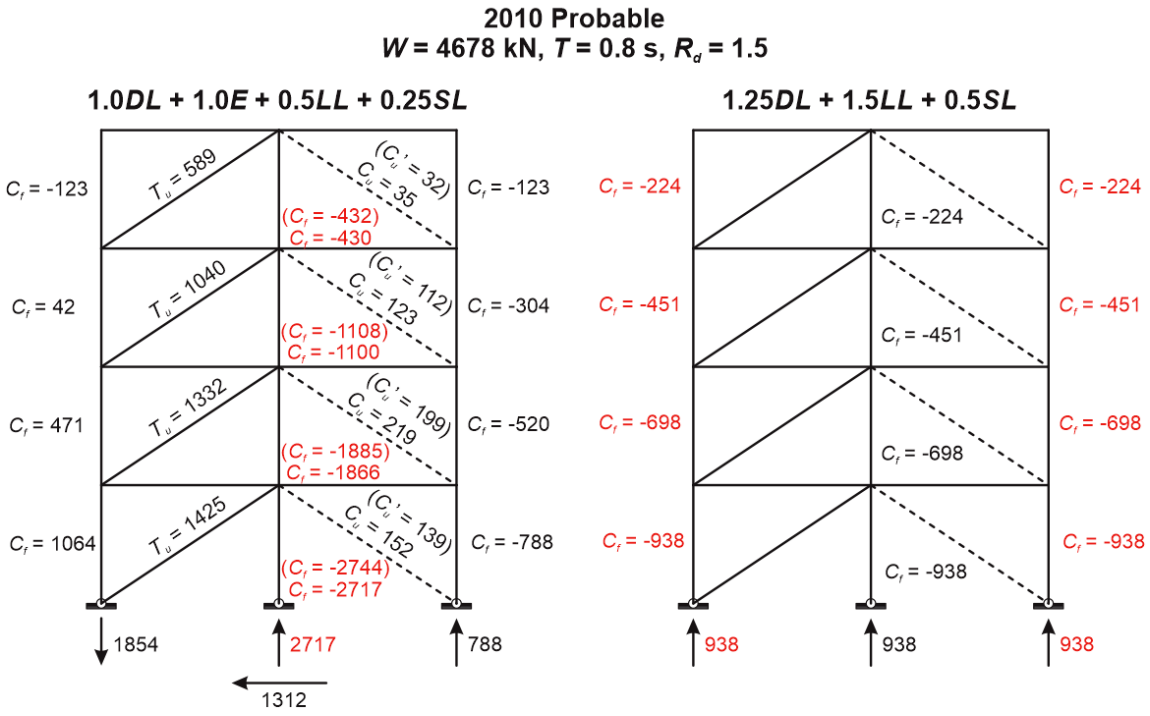

Figure 2.8: Design force based on brace probable capacity

2.3.2 Members assessment

The forces imposed on the columns and beams when brace forces reach C_u and T_u are shown in Figure 2.8. In the figure, the values in brackets are forces that develop when the compression brace reaches its post-buckling capacity, C'_u. As shown, this condition results in slightly greater axial compression forces in the central column. Tables 3.12 and 3.13 show the evaluation results for columns and beams. The probable resistance of these elements were considered in the calculations to reflect their likely conditions, i.e., using ϕ = 1.0 and R_yF_y = 385 MPa. As shown, beams and columns of the existing braced frame are all adequate. Columns even possess extra capacity that could be exploited for the retrofit of the structure, if that was necessary. Based on this assessment approach, buckling of the central column at the first level would not be expected even if all braces reached their probable resistances (stress ratio = 0.91).

Table 2.12: Column resistance demand-to-capacity ratios

Level	Center Column	$C_{u\text{-}10}$ (kN)	$C_{f\text{-}10p}$ / $C_{u\text{-}10}$	Side Column	$C_{u\text{-}10}$ (kN)	$C_{f\text{-}10p}$ / $C_{u\text{-}10}$
4&3	W200X52	1593	0.69	W200X36	847	0.53
2& 1	W310X79	2968	0.91	W200X52	1593	0.59

Table 2.13: Beam resistance demand-to-capacity ratios

Level	Beam Section	Ratio	Governed failure mode
4	W310X28	0.76	Overall member str.
3	W360X39	0.85	Overall member str.
2	W410X39	0.99	Overall member str.
1	W360X45	0.93	Overall member str.

2.3.3 Connection assessment

The resistance of the brace connections should exceed the brace forces shown in Figure 2.8 in order to prevent connection failure. The probable resistance of the connections are used in this verification with $\phi = 1.0$ and $R_y F_y$ = 385 MPa. For limits states associated to fracture, values of the probable ultimate tensile stress are not given in CSA S16-09 and the value specified in AISC 341-05 (AISC 2005) for angle sections and plates was adopted: $R_t F_u$ = 495 MPa, which corresponds to 1.10 F_u (F_u = 450 MPa). For bolts in shear, the nominal ultimate stress was considered (F_{ub} = 825 MPa) assuming that bolt strength does not vary as much as for structural steels used in shapes and plates. Connection assessment results are shown in Table 2.14. As shown, the brace connections are still too weak to achieve inelastic response in the bracing members and the governing failure mode is still net section rupture except bolt shear failure in connections at the second floor. Both failure modes may exhibit only limited ductility. This is the same critical seismic deficiency as found when applying NBCC 2010 and CSA S16-09 provisions.

Table 2.14: Connection failure modes and demand-to-capacity ratios

	1st floor		2nd floor		3rd floor		4th floor	
$T_{f\text{-}10p}$ (kN)	1425		1332		1040		589	
Failure mode	$T_{u\text{-}c\text{-}10}$ (kN)	$T_{f\text{-}10p}$ / $T_{u\text{-}c\text{-}10}$	$T_{u\text{-}c\text{-}10}$ (kN)	$T_{f\text{-}10p}$ / $T_{u\text{-}c\text{-}10}$	$T_{u\text{-}c\text{-}10}$ (kN)	$T_{f\text{-}10p}$ / $T_{u\text{-}c\text{-}10}$	$T_{u\text{-}c\text{-}10}$ (kN)	$T_{f\text{-}10p}$ / $T_{u\text{-}c\text{-}10}$
Net rupture of angle	1307	**1.09**	1212	1.10	937	**1.11**	374	**1.57**
Block shear failure of angle	2505	0.57	2117	0.63	1389	0.75	665	0.89
Bearing failure of angle	3772	0.38	3233	0.41	2245	0.46	1078	0.55
Bolt shear failure	1383	1.03	1185	**1.12**	988	1.05	593	1.00
Net rupture of gusset plate	1693	0.84	1316	1.01	1152	0.90	563	1.05
Block shear failure of gusset plate	2930	0.49	2481	0.54	1635	0.63	798	0.74
Bearing failure of gusset plate	2515	0.57	2156	0.62	1572	0.62	808	0.73

2.3.4 Summary of seismic assessment based on probable resistance

This second assessment approach assuming all members have their probable resistance confirms the main finding of the previous assessment using factored design forces and factored resistances from current code provisions, i.e., the brace connections represent the most critical deficiency in this existing braced frame designed using the 1980's design standards. The connection problem can be divided into two parts. The first part is related to insufficient strength, i.e., the connections are expected to be the first elements to reach their capacity in braced frame. The second part is the failure mode of the connections: the rupture on the net section may not provide enough ductility to accommodate the inelastic demand imposed on the whole braced frame. As mentioned before, the consequence of a premature connection failure may lead to soft-storey phenomenon and even complete collapse of the existing structure under a strong seismic event. Thus, a retrofit of the brace connections is necessary.

2.4 Proposed retrofit strategies

According to the characteristics of the connection deficiency, two basic retrofit strategies can be adopted. The first approach consists in increasing the strength of the connections to solve the lack of resistance issue. The second approach consists in increasing the ductility of the critical failure modes of the connections. Either approach can be used: if the connection resistance is increased beyond the force demand corresponding to the brace probable resistance, connection ductility is not required anymore because ductility will be provided by the bracing members; if, on the contrary, sufficient connection ductility is provided such that the entire expected inelastic demand can be accommodated in the connections, the connections will act as fuses in the system and the brace connections will not need any reinforcement.

The first floor of the structure is considered to be the most critical storey in the building because the seismic energy is transmitted from the ground to the structure at that location. P-delta effects that may lead to building collapse are also more important at that level. Thus, the brace connections at the first floor are selected as the typical double angle brace connection to be studied to develop possible retrofit strategies to address the connection deficiency. Figure 2.9 shows the detail of the existing connection for double angle brace at the first floor. Examination of the configuration for this connection leads to three possible retrofit strategies that are described in the next sections.

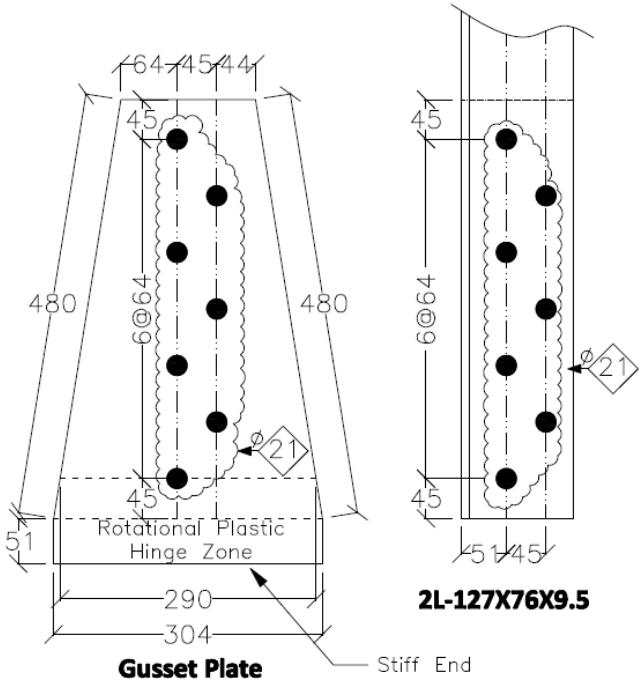

Figure 2.9: Existing brace connection at level 1

2.4.1 Retrofit strategy I

The first strategy is to strengthen the connection. Based on the assessment results, it is found that the existing brace connection is not strong enough and, therefore, cannot transfer large enough forces to the double angle braces so that the braces can dissipate energy. One way to strengthen the connection is by welding additional cover plates to the short legs of each angle in the region where angle net section rupture is expected. Additional plates can increase the net cross-section area of the double angle brace member in the connection region and force brace yielding in the gross cross-section. Such a connection reinforcement is already being used in practice to increase brace connection resistance of braced frames designed in accordance with current design codes (Figure 2.10).

Figure 2.10: Connection strengthen by welding additional plates (Tremblay 2013, personal communication)

Equation 2.26 is used to calculate the connection resistance with cover plates. This equation is proposed by Haddad and Tremblay (Haddad and Tremblay, 2006). In this expression, A_n is the double angle net cross-section area, and A_{cp} is the cross section area of cover plate. To calculate the probable resistance, the following values are used: ϕ_r= 1.0, ϕ = 0.75, and U= 0.884. When using the 7.93 x 45 reinforcement plates shown in Figure 2.11, the resulting probable resistance is 1682 kN, which is larger than the probable yielding capacity of the double angle brace, T_u = 1425 kN. Thus, it is possible to strengthen the brace connections up to a point corresponding to the capacity design concept where the brace member acts as a “fuse” to dissipate energy. The disadvantage of

this retrofit strategy is that large lateral forces will be induced in the existing structure and foundations, as was discussed when describing the assessment based on probable resistances.

$$T_r = \left(\phi_r \times F_u \times A_n + \phi \times A_{cp} \times F_u\right) \times U \tag{2.26}$$

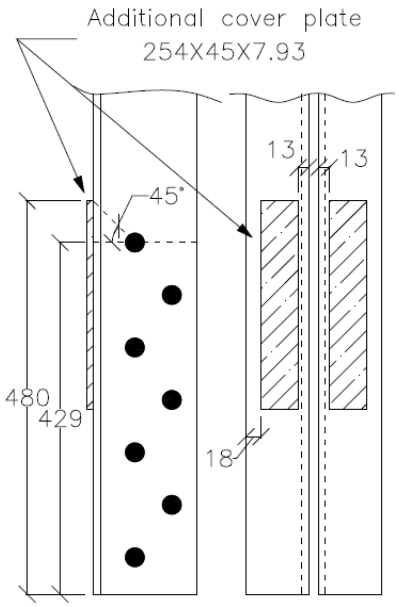

Figure 2.11: Connection strengthen by welding additional plates

2.4.2 Retrofit strategy II

The second strategy consists in using the brace connections to work as "fuses" instead of the bracing members themselves. This strategy requires that the connection failure mode can provide the required local ductility corresponding to the global ductility of the system, as represented by the R_d factor equal to 1.5. The plan of this retrofit strategy is shown in Figure 2.12. Four slotted holes are created at the end of the gusset plates. The shape of the steel segments remaining between the slotted holes are similar to small steel coupons. For this particular connection, the size of these "steel coupons" is 2.0 in. by 0.5 in., which approximately corresponds to the dimensions of a standard steel coupon as specified in ASTM-E8 standard for tension testing. These "steel coupons" may provide sufficient ductility when the connections is subjected to tension forces. In strategy, the net cross-section area of the gusset plate must be reduced such that the strength of the gusset plate in tension on net section will control the seismic induced force demand on the connections and, thereby, on the bracing members and the entire braced frame. The expected failure mode of this retrofitted connection is rupture in tension on the net section of the gusset plate. The probable

capacity associated to this failure mode for the detail shown in Figure 2.12 is 1272 kN, which is less than the probable capacity of angle net section rupture failure mode ($T_{u\text{-}c}$ = 1310 kN in Table 2.14). Thus, the axial force on the brace can be controlled (limited) by introducing this weak link in the gusset plate. However, this retrofit scheme presents two main challenges. First, the ductility performance of the connection retrofitted using this strategy is unknown and must be examined through an experimental program. The second challenge is the implementation of the strategy in a real structure as it may be difficult to access the connection and proceed with the creation of the slotted holes on existing gusset plates on site.

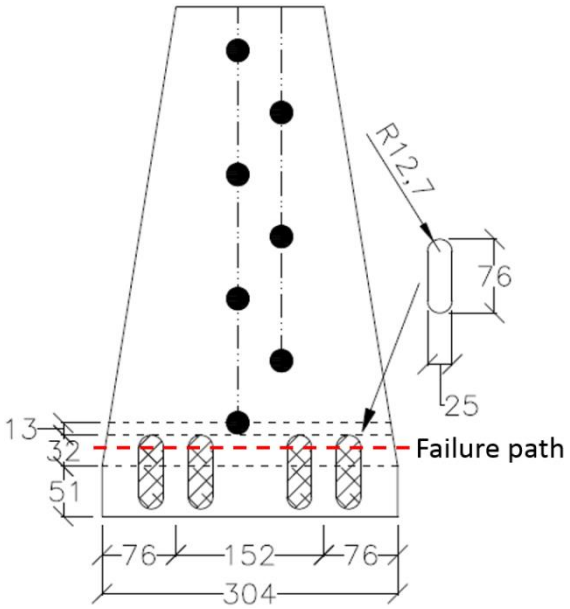

Figure 2.12: Increasing ducility and controlling force of gusset plate net rupture failure mode

2.4.3 Retrofit strategy III

The objective and concept behind the third retrofit strategy are similar to those of the previous one: increasing ductility and controlling forces. Tear-out of the bolts in the gusset plate is promoted instead of net section rupture of the gusset plate. As shown in Figure 2.13, the distance between two existing holes is reduced by adding small holes between them. This reduces the gross area resisting in shear the force imposed in bearing by the bolts to the gusset plate. Ideally, under tension forces, the bolts will be in contact with the holes at the beginning. Then, the bolts will bear against the small steel segments located between the holes and the additional small holes. The small steel segments are expected to eventually fail in shear along their two sides parallel to the load. During

this process, a certain amount of ductility can be developed. To calculate the capacity associated to this failure mode, the shear resistance part of the block shear resistance in Equation 2.18 is used. The probable yield and tensile stresses are used instead of the nominal F_y and F_u values. In addition, ϕ_u is taken equal to 1.0 to calculate the probable resistance for this failure mode. For the geometry shown in Figure 2.13, that probable resistance is equal to 1127 kN. Again, this force is lower that the brace probable resistance and the force demand in the braced frame can be controlled by this failure mode. Two issues need to be addressed for this retrofit strategy. First, the ductility capacity of the intended failure mode is unknown and must be verified by physical testing. Second, the accuracy of the equation used to predict the capacity of the failure mode is not guaranteed because the shear failure plane does not necessarily follows a perfect straight line.

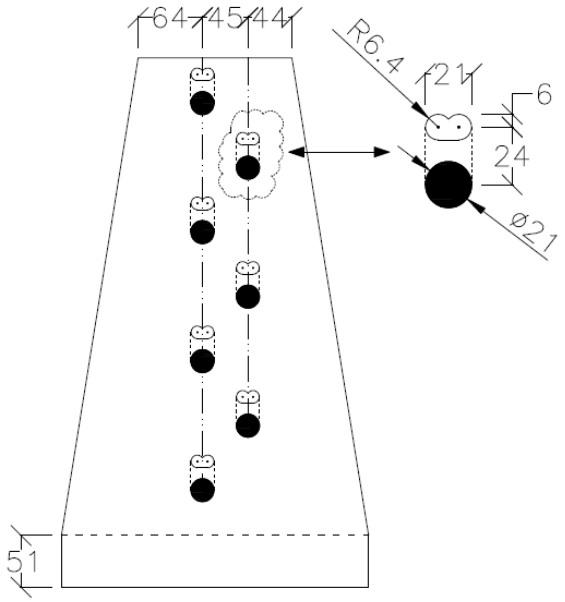

Figure 2.13: Increasing ductiltiy and controlling force by reducing area in shear

2.4.4 Comparison of Retrofit Strategies

The factored and probable resistances of the original connection and each retrofitted connection are summarized in Table 2.15. As discussed in Section 2.4.1 to 2.4.3, the design objective of each retrofitted connection can be achieved based on its probable resistance.

Table 2.15: Factored and probable resistance capacities of connections

Resistances	Gross yielding of angle (kN)	Original (kN)	Retrofit I (kN)	Retrofit II (kN)	Retrofit III (kN)
Factored	999	893	1331	892	720
Probable	1425	1310	1682	1272	1127

2.5 Summary

Based on the study performed in Chapter 2 on the seismic loads in NBCC 1970 to NBCC 2010, it was decided to study a low-rise 4-storey ficitious steel building located in Vancouver. A tension-only braced frame designed with built-up back-to-back double angle braces was chosen. One braced frame of the structure was designed according to the provisions of NBCC 1980 and CSA S16.1-M78. These codes were published before the implementation of capacity design seismic provisions.

The braced frame was assessed by applying the provisions of the current NBCC 2010 and CSA S16-09. The brace connections were found to presentthe most critical deficiencies in the structure. A second assessment was performed by using the probable resistances of members and connections. Again, premature brace connection failure was identified as the most likely failure scenario in case of a strong earthquake. Brace connection failure may lead to soft-storey response and total collapse of the structure. In that case, it is expected that the brace connections at the first level would be the most critical since this level is the first one to resist the seismic demand. Three retrofit strategies have been proposed to address this deficiency: one where the connection strength is increased and two where the connection ductility is enhanced while its strength is reduced. The second and third schemes are preferred because the force demand on the structure and the foundations is lower and can be controlled. However, in both cases, the ductility capacity of the proposed retrofitted connections need to be verified through experiemtnal investigation.

CHAPTER 3: QUASI-STATIC TEST PROGRAM AND RESULTS

The bracing members made from 2L-127x76x9.5 angles with long legs back-to-back used at the first floor of the prototype building are selected to perform quasi-static tests because they are considered to be the more critical braces in the structure. Coupon tension tests are used to measure the steel properties for 127x76x9.5 angle and gusset plate material. A quasi-static cyclic test is also performed on an L-76x51x8.0 brace cut from an existing building that was built in 1960's for comparison purposes.

3.1 Ancillary (Coupon) tests

3.1.1 Introduction

The steel yield strength and tensile strength are very important properties to evaluate the strength and ductility of steel members. Knowledge of these properties for the seismic assessment of an existing steel structure can be very useful as the governing failure modes and the ductility associated to those modes may depend on the ratio between the two strength properties (F_y/F_u). In order to obtain accurate values for these properties, coupon tension tests were performed on the material used for the fabrication of the brace and gusset plate specimens.

According to the CSA S16 steel design standard, the minimum specified yield strength and tensile strength for the steel used are respectively 300 MPa and 450 MPa for CSA G40.21-300W steel. According to CSA S16-09, the probable yield strength, R_yF_y, must be taken as equal to 385 MPa for this material. The probable tensile strength is not specified in CSA S16-09. According to the AISC 341-05 seismic design provisions for steel structures, the probable tensile strength is calculated by multiplying the specified value by an R_t factor. In that standard, R_t is equal to 1.1 for hot rolled structural shapes made of ASTM A572 Grade 42 ksi (290 MPa) steel, the U.S. grade closest to the CSA G40.21-300W steel. Using that value, R_tF_u would be equal to 495 MPa.

For the fabrication of the test specimens for the test program, CSA G40.21-300W steel was specified for the fabrication of the angles and gusset plates. From the mill test reports that were obtained, the steel yield and tensile strength values for the steel used in the fabrication of the L-127x76x9.5 angles are 346 MPa and 493 MPa, respectively. These two values for the gusset plates are 391 MPa and 549 MPa.

3.1.2 Coupon test specimens

Coupon tests were performed on 9 coupons with a 200 mm gage length, including 6 coupons cut from the angles and 3 coupons cut from gusset plates. All coupons were fabricated (machined) by Proto-Concept according to the ASTM E8 and ASTM A370 coupon test standards.

As shown in Figure 3.1, 6 angle coupons are cut from the long leg and the short leg of 3 L-127x76x9.5 angle segmentshaving3 feet in length. Table 3.1 shows the geometrical properties of these coupons. The three segments are respectively labelled 40, 41 and 42. The letter “A” in the coupon designation means that the coupon was cut from the long leg of the angles, and the letter “B” means that the coupon was cut from the short leg. The average measured thickness for the long leg coupons is 9.94mm, which is larger than the 8.91mm thickness measured for the short leg coupons. The average thickness for all measured coupons is 9.42mm, which is 1% less than the 9.53mm nominal thickness for the angles. The geometrical properties of the 3 coupons cut from the gusset plate with 1/2" (12.7 mm) nominal thickness is also shown in the second part of Table 3.1. The measured average thickness of these coupons is 12.65 mm, which is almost the same as the nominal thickness.

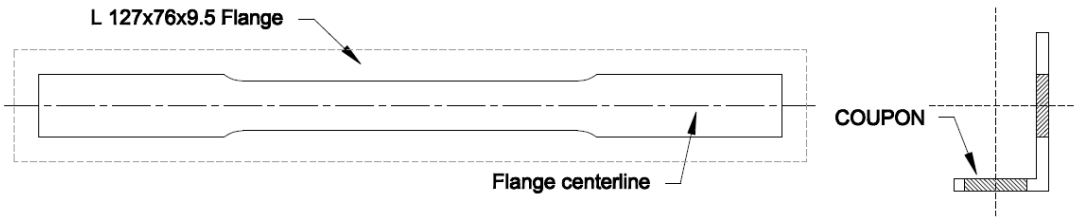

Figure 3.1: Angle coupon fabrication

Table 3.1: Geometrical properties of the coupons

Coupon No.	W (mm)	t (mm)	A(mm^2)
C40A	38.13	9.95	379.6
C40B	38.24	8.93	341.4
C41A	38.11	9.92	378.2
C41B	38.25	8.90	340.5
C42A	38.10	9.94	378.9
C42B	38.08	8.90	339.1
G01	40.21	12.66	509.2
G02	40.19	12.65	508.3
G03	40.26	12.64	509.0

3.1.3 Coupon test setup

All coupon tests were performed in a high stiffness 2.5 MN Tension/Compression capacity INSTRON load frame. In the testing machine, the coupons are clamped by using hydraulic grips. An EPSILON 3543-050M extensometer with a resolution of 0.1μm was used to measure the elongation of the coupons over the 200 mm gage length.

3.1.3.1 Loading protocol for coupon testing

Coupon tests are monotonically displacement controlled. The initial displacement rate applied in the test is equal to 0.0115mm/s. The rate is gradually increased by 5 to 0.0575mm/s after the strain hardening occurred approximately 25 minutes after the beginning of the tests. The rate change is done in 5 consecutive steps, increasing the rate by 0.092 mm/s at each time. Each step lasted for 1 minute.

3.1.4 Coupon test results

3.1.4.1 Coupons cut from the angles

The measured overall stress-strain curves of all tested angle coupons are plotted in Figure 3.2a. Figure 3.2b shows the yield strength of the angle coupons. The measured mechanical properties are given in Table 3.2. The yield strength (F_y) is the average value along the yield plateau. The tensile strength (F_u) values are obtained by dividing the maximum applied tension force measured

in the tests by the initial coupon cross-section area. Average yield and tensile strength values for all coupons are calculated based on the cross-section area of each coupon. As shown in Table 3.2, the coupons cut from the short leg of the angles have higher yield and tensile strengths than the coupons cut from the long legs. On average, the yield strength is 12.3% higher (357 *vs.* 318 MPa) and the tensile strength is 2.7% higher (497 *vs.* 485 MPa) for the long leg coupons. However, the coupons cut from the long legs have higher elongation capacity: the average elongation for the long leg coupons is 25.9%, which is higher than the 23.1% value obtained from the short leg coupons.

The weighted average values for the entire cross-sections were determined based on the respective area of the individual legs, where 4 mm radius was considered in the corner and at the toes. In addition, researchers (Adluri & Madugula, 1995; St-Onge, 2012) have found that F_y in the corner is larger than F_y in the legs. The survey by St-Onge (2012) shows that the ratio between F_y in the corner and F_y in the leg can be taken as 1.16 on average. Using this values, a weighted average value F_y = 336 MPa is obtained for the entire angle cross-section. The average values obtained for F_y and F_u are also given in Table 3.2. Comparing the test results and the mill test report values for the angles, it is found that the yield strength from the mill test report is 1.03% higher than the value obtained from the coupon tests (346 *vs.* 336MPa). For the angles, the tensile strength from both the mill test report and the coupon tests are almost the same: 493 MPa (mill tests) and 491MPa (coupon tests). The measured average yield strength from the coupon tests is 12.7% lower than the 385 MPa minimum R_yF_y value specified in CSA S16-09. The measured average tensile strength from the coupon tests (491 MPa) is similar to the 495 MPa code value.

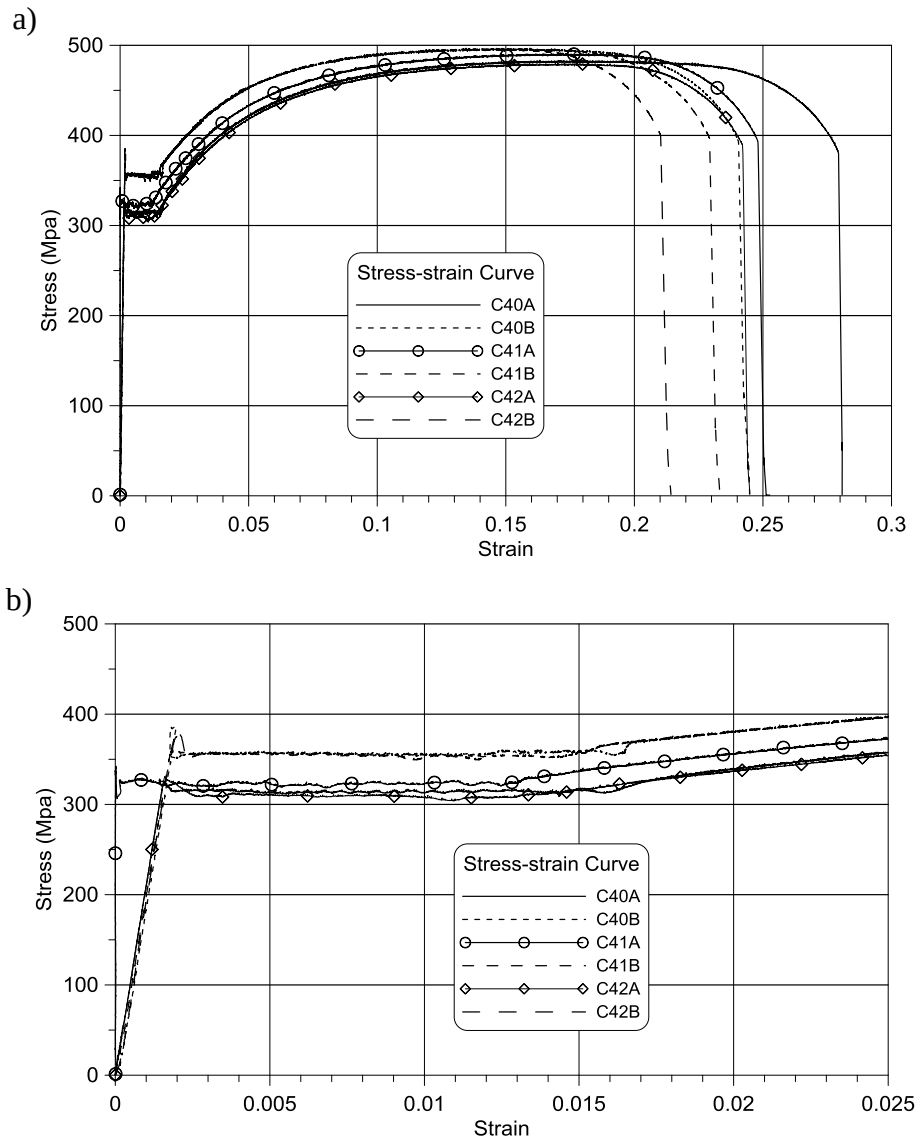

Figure 3.2: Stress-strain curve for angle coupon tests: a) Overall stress-strain curve; b) stress-strain curve before strain hardening

Table 3.2: Measured mechanical properties of the angles from coupon tests

Coupon No.	F_y (MPa)	F_u (MPa)	Fracture Elongation (%)
C40A	316	484	28.1
C40B	358	496	24.5
C41A	326	491	25.2
C41B	357	497	23.4
C42A	311	480	24.5
C42B	356	496	21.4
Average values	336 (A+B) 318 (A) 357 (B)	491 (A+B) 485 (A) 497 (B)	24.7 (A+B) 25.9 (A) 23.1 (B)

3.1.4.2 Coupons cut from the gusset plates

The measured overall stress-strain curves for all tested coupons cut from the gusset plates are plotted in Figure 3.3a. Figure 3.3b shows the yield strength of these coupons. For all coupons, a progressive transition was observed between the elastic and yielding phases and the 0.2% offset method was used to measure the steel yield strength (F_y). As shown in Table 3.3, the average yield strength of the coupons cut from the gusset plates is 395 MPa, which is 1% higher than the value from the mill test report (391 MPa) and 2.7% higher than the CSA S16-09 R_yF_y value (385 MPa). The average tensile strength (464 MPa) is closed to the code value but is much lower than the value given in the mill test report (549 MPa). This suggests that an error occurred in the mill test report.

a)

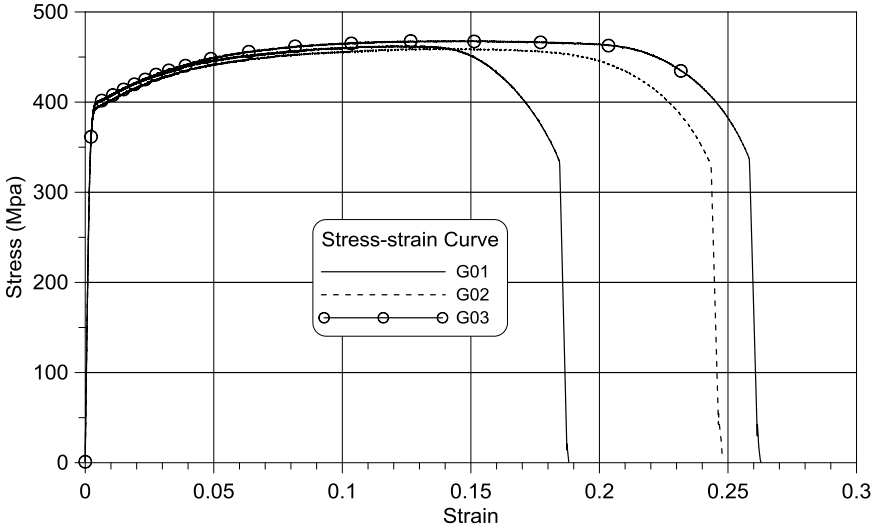

b)

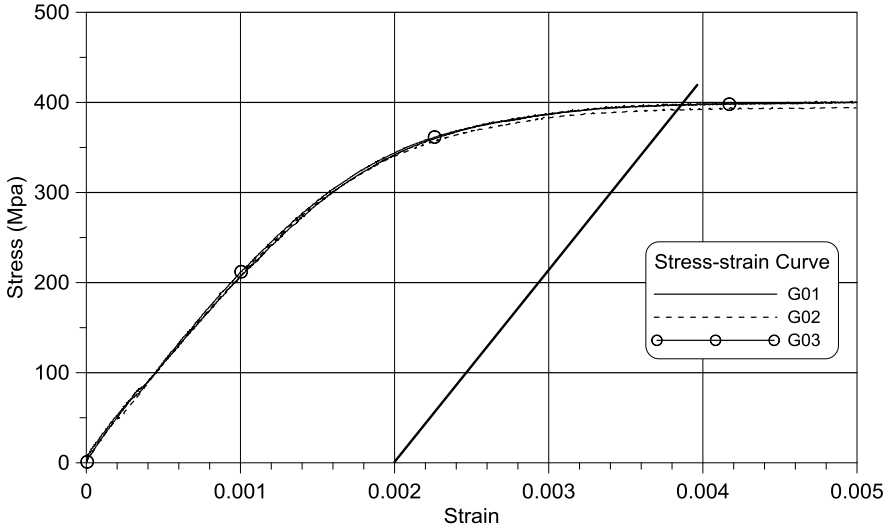

Figure 3.3: Stress-strain curve for gusset plate coupon tests: a) Overall stress-strain curve; b) stress-strain curve up to yielding point

Table 3.3: Measured mechanical properties from coupon tests

Coupon No.	F_y(MPa)	F_u(MPa)	Fracture Elongation (%)
G01	396	463	18.9
G02	392	460	25.0
G03	398	468	26.4
Average	395	464	23.4

3.1.5 Discussions based on coupon test results

The mill test and coupon test results show that CSA G40.21-300W steel can have different yield and tensile strength values depending on the steel section. The hot-rolled L shapes have a lower yield strength than the plate used for the gusset plates. However, the tensile strength of the angles is higher. The elongation at facture for all the coupons are almost the same in all cases. In addition, the probable yield and tensile strength values are close to the values specified in codes in CSA S16-09 and AISC 341-05 standards.

If the yield and tensile strength values from the coupon tests are used to replace the code probable yield and tensile strengths for the seismic assessment of the structure in Section 2.3 the assessment results may change. For example, the probable yield tensile strength of the double angle braces at

the ground floor, T_u in Figure 3.8, reduces from 1425 kN to 1243 kN when using the measured yield strength of 336 MPa. However, the probable resistance associated to the tension rupture on the net section for the connection of this brace only slightly changes ($T_{u\text{-}c}$ = 1299 kN *vs.* 1310 kN in Table 2.8) because the probable tensile strength in the assessment (495 MPa) is almost the same as the measured tensile strength (491 MPa). In this case, the differences between code and measured strength values are favorable as the double angle braces may yield before failure at the end connections (T_u = 1243 kN smaller than $T_{u\text{-}c}$ = 1299 kN based on F_u = 491 MPa). An opposite assessment conclusion was found in Chapter 2.

Even if the behaviour of the structure based on coupon test results may not correspond to the assessment results of Chapter 2, the double angle braces and its end connections as designed in Chapter 2 are kept unchanged for the quasi-static tests, the hybrid tests, and the OpenSees models used for the building analyses that were performed later. This is justified by the fact that the difference between the connection net section rupture probable resistance (1299 kN) and the brace probable yield strength (1243 kN) is small (5%), and that the governing failure mode may remain unchanged and that the ductility capacity when the two strength values are that close is unclear.

3.2 Quasi-static test program

The quasi-static test program on the first-storey angle brace and its end connections is performed to verify the assessment predictions made in Chapter 2, collect data for the calibration of the OpenSees model, and study the behaviour of the braces under cyclic inelastic loading.

3.2.1 Introduction

The test matrix adopted for this research is shown Table 3.4. As shown, two different brace lengths are used because two different test platforms were used: an existing pinned 7500 mm X 4087 mm vertical frame test platform (Figure 3.4a) and an 12 MN load frame platform (Figure 3.4b). The main objective of the test in the vertical frame was to collect data on the inelastic cyclic response of the brace when mounted in a frame similar to the frame in the prototype building. Only one test of this type was performed. For this test, it was decided to avoid premature connection failure such that the response of the brace could be measured up to large storey drift demand. This was done by reinforcing the brace end connections to prevent net section rupture, as suggested for Retrofit strategy I presented in Chapter 2. The data collected could then be useful for the calibration of

brace models over subjected to large inelastic deformation cycles while verifying the adequacy of the Retrofit strategy I.

For the tests performed in the 12 MN load frame, the focus was on the cyclic inelastic response of the brace connections. Three tests were performed: one test on the original brace connection design and two tests where the brace connections were retrofitted according to the two strategies II and III implemented in the gusset plate, as discussed in Section 3.5. The test specimens included the entire brace length because the brace response can influence the demand imposed on the brace connections. In particular, it was important to evaluate the share of inelastic demand between the two end connections. It was also critical to impose the flexural demand induced upon buckling and subsequent straightening of the brace in each loading cycle. Comparison of the tests performed in the two different test platforms on the original brace design would also allow investigating the influence of the brace boundary conditions and loading conditions on the brace-connection assembly.

Table 3.4: Test program

<table>
<tr><th>Test Name</th><th>Test Specimen</th><th>Brace Length (mm)</th><th>Gusset Plate type</th><th>Test Platform</th><th>Loading Protocol No.</th><th>Brace Net Section</th></tr>
<tr><td>VF-S-C-1</td><td rowspan="4">2L-127x76x9.5</td><td>6440</td><td>Original</td><td>Pinned vertical frame</td><td>1</td><td>Reinforced</td></tr>
<tr><td>LF-O-C-1</td><td rowspan="3">6095</td><td>Original</td><td rowspan="3">12 MN load frame</td><td rowspan="3">2</td><td rowspan="3">Original</td></tr>
<tr><td>LF-R1-C-1</td><td>Strength Reduced 1</td></tr>
<tr><td>LF-R2-C-1</td><td>Strength Reduced 2</td></tr>
</table>

a)

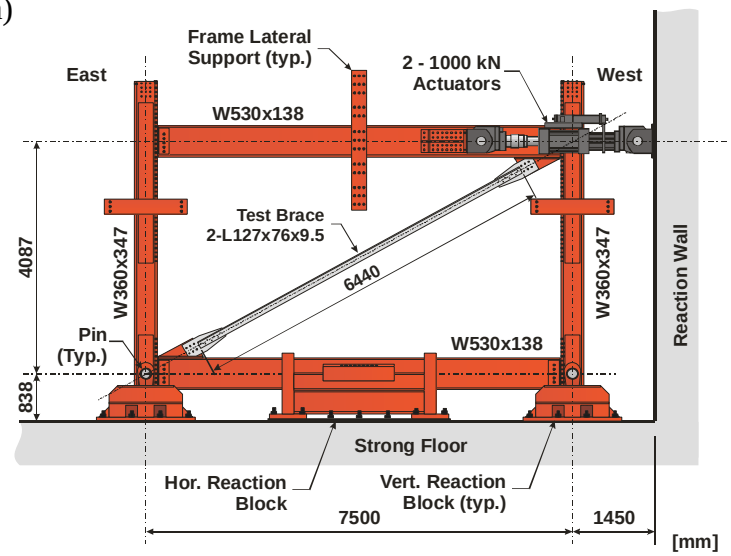

Figure 3.4: Test platforms: a) Pinned vertical frame; b) 12MN load frame

b)

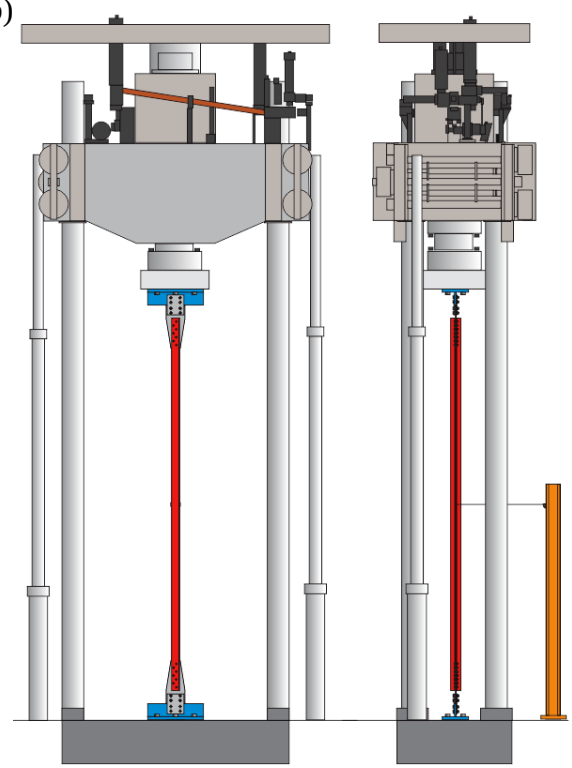

Figure 3.4: Test platforms: a) Pinned vertical frame; b) 12MN load frame (continued)

3.2.2 Brace properties

All the braces used in the quasi-static and hybrid tests have the same section 2L-127x76x9.5 and were all fabricated by the CANAM Group steel fabricator using the G40.21-W300 steel from the same heat. Hence, a typical gross cross section area could be used for all braces to simplify the data reduction and analysis process. The ratio between the effective average thickness and the nominal thickness (9.53 mm) was multiplied the nominal cross section area (3700 mm^2) specified in the steel handbook to obtain the actual cross-section area. Due to the different thickness between the long and short legs of the angle section, a total of 50 thickness measurements were taken randomly along each of the two angle legs using a micrometer with 0.01 mm resolution. The average thickness for the long and short legs are respectively 9.90 mm and 8.92 mm. The effective average thickness for L-127x76x9.5 is 9.41 mm, which is 1.23% thinner than the nominal thickness. Thus, the actual gross cross-section area is taken equal to 3653 mm^2.

3.2.3 Pinned vertical frame test

3.2.3.1 Test specimen

The 2L-127x76x9.5 built-up double angle brace for pinned vertical frame test is shown in Figure 3.5. The brace length is 6440 mm, as governed by the dimensions of the test frame. This is slightly longer than the brace length in the prototype building (6095 mm). It is believed that this 5.7% difference in length had small effects on the brace response. The test length was specified in the numerical models used for calibration purposes. The total specimen length considering the brace and the end connections is 7043 mm. One stitch connector is welded at the brace mid-length, as was the case in the prototype building. The measured out-of-straightness is approximately 12mm in the out-of-plane (weak axis) direction. It was measured using a laser mounted on the edge of gusset plate. The laser generated a laser beam parallel to the center line of the brace. The distance between the laser beam and the center of mid stitch is the out-of-straightness. Gusset plate dimensions are also shown in the figure.

As described in Table 3.4, the brace connections in this test were strengthened to develop the full brace capacity. As shown in Figure 3.5, the brace is connected to the gusset plates by means of seven ¾” A325 bolts. The figure shows the double angle brace specimen with the 254x45x7.9 mm additional cover plates welded to the outstanding (short) legs of the double angle brace to reinforce

the brace net section. Welding was done in the Structural Engineering laboratory at École Polytechnique of Montréal. The distance from the end of the cover plates to the end of the brace is 480 mm, which gives a distance of 51 mm between the inner end of the cover plates to the center line of the first bolt hole, i.e., the same distance as the distance between the center of the first bolt hole to the angle heel. This retrofit strategy could be easily implemented.

For this test, the gusset plate of the brace assembly was previously bolted to a strong connecting bracket already present in the pinned vertical frame. As shown in Figure 3.6, an additional cover plate (CP-VF) was welded to the end of gusset plates to make sure that this bolted connections between the gusset plates and the brackets remained elastic during the test.

3.2.3.2 Test setup

Figure 3.7 shows a photo of the test setup in the pinned vertical frame test platform. The whole brace is connected to the stiff brackets of the test frame using six 1” A490 bolts acting in single shear. These bolts were pre-tensioned using the turn-of-nut method: a (1/3 turn rotation was applied after snug-tight using an air impact gun. The bolts between the braces and the gusset plates were only snug-tightened, as was done in the 1980's for this application.

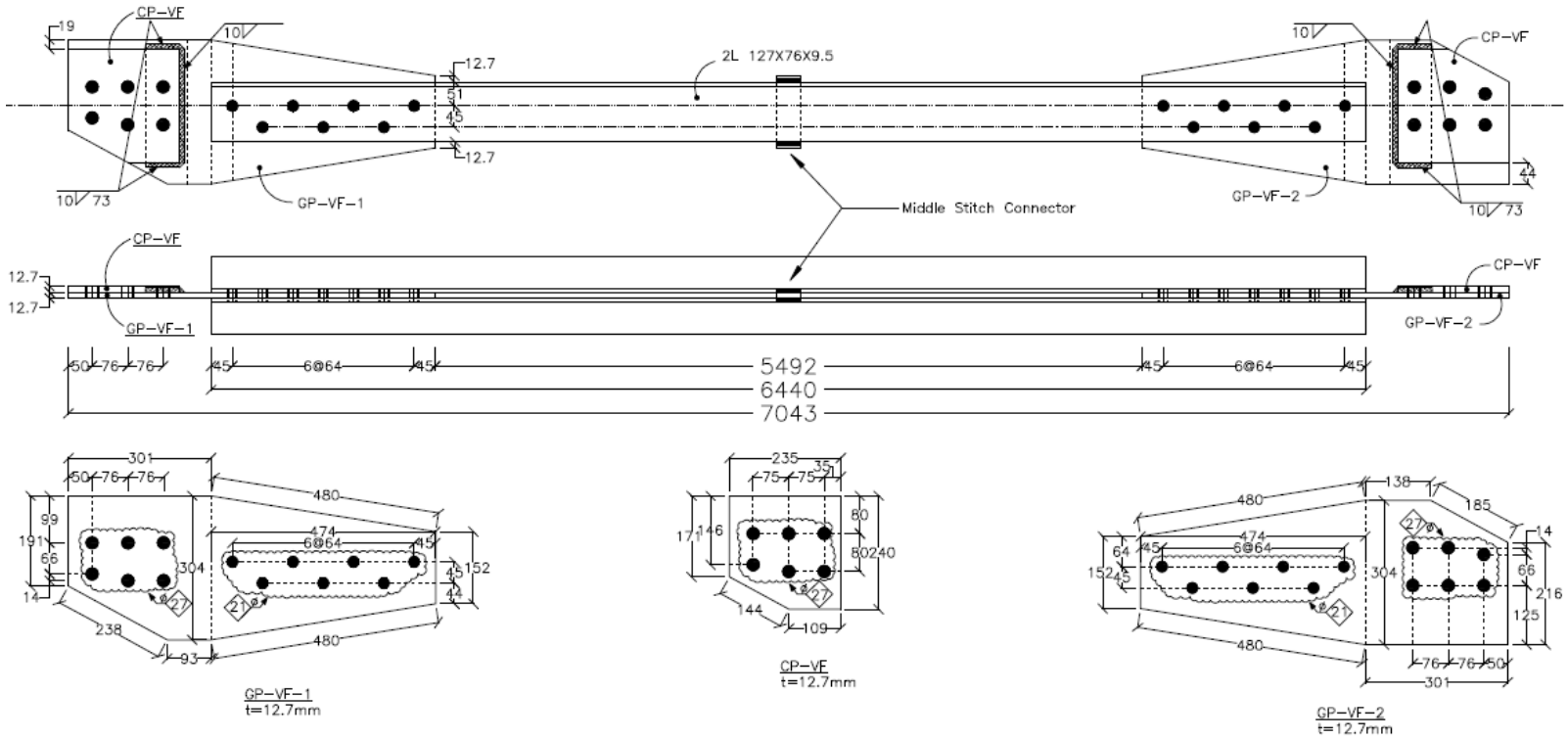

Figure 3.5: Brace using in pinned vertical frame test

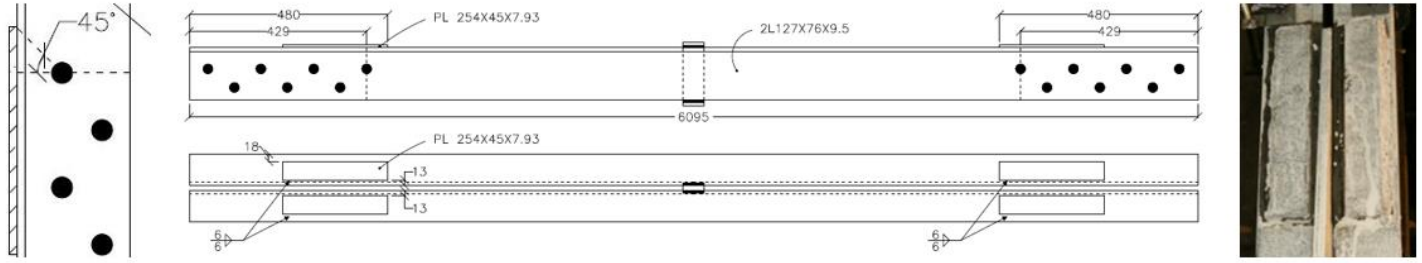

Figure 3.6: Strengthened brace

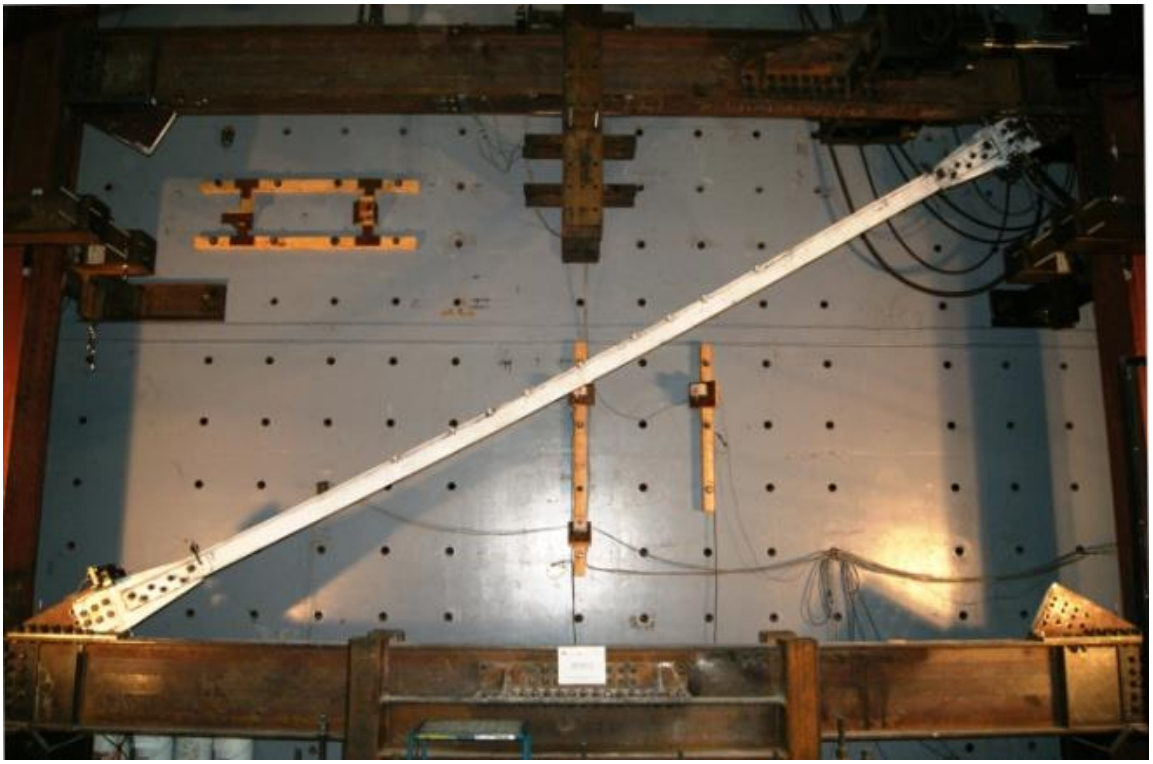

Figure 3.7: Photo of the test specimen mounted in the pinned vertical frame

3.2.3.3 Instrumentation

Two INTERTECHNOLOGY SP635 string pots that have a maximum elongation capacity of 635 mm and a resolution of 1 pm (10^{-12}) were used to measure the whole axial brace deformations (brace deformation plus connection deformation). Four INTERTECHNOLOGY SP127 string pots were used to record the connection axial deformations. Figure 3.8a shows the configuration of these string pots. At end each, one SP635 and two SP127 string pots are fixed to a T-shape connector. The connector is welded by tack welding on the edge of the gusset plate, at mid-length of the rotational hinge region. Figures 4.8b and 4.8c show the string pots at the bottom and top brace connections. In the transverse direction, the SP635 string pot at the bottom connection is located between the two SP127 instruments. As shown in the figure, the end of the spool of the string pot is connected with a fishing wire to a short metallic pole welded at the mid-length of the rotational hinge region of the gusset plate located at the other (opposite) brace end, such that the entire brace axial deformations can be measured. The average total elongation is obtained from the two SP635 string pots. The frame drift obtained from the displacement transducers built-in the actuators is used to control the imposed displacement in the test. For each end connection, the average

elongation from two SP127 string pots is used to obtain the deformation of the connections. As shown in the figure, two short poles were clamped (not welded) to the short legs of the brace at the end of the reinforcement plates.

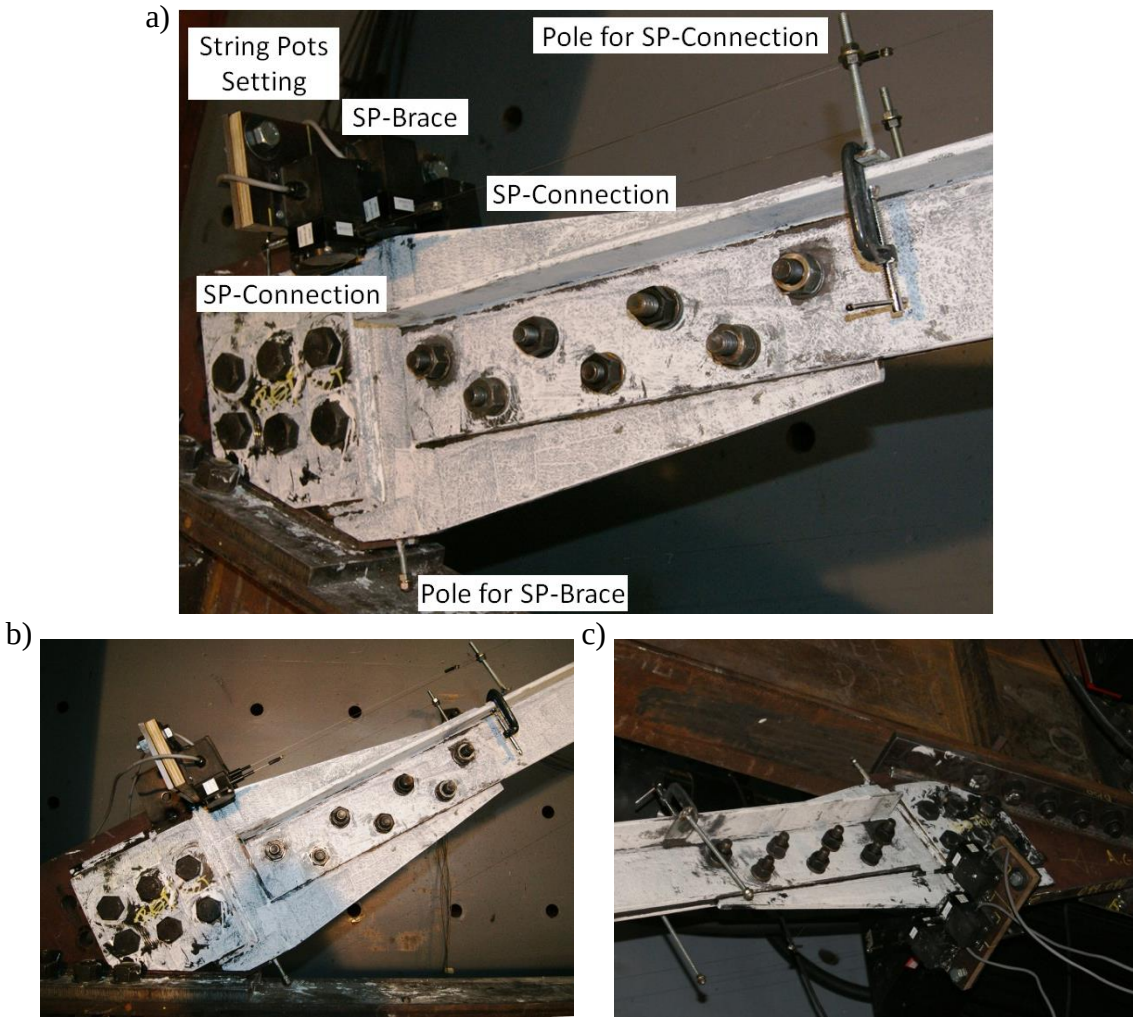

Figure 3.8: Displacement (string pots - SP) transducers for axial deformations: a) location and installation; b) bottom connection; c) top connection

To measure the out-of-plane displacements of the brace upon buckling, nine SP1270 string pots with a maximum elongation capacity of 1270 mm were connected to nine pin clamps shown in Figure 3.9a. These clamps were placed close to the edge of the short leg of one of the two angles at 1/4, 5/16, 6/16, 7/16, 1/2, 9/16, 10/16, 11/16, and 3/4 of the brace length. The string pots were mounted on wooden plates clamped to an inclined HSS member parallel to the brace (Figure 3.9b). The HSS member was supported by two vertical columns. The simple frame formed by the HSS member and the two columns was placed approximately 4 m away from the pinned vertical frame.

Another pin clamp was mounted at the mid-length of the brace on the short leg of the other angle of the brace (Figure 3.9a). Three string pots mounted on the laboratory reaction wall were connected to that additional pin clamp to trace the 3D position of the mid-length of the brace.

a)

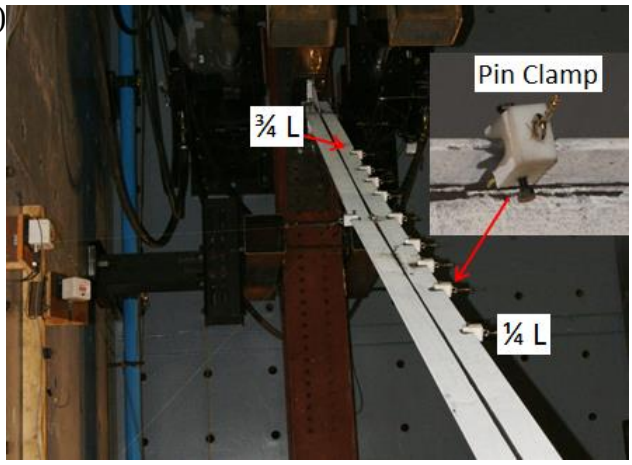

b)

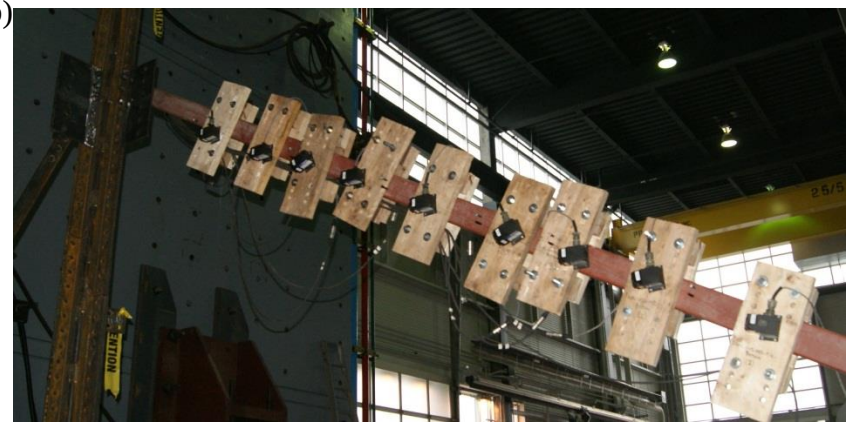

Figure 3.9: String pots in lateral direction: a) pin clamps; b) string pots

3.2.3.4 Loading protocol

The loading protocol is shown in Figure 3.10. A positive storey drift induces tension in the brace specimen. The loading protocol includes several loading excursions at small deformation amplitude (0.1% storey drift), which represent the elastic demand experienced in the building history. Several cycles at 0.2% drift are expected to buckle the tension-only brace. Progressively increasing the displacement amplitudes in subsequent cycles was expected to gradually introduce damage. The applied amplitudes are 0.3%, 0.4%, 0.5%, 0.6%, 0.8%, 1.0%, 1.2%, 1.5%, 2.0%, 3.0%, and 4.0% of storey drift. The maximum value (4% storey drift) is the deformation capacity

of this test platform. The test will be stopped after reaching this limitation to avoid introducing damage to the test platform. A displacement rate of 0.3 mm/s was used.

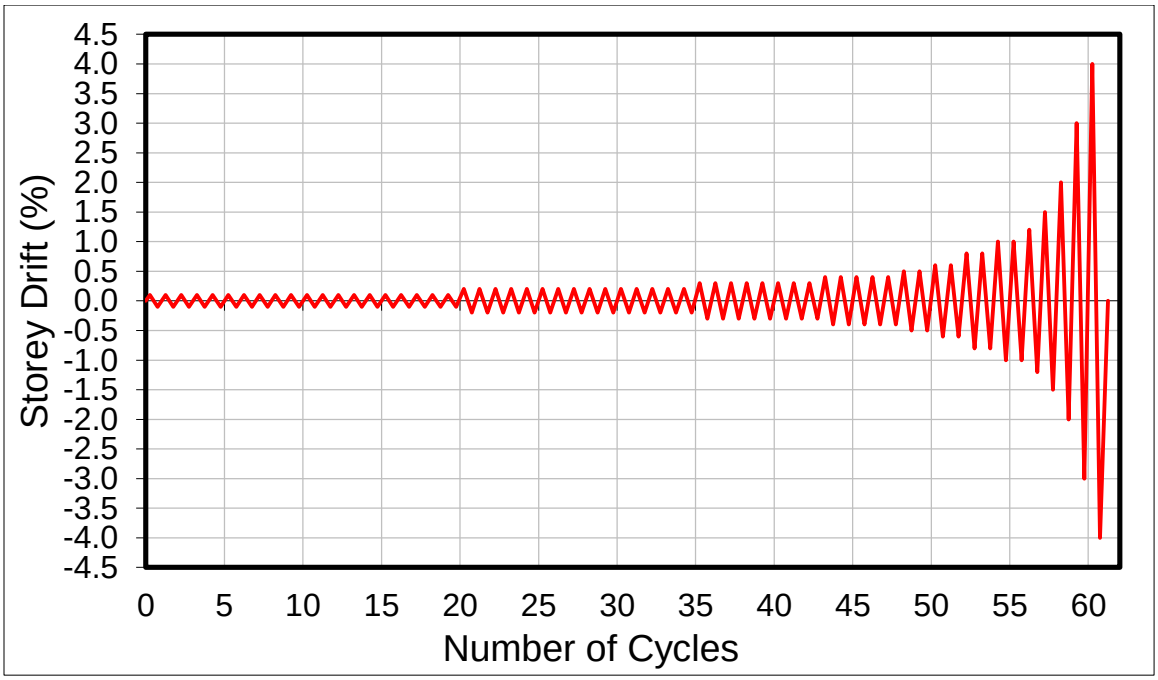

Figure 3.10: Loading protocol for test in pinned vertical frame

3.2.4 The 12MN load frame test

3.2.4.1 Test specimen

The double angle braces used in the 12MN load frame tests have the same brace section, brace configuration, and end connections as the brace used in the pinned vertical frame test. The total brace length is changed to be 6095 mm, which is the design length of the brace at the first level of the fictitious building. In the 12 MN load frame, the brace end gusset plates were bolt-connected to T-shape brackets previously mounted in the load frame. In order to fit with this test setup, the portion of the gusset plate that was reinforced with a cover plate to ensure elastic response of the connections to the brackets were changed to the rectangular shape shown in Figure 3.11. The gusset plate shown in this figure is referred to as the original brace connection design. This original gusset plate design was then modified to accommodate the two types of retrofitted gusset plates that were proposed in Chapter 2. The fabrication procedure for the first retrofit scheme is shown in Figure 3.12a. Four rows of three 25.4 mm (1”) holes are drilled in the gusset plate, between the end of the

brace member and the reinforcement cover plate. Then a portable grinder with a cutting blade is used to cut the small steel pieces between holes to form four smooth parallel slotted holes. With this strategy, the gusset plates are expected to yield in tension over the segments located between the parallel, 76 mm long slots. Preparation of the gusset plates for the second retrofit strategy is shown in Figure 3.12b. This time, a magnetic drill is used to drill two 6.4 mm (1/4") holes in the gusset plates in front of the holes of the bolts connecting the brace to the gusset plates. The objective is to create weak steel segments in front of each of these bolts. These segments are expected to yield in shear when subjected to bearing forces imposed by the bolts when the brace acts in tension.

In an actual building, these two retrofit schemes would be realized on site, without removing the gusset plates. Hence, efforts were made in the laboratory to use the tools that would be employed to implement the retrofit strategies in an actual structure.

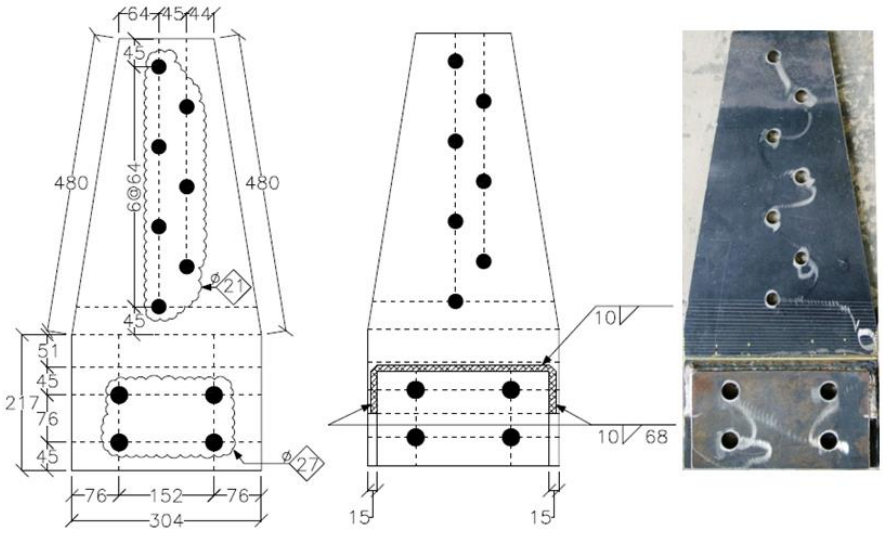

Figure 3.11: Original gusset plate

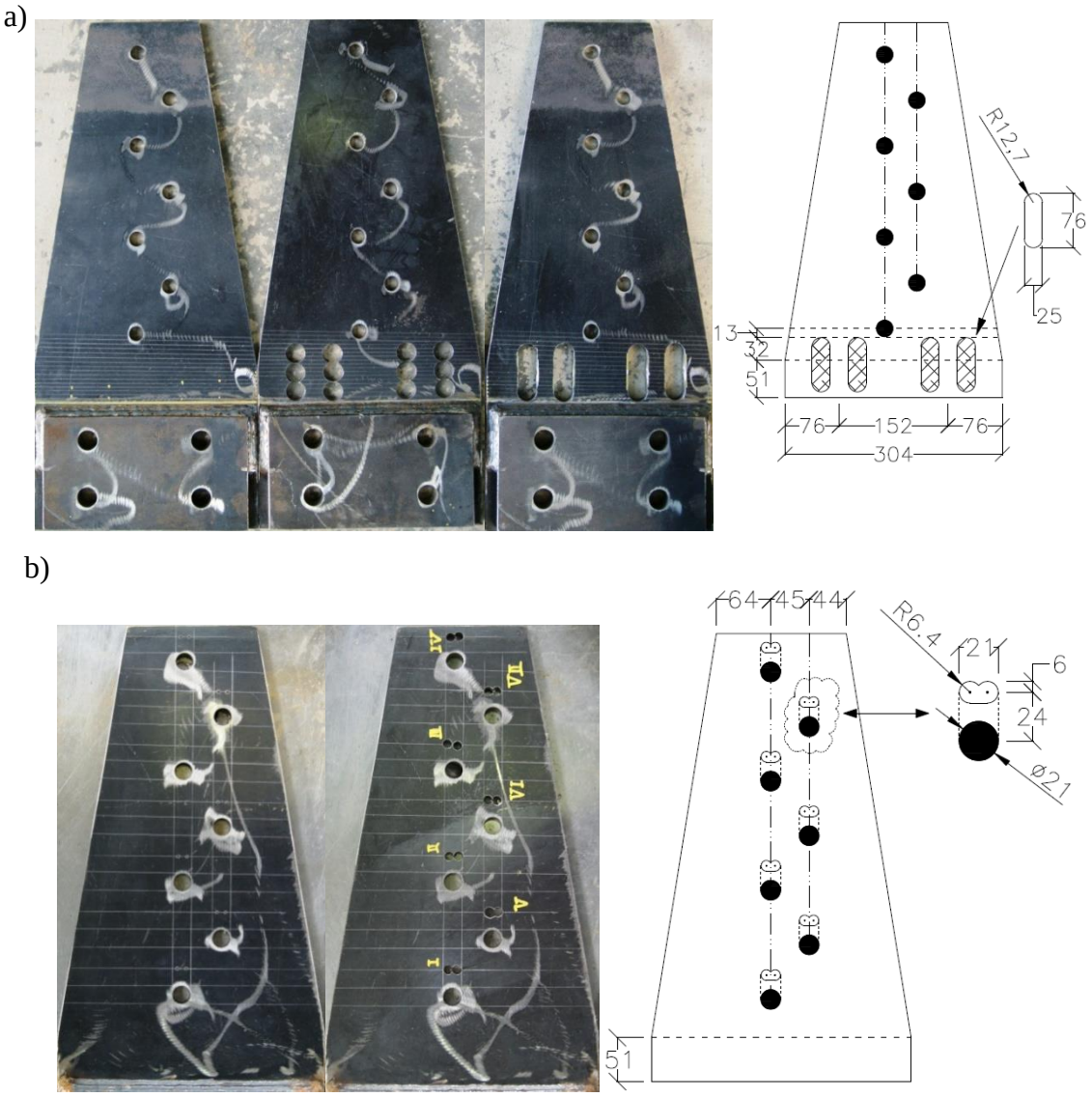

Figure 3.12: Retrofitted gusset plate preparation: a) retrofit strategy II; b) retrofit strategy III

3.2.4.2 Test setup

The test setup is shown in Figure 3.13. The T-shaped brackets are connected to the load frame actuator upper platen and the load frame base plate using six 51 mm (2”) socket head A574 screws. The screws were tightened by applying 3500 psi torque using a hydraulic wrench. The brace specimens are connected to the T-shaped brackets using eight 25.4 mm (1”) A490 bolts. An air impact gun was used to tight these bolts using the turn-of-nut procedure.

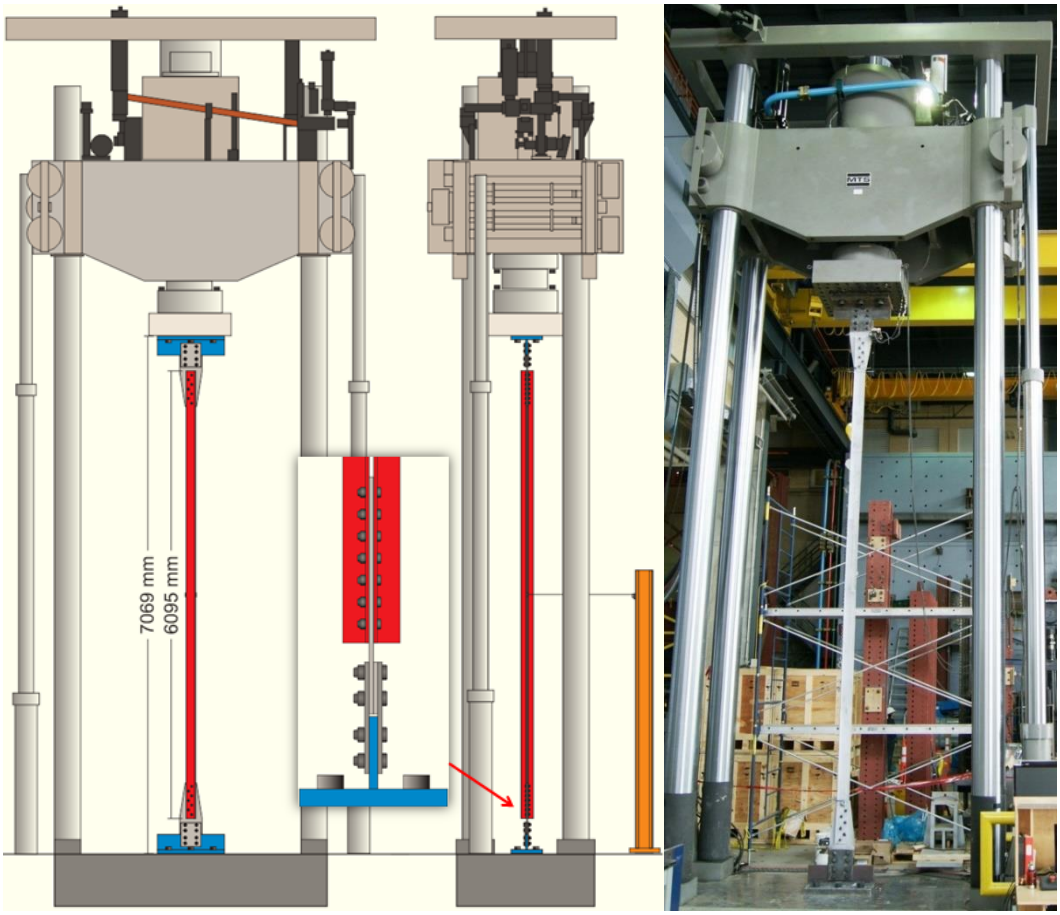

Figure 3.13: Test setup in 12MN load frame

3.2.4.3 Instrumentation

The instrumentation in the 12MN load frame is shown in Figure 3.14. For the axial deformations, it is the same as the instrumentation used in the pinned vertical frame. The average axial deformations from the two SP35 string pots in the axial direction is used to control the test in the 12MN load frame. Two string pots were used at each brace end to measure the axial deformations in the brace end connections. In the lateral direction, only one SP1270 string pot was used to record the out-of-plane deformation at mid-length of the brace.

a)

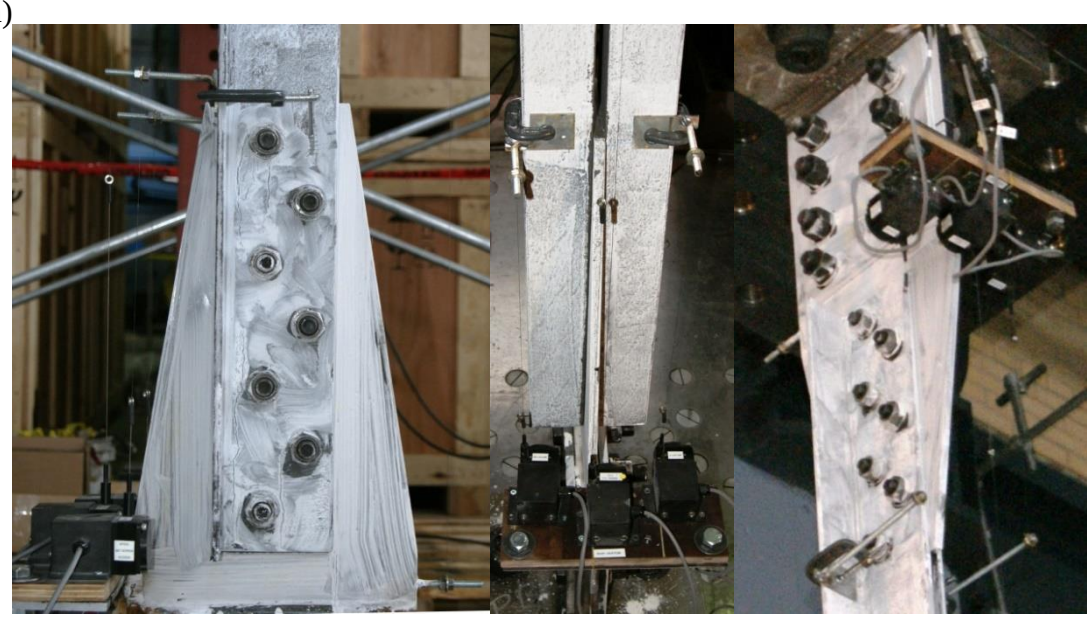

b)

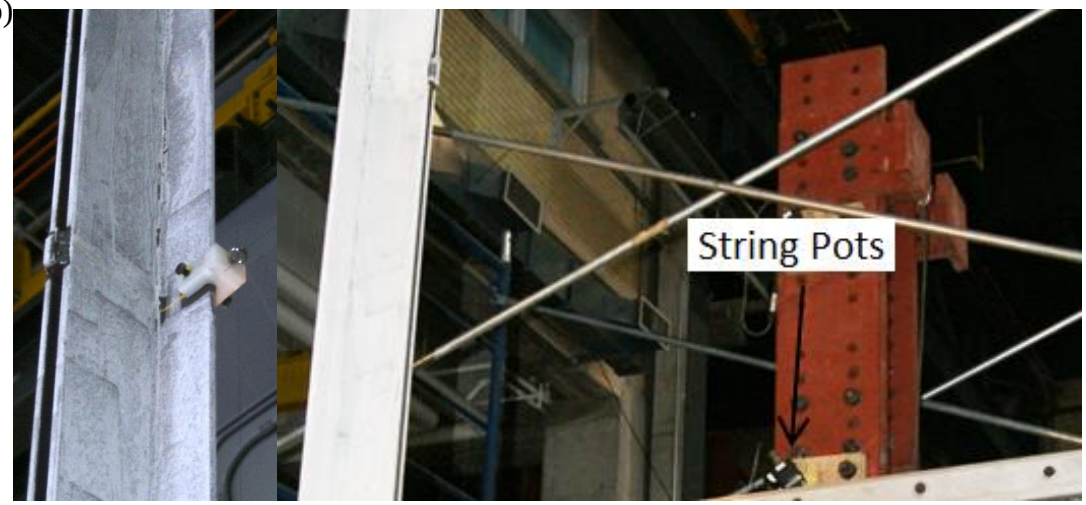

Figure 3.14: Instrumentation in the 12 MN load frame tests: a) axial direction; b) lateral direction

3.2.4.4 Loading protocol

The loading protocol is based on the loading protocol used in the pinned vertical frame test. The storey drift at each peak points and number of cycles are exactly the same. However, the displacement at each peak points is different. Figure 3.15 shows the braced frame, which has the same dimension as the fictitious building, used to develop the loading protocol. The storey drifts (Δ/h_s) are converted to brace axial deformations (δ) that are used to control the cyclic test in 12 MN load frame. The brace axial deformations correspond to the deformations that develop in the whole brace (L_b), which includes the net brace deformations (δ_b) and the connection deformations (δ_c).

Figure 3.16 shows the loading protocol used in the 12 MN load frame. The maximum equivalent storey drift in this loading protocol is 5%. The displacement rate is the same as the one used in the pinned vertical frame test, i.e., 0.3 mm/s. It corresponds to 49.2με/s.

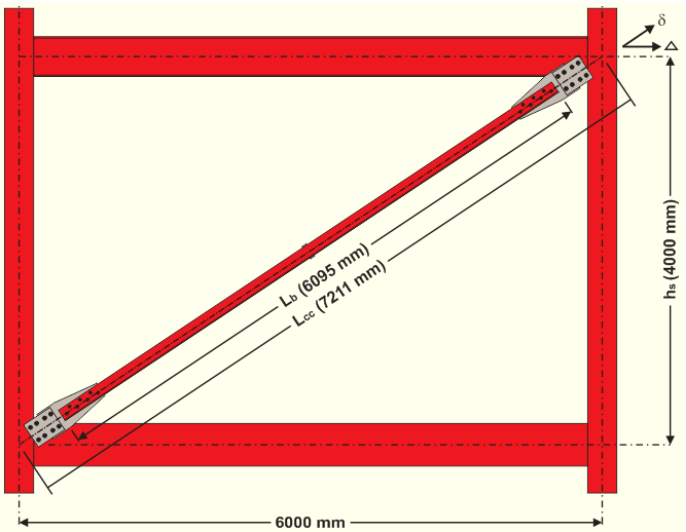

Figure 3.15: Braced frame used to develop loading protocol

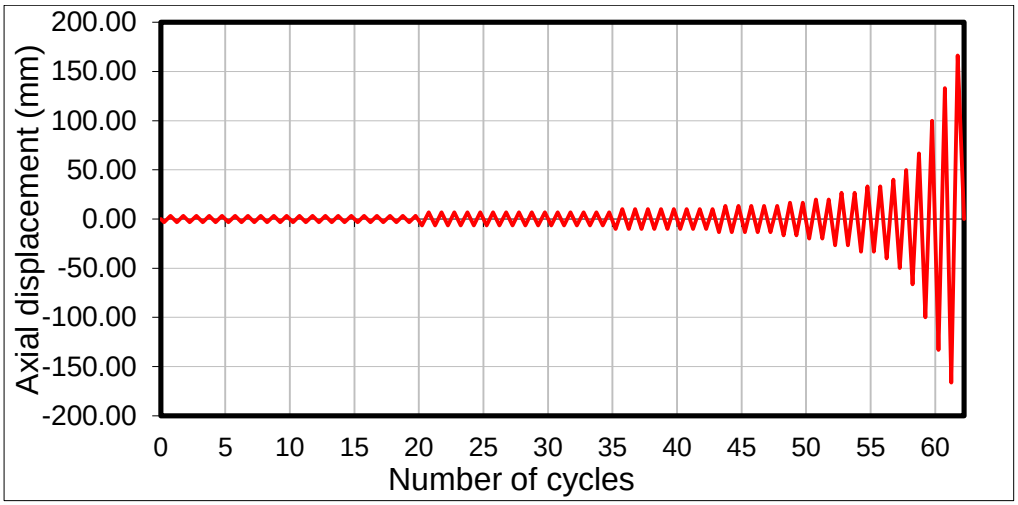

Figure 3.16: Loading protocol used in 12 MN load frame tests

3.3 Quasi-static test - Observed behaviour and results

3.3.1 Test VF-S-C-1 (Retrofit strategy I) (Specimen No. 1)

In this test, a built-up double angle brace with strengthened connections is tested in the pinned vertical frame.

3.3.1.1 Observed behaviour

In the first 20 cycles with 0.1% storey drift amplification, the brace remained elastic. As shown in Figure 3.17a, no change in the spacing between the two angles could be observed. Buckling of the brace happened in the first cycle with 0.2% storey drift amplitude. As expected by calculation, the brace buckled in the out-of-plane direction. After brace buckling, the width of the gap between the vertical legs of the two angles began to reduce upon imposing compression loading. Figure 3.17b shows the behaviour in these cycles. The axial deformation of the brace was approximately 5.5 mm in these cycles, which is about 2 mm less than the expected axial deformation in brace. This is attributed to the slackness present in due to the beam-to-column connections with slotted holes used in the pinned vertical test frame. Light noise from slippage of the hand tightened bolts could be heard in the test. In the 0.3% storey drift cycles, the long legs of the two angles came into contact with each other for the first time. As shown in Figure 3.17c, the gap is closed in the region extending between 1/4 and 5/16 of the brace length. At this time, the heel of the angles are in contact whereas a gap still exists between the toes of the angles (Figure 3.17d). Upon buckling of the brace in the cycles with 0.4% storey drift amplitude, the two angles came into contact with each other in the upper half segment of the brace for the first time from 10/16 to 11/16 of the brace length. This is shown in Figure 3.17e. Slippage of the 25.4 mm (1”) bolts that had been pre-tensioned was observed in the first cycle with 0.3% and 0.4% storey drift amplitudes. Due to this slippage, vibration of the steel wires of the string pots and shifts in the string pot readings could be noticed.

Once the displacements increased to 0.5% storey drift, the two vertical legs started to deform toward each other under increasing tension forces, as shown in Figure 3.17f. At the same time, yielding was observed for the first time in the gusset plates. In the following cycles, no significant changes in brace behaviour in the compression phase was observed until the cycles with 1.0% storey drift amplitude. In Figure 3.17g, the toes of the two angle long legs came into contact for the first time when applying compression loading to the brace. Gross cross section yielding of the double angle brace started in these cycles as well. Brace in-plane bending under tension forces became obvious in the region around the brace end connections in the cycles with 1.2% storey drift amplitude (Figure 3.17h). In-plane bending is caused by the eccentricity between the brace cross-section and the brace end connection. In the following cycles, the brace axial deformation increased

in the tension phases, whereas brace lateral deformations increased during the compression phases as the imposed displacement amplitudes increased. In the last two cycles of the test, the brace passed 3% storey drift in compression, and still sustained 4% storey drift in tension without failure.

The test was stopped at 0 kN force after having passed 4% storey drift. Figures 4.18a and 4.18b show the yielding of the end connection after the test. The residual deformed shape of the double angle brace is shown in Figure 3.18c. In the figures, the non-uniform white color of the whitewash on the brace is caused by flaking off due to the elongation of the brace in tension. After disassembling the brace, it was found that the last hole (closest to the angle end) in the gusset plate for ¾" bolts had the largest bearing deformation (Figure 3.18d). In addition, the deformed direction is not exactly parallel with the axial load direction. This is attributed to the in-plane bending that probably imposed additional forces to this bolt. However, no deformation of this hole could be observed in the brace member.

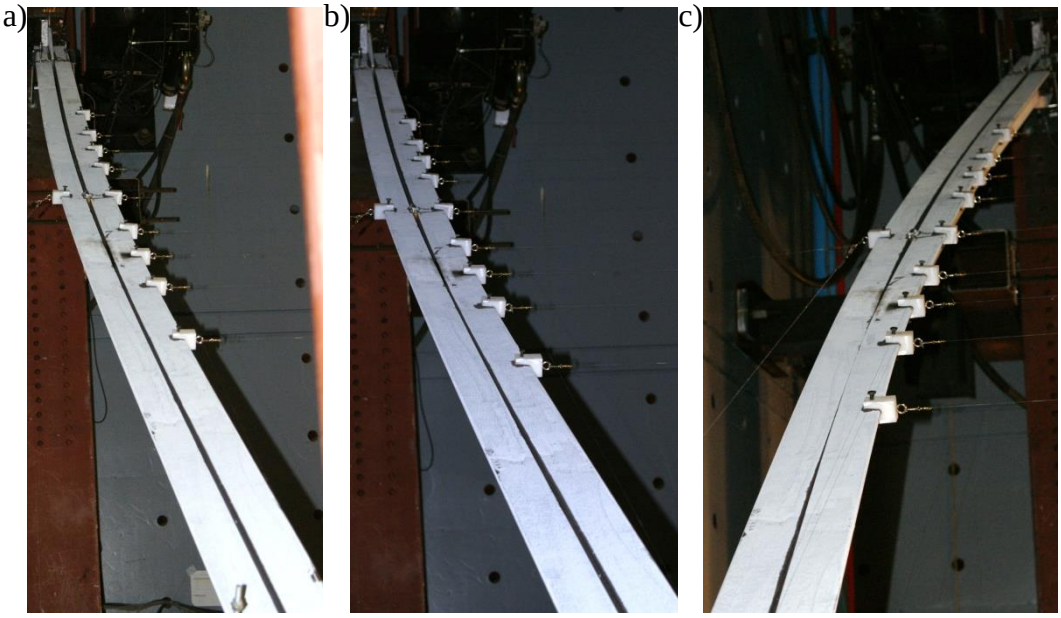

Figure 3.17: Specimen No. 1 - Observed behaviour during the test: a) elastic elongation; b) buckling of brace; c) gap closed in the lower brace segment; d) gap left between the toes of the long legs; e) gap closed in the upper brace segment; f) gap closing between the two vertical legs under brace tension loading; g) contact between the toes of the long legs under compression; h) in-plane bending

d) e) f)

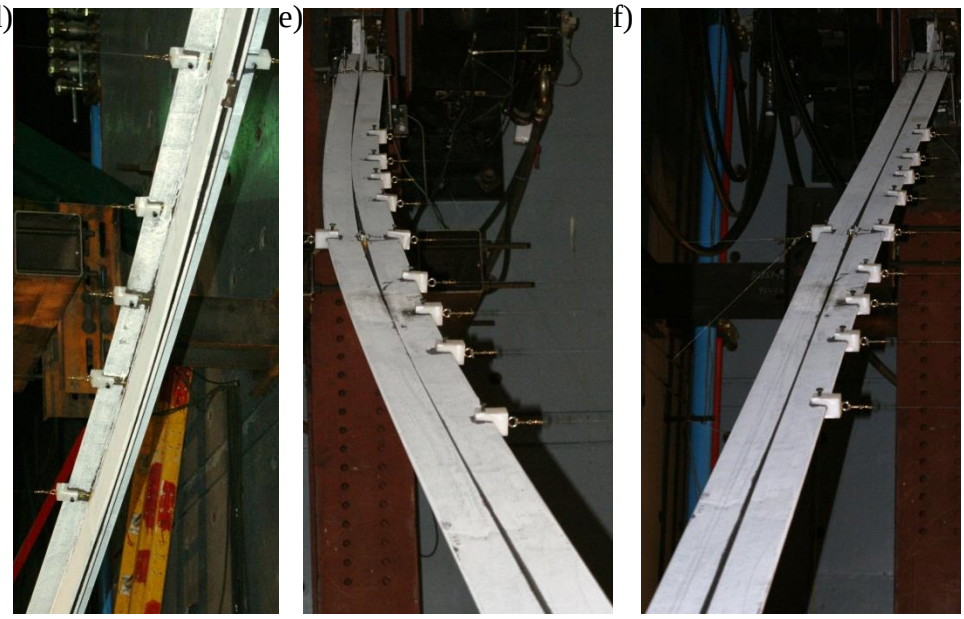

g) h)

Figure 3.17: Specimen No. 1 - Observed behaviour during the test: a) elastic elongation; b) buckling of brace; c) gap closed in the lower brace segment; d) gap left between the toes of the long legs; e) gap closed in the upper brace segment; f) gap closing between the two vertical legs under brace tension loading; g) contact between the toes of the long legs under compression; h) in-plane bending (continued)

a)

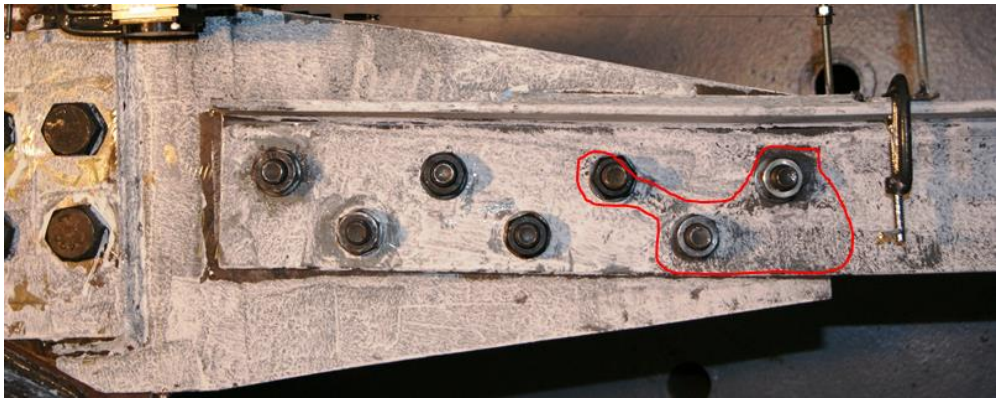

b)

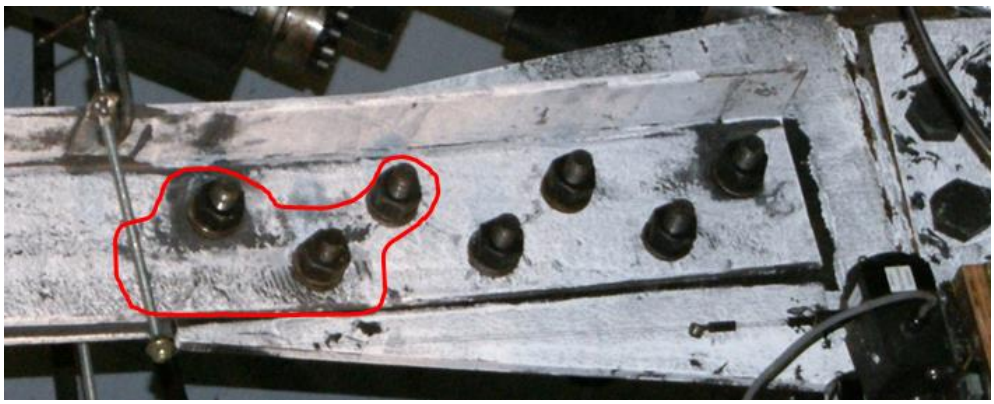

c)

Figure 3.18: Specimen No. 1 - Damage to end connections after the test: a) yielding in the bottom connection; b) yielding in the top connection; c) residual deformed shape of the brace; d) hole elongation in the gusset plate

d)

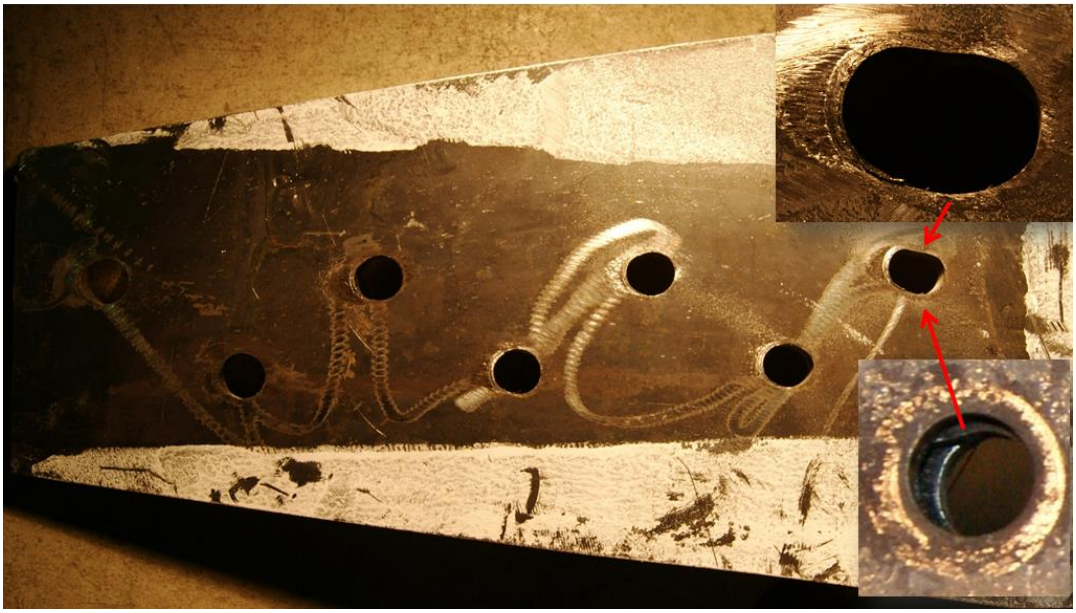

Figure 3.18: Specimen No. 1 - Damage to end connections after the test: a) yielding in the bottom connection; b) yielding in the top connection; c) residual deformed shape of the brace; d) hole elongation in the gusset plate (continued)

3.3.1.2 Test results

The main response parameters for this specimen are summarized in Table 3.5. Figure 3.19 shows the overall brace hysteretic axial response including connection deformations. In the graph, the load is normalized with respect to the brace yield tensile resistance determined with the average measured yield strength. The brace with the strengthened net section at the end connections exhibited good energy dissipating response under tension loads. Buckling in compression occurred at a relatively small load and the energy dissipating capacity is limited under compression load, as expected for bracing members of a tension-only braced frame. At 4% storey drift in tension, the overall brace elongation is 2.13%. The overall brace deformation is approximately 2% at 3% storey drift in compression side. These values are smaller than the respective theoretical brace elongation values of 3.51% 2.63%. This is attributed to the slackness in the connections of the frame test platform. As shown, the brace developed a yield tensile resistance equal to 1.1 times the expected brace tensile yield strength. Two reasons may explain this observation: the material yield strength or the cross-section dimensions of the brace do not correspond to those measured in the ancillary test program. Strain hardening developed in the last tension cycle of the test, i.e., after the brace

overall axial elongation reached approximately 2%. The maximum load reached in the test was equal to 1460 kN.

Table 3.5: Key response parameters for specimen No.1

Specimen Number 1 (VF-S-C-1)	
Failure mode	No failure
Maximum brace load	1460 kN (1.19 AR_yF_y)
Maximum equivalent storey drift	4%
Maximum total brace deformation	138 mm (2.13% L)
Maximum total connection deformation	28 mm (0.43% L)
Maximum net brace deformation	110 mm (1.7% L)

a)

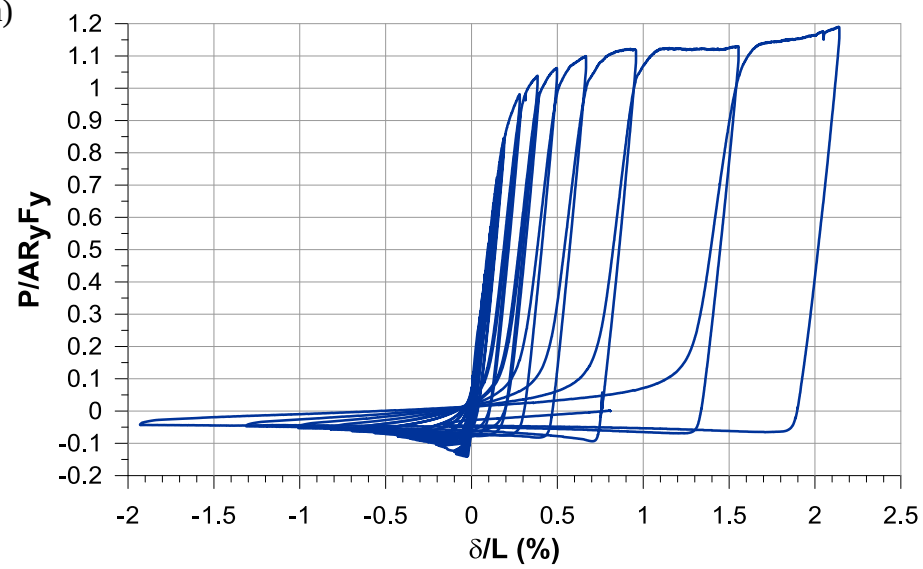

Figure 3.19: Specimen No. 1 - Overall brace response: a) axial displacement; b) storey drift

b)

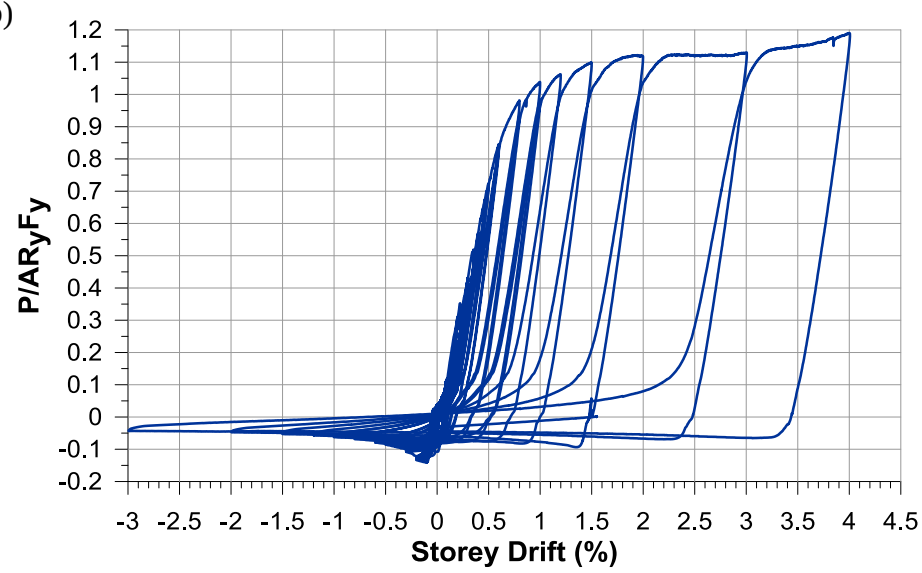

Figure 3.19: Specimen No. 1 - Overall brace response: a) axial displacement; b) storey drift (continued)

Figure 3.20 shows the brace lateral deformations at the middle, one-quarter, and three-quarter of the brace length. The response in this figure is up to 2% storey drift in tension and 1.5% storey drift in compression because the string pots used to record the lateral deformations at one-quarter and three-quarter of the brace length were disconnected after 2% storey drift in tension. As shown in the figure, the lateral deformation at ¼ brace length is slightly larger than the deformation at ¾ brace length. This is consistent with the observed behaviour during the test: the gap between the two angles closed sooner in the lower brace segment. Moreover, due to the permanent brace elongation gradually increasing in the tension excursions, the curves shift upward at cycles with larger amplitudes. In addition, the lateral deformations are always positive, even in the tension phases. This is because the two legs move toward each other, and the lateral instruments are connected to only one leg.

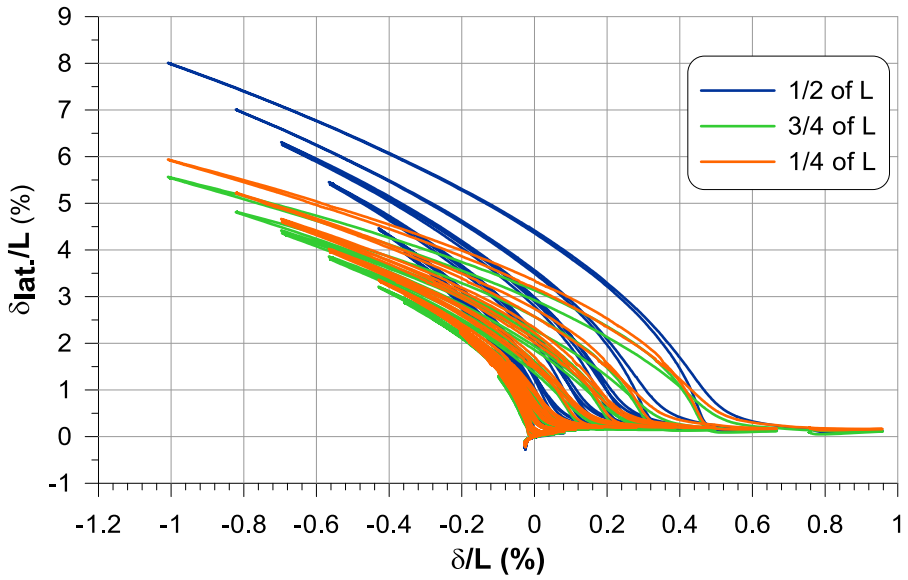

Figure 3.20: Specimen No. 1 - Lateral deformation *vs.* axial displacement

The measured connection response is shown in Figure 3.21a. The connection deformation includes yielding of the brace in the connection regions, yielding of the gusset plates, bearing of the bolts against the connected elements, shear deformations of the bolts, and slippage of the bolts. The two end connections withstood the entire loading protocol, without failure. The strengthened connections achieved the design objective of developing gross section yielding of the brace. The brace elongation dissipates the majority of the energy corresponding to the applied load. The brace connections mainly deformed during the tension excursions because the brace axial loads in compression were too small to deform the connections. The two end connections developed a total deformations corresponding to 0.43% of the total brace length, which is approximately 20% of the overall brace axial deformation. This corresponds to 0.8% equivalent storey drift. In this figure, the connection response on the tension side is more accurate than the response on the compression side because the average deformation from the two string pots that were used to measure the deformation in one connection did not function properly due to the gusset plate bending about the rotational hinge zone as shown in Figure 3.22. However, this is not important because the connection deformations under compression forces are very small, and the compression loads are also very small.

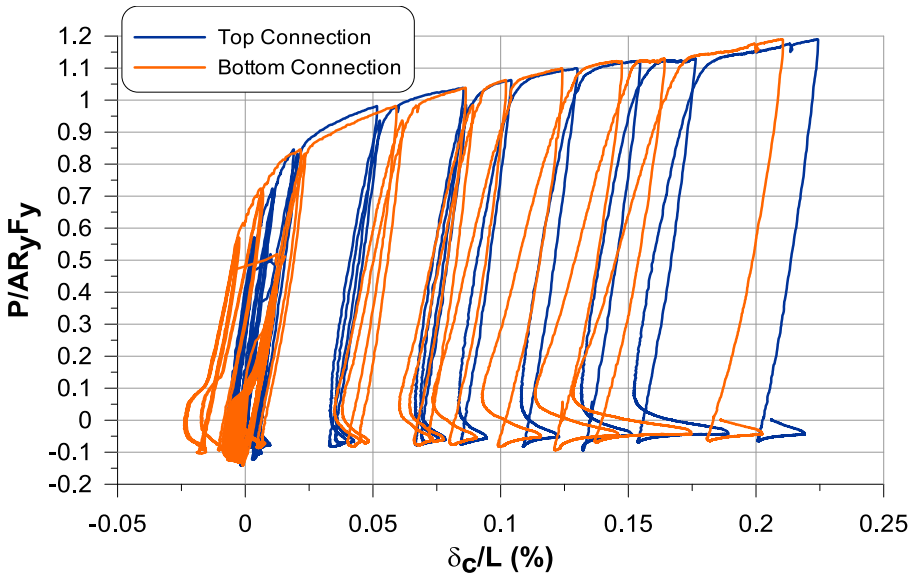

Figure 3.21: Specimen No. 1 - Brace connection response in axial direction

The net brace response on the tension side is shown in Figure 3.22. The net brace deformation response is obtained from overall brace deformation response minus the total deformation of the two end connections. Because of the lack of accuracy in the measurement of the connection deformations in compression, as discussed in previous paragraph, the net brace response on the compression side is not shown. The net brace yielding corresponds to 1.7% of the brace length, which is approximately 3.2% equivalent storey drift. Hence, the majority of the brace ductility and energy dissipation are from the yielding of the bracing member. Combining the net brace response and the overall brace response (Figure 3.19b), yielding of the brace gross section starts at the cycles with 1.0% storey drift amplitude. In addition, strain hardening of the brace starts at 1.5% overall brace deformation, which is 1.2% net axial brace deformation.

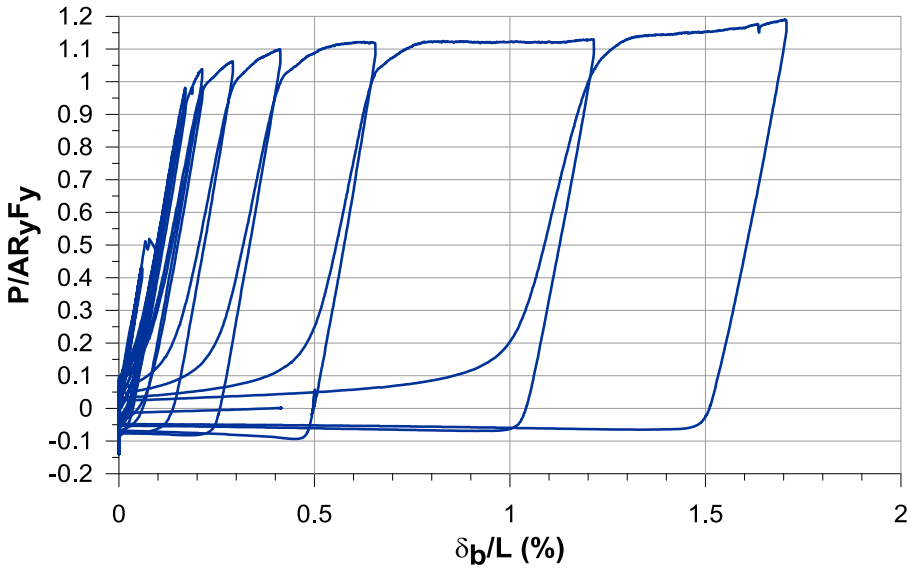

Figure 3.22: Specimen No. 1 - Net brace response under tension

This test shows that adopting a retrofit strategy where the net section of the brace is strengthened can be very successful to achieve ductile brace response. By welding cover plates to the short legs of the angles in the connection region, the connection can become strong enough to develop yielding of the brace which, in turn, can provides most of the ductility and the energy dissipation capacity in a braced frame. In short, this retrofit strategy I can be recommended, provided that the forces induced by the bracing members can be resisted by the other structural components of the braced frames.

3.3.2 Test LF-O-C-1 (Original connection design) (Specimen 2)

This is the first test performed in the 12 MN load frame. A double angle brace with the original connection design is tested.

3.3.2.1 Observed behaviour

Generally, the overall brace behaviour under compression force is similar to the observed behaviour in test VF-S-C-1. Figure 3.23a shows the buckling behaviour of the brace. Figure 3.23b shows the out-of-plane bending of the brace about the rotational hinge in the gusset plate. For the behaviour under tension, the brace connections started to yield at 16.5 mm axial displacement, which is equivalent to 0.5% storey drift as shown in Figure 3.23c. In-plane bending of the brace in the connection regions was observed at 0.6% equivalent storey drift, as shown in Figure 3.23d. In

the subsequent cycles, the brace stopped deforming in the connection regions. Yielding of the bracing member was observed. The connection was stronger than what we expected. Finally, the top connection broke at 4.2% equivalent storey drift, during the cycle from -4% to 5% storey drift with the imposed axial displacement reached 135 mm.

Figure 3.23: Specimen No. 2 - Observed behaviour during the test: a) Buckling of the brace; b) out-of-plane bending about gusset plate hinge; c) yielding on net section; d) in-plane bending of the brace in the connection region

Failure of the specimen occurred by rupture on the net section of the brace happens at the top connection, as shown in Figure 3.24a. The failure plane followed a zigzag pattern, not a straight line: it started at the angle toe of the long leg, close to the second bolt hole, then crossed the first bolt hole (closest to the brace center) and then continued to the rest of the long leg and passed

through the whole short leg up to the toe of the short leg. Necking of the brace cross-section could be observed at both ends of the failure plane. Figure 3.24c shows the necking of the short leg. Initiation of cracking at the position of the second bolt hole coincides with the location where steel yielding initiated in the connection due to stress concentration, bolt bearing, and in-plane brace bending. Figure 3.24d shows cracks around the bolt hole after the test. Necking of the brace was also observed in the bottom connection, as shown in Figure 3.24e, but this was less clear. This suggests that the bottom connection stopped deforming at a certain point because the top connection became the weakest point in the whole brace-connection assembly. Yielding of the gusset plate is shown in Figure 3.24f.

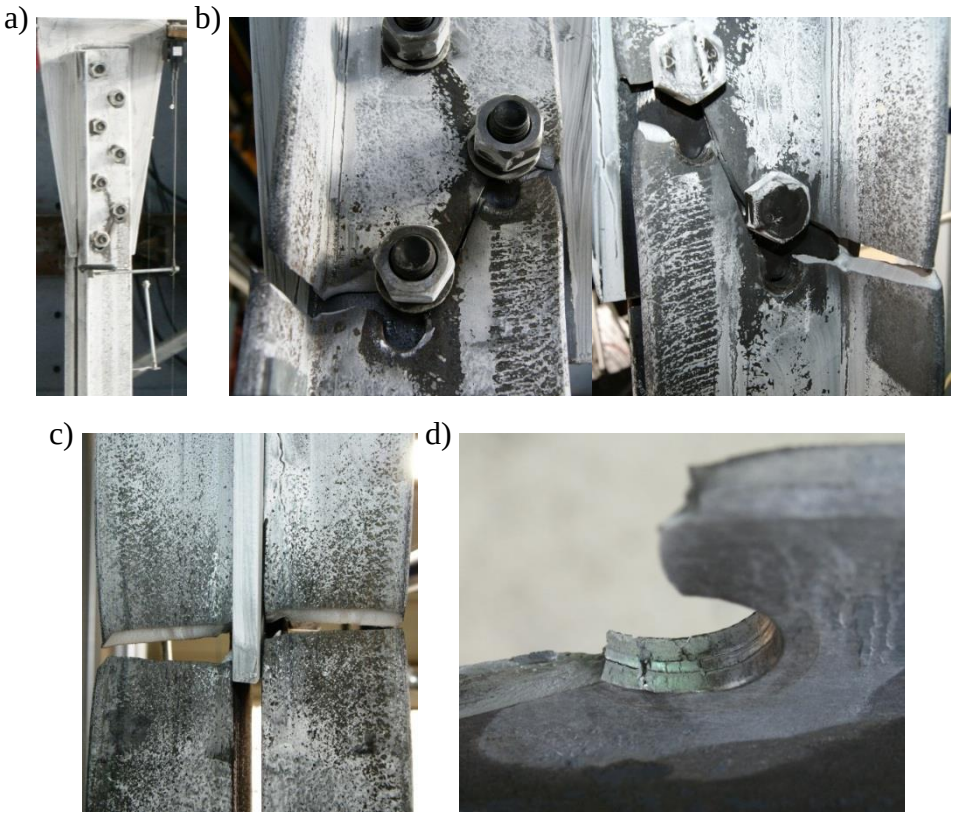

Figure 3.24: Specimen No. 2 - Observed damage after the test: a) net section rupture at connection; b) fracture plane; c) necking on short leg; d) cracks near bolt hole; e) necking at net section in the bottom connection; f) yielding of the gusset plate

e)

f)

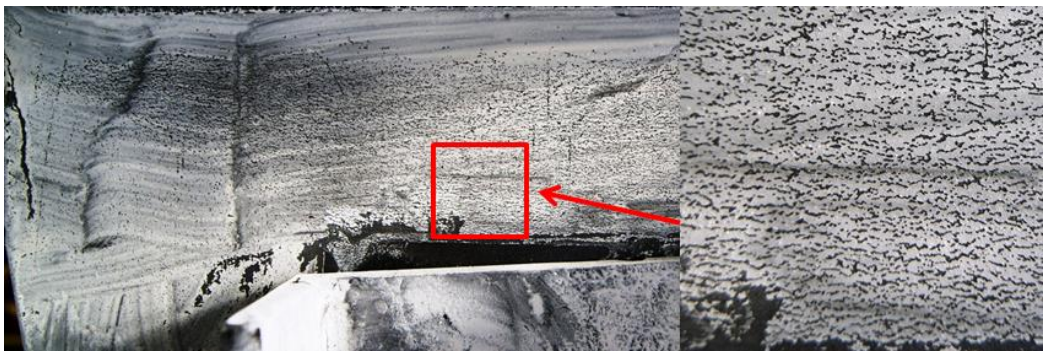

Figure 3.24: Specimen No. 2 - Observed damage after the test: a) net section rupture at connection; b) fracture plane; c) necking on short leg; d) cracks near bolt hole; e) necking at net section in the bottom connection; f) yielding of the gusset plate (continued)

3.3.2.2 Test results

The main response parameters for this specimen are summarized in Table 3.6. Failure point is the point where cracks in the connection region were observed, which corresponds to the point where the maximum force recorded in many cases. Net section rupture of the connection occurred at a load of 1423 kN. This is 10% higher than the probable resistance of the connection based on measured material properties (1299 kN). This means that the current equation in CSA S16-09 that is used to calculate net section rupture capacity is conservative. Based on Equation 2.18, the resistance associated to net section rupture depends on the effective net cross section area and the probable tensile strength of steel. The tensile strength obtained from the coupon tests is reliable because very consistent F_u values were obtained from both the short and long angle legs. Hence, the error probable comes from the effective net cross section area. According to the S16-09 requirement, only 80% of the net cross section can be considered as the effective net cross section

for this connection configuration to account for shear lag effects. This reduction may too conservative for this particular connection configuration. Stress on the net section may also be redistributed due to the yielding observed in the connection and this redistribution may be more important under cyclic loading.

As shown in the overall brace response of Figure 3.25, the brace reached its yield tensile strength before connection failure. The brace yield strength is 10% higher than the expected yielding capacity. As was observed in the pinned vertical frame test, this is likely because variability in the material yield strength compared to the coupon tests.

Table 3.6: Key response parameters for specimen No.2

Specimen Number 2 (LF-O-C-1)	
Failure mode	Brace net section rupture
Maximum brace load	1423 kN (1.16 AR_yF_y)
Brace load at failure	1423 kN
Equivalent storey drift at failure	4.2%
Total brace deformation at failure	135 mm (2.2% L)
Total connection deformation at failure	19.7 mm (0.32% L)
Total net brace deformation at failure	115.3 mm (1.89% L)
Connection deformation failed connection at failure	13.8 mm (0.23% L)

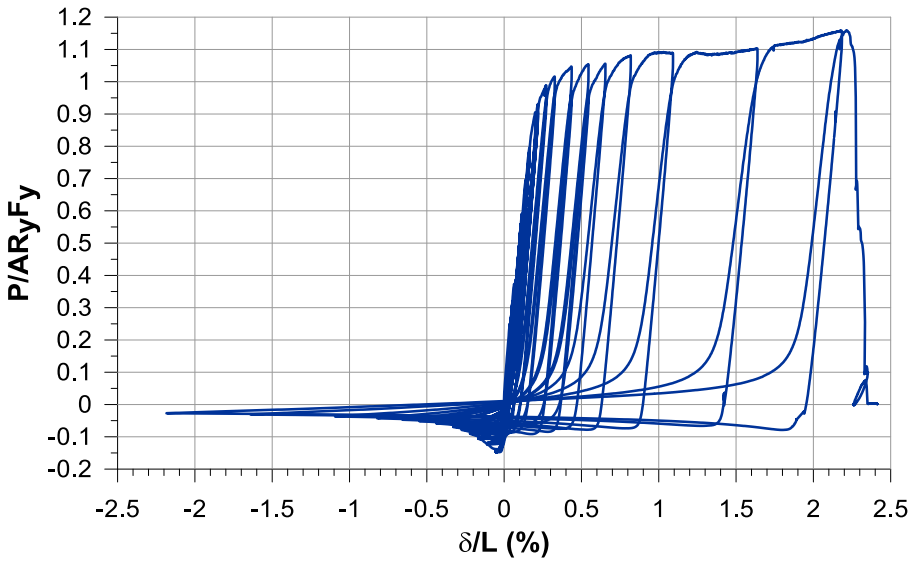

Figure 3.25: Specimen No. 2 - Overall brace response

From the connection response in Figure 3.26, the fracture load level is almost the same as the load level reached in the previous cycle at 4% storey drift on the tension side. The connection sustained one more cycle and then broke at the same force level, probably due to the fatigue under cyclic loading. The two connections could provide a total of up to 19.7 mm elongation in the test, which is about 0.32% of the brace length. After the top connection reached its maximum force level, it deformed another 3 mm while the force level didn't decrease much. In addition, the net brace elongation is 1.89% of the brace length, as shown in Figure 3.27. Figure 3.28 shows the lateral deformation at the brace mid-length. The tested double angle brace is very flexible with 940 mm lateral deformations recorded at 4% storey drift under compression.

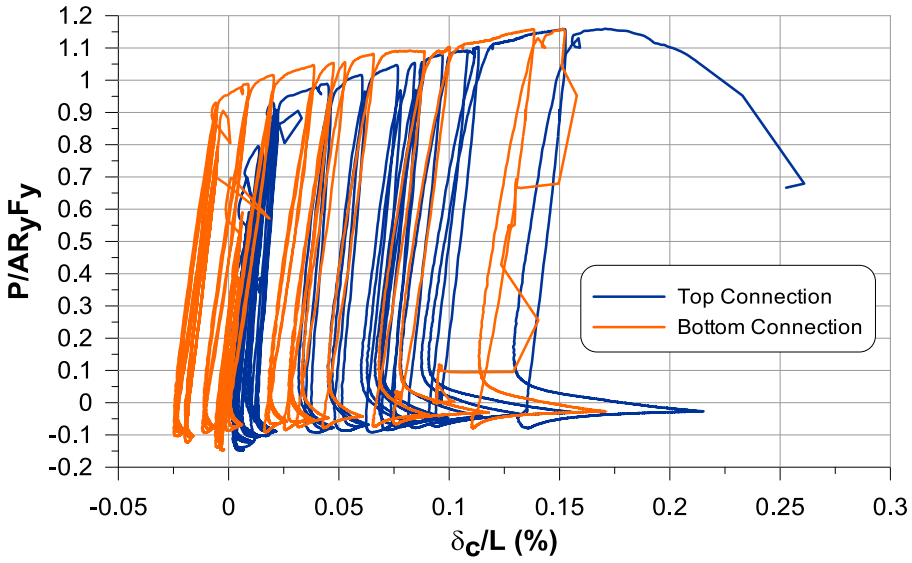

Figure 3.26: Specimen No. 2 - Connection response in axial direction

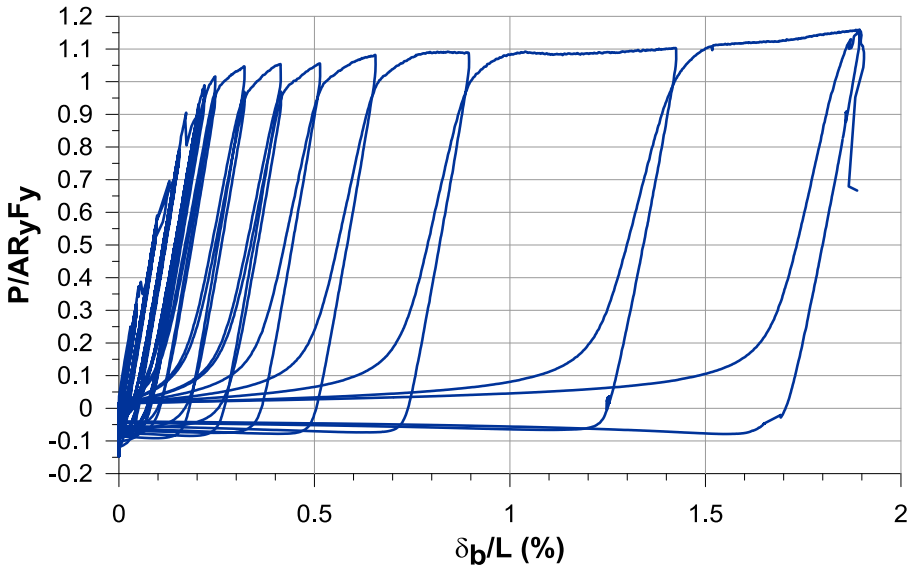

Figure 3.27: Specimen No. 2 - Net brace response under tension load

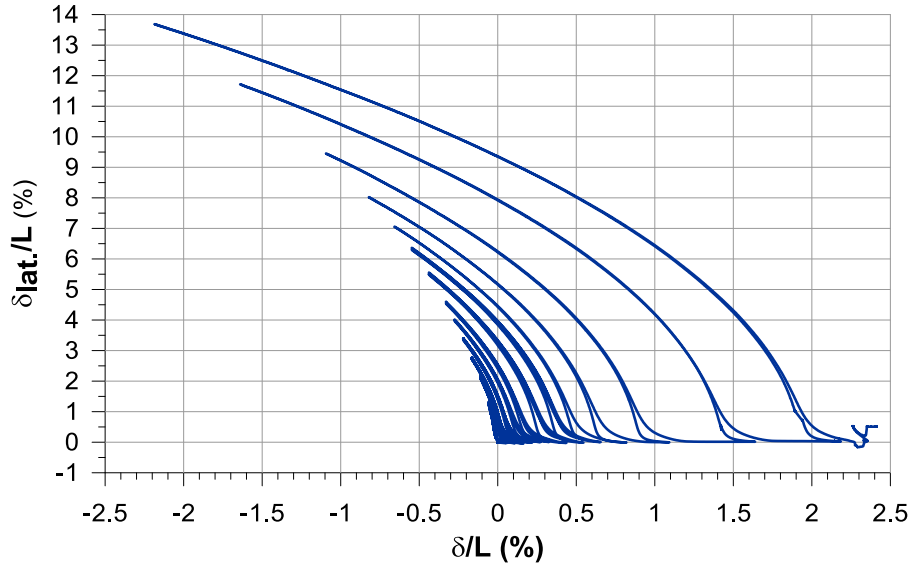

Figure 3.28: Specimen No. 2 - Lateral deformation *vs.* axial displacement

Based on the test results, the original connection design was strong enough to trigger gross section yielding of the brace and the brace exhibited good ductility with large overall axial deformation capacity. Although the specimen eventually failed at one of the brace end connections, the test suggests that it would not be necessary to retrofit this brace-connection assembly because of the ductility that was achieved. However, this behaviour is probable heavily dependent on material properties, meaning that another, less ductile response could have been observed had the material

properties been slightly different. It is also possible that steels used in the 1980's do not have the same properties as the steel that was used to fabricate the test specimens. The code equation for net section rupture with shear lag effects may also be too conservative, leading to incorrect prediction of the brace connection. Thus, the two proposed retrofit strategies aiming at reducing the connection strength and increasing the connection ductility are still of interest in cases where brittle connection failure is likely.

3.3.3 Test LF-R1-C-1(Retrofit strategy II) (Specimen 3)

Retrofit strategy II is applied to the end connections used in this test. The design objective of this retrofitted connection design with slotted holes drilled in the gusset plate is to control the force level in the braced frame while improving the ductility capacity of the system.

3.3.3.1 Observed behaviour

The retrofitted connections before the test are shown in Figure 3.29a. In the test, yielding of the retrofitted gusset plate started at 0.3% equivalent storey drift. As show in Figure 3.29b, yielding started on the left hand side due to the in-plane bending response of the brace and the location of the last bolt hole. The whole gusset plate yielded non-uniformly at 19.97 mm total axial displacement, which corresponds to 0.6% storey drift (Figure 3.29c). Finally, the test was stopped at 1.0% equivalent storey drift, after tension rupture had developed at the bottom connection over nearly half the width of the net section of the gusset plate across the slotted holes (Figures 4.29d and 4.30). The test was interrupted at this point because of the significant in-plane bending deformations that had formed and could have damaged the string pots. In Figure 3.29d, necking was observed between the slotted holes and the two sides of the gusset plate. Two cracks developed in the two segments where yielding was first observed in the gusset plate. The double angle brace remained elastic during the test. At the end of the test, yielding developed at the net cross section of the brace around the first and second bolt holes in the connection region. The overall brace response in compression was similar to the one observed in the previous cyclic tests.

a)

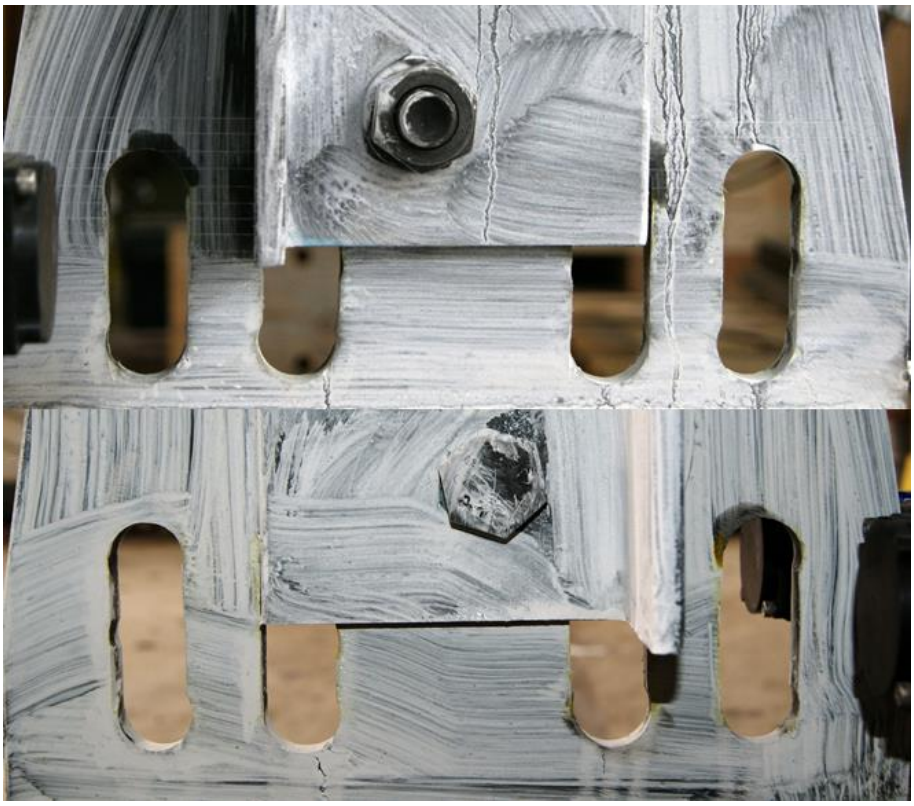

b)

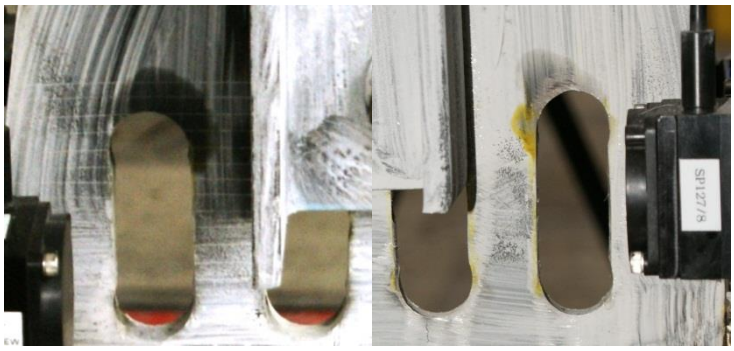

Figure 3.29: Specimen No. 3 - Observed behaviour of gusset plate in the region with slotted holes during test: a) before test; b) initiation of yielding near the slotted holes; c) yielding of the whole gusset plate; d) necking and initiation of tension rupture of the gusset plate

c)

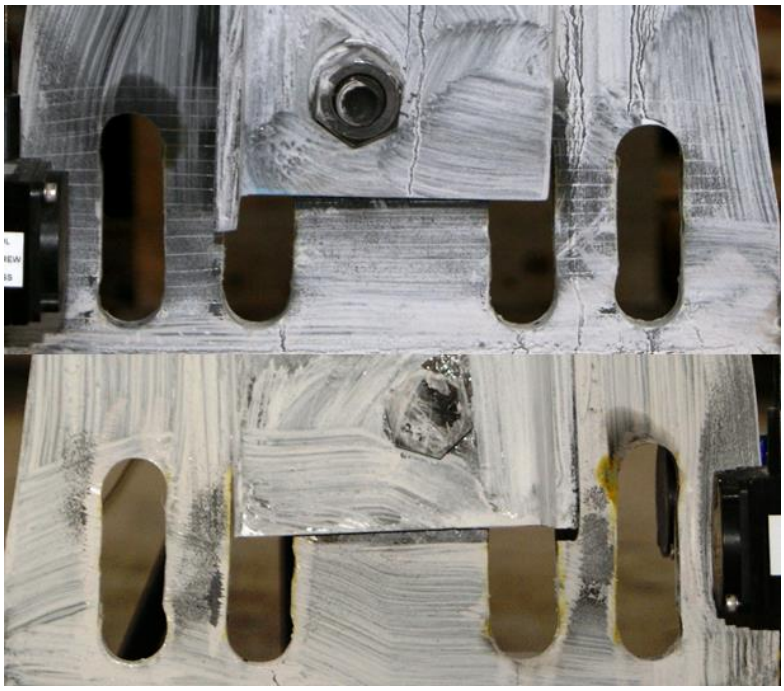

d)

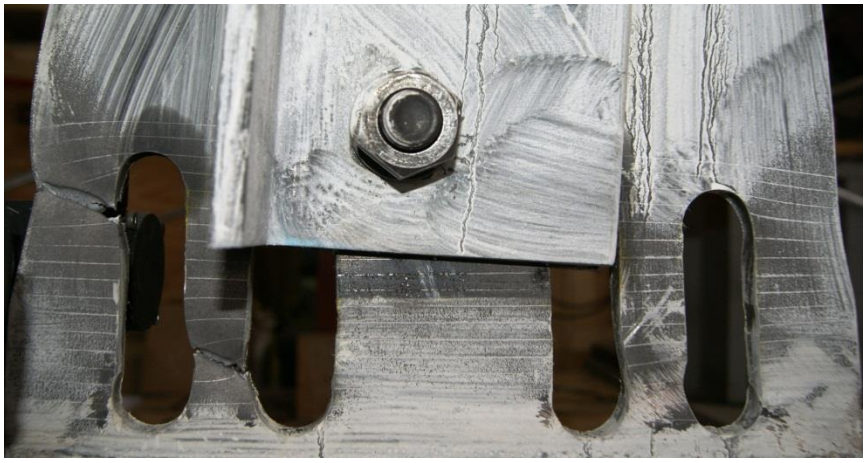

Figure 3.29: Specimen No. 3 - Observed behaviour of gusset plate in the region with slotted holes during test: a) before test; b) initiation of yielding near the slotted holes; c) yielding of the whole gusset plate; d) necking and initiation of tension rupture of the gusset plate (continued)

Figures 4.30a and 4.30b show the region with the slotted holes in the gusset plate at the bottom and top connections after the test. Light grey areas in the figure correspond to regions where yielding took place during the test. No crack developed in the gusset plate at the top connection because the deformations in that gusset stopped once cracking initiated at the bottom of gusset plate. The yielding direction and pattern is the same from the left hand side to the right hand side due to brace in-plane bending and the position of the last bolt hole.

a)

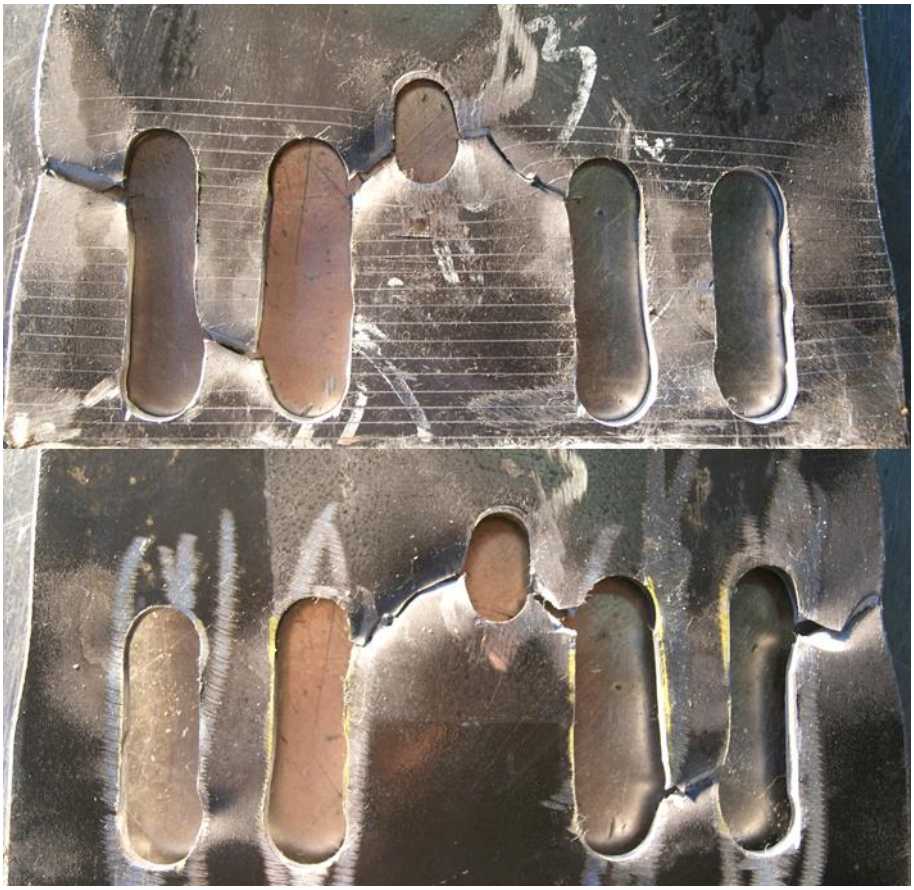

Figure 3.30: Specimen No. 3 - Observed behaviour of gusset plate in the region with slotted holes after test: a) gusset plate at bottom; b) gusset plate at top

b)

Figure 3.30: Specimen No. 3 - Observed behaviour of gusset plate in the region with slotted holes after test: a) gusset plate at bottom; b) gusset plate at top (continued)

3.3.3.2 Test results

The main response parameters for this specimen are summarized in Table 3.7. In the test, tension rupture on the net section of the gusset plate occurred at a load equal to 1174 kN. This is 8.5% lower than the expected design value, which is 1272 kN. This reduced strength is attributed to the non-uniform stress distribution that resulted from brace in-plane bending and asymmetric location of the bolt holes. This led to premature failure of the steel on the left-hand side of the gusset plate. The design objective of controlling the force level was achieved. As shown in Figure 3.31, the overall brace elongation at failure is 0.51% of the brace length, which is approximately 31 mm. Figure 3.32 shows the connection responses. As shown, due to the strain hardening response, similar level of inelastic deformations took place in both connections, which is a desirable behaviour. In total, the two connections provided 22.8 mm elongation, which corresponds to 0.37% of the brace length. From the initiating of crack (failure point) to fracture, another 1.8 mm deformation was obtained from the fractured connection. When comparing with the original

connection, the retrofitted connection with slotted holes resulted in 16% more elongation capacity, which satisfies the second objective of improving the system ductility. The net brace response is shown in Figure 3.33. The curve reflects nearly perfectly linear response in tension, meaning that the bracing member remained nearly elastic until the end of the test. In addition, very limited energy was dissipated by the brace under tension loading.

Table 3.7: Important response parameters for specimen No.3

Specimen Number 3 (LF-R1-C-1)	
Failure mode	Gusset net section rupture
Maximum brace load	1174 kN (0.96 AR_yF_y)
Brace load at failure	1174 kN
Equivalent storey drift at failure	0.93%
Total brace deformation at failure	30.8 mm (0.51% L)
Total connection deformation at failure	22.8 mm (0.37% L)
Total net brace deformation at failure	8 mm (0.13% L)
Connection deformation failed connection at failure	12.3 mm (0.2% L)

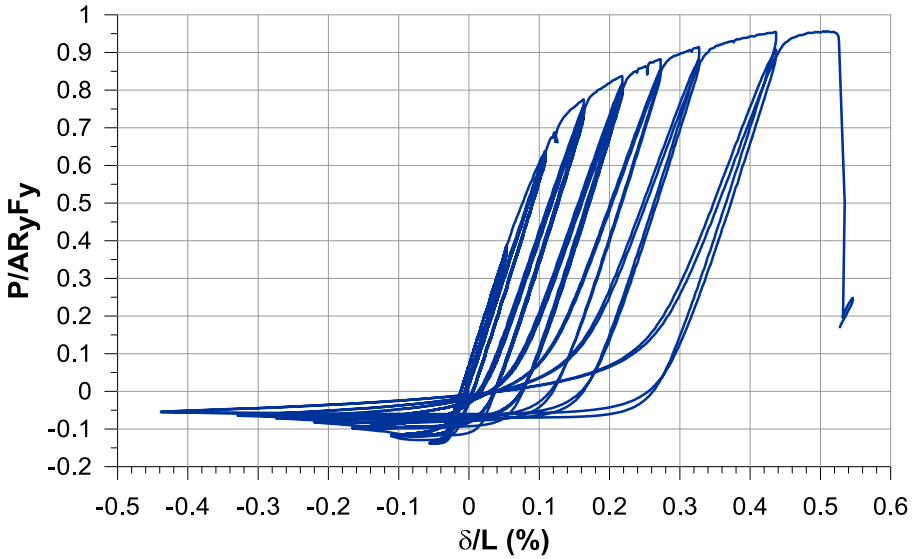

Figure 3.31: Specimen No. 3 - Overall brace response

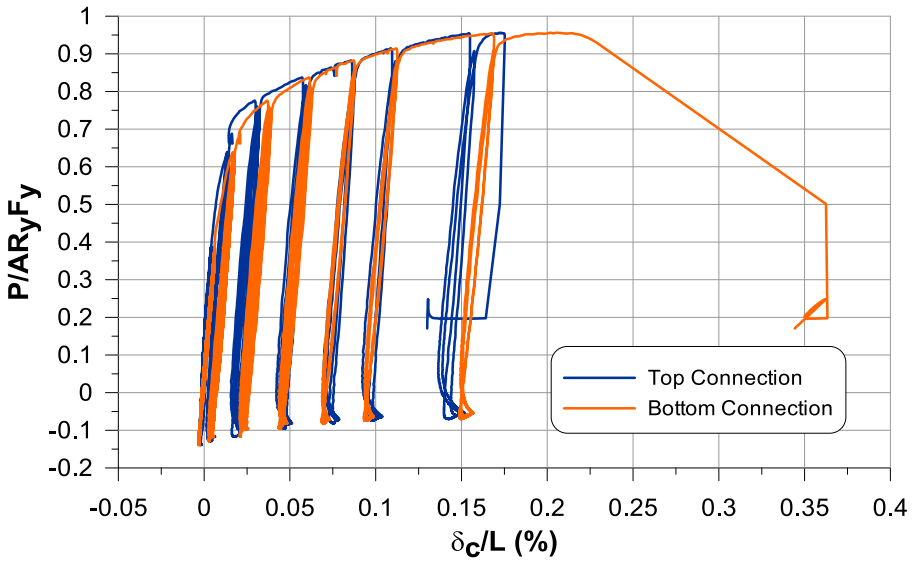

Figure 3.32: Specimen No. 3 - Brace connection response in axial direction

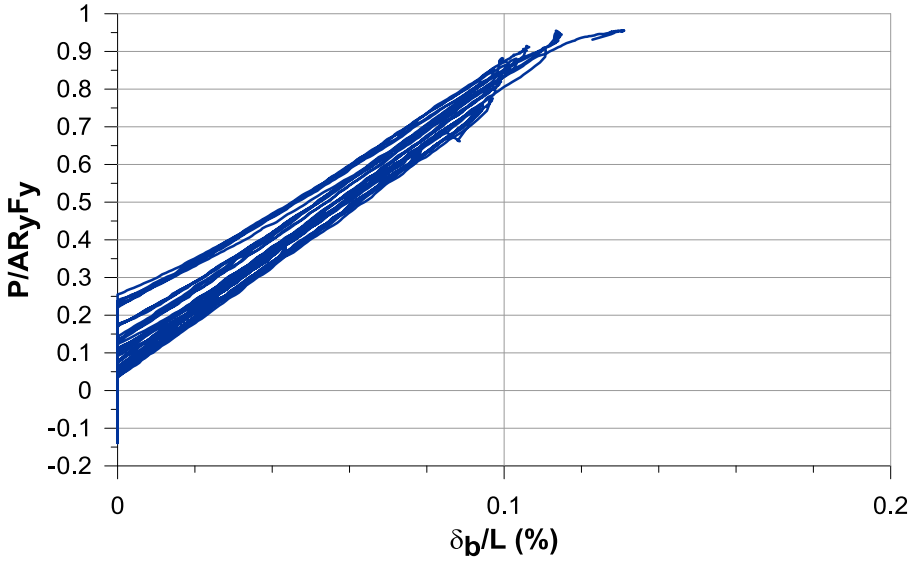

Figure 3.33: Specimen No. 3 - Net brace response

Based on the test results, the force level could be controlled with the proposed retrofitted connection while increasing the connection ductility. However, the overall brace ductility capacity has been reduced because the brace remained nearly perfectly elastic. Failure occurred at 1% equivalent storey drift, which would be acceptable only for braced frames of the Conventional Category (Type CC). In view of the limited capacity of the brace-connection assembly, it is necessary to verify through nonlinear time history analysis if the slotted holes used in the gusset

plates can provide sufficient inelastic deformation capacity before failure to prevent overloading of the frame components. This task will be performed in the subsequent chapters.

3.3.4 Test LF-R2-C-1 (Retrofit strategy III) (Specimen No. 4)

Connections with retrofit strategy III where the strength of the connections is reduced by promoting shear yielding of gusset plate segments located in front of the connecting bolts are used in this test. The assembled brace-connection assembly in the 12 MN load frame looks the same as the brace configuration in Test LF-O-C-1 because the retrofitted gusset plates are covered by the brace and the retrofit scheme is not visible in the connection region.

3.3.4.1 Observed behaviour

The behaviour observed in this test was different from what was expected. It is similar to the behaviour observed in Test LF-O-C-1 built with the original connection design. The retrofitted connections was found to be too strong to engage shear yielding of the steel segments created in front of the connecting bolts. Instead yielding took place in the gross and net section of the bracing members. The brace eventually failed in tension on net section at an axial displacement in the tension direction of 144 mm. The test was then stopped at approximately 4.4% equivalent storey drift in the cycle where the equivalent storey drift was gradually increased from -4% in compression to 5% in tension.

The specimen with retrofitted connections was more ductile than the original brace-connection design. As shown in Figure 3.34a, the relative movement between the brace and the gusset plate in the connection region is more pronounced. The failure plane in the angle brace at the top connection is shown in Figure 3.34b. The fracture line combined shear and tension failure along the zig-zag net brace section. Figures 4.34c and 4.34d show the top and bottom gusset plates after the test. Generally, the steel segments in front of behind the first hole and the last hole have the largest deformations induced by bolt bearing. In addition, the steel material in the vicinity of all the additional small holes that have been drilled has sustained some degree of inelastic deformation. They then dissipated some energy during the test.

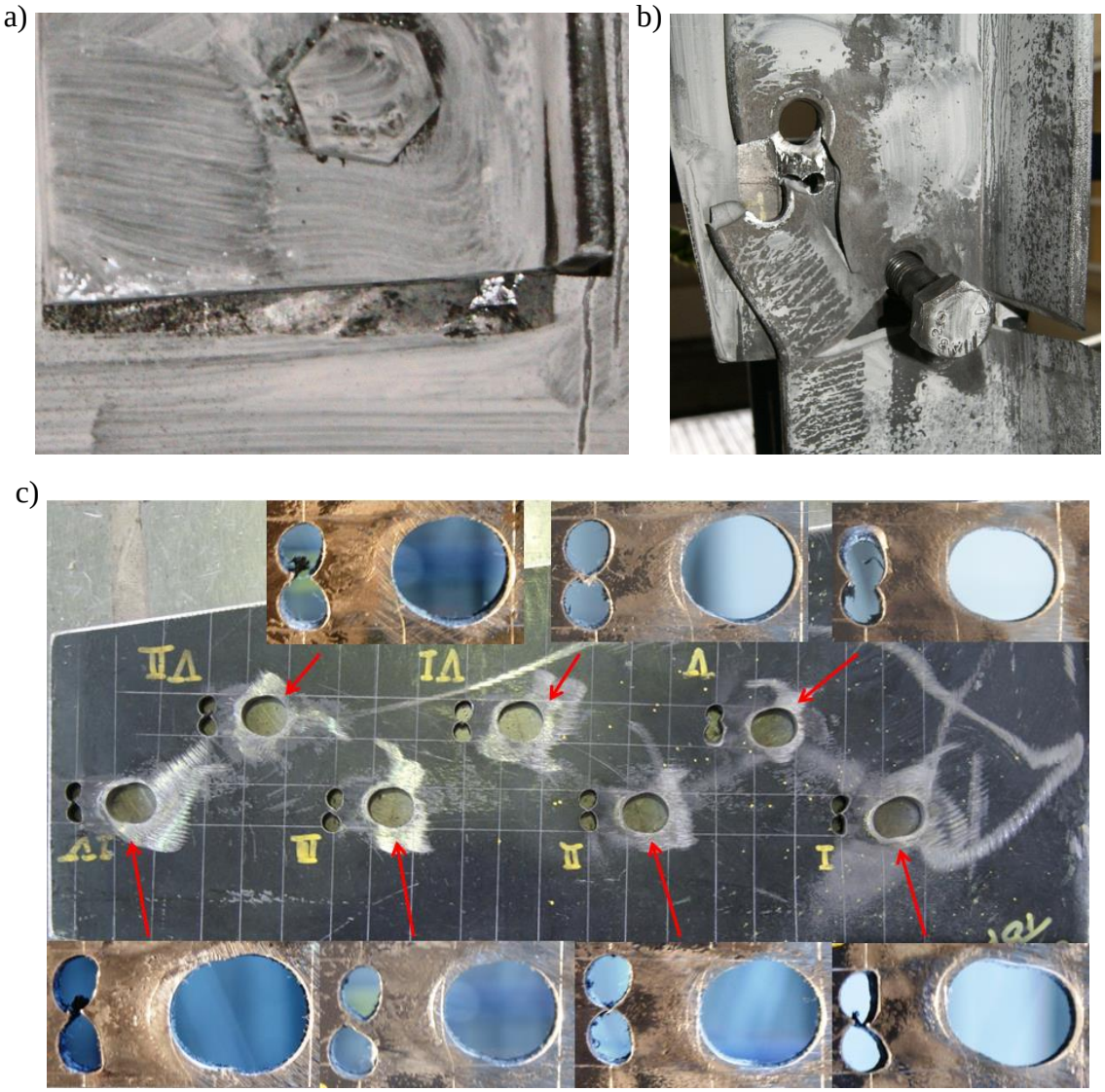

Figure 3.34: Specimen No. 4 - Observed damage after the test: a) relative displacement between the brace and the gusset plate; b) fracture plane; c) & d) local inelastic deformations near the bolt holes in the top (c) and bottom (d) gusset plates

d)

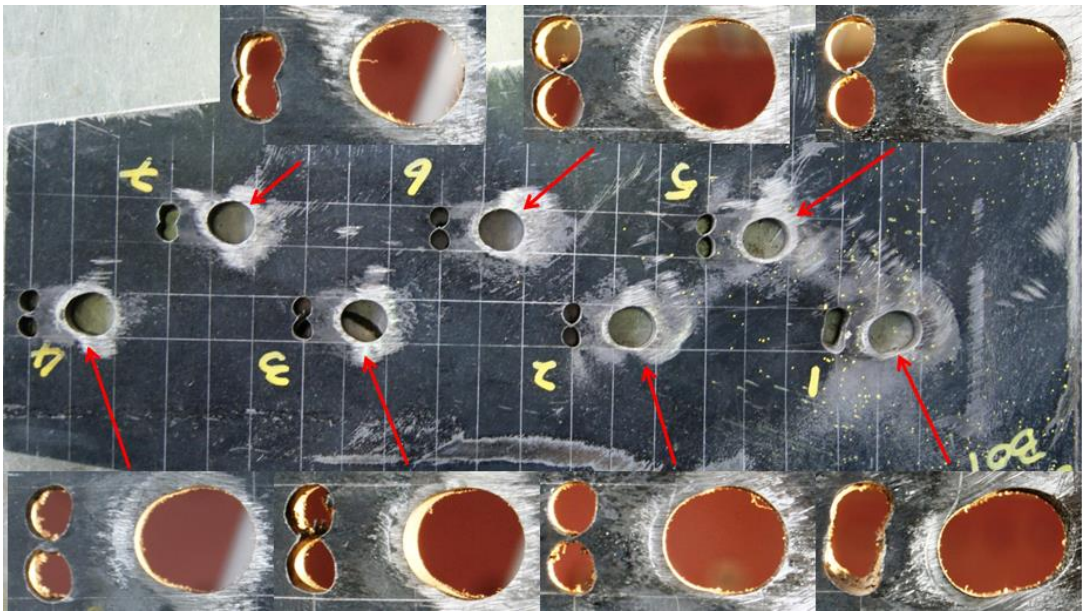

Figure 3.34: Specimen No. 4 - Observed damage after the test: a) relative displacement between the brace and the gusset plate; b) fracture plane; c) & d) local inelastic deformations near the bolt holes in the top (c) and bottom (d) gusset plates (continued)

3.3.4.2 Test results

The main response parameters for this specimen are summarized in Table 3.8. Figure 3.35 shows the overall brace hysteretic response. The maximum force that developed in this specimen was 1415 kN, as governed by the tension rupture of the angle brace at the net section. According these results, the maximum resistance developed in the specimen during the test was not controlled by the retrofitted connection and the proposed retrofit scheme failed at achieving the main objective which was to limit the force demand on the connection and the brace. The resistance of that specimen is almost the same as the one measured in Test LF-O-C-1 (1423 kN, see Table 3.6). As show in Figure 3.36, inelastic deformations took place in both gusset plates. The total deformation of the two connections is 0.55% of the brace length, which is larger than that obtained for the original connection design (0.39% *L*, see table 4.6). Yielding in the top gusset plate started at a tension load of 860 kN, which is lower than the yield force of the bottom gusset plate (approximately 1100 kN). This difference is probably due to differences in the geometry of the steel segments between the 19.1 mm (¾") bolt holes and the additional smaller holes drilled in the gusset plates. The difference in resistance between the two gusset plates gradually reduced as inelastic deformations took place in the gusset plates. As shown in Figure 3.37, the net brace

elongation at failure is 110 mm, which shows that the brace contributed significantly to the specimen ductility.

Table 3.8: Key response parameters for specimen No.4

Specimen Number 4 (LF-R2-C-1)	
Failure mode	Brace net section rupture
Maximum brace load	1415 kN (1.15 AR_yF_y)
Brace load at failure	1210 kN
Equivalent storey drift at failure	4.31%
Total brace deformation at failure	144 mm (2.34% L)
Total connection deformation at failure	33.7 mm (0.55% L)
Total net brace deformation at failure	110 mm (1.79% L)
Connection deformation failed connection at failure	21.6 mm (0.35% L)

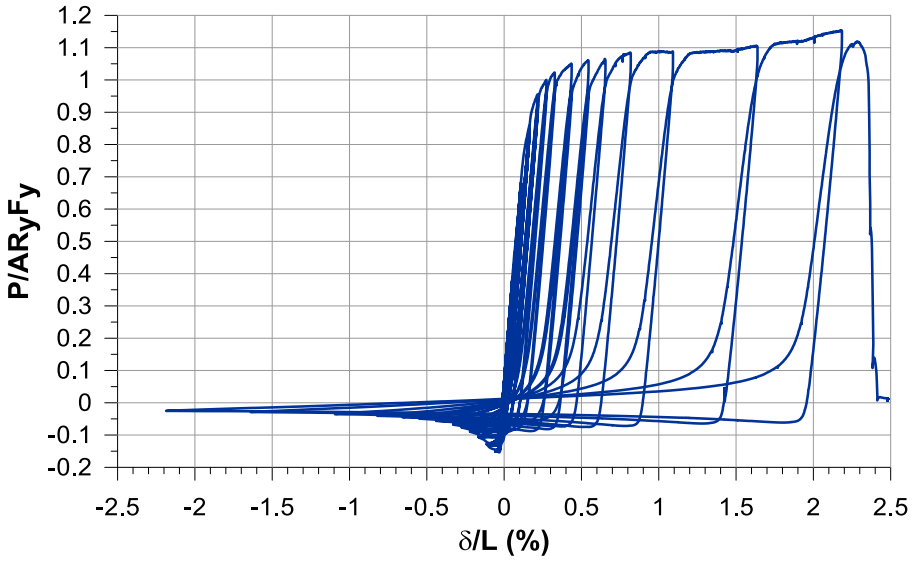

Figure 3.35: Specimen No. 4 - Overall brace response

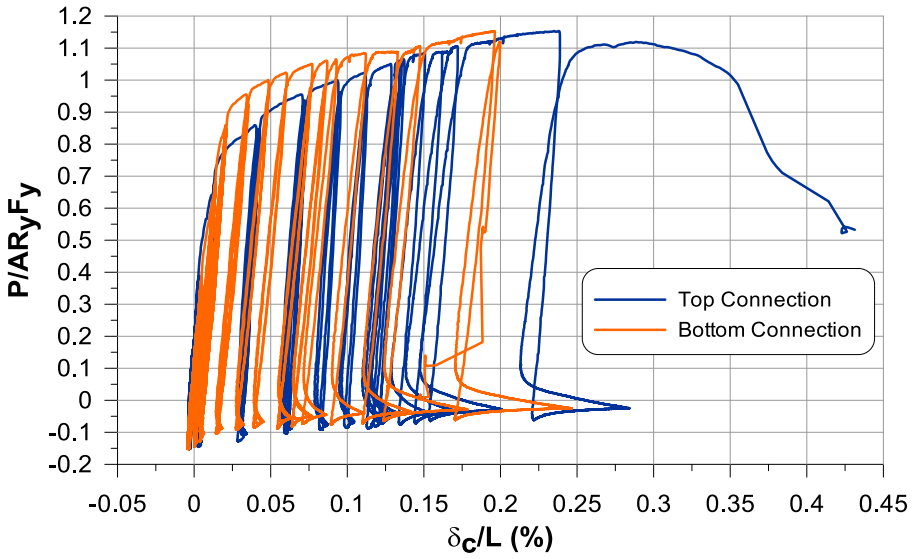

Figure 3.36: Specimen No. 4 - Connection response

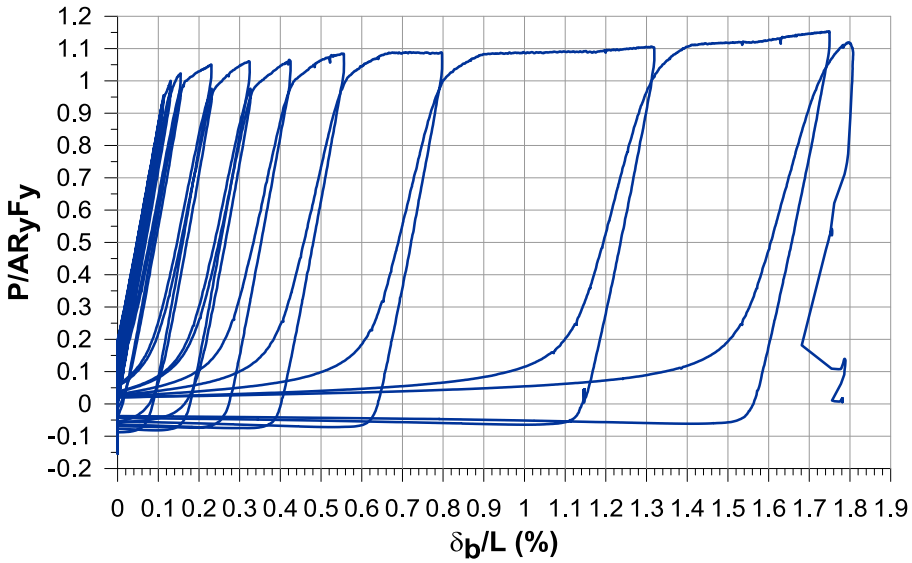

Figure 3.37: Specimen No. 4 - Net brace response

As mentioned, this specimen with retrofitted connections exhibited a higher global ductility compare to the original design. However, the ductility of the connection detail was still limited. In addition, the response of the retrofitted connection appeared to be difficult to control. In particular, it seems to be hard to accurately predict the yield and ultimate strengths of this connection. Further study is needed before this retrofit strategy can be implemented in practice.

3.3.5 Comparison of Retrofit Strategies

Based on the steel properties obtained from coupon tests, the resistances of the original connection and of each of the retrofitted connection were recalculated. The recalculated resistance together with the resistances obtained from the cyclic tests are summarized in Table 3.9. The building assessment results may be affected corresponding to the recalculated resistances of the connections. Of key importance, the results show that gross yielding of angle can happen before the net section rupture of the angle brace in the original connection. This result is opposite to that obtained from the evaluation based on probable resistances. However, it is consistent with the cyclic test results. This means that the ductility performance of a braced frame with the original brace connection may be better than what was expected. Both the recalculated resistance and cyclic test results show that the design objectives of retrofit strategies I and II are achieved. As discussed in Section 3.3.4, retrofit strategy III is not expected to perform well.

Table 3.9: Factored, probable and measured connection resistances

Resistances	Gross yielding of angle (kN)	Original (kN)	Retrofit I (kN)	Retrofit II (kN)	Retrofit III (kN)
Factored	999	893	1331	892	720
Probable	1425	1310	1682	1272	1127
Coupon	1243	1299	1655	1305	1100
Cyclic Test	1375	1423	> 1460	1174	> 1415

3.4 Additional quasi-static cyclic tests

After completing the originally planned test program, it was decided to conduct two additional more tests to study further some interesting points. First, an angle section with bolted end connections fabricated in the 1960s and recuperated from an existing structure was tested to verify if the steel properties could influence the brace response. Especially, the strength and ductility associated to the tension rupture on the brace net section was of interest. Second, a new connection

retrofit strategy (Retrofit strategy IV) is proposed to reduce the connection strength without affecting the ductility of the connection.

3.4.1 Test LF-OLD-C-1 (Old angle brace) (Specimen 5)

In Test LF-O-C-1, the net section rupture of a double angle brace in the connection region was not as brittle as per our expectations. However, Caruso and Rogers (2011, personal communication) observed in tests performed on old angle braced at McGill University that this type of failure mode could be very brittle. One possible reason may be the steel properties such as the carbon content. In Test LF-O-C-1, the double angle brace and gusset plates were designed using CSA S16.1-M78 standard, but the steel used to fabricate the brace and the plates were G40.21-300W steel produced according to current (recent) fabrication standards. In order to verify if actual old angle braces could behave differently, especially the ductility capacity and resistance of the net section rupture mode, a rusted angle brace cut from an existing building was tested in this study.

3.4.1.1 Test specimen

The specimen is a rusted double angle brace 2L-76x51x7.9 (2L-2"x3"x5/16") with 3440 mm length. It was cut from a chevron braced frame in an existing building structure that was built in the 1960s. The dimensions of the original braced frame are unknown. Figure 3.38 shows a sketch of the braced frame with the dimensions that were assumed to develop the test displacement protocol. The double angle brace is shown in Figure 3.39. Three stitch connectors are used along the brace length, with a distance between the stitch connectors of 850 mm. At the brace ends, three 15/16”holes for A325 7/8” bolts are arranged in a single line in the long leg were used for the brace connections. The center-to-center spacing between the holes is 76 mm (3”) and the edge distance and the end distance are both equal to 38 mm (1.5”). The steel grade is unknown. In order to study single angle behaviour under cyclic loading and obtain data to calibrate numerical finite element models of single angle brace in OpenSees, this double angle brace was separated into two single angle braces. One angle is selected to test in the single angle cyclic test. Figure 3.40 shows one of the separated braces. Six 7/8” A325 original bolts shown in Figure 3.41 were used to connect the brace to gusset plate. These bolts were recuperated moved from the same structure as the angle brace specimens. Two new gusset plates designed to be strong enough to remain elastic during the test were fabricated in the Structural Engineering Laboratory of École Polytechnique of Montréal. Figure 3.42 shows the

drawing of the gusset plate. Five measurements of the brace angle thickness were taken in the short and long legs of the angle along the specimen length. The average thickness for the short and long legs are 8.046 mm and 8.148 mm, which is slightly higher than the nominal thickness for this angle size (7.94 mm). The long leg is thicker than the short leg, as was the case for the L127x76x9.5 angles used in the original test program, but the difference is much smaller: 1.3% in this old brace compared to 11% in the newer double angle brace specimens. The effective average thickness is 8.097 mm, which is 2% thicker than the nominal thickness 7.94 mm specified in steel standards. Hence, the effective cross section area for this brace is 964 mm^2, greater than the nominal cross section area of 945 mm^2.

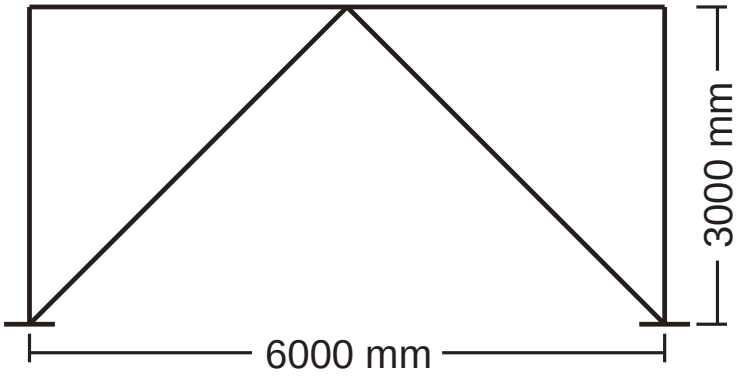

Figure 3.38: Sketch of existing chevron braced frame

Figure 3.39: Rusted double angle brace

Figure 3.40: Separated double angle brace

Figure 3.41: Original 7/8”A325 bolts

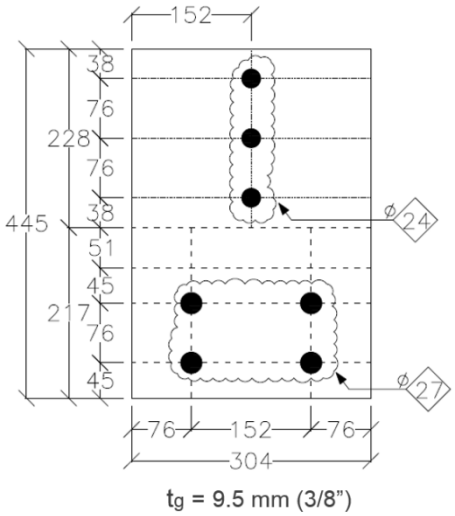

Figure 3.42: Sketch of the gusset plate fabricated for the test

3.4.1.2 Test setup

This test is carried out in the 12MN load frame test platform. Figure 3.43 shows the test setup. The same T-shaped brackets were used in this test. The gusset plates are connected to the T-shaped brackets using four 25.4 mm (1”) A490 high strength bolts. These bolts were pre-tensioned. Hence, load eccentricity exists in the test. Old bolts are tightened by hand, and impact gun is used to torque the 1” bolts.

3.4.1.3 Instrumentation

Instrumentation in this test is the same as the instrumentation in the other 12MN load frame tests. The only difference is the poles using to connect the spools of the string pots that were used to measure the connection deformations because only one short flange was available in this single

angle test to clamp the instrument supports. Figure 3.44 shows the string pots at the bottom gusset plate.

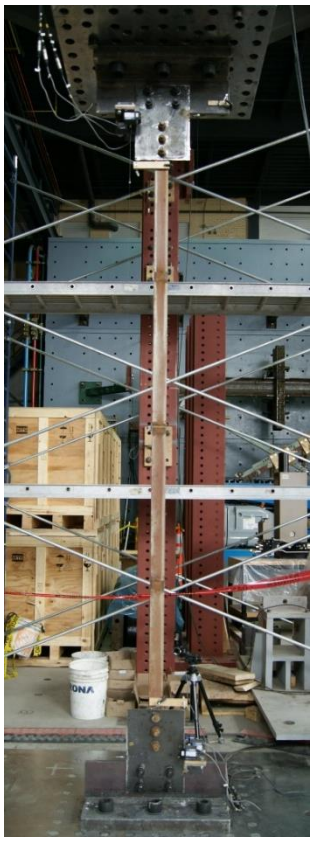

Figure 3.43: Test setup for old single angle brace test

a) b)

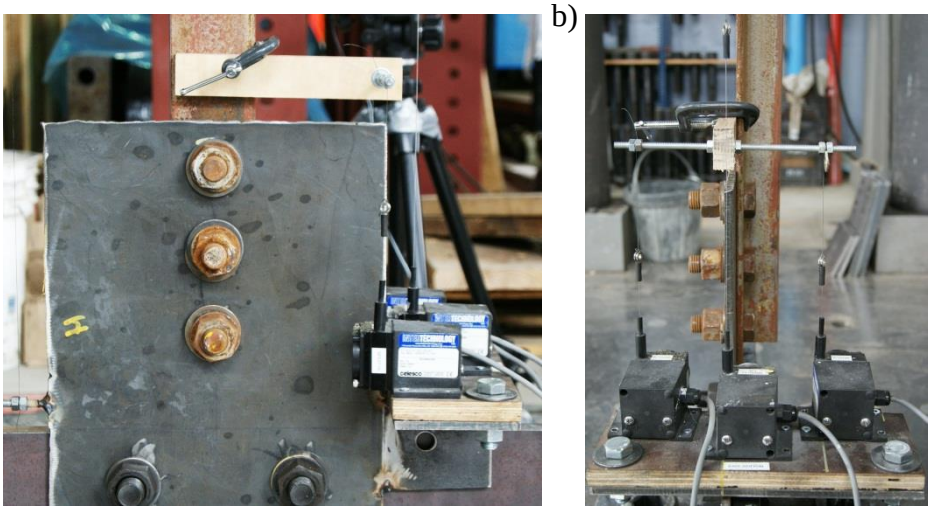

Figure 3.44: Instrumentation at the bottom gusset plate: a) front view; b) side view

3.4.1.4 Loading protocol

The loading protocol used in this test is the one proposed in FEMA 461 (ATC, 2007). This protocol was suggested by A. J. Caruso and Professor C. Rogers of McGill University who used a similar loading protocol in their old brace cyclic tests. Figure 3.45 shows the loading protocol. It starts with 6 cycles of initial displacements at 50% expected yield force. To be conservative, a steel yield strength value of 248 MPa was used to calculate the initial displacement level, which is 2.13 mm based on calculations. Then, the amplitude is increased by 40% of the previous amplitude for each successive group of 2 cycles until a brace deformation corresponding to a maximum anticipated storey drift of 2%, is reached. This storey drift level is considered to be the maximum value for a seismic force resisting system with limited ductility. Based on the braced frame dimensions shown in Figure 3.38, the corresponding brace axial deformation is 34.4 mm at the 2% storey drift. Hence, the last displacement amplitude in the test protocol before reaching the expected storey drift is 31.43 mm (2.13 mm x 1.4^8). After the expected storey drift has been reached, the displacement is increased by 30% for each successive group of 2 cycles until the end of the test. The first displacement amplitude after the 2% anticipated storey drift is 40.86 mm (31.43 x 1.3). The end of the testing protocol is 89.78 mm (31.43 x 1.3^4), which is approximately equal to 5% equivalent storey drift. The displacement rate in the test is 0.3 mm/s, which corresponds to 87.2 με/s.

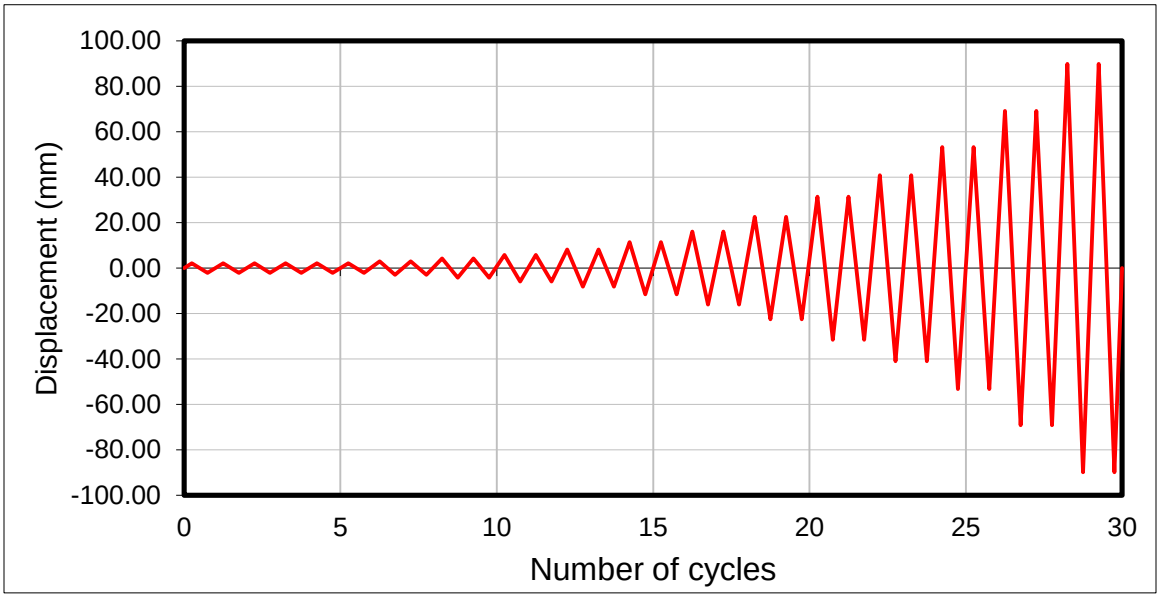

Figure 3.45: Loading protocol for Test LF-OLD-C-1

3.4.1.5 Observed behaviour

Assuming F_y = 248 MPa and F_u = 414 MPa, net section rupture was expected for this brace connection (T_u = 263 kN, $T_{u\text{-}c}$ = 206 kN). The failure plane would be perpendicular to the brace longitudinal axis and cross the first bolt hole closest to the center of the brace. Moreover, for an angle connected through one leg with only three bolts forming a single line, the shear lag factor in CSA S16-09 is 0.6, based on the work by Kulak and Wu (1993). This is more critical than the 0.8 factor that applied for the L127x76x9.5 double angle braces used in the original test program.

Figure 3.46a shows the location where net section rupture was likely to occur. Based on previous test, we also expected that the most critical region would be in the region of the net section located between the first bolt hole and the toe of the short angle leg. Yielding started in that region at a 5.85 mm displacement, as shown in Figure 3.46b. Then the yielded area increased in this region in the subsequent cycles as shown in Figure 3.46c. Necking of the brace at the angle toe close to the first bolt hole was observed at a displacement of 16.06 mm (Figure 3.46d). In the following cycles, the entire brace gross section yielded uniformly until the tension loading phase in the first cycle with 69.15 mm displacement. A crack then initiated close to bolt hole, which is shown in Figure 3.46e. In the tension loading phase of the second cycle with 69.15 mm displacement, complete tension rupture occurred over the most critical region of the net section, as shown in Figure 3.46f. Finally, the fracture line passed through the whole brace net section at around 70 mm displacement in the cycle from -69.15 mm to 89.90 mm displacement. The failure place is at the exact location where net section rupture was expected. Figure 3.46g shows the net section close to complete rupture at that location.

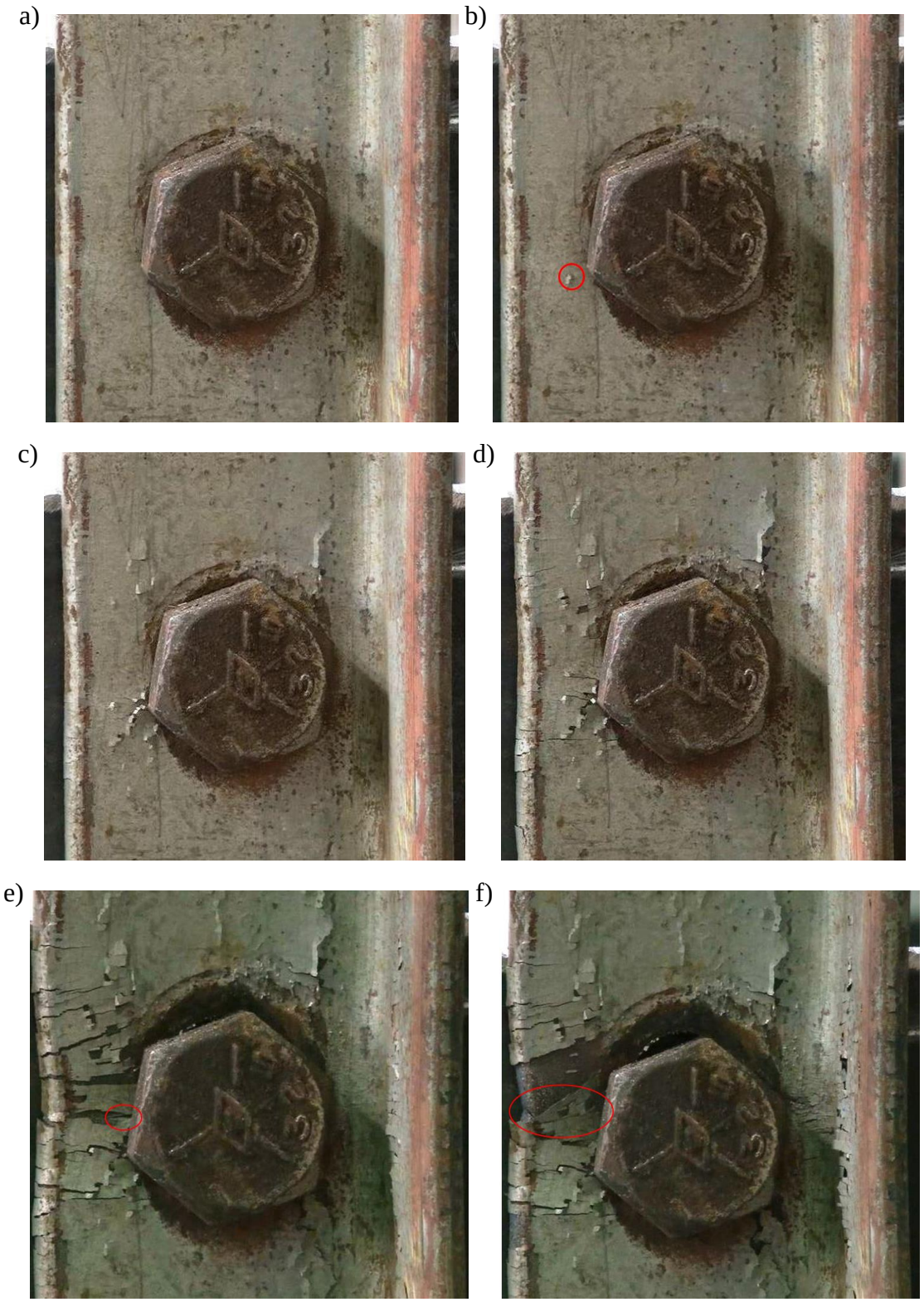

Figure 3.46: Specimen No. 5 - Net section of the old angle brace: a) before test; b) at initiation of yielding; c) upon increasing yielding; d) at necking; e) at initiation of cracking; f) at fracture of the critical region; g) near complete net section rupture

g)

Figure 3.46: Specimen No. 5 - Net section of the old angle brace: a) before test; b) at initiation of yielding; c) upon increasing yielding; d) at necking; e) at initiation of cracking; f) at fracture of the critical region; g) near complete net section rupture (continued)

During the test, other aspects of the behaviour of the single angle brace could be observed under cyclic loading. Figure 3.47a shows in-plane bending of brace under tension loading due to loading eccentricity between the center of gravity of the angle section and the center line of the connecting bolts. When the brace buckled, the buckled shape combined major out-of-plane bending and minor in-plane bending as shown in Figure 3.47b. At the mid-length of the brace, the two legs opened under the compression force, which resulted in an inner angle greater than 90 degrees (Figure 3.47c and 4.47d). In addition, Figure 3.47e and 3.47f shows the bending observed in the gusset plate at the end brace connections.

The residual shape of the brace after the test is shown in Figure 3.48a. The upper and the lower segments of the brace are still straight after the test, which means that only the connections and the middle part of the brace deformed (three plastic hinges) when the brace buckled. The fractured brace cross-section is shown in Figure 3.48b.

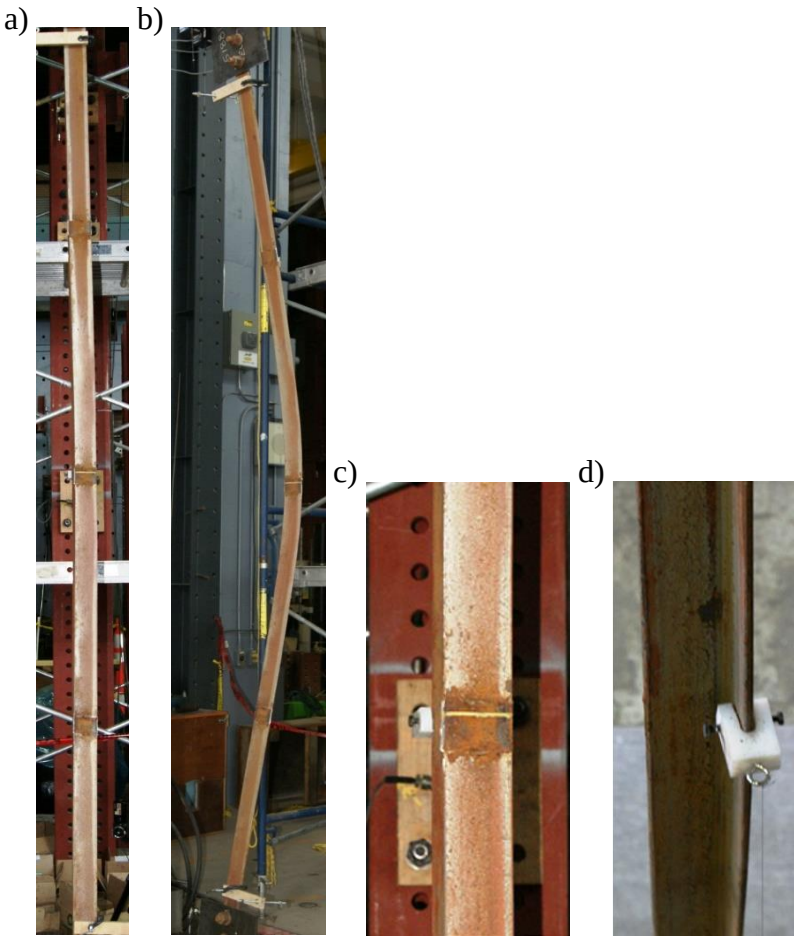

Figure 3.47: Specimen No. 5 - Observed behaviour during the test: a) in-plane bending; b) buckling of brace; c) opening of the legs (front); d) opening of the legs (back); e) bending at top connection; f) bending at bottom connection

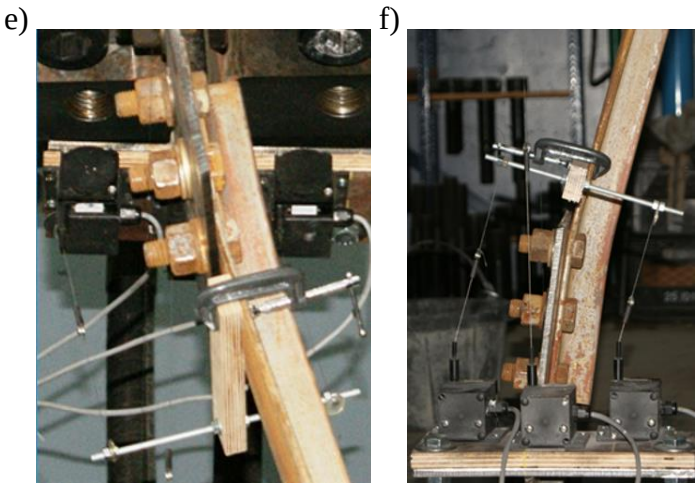

Figure 3.47: Specimen No. 5 - Observed behaviour during the test: a) in-plane bending; b) buckling of brace; c) opening of the legs (front); d) opening of the legs (back); e) bending at top connection; f) bending at bottom connection (continued)

a) b)

Figure 3.48: Specimens No. 5 - observed damage after the test: a) residual deformed shape; b) failed cross section

3.4.1.6 Test results

The main response parameters for this specimen are summarized in Table 3.10. The overall brace response is shown in Figure 3.49. Stiffness degradation of the brace occurred at an axial displacement of approximately 64 mm, and brace failure occurred at 64.1 mm axial displacement. This corresponds to 1.86% of brace length elongation, which is 3.72% storey drift. Hence, although the brace failed by tension rupture on net section, the chevron braced frame would have still exhibited a ductile behaviour in a severe seismic event. In the connection response of Figure 3.50, the connection starts to yield at a tension force of 126kN, and the maximum force reached during test was 323 kN. The ratio between the two values is 2.56, which is much more than the ratio expected between tensile and yield strengths for structural steels. Normally, the F_u to F_y ratio is

between 1.2 and 1.5. The corresponding average axial stresses on the angle net section (753 mm^2) are 167 MPa and 429 MPa.

In addition, the total deformation of two connections at complete fracture is 27.7 mm (17.5 mm at failure), which corresponds to 0.81% of the brace length and an equivalent storey drift of 1.6%. Figure 3.51 shows the net brace axial hysteretic response. Yielding of the brace cross section is evident in the figure. The net brace deformation at failure is 39.7 mm and the brace yield resistance is 320 kN. According to this yield force and brace gross cross-section area, the yield strength of the steel can be estimated as equal to 339 MPa.

These values combined with the observations made in the tests suggest that yielding initiated in the critical region of the brace net section at the low (125 kN) load due to combined tension, including shear lag effects, and in-plane bending conditions. Failure at the net section under the 323 kN load, just above the 320 kN gross yield strength of the brace, suggests that fracture took place because strain hardening had just initiated in the brace gross cross-section or because of fatigue effects in the net section. Applying a shear lag factor of 0.6 to the computed tensile strength of 429 MPa, it results in a tensile strength of 715 MPa. This very high, unlikely value, suggests that a shear lag factor of 0.6 for a three-bolt single leg angle connection is probably too conservative.

Table 3.10: Key response parameters for specimen No.5

Specimen Number 5 (LF-OLD-C-1)	
Failure mode	Brace net section rupture
Maximum brace load	323 kN (1.3 AR_yF_y)
Brace load at failure	323 kN
Equivalent storey drift at failure	3.72%
Total brace deformation at failure	64.1 mm (1.86% L)
Total connection deformation at failure	17.5 mm (0.51% L)
Total net brace deformation at failure	46.6 mm (1.35% L)
Connection deformation failed connection at failure	8.7 mm (0.25% L)

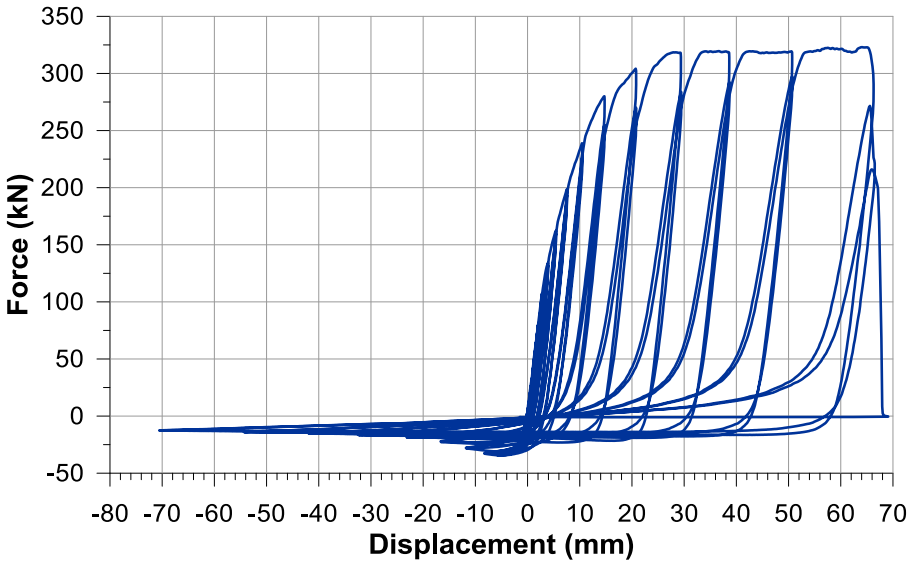

Figure 3.49: Specimen No. 5 - Overall brace response

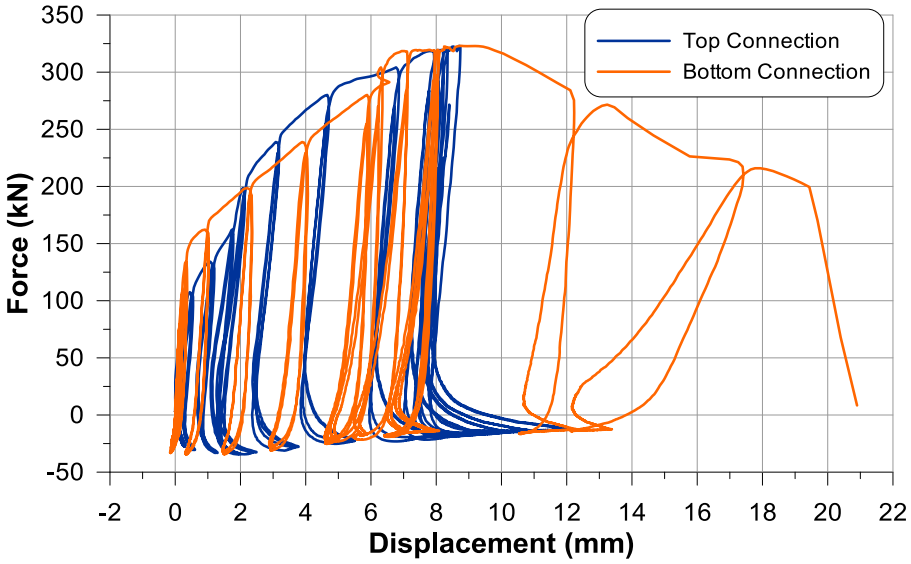

Figure 3.50: Specimen No. 5 - Connection displacement *vs.* force

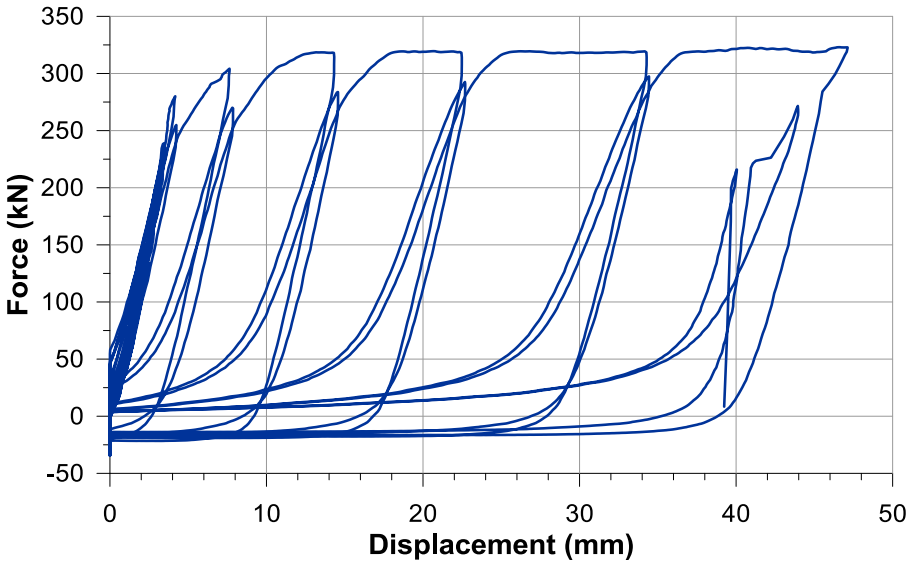

Figure 3.51: Specimen No. 5 - Net brace response

Based on these test results, net section rupture of this old single angle brace showed some ductility. A similar observation was made after Test LF-O-C-1 on the original connection. Some ductility was also observed in tests by Castonguay (2009) and Kulak and Wu (1993). In Tests LF-O-C-1 and this test on the rusted old brace, the resistances associated to gross section yield and net section rupture were very close, which allowed yielding to develop in the bracing member, while significantly increasing the overall ductility of the assembly. Hence, although the rupture on net section in connections can be considered as a low ductility failure mode, its ductility is highly dependent on the steel properties and connection geometry. In addition, the overall brace ductility also depends on the relative connection and brace resistance levels. If the connection failure strength is much larger than the brace tensile yield strength, brace yielding can be triggered before connection, failure and the overall brace ductility can be greatly increased.

3.4.2 Test LF-R3-C-1 (Retrofit strategy IV) (Specimen 6)

Based on the results obtained from the previous tests and knowledge gained on the net section failure mode for angle braces, a new retrofit strategy that may control the force level without decreasing the ductility was proposed for the connections. Figure 3.52 illustrates this Retrofit strategy IV for the 2-L127x76x9.5 double angle brace selected for the original test program. A total of four additional 7/8” holes are created in the connection region of the double angle brace two in each of the two legs of each of the two angles. These holes are added with the idea of reducing the

net cross section area and therefore control the force level that can be transmitted by the connection. No bolts are used in these additional holes (and no additional holes are drilled in the gusset plates). Although the additional holes is likely to change the failure plane from a zig-zag line to a straight line, the net section rupture of the brace is expected to remain essentially the same and the connection ductility capacity should be similar to that observed for the original connection. The T_{u-c} value of this retrofitted connection is 1046 kN based on the T_{u-c} obtained from Test LF-O-C-1 for brace net rupture, 1423 kN, because force resisting capacity of these two connections relate to the net cross section area of therm. In Test LF-O-C-1 net area of brace is 3303 mm^2, which is 36% larger than the net cross section area of this retrofitted connection (2429 mm^2). The retrofitted connection resistance is less than the probable yielding capacity of brace (1227 kN). Hence, the force level in the brace is controlled by the proposed retrofit strategy. These holes are drilled using a magnetic drill in the Structures laboratory. Except for the new retrofit scheme, the test specimen, test setup, instrumentation, and loading protocol are the same as those used for the other quasi-static tests performed on the double angle brace specimens tested in the 12 MN load frame. Figure 3.53 shows the retrofitted connection.

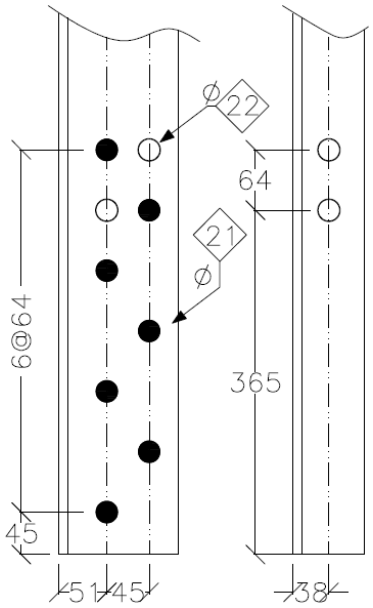

Figure 3.52: Plan of Retrofit strategy IV for connection

Figure 3.53: Retrofitted connection preparation

3.4.2.1 Observed behaviour

During the test, yielding started at an axial displacement of 9.98 mm and a force of approximately 600 kN. However, no deformation could be observed at the bottom connection at that time. The situation at the top connection was unknown because of the difficulty to access the upper end of the specimen during the test. The behaviour is very similar as in Test LF-O-C-1. At 0.8% equivalent storey drift, one leg of the double angle brace at the top connection fractured. The test was then stopped. Figure 3.54a shows this failure mode with net section failure in Angle 1 (L1) on a straight failure line, as was expected. Necking was observed at both legs of the two angles (L1 and L2). In the figure, the holes with a red circle are the additional holes. Due to the bolt bearing, damage is observed around the inner face of the holes used for the bolts. In Figure 3.54a, one crack initiated at the edge of a bolt hole in the long (connected) leg of angle 2 (L2) that did not fail, indicating that failure of that second angle was imminent. The bottom connection after the test is shown in Figure 3.54c. The inner face of the additional hole is much smoother than the inner face of the hole for bolts.

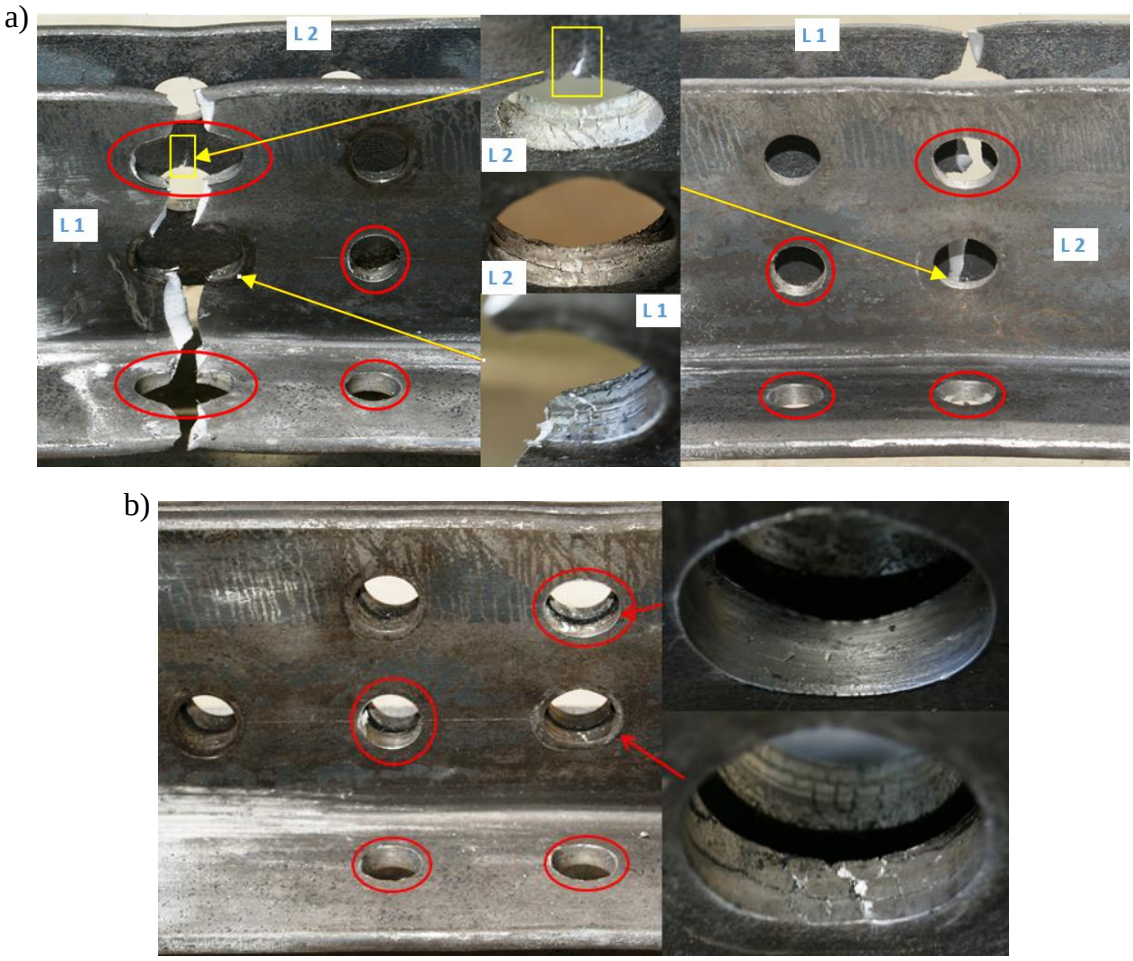

Figure 3.54: Specimen No. 6 - Observed behaviour: a) top connection after test; b) bottom connection after test

3.4.2.2 Test results

The main response parameters for this specimen are summarized in Table 3.11. Figure 3.55 shows the overall brace hysteretic response. The maximum elongation of the brace is 20.7 mm, which corresponds to 0.34% of the brace length. This is smaller than the overall brace elongation at failure measured in test LF-O-C-1. The axial force that developed at connection fracture came close to the gross yield strength of the brace, which is 1227 kN. The force level was controlled by the retrofitted connection. However, the local ductility capacity from connections decreased much. The expected performance of this retrofit connection is not achieved. This is because of the totally different performance between two connections. As show in Figure 3.56, the bottom connection appears to be stronger than the top connection, as yielding. The bottom connection probably could resist much higher forces because the forces were more uniformly distributed between the two angles. In the

top connection, it is expected that one angle was carrying nearly all loads at the beginning of the test, which leads to the situation where yielding started earlier and fracture developed in only one angle in that connection. In Figure 3.56, the gradually increasing resistance of the top connection very likely reflects the progressive engagement of the second angle in resisting the applied load. This shows that connection response for double angle (and any built-up brace members) is dependent on the initial distribution of loads, which depends on the fabrication tolerances (relative longitudinal position of the bolt holes in the two angles). When large discrepancies exist and the connection has limited ductility, it is possible that connection failure occurred before the two angles develop their full strength, as was possibly the case in that particular test. The resulting fracture resistance of the connection was slightly less than the brace yield strength and the bracing member remained nearly elastic up to the end of the test, as shown in Figure 3.57.

Table 3.11: Key response parameters for specimen No.6

Specimen Number 6 (LF-R3-C-1)	
Failure mode	Brace net section rupture
Maximum brace load	1204 kN (0.98 AR_yF_y)
Brace load at failure	1204 kN
Equivalent storey drift at failure	0.62%
Total brace deformation at failure	20.7 mm (0.34% L)
Total connection deformation at failure	13.2 mm (0.22% L)
Total net brace deformation at failure	7.5 mm (0.12% L)
Connection deformation failed connection at failure	10.3 mm (0.17% L)

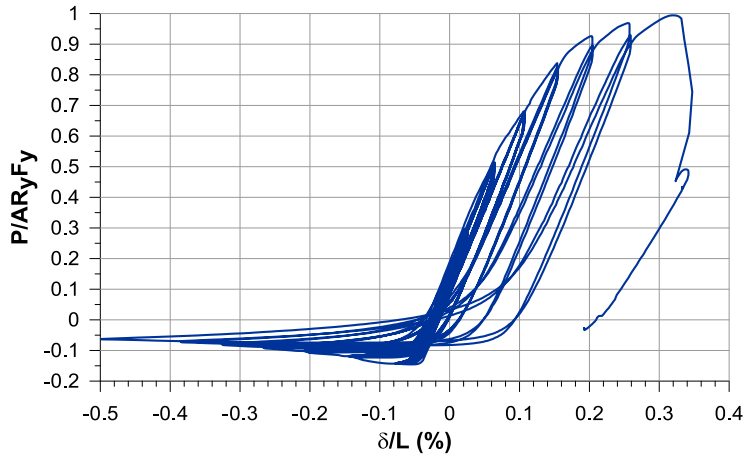

Figure 3.55: Specimen No. 6 - Overall brace response

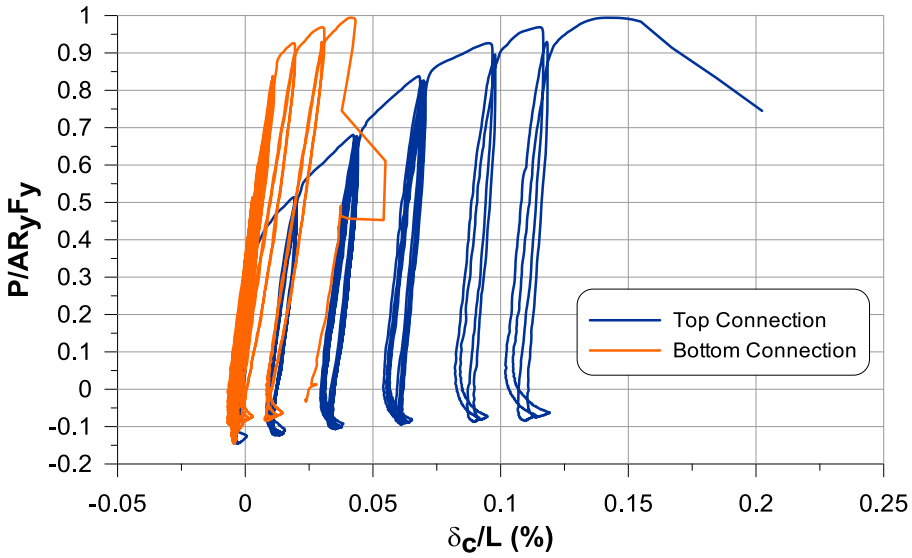

Figure 3.56: Specimen No. 6 - Connection response

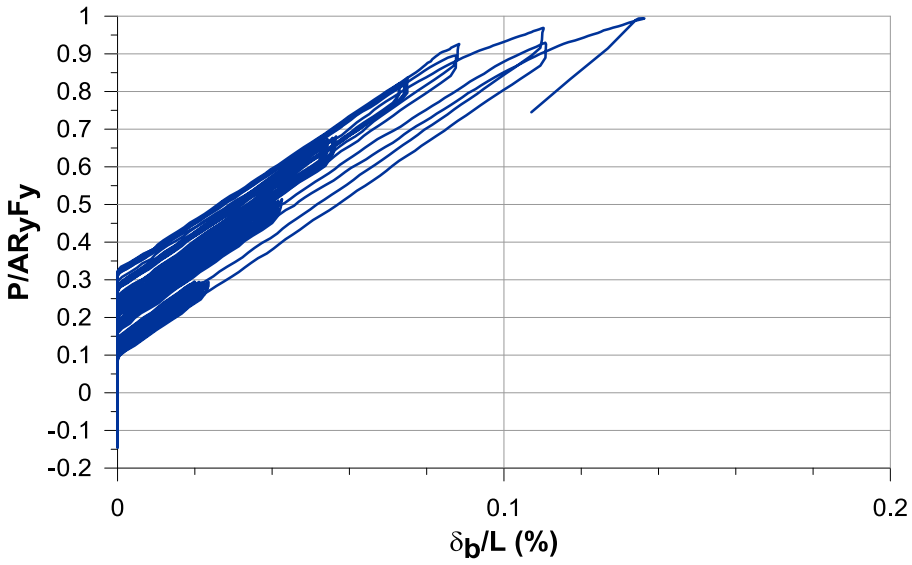

Figure 3.57: Specimen No. 6 - Net brace response

The design objective for this Retrofit strategy IV was not achieved. Force level in the brace was controlled, but the connection was not ductile enough. If the bottom connection has similar ductility performance as the top connection, the ductility capacity of this retrofitted connection should be much better. However, the performance of connections using this retrofit strategy is difficult to control in a real situation because deformations and damage in the two angles can be different. Small differences may lead to large impact on stress distributions. Thus, extensive research on the behaviour and performance of this retrofit strategy is required.

3.5 Summary

This chapter described the quasi-static cyclic experimental program. The results of the coupon tests are presented at the beginning of the chapter. The original test program included four cyclic tests: one test performed in a pinned vertical frame and three tests performed in a 12 MN load frame are described. Two other tests were added in the 12 MN load frame. The double angle brace with the original connection design was found to be stronger and more ductile than expected. Retrofit strategy I which consists in strengthening the net section are of the brace at the connection worked well: the ductility of the brace-connection assembly was increased; however, the force increased as well, which may impact on the performance of other braced frame elements. In the second retrofit strategy, slotted holes were drilled in the gusset plates to control the connection strength and increase its ductility. The system worked as intended: although the overall brace ductility

decreased, the local ductility capacity of this retrofitted connection increased without increasing the force demand. The third retrofit strategy consisted in creating weak steel segments in the gusset plates that would yield in shear. The performance of this third retrofit strategy was not good as the resistance was too high and the expected failure mode was not achieved.

Based on test results from the first four quasi-static tests, two additional tests were performed to further study the net section rupture mode of angle braces. One old single angle brace cut from an existing braced frame built in the 1960s was tested. Net section rupture occurred, as expected. The failure mode was accompanied with some ductility, as in the previous tests, which confirmed that net section rupture is a failure mode with some limited ductility. A fourth retrofit strategy was studied in the last test: additional holes were introduced at the brace net section to control the force demand. As expected, the connection capacity was reduced. However, connection failure seems to have occurred prematurely, likely due to uneven force distribution between the two angles, and brace yielding did not develop. This resulted in a reduction of the global ductility for the retrofitted brace-connection assembly.

CHAPTER 4: OPENSEES MODEL AND CALIBRATION

In this chapter, a numerical model is proposed and validated to simulate the inelastic seismic response of long leg, back-to-back built-up double angle braces including brace connection failure. The model is developed in the OpenSees platform, and examined through physical tests that were presented in Chapter 3. Sensitivity analyses are carried out to examine the influence of the number of fibres, number of elements, and number of integration points on the brace response predictions.

4.1 OpenSees modelling

The model accounts for several factors including flexural buckling of the individual angles, angles acting in pairs, physical contact between the two angles, the influence of the stitch connections on the buckling and post-buckling responses of the angles, and the nonlinear flexural and longitudinal responses of the end connections. The model is first introduced to study the flexural buckling response of a single-angle member. The model is then extended to reproduce the cyclic inelastic response of a double-angle bracing member, including the inelastic end-connections behaviour. Buckling strength of single and double angle members are validated by comparison with current design equations for compression members.

4.1.1 Single angle model

The angle section model uses force-based beam-column element and the fiber section representation of the cross-section. Initial out-of-straightness and residual stress conditions are accounted. A single angle section L-127x76x9.5 is selected to illustrate the numerical model because it is the shape used in the cyclic tests presented in Chapter 3. Therefore, model validation is more convenient. As shown in Figure 4.1a, the brace is modelled using 16 nonlinear forced-based beam-column elements. Each element includes 4 integration points. The cross-section of each element is discretized using rectangular fibres. As shown in Figure 4.1b, a total of 160 fibers are used, which includes 20 layers along the width of each of the two angle legs and 4 layers of fibres across the angle thickness. Nonlinear material response is reproduced with the uniaxial Giuffré-Menegotto-Pinto (*Steel02*) steel material object exhibiting both kinematic and isotropic strain hardening properties. The *Steel02* material also accounts for Baushinger effect on the initiation of yielding in the second and subsequent yielding excursions under cyclic inelastic loading. This modelling technique has already been successfully used in past studies on HSS

bracing members (Aguero et al. 2006; Uriz et al. 2008). Residual stresses can also be accounted for when using the *Steel02* material (Lamarche and Tremblay 2011). Although a flat yield plateau can be observed after initiation of yielding of an angle section, which is typically not the case for HSS sections, this plateau is neglected here when using the *Steel02* material. It is believed that the error is small and will not influence much the response predicted for bracing members, especially when the brace response is influenced by connection behaviour as is the case in this study. Hence, in spite of this limitation, the *Steel02* material is adopted for the brace model. Parameters used to define the *Steel02* material assigned to angle braces are shown in Table 4.1. These parameters (excluding the F_y value) had been used for the HSS brace numerical model in analysis carried out by Aguero et al. (2006). Residual stresses linearly varying across the width of the angle legs are assigned to the cross-section fibers, based on the measurement data collected by Adluri and Madugula (1995). Figure 4.1c shows the adopted residual stress distribution for the L-127x76x9.5 section.

The section aggregator command is used to aggregate elastic torsional stiffness to the fiber defined angle section. Corotational geometric coordinate transformation is used to predict the buckling response. Initial out-of-straightness is included by means of a half-sine initial deformation configuration with maximum deformation equal to L/500specified at the brace mid-length.

Figure 4.1: Single angle model: a) Beam-column elements; b) Brace cross-section with fibers and residual stress patterns; c) Residual stress measurements considered for the L-127x76x9.5 model (from Adluri and Madugula 1995)

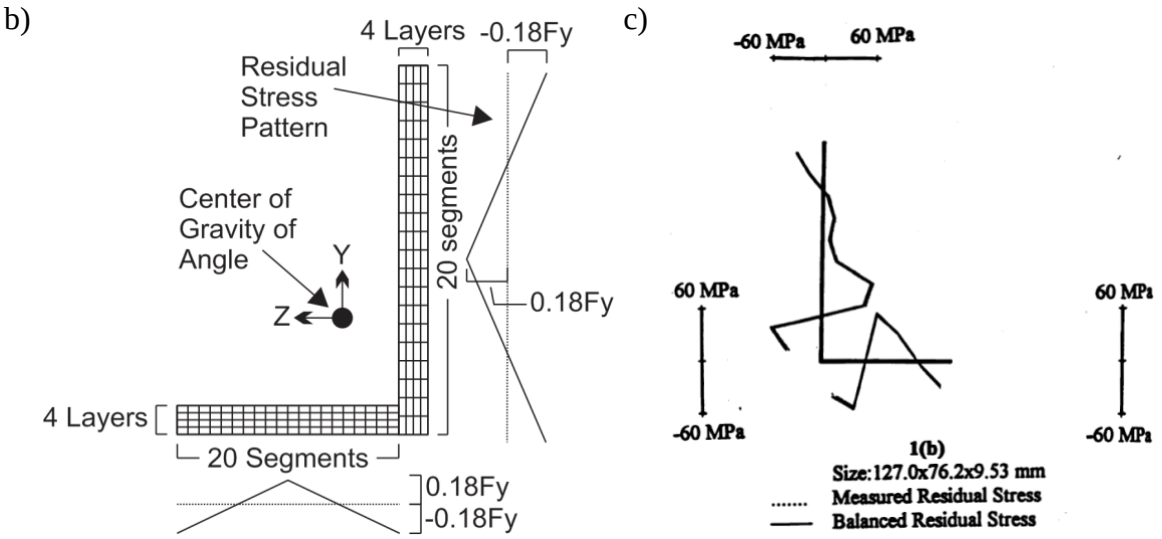

Figure 4.1: Single angle model: a) Beam-column elements; b) Brace cross-section with fibers and residual stress patterns; c) Residual stress measurements considered for the L-127x76x9.5 model (from Adluri and Madugula 1995) (continued)

Table 4.1: Parameters used to define the *Steel02* material

F_y	*E0*	*b*	*R0*	*CR1*	*CR2*	*a1*	*a2*	*a3*	*a4*	Siglnit
0.336	200	0.0042	30	0.925	0.15	0.4	22	0.4	22	Residual stress
Fy obtained from coupon tests in Chapter 3. $b = 0.1 \times F_y / 0.04 / E0$										

To verify the buckling shape of a single angle brace, a brace length of 6095 mm is selected as it corresponds to the brace length in the 6 m wide and 4 m storey height braced frame of the prototype building studied. Both brace ends are assigned as fixed about both flexural axes. The brace is analyzed under nonlinear static incremental (push-over) analysis in which a 20 mm negative deformation inducing compression is gradually applied at one end of the brace in 1000 steps. In general, single angle braces buckle about the minor principal axis of their cross section. Figure 4.2 shows the buckled shape of the brace in Y and Z directions at the end of the analysis for three different initial imperfections (δ_o) conditions: out-of-straightness in both Y and Z directions, out-of-straightness only in Y direction, and out-of-straightness only in Z direction. Generally, the lateral displacements along the Z direction are approximately 3.4 times larger than the displacements along the Y direction at the end of the analysis, where the single angle brace had buckled. According to the Steel design standard, this ratio is 2.7. The reason leading to this

difference is the buckling of single angle brace. Once the single angle brace buckled, the angle between two legs is larger than 90 degrees. Test LF-OLD-C-1 in Chapter 3 exhibited this behaviour. The ratio between Z direction displacement and Y direction displacement is the same as the value provide by the Steel design standard, when single angle brace reached buckling load. In addition, the different imperfection conditions lead to differences of about 8% and 3% in lateral deformations along the Y and Z directions, respectively. These differences are small and can be ignored. Thus, initial imperfection will be only applied in the Z direction to simplify the model.

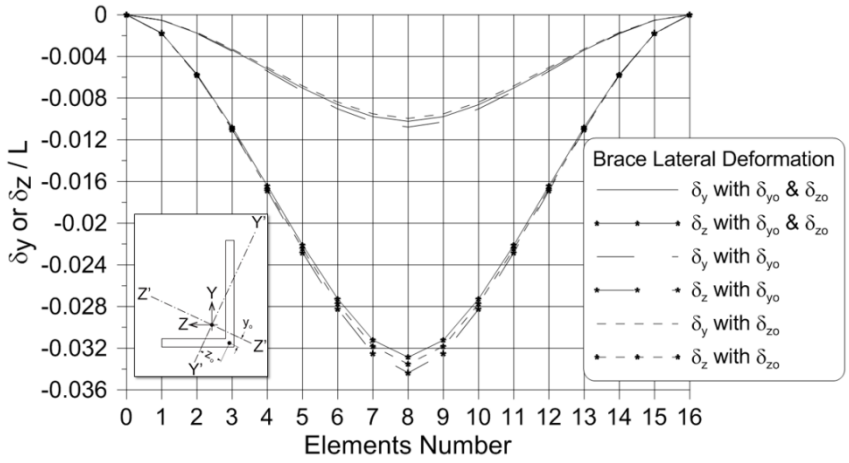

Figure 4.2: Lateral deformation in Y and Z directions at the end of analysis resulting from different initial imperfection conditions

The buckling strength obtained from the analysis is validated by comparing with the nominal (unfactored) compressive resistance specified in the CSA S16-09 Canadian design standard shown in Equation 4.1 for flexural buckling, C_n:

$$C_n = AF_y(1 + \lambda^{2n})^{-1/n},\ \lambda = \frac{KL}{r}\sqrt{\frac{F_y}{\pi^2 E}} \tag{4.1}$$

where A is the gross cross-sectional area of the member, F_y is the steel yield strength, taken equal to 345 MPa for this comparison,$\lambda$is the non-dimensional brace slenderness, n = 1.34 for angles, KL is the member effective length, r is the radius of gyration of the cross-section about the minor principal axis, $r_{Y'}$, and E is the Young's modulus (E = 200000 MPa). The calculations are performed for 60 different lengths to obtain 60 different $KL/r_{y'}$ ratios varying from 20 to 200. A factor K = 0.5 is used in Equation 4.1 to represent the fixed end conditions of the model. In Figure 4.3, the model predictions are very close to the values obtained with the code equation.

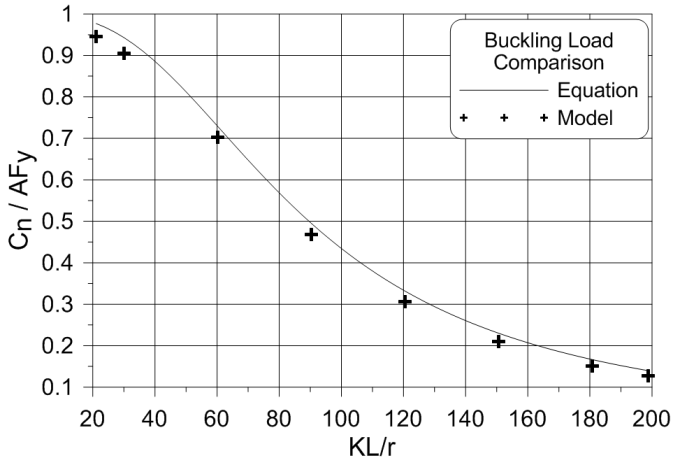

Figure 4.3: Buckling load comparison between CSA equation and modelling analysis

4.1.2 Long leg back to back built-up double angle and connection model

Figure 4.4a shows the model used for the double angle bracing member built with two L-127x76x9.5 angles with long legs back-to-back. This built-up double angle brace model is an extension of the single angle brace model. Two single angle brace models are connected back-to-back using *elastic beam column* elements linking together the centres of gravity of the individual angles at each end and mid-length of the brace. As shown in Figure 4.4b, one simple 3D stiff *elastic beam column* element is used at the brace mid-length to simulate the only stitch connector welded between the two angles at the double angle brace mid-length. This elastic beam column element is assigned a very high stiffness by using large cross section area, Young's modulus, and moment of inertia. In Figures 5.4c and 5.4d, stiff *elastic beam column* elements and *ZeroLength* elements with *elastic-perfectly plastic gap* material are used at each pair of nodes of the brace member to reproduce the contact behaviour between the two angles when they buckled. Zero stiffness and strength properties are specified for the gap elements in tension. In compression, these elements are assigned 12.7 mm initial clear distance, corresponding to the thickness of the gusset plates, as well as high stiffness and strength properties. *ZeroLength* elements are used to represent the brace-to-gusset connections. As shown in Figure 4.4d, these *ZeroLength* elements are connected to a node located at the mid-length of *elastic beam column elements* connecting together the two angles at the brace ends. Three different properties are assigned to these *ZeroLength* elements: 1) *Pinching4* material properties for nonlinear axial load-deformation response due to local yielding of the brace member and gusset plate in the brace connection region, bearing of the bolts against

the connected elements, shear deformations of the bolts, and slippage of the bolts, 2) uniaxial Giuffré-Menegotto-Pinto (*Steel02*) steel material properties for nonlinear flexural response due to bending of the gusset plates upon buckling and subsequent straightening of the brace, and 3) elastic properties for torsional response. The same proposed stiff *elastic beam column* elements are used along the brace longitudinal axis to connect the brace-to-gusset connections to fix end supports. In a braced frame OpenSees model, these *elastic beam column* elements are connected to the frame's beams or columns.

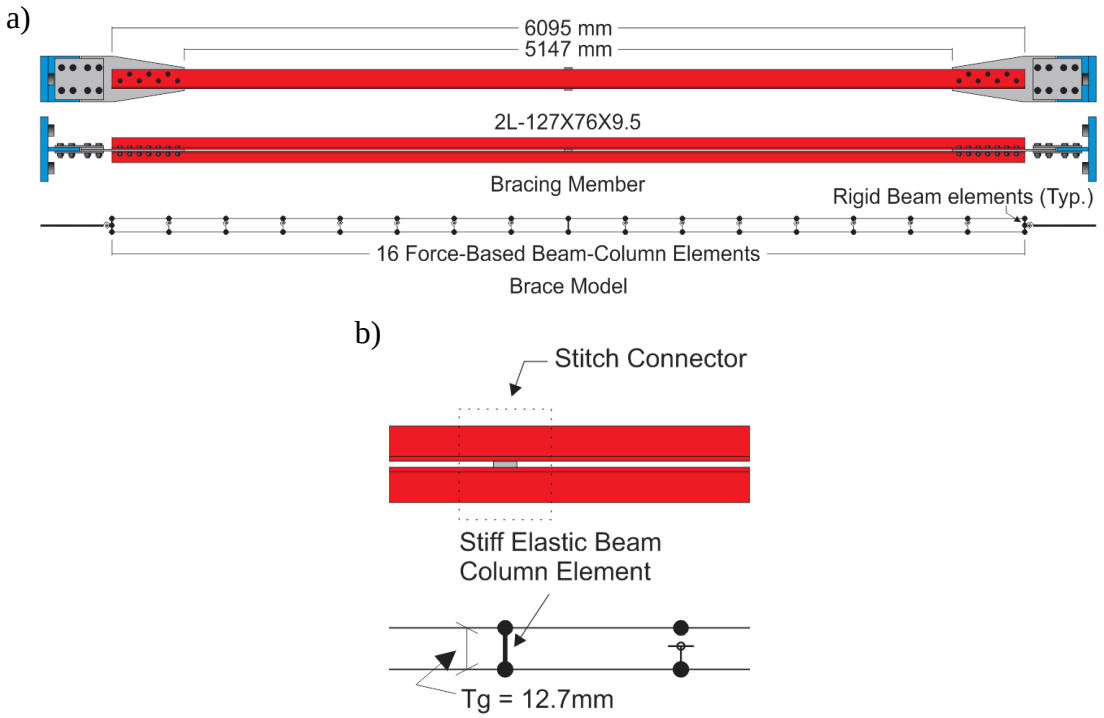

Figure 4.4: Built-up double angle brace model: a) Brace configuration and overall model; b) Stitch connection at the brace mid-length; c) Brace cross-section with fibers and residual stress patterns; d) Contact elements and brace end connection modelling

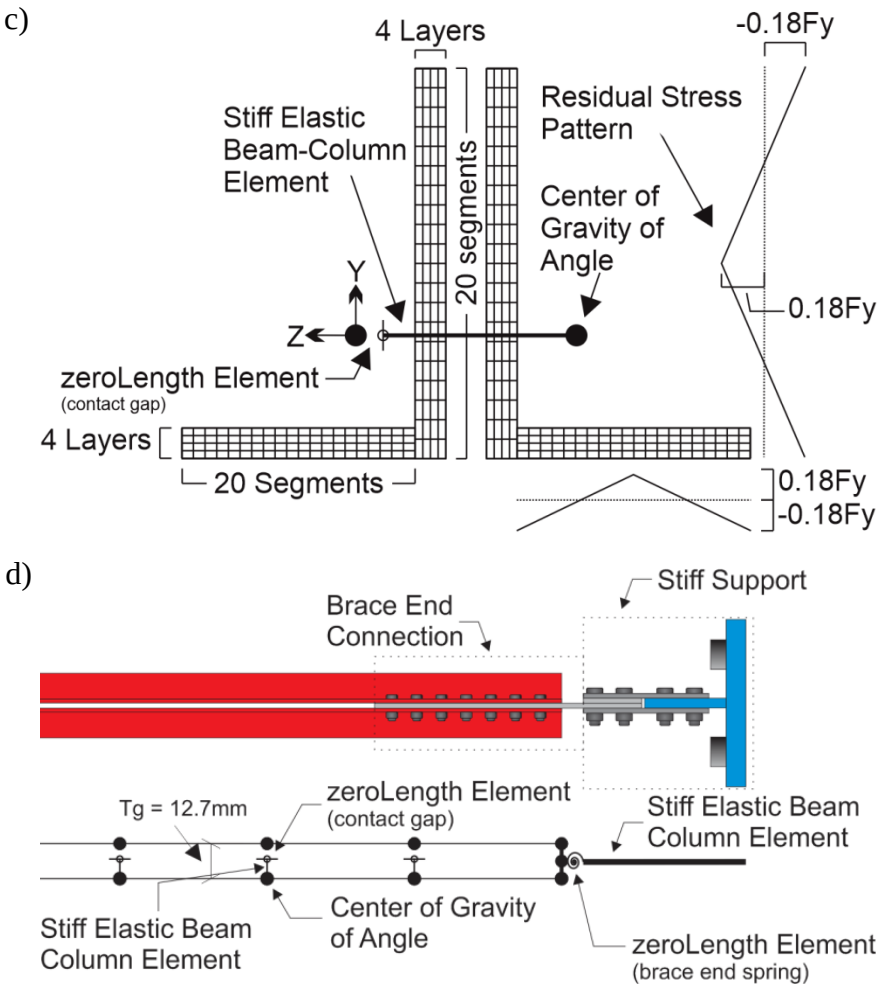

Figure 4.4: Built-up double angle brace model: a) Brace configuration and overall model; b) Stitch connection at the brace mid-length; c) Brace cross-section with fibers and residual stress patterns; d) Contact elements and brace end connection modelling (continued)

4.1.3 Material details in *ZeroLength* element for connections.

In the axial direction, the *Pinching4* material is used for the brace end connections. The hysteretic response of the *Pinching4* material is based on pre-defined load-deformation relationship. A total of 4 load-deformation (stress-strain) points can be specified on either deformation side to define the envelope of the hysteretic response, as show in Figure 4.5. The location of the first point on the tension side (positive load and positive deformation) is where the connection response becomes nonlinear (e.g., initiation of yielding). The second point corresponds to initiation of strain-hardening response. For last two points, there are two possible cases. If the connection eventually fractures, the third point corresponds to the load-deformation values reached at failure and the last point is used to define the residual resistance in the post-peak region. For the type of connections

studied herein, the residual resistance would typically be zero. However, in order to avoid convergence problems, it is recommended to specify a small residual force value. In addition, partial failure occurs when the maximum load is reached, and the post-peak decreasing resistance of the connection can be reproduced using the fourth point. The negative stiffness slope between the third point and the fourth point can be used to simulate the behaviour after the fracture was initiated. If connection failure is not expected in the analysis, the fourth point can be set at the maximum load level and at a maximum deformation that can be sustained by the connection. The third point can then be used between the second and last points to refine the load-deformation response of the connection model.

On the compression side, due to the fact that the brace buckling load is relatively small, the response of the connection in axial direction is considered as elastic. The load level of the first point is then set slightly larger than the anticipated brace buckling load because elastic connection response is specified in compression. In the connection model, *rDispP*, *rDispN*, *rForceP*, and *rForceN* were specified as 1.0. The floating point value defining the ratio of strength developed upon unloading from negative load to the maximum strength (*uForceP*) or minimum strength (*uForceN*) developed under monotonic loading are 0.95 and 0.1 respectively. Stiffness degradation, strength degradation, and damage properties were omitted.

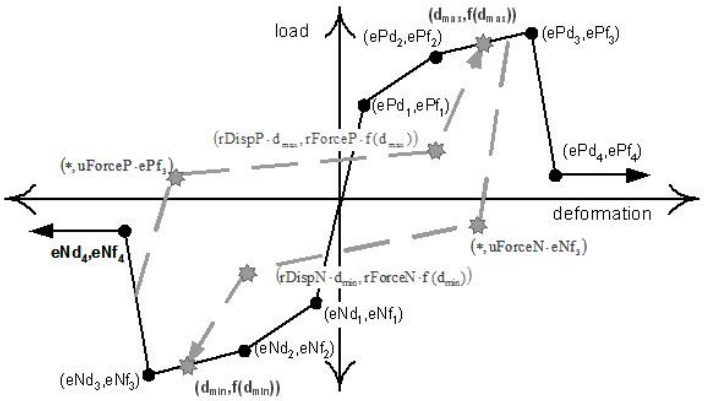

Figure 4.5: Pinching4 material in OpenSees (Mazzoni et al., 2009)

For bending of the brace end connections towards the out-of-plane direction, the properties of uniaxial Giuffré-Menegotto-Pinto (*Steel02*) material for nonlinear flexural response are obtained from a three-dimensional finite element analysis performed using the SAP2000 computer program

(CSI 2008) model shown in Figure 4.6. This analysis gives the equivalent flexural stiffness of the gusset plate to be specified to the rotational *ZeroLength* spring element. The flexural strength is obtained based on the plastic section modulus and steel yield strength of the gusset plate. Hence, the axial-flexure interaction on the flexural strength of the gusset plate is omitted in the model.

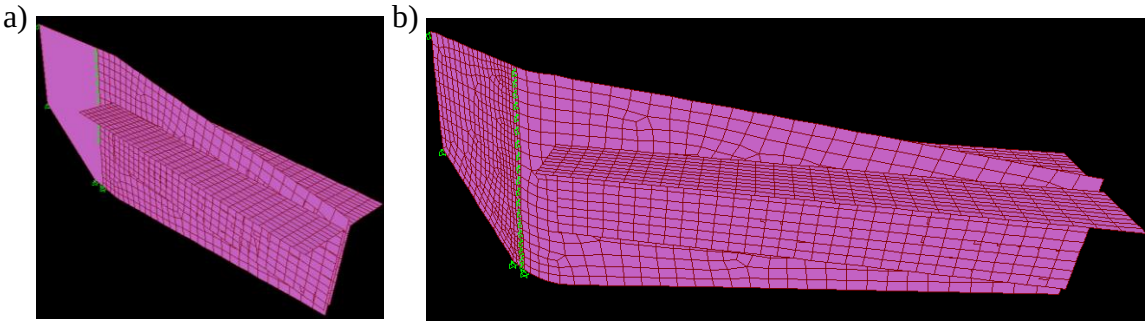

Figure 4.6: Connection SAP2000 model: a) original shape; b) bent shape

4.2 OpenSees model validation

The proposed numerical models for single angle and double angle braces and their connections are validated using the results from the four tests described in Chapter 3: VF-S-C-1, LF-O-C-1, LF-R1-C-1, and LF-OLD-C-1.

4.2.1 Test VF-S-C-1

In the numerical model of Test VF-S-C-1, *elastic beam column* element was used to model the elastic beams and columns in the test setup. Real beam (W530x138) and column (W360x347) sizes were specified in the numerical element. The numerical model is very similar as the test setup shown in Figure 4.4a. The controlling displacement was applied horizontal at the top of right column which is the node where beam, column, and brace met.

Figure 4.7 shows the model calibration results for the double angle brace cyclic test. In Figure 4.7a, the overall brace hysteretic response obtained from the proposed numerical model can simulate the test results correctly except that the hysteretic curve from the numerical model slightly shifts in few tension loading cycles. This small difference comes from the connection model. Yielding stress and strain, maximum stress and strain and buckling load are reproduced accurately in the numerical model. Due to the slackness in beam to column connections in pinned vertical frame test platform, applied axial deformation on double angle brace in the experimental test and numerical model are

different, even if the same loading protocol is used. The slackness leads to curve shifting in brace lateral deformation as illustrated in Figure 4.7b. As shown in Figure 4.7c, similar connection hysteretic response curves are obtained from the tests and the numerical model analysis.

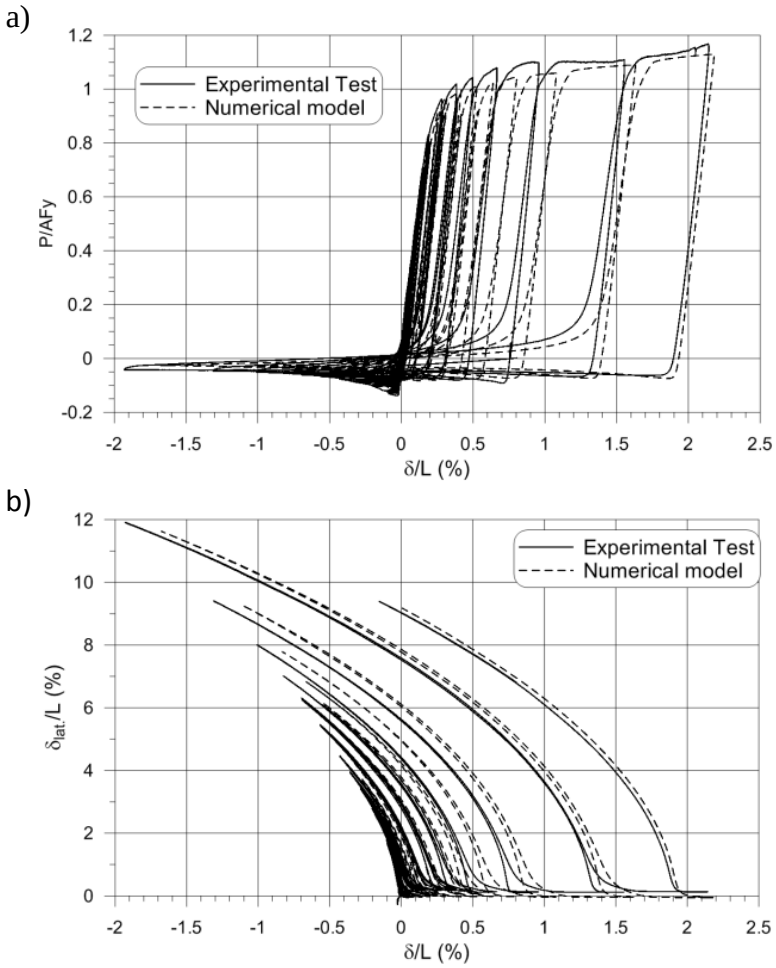

Figure 4.7: Model calibration for Test VF-S-C-1: a) brace hysteretic behaviour; b) brace lateral deformation; c) response of bottom connection

c)

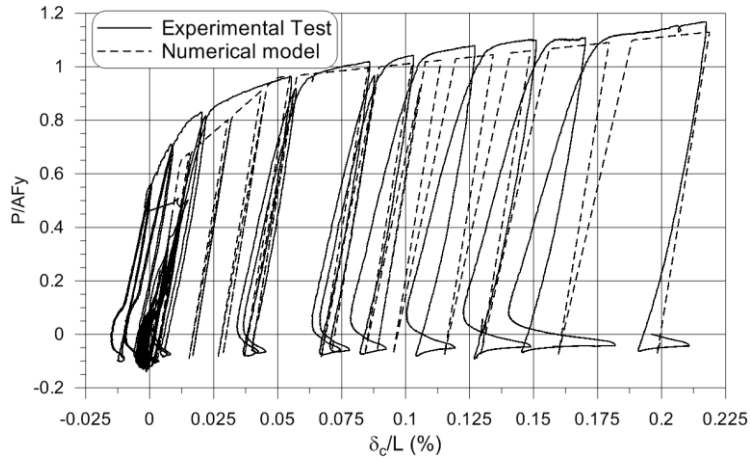

Figure 4.7: Model calibration for Test VF-S-C-1: a) brace hysteretic behaviour; b) brace lateral deformation; c) response of bottom connection (continued)

4.2.2 Tests LF-O-C-1 and LF-R1-C-1

Numerical model for tests carried out by the vertical load frame is simpler than the numerical model for Test VF-S-C-1. The sketch of the model is shown in Figure 4.4a. Both end nodes are fully fixed to simulate the boundary condition for the test setup excepting that the axial direction of the right end node is free to applied loading protocol.

Very good correlations are obtained between the numerical model analysis and the results from Test LF-O-C-1 with the original connection design and Test LF-R1-C-1 with the end connections retrofitted with the slotted holes. In the first test, the maximum resistance was measured when tension rupture occurred on the brace net section. As shown in Figures 5.8a and 5.8c, the peak resistance and connection failure in the test and the numerical simulation occur in the same loading cycle and at the same brace and connection deformations. In the 12 MN load frame test platform, no slackness existed in the test setup and the axial displacement *vs.* lateral deformation curves shown in Figure 4.8b match perfectly. Figure 4.9 shows the numerical model validation results for test LF-R1-C-1. The performance of the numerical model is again very good with excellent prediction of the failure point.

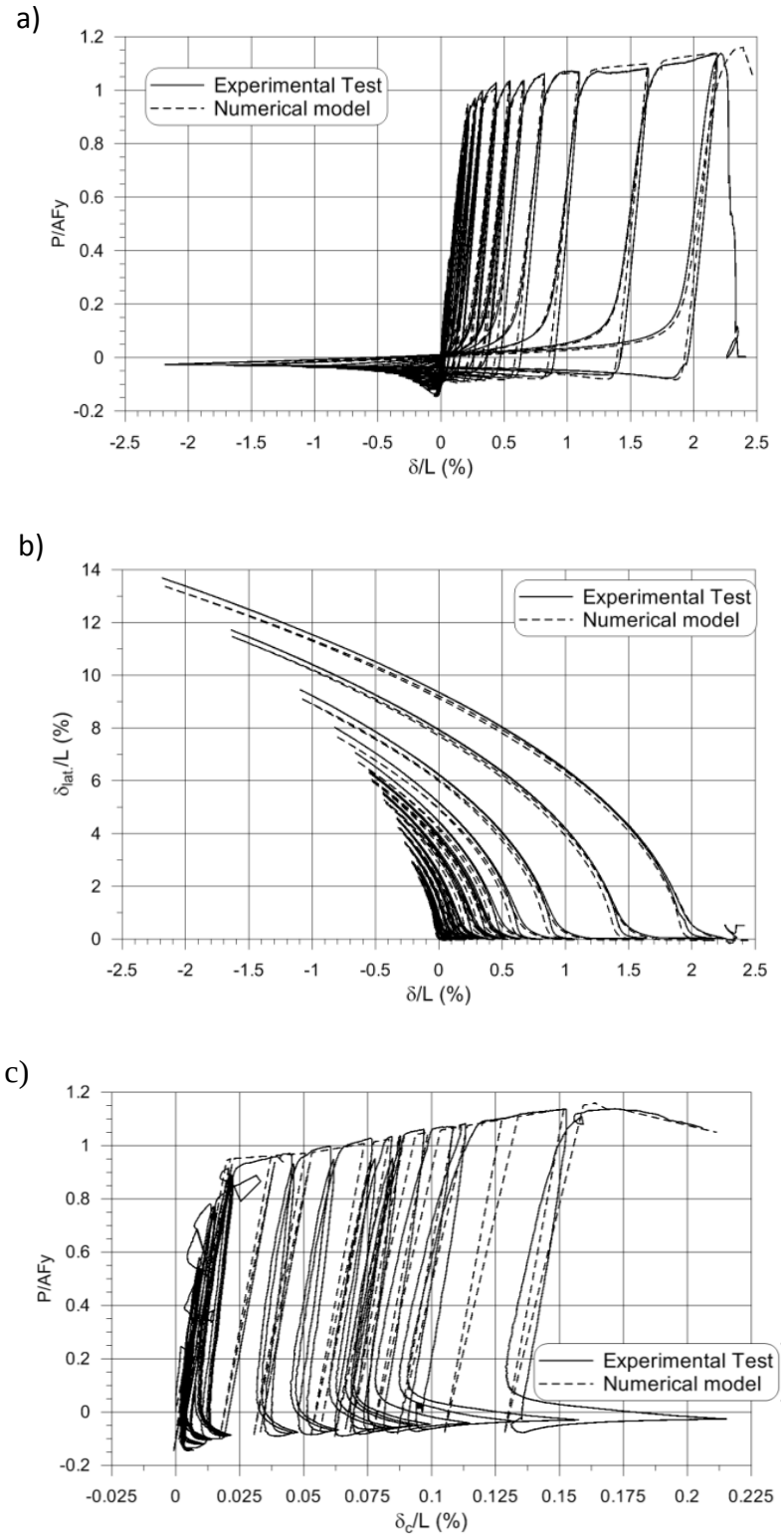

Figure 4.8: Model calibration for test LF-O-C-1: a) brace hysteretic behaviour; b) brace lateral deformation; c) brace connection response

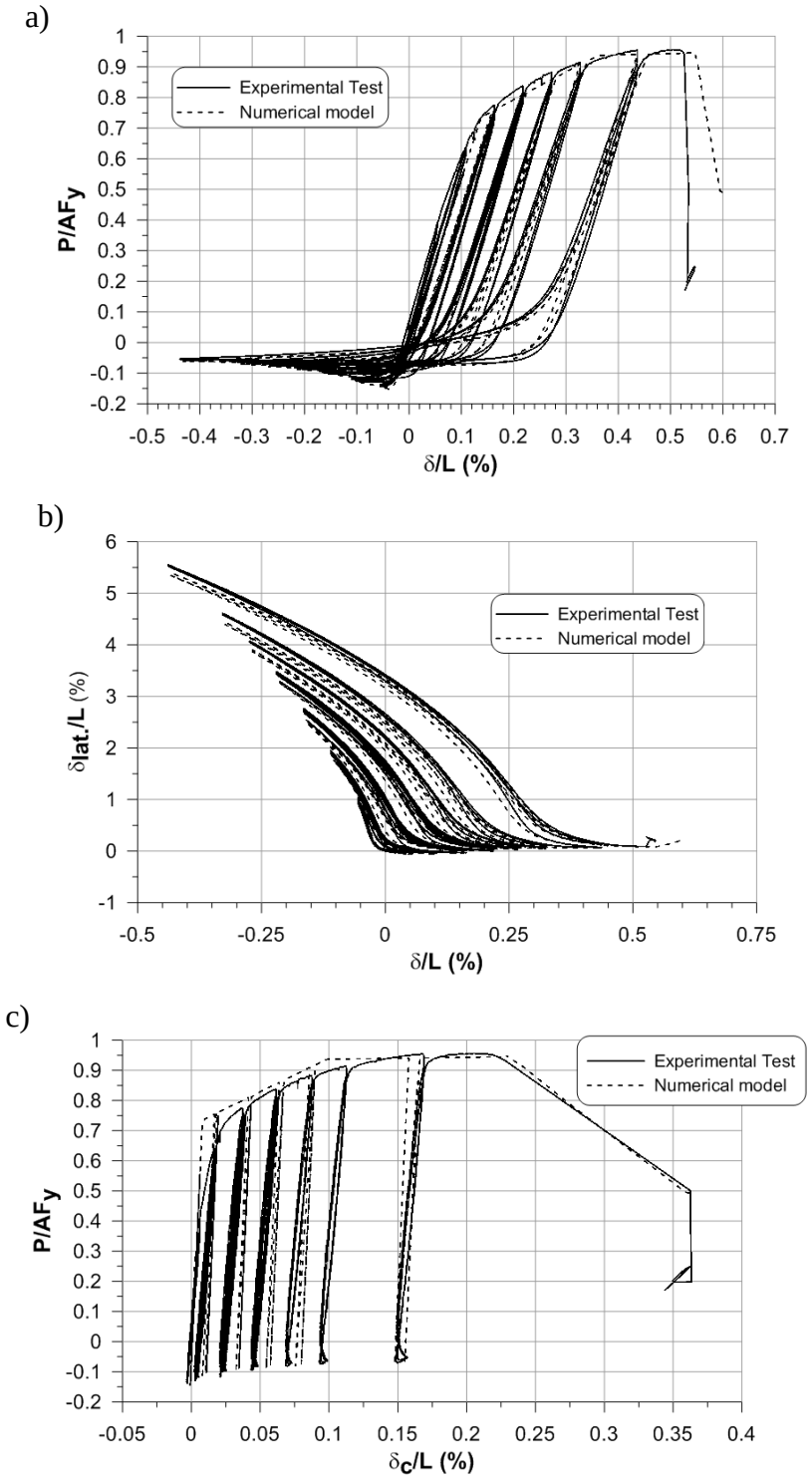

Figure 4.9: Model calibration for test LF-R1-C-1: a) brace hysteretic behaviour; b) brace lateral deformation; c) brace connection response

4.2.3 Test LF-OLD-C-1

The single angle OpenSees model is modified to calibrate the L-76x51x7.9 single angle cyclic Test LF-OLD-C-1. The brace length is changed to 3440 mm in the model. *ZeroLength* elements are added at both ends of the brace to reproduce the connection response observed in the test. Figure 4.10 shows the calibration results. Good match is obtained between the test and model analysis results. In particular, the strength degradation that followed the net section tension failure is generally well reproduced with the OpenSees model.

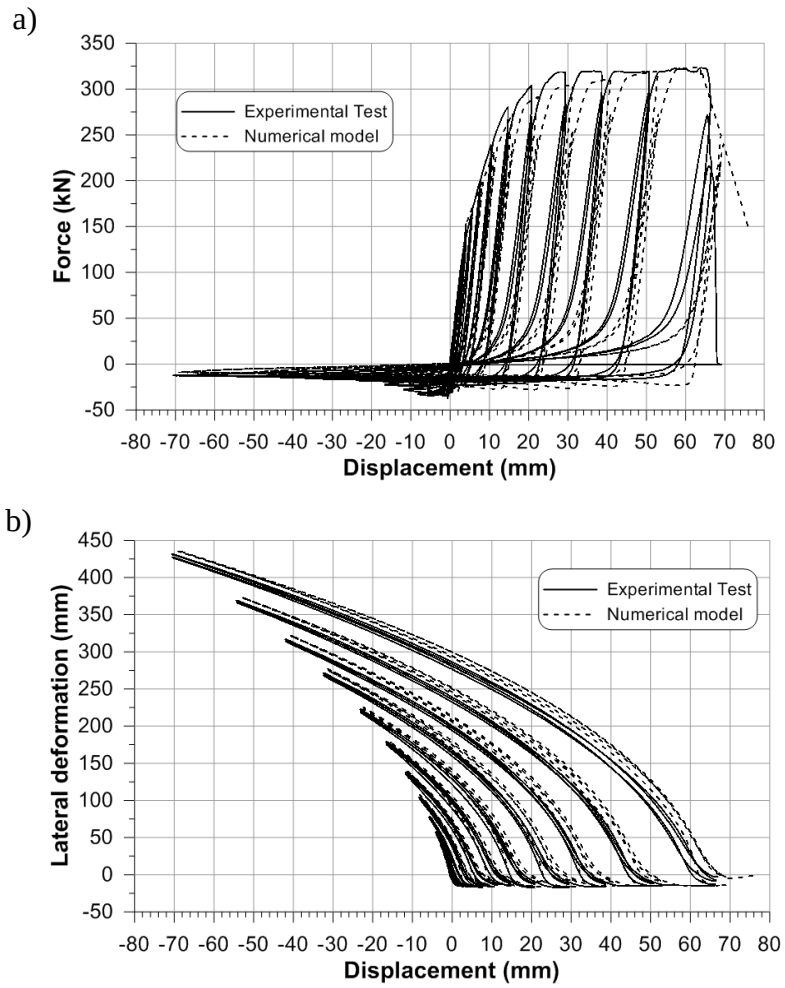

Figure 4.10: Model calibration for Test LF-R1-C-1: a) brace hysteretic behaviour; b) brace lateral deformation; c) brace connection response

c)

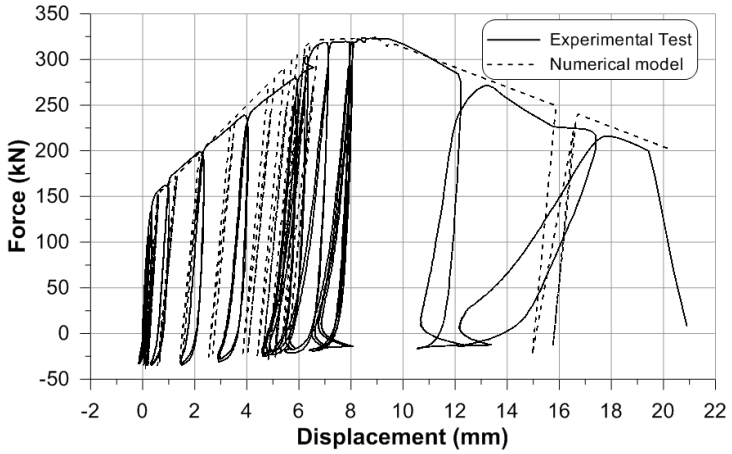

Figure 4.10: Model calibration for Test LF-R1-C-1: a) brace hysteretic behaviour; b) brace lateral deformation; c) brace connection response (continued)

4.2.4 Convergence problem

The convergence problem is the most critical difficulty that was met in the development and validation of the brace models. However, no specific rules are formulated to avoid this problem. This mainly results from the large number of nonlinearities, including stiffness degradation, specified in these models. It is difficult to propose a very effective method to address the convergence problem because the cause of this problem can be complex. Three methods can still be used to deal with this problem. Firstly, appropriately reducing the number of elements in the model reduces the volume of calculations, which can help avoiding convergence problems. Second, increasing the number of analysis steps at points where highly nonlinear response or stiffness degradation is likely can smooth the model calculations and contribute to convergence of the solution. Third, slightly modifying some model parameters may lead to unexpected good analysis performance, which means fewer convergence problems. In many instances, the analysis results were found to be nearly unchanged when applying the modifications to the model, indicating that the integration scheme can be more sensitive to some model parameters compared to the brace response. From this experience gained in this project, it was found that these parameters include, but may not be limited to brace's yield stress and strain-hardening ratio in the *Steel02*material used for the angle brace model, the post-peak residual resistance and maximum deformation in the *Pinching4* material used for the connection model.

4.3 Sensitivity Analysis

Model sensitivity analysis can provide useful data to verify and improve the accuracy and effectiveness of the numerical model for future numerical simulations. The number of integration points, the number of elements along each angle member, and the number of fibre layers across the angle thickness were varied to examine the influence of these parameters on the brace response. In this sensitivity analysis, a stiff elastic material was used for the axial response of the *ZeroLength* element simulating the brace end connections, instead of the *Pinching4* nonlinear material. This simplification aimed at focusing the study on the brace inelastic response rather than on the combined brace and connection nonlinear responses. The loading protocol used in the 12 MN load frame test program was used in the sensitivity analysis. The buckling load (P_u), the hysteretic energy dissipated over the entire loading protocol (E_H), and the maximum lateral displacement at brace mid-length (δ_{lat}.) are the response parameters selected for comparison.

The influence of the number of integration points is examined for a model with 16 elements, 4 layers of fibres and one stitch connector between the two angles. The other parameters for this model are identical to those used in the model employed to simulate the brace specimen in the 12 MN load frame test. In Figure 4.11, it is shown that 3 integration points are sufficient to properly predict the buckling load and the energy dissipation capacity of the brace. No definite trend is observed for the lateral displacements but the results indicate that good predictions are obtained with 2 to 5 integration points.

In Figure 4.12, the effect of varying the number of elements and the number of fibre layers across the angle thickness are examined. For this study, the elements were modelled with 3 integration points, based on the results obtained in Figure 4.11. In Figure 4.12, the results are normalized with respect to those obtained with 32 elements and 16 fibre layers. The results show that accurate predictions are generally obtained when using 8 elements along the brace length, which is consistent with the results by Aguerro et al. (2006). However, buckling load predictions can be improved slightly when using 16 elements instead of 8. The number of fibre layers seems to have relatively smaller influence on the brace response. Using 4 layers in combination with 8 elements appears to be sufficient to achieve good predictions.

The compressive resistance and energy dissipation capacity of double angle bracing members are both expected to increase as the number of stitch connectors is increased. This influence is examined in Figure 4.13. The numerical model used to perform this study is the same model that was adopted in the sensitivity analysis with 3 integration points, 8 elements, and 4 fibre layers. Both the buckling load and the energy dissipation capacity exhibit the anticipated trend as the number of stitches is increased. Lateral displacements at the brace mid-length also tend to increase when using more closely spaced stitch connectors. The discrepancy observed for the brace with 3 stitches is due to the position of the stitches relative to the buckled shape which is shown in Figure 4.14. For the double angle brace with 3 stitches, the lateral deformed shape between stitches is more flat than the shape from other two brace.

In Figure 4.13a, the prediction of the brace compressive strength based on the AISC Specification (AISC 2010) requirements for built-up sections are indicated on the figure. In AISC specification, the modified slenderness ratio of built-up member is calculated using Equation 4.2. For these calculations, a K factor of 0.92 was used for brace overall buckling about the axis of symmetry, as determined by comparing the AISC predictions with the buckling load measured in the 12 MN load frame test with one stitch connector. An effective length factor of 0.5 was also used for local buckling of the individual brace angles between the stitches, as recommended in the AISC Specification for welded stitches. As shown, a similar influence of the number of stitches on the brace compressive strength is obtained from the numerical model and the AISC 360-10Specification. However, the effect of the number of stitch connectors is larger in the model analysis than in the AISC equation.

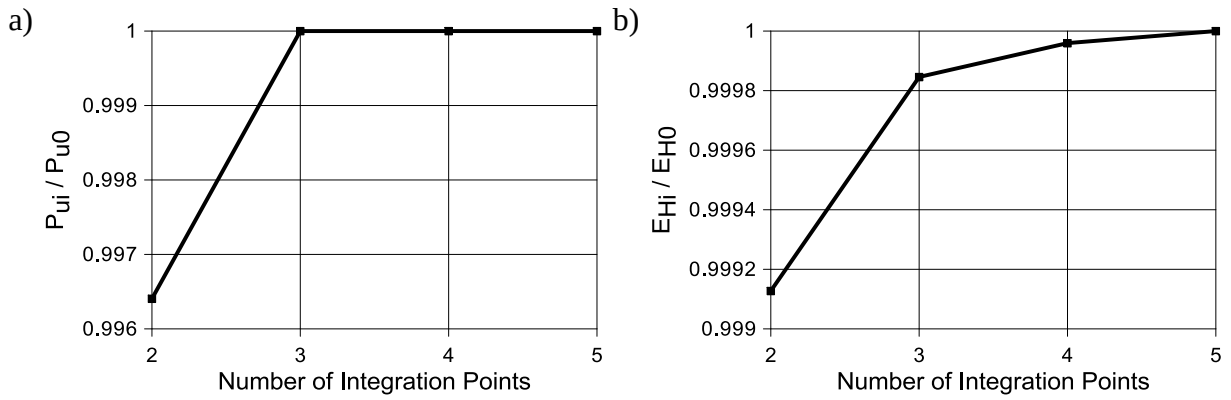

Figure 4.11: Influence of the number of integration points on the: a) Buckling load; b) Energy dissipation; c) Lateral displacement at brace mid-span

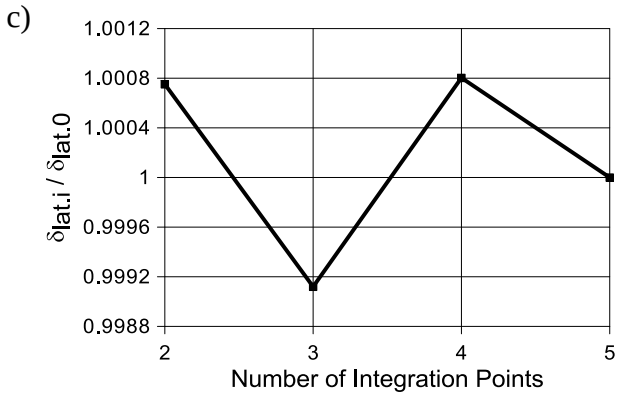

Figure 4.11: Influence of the number of integration points on the: a) Buckling load; b) Energy dissipation; c) Lateral displacement at brace mid-span (continued)

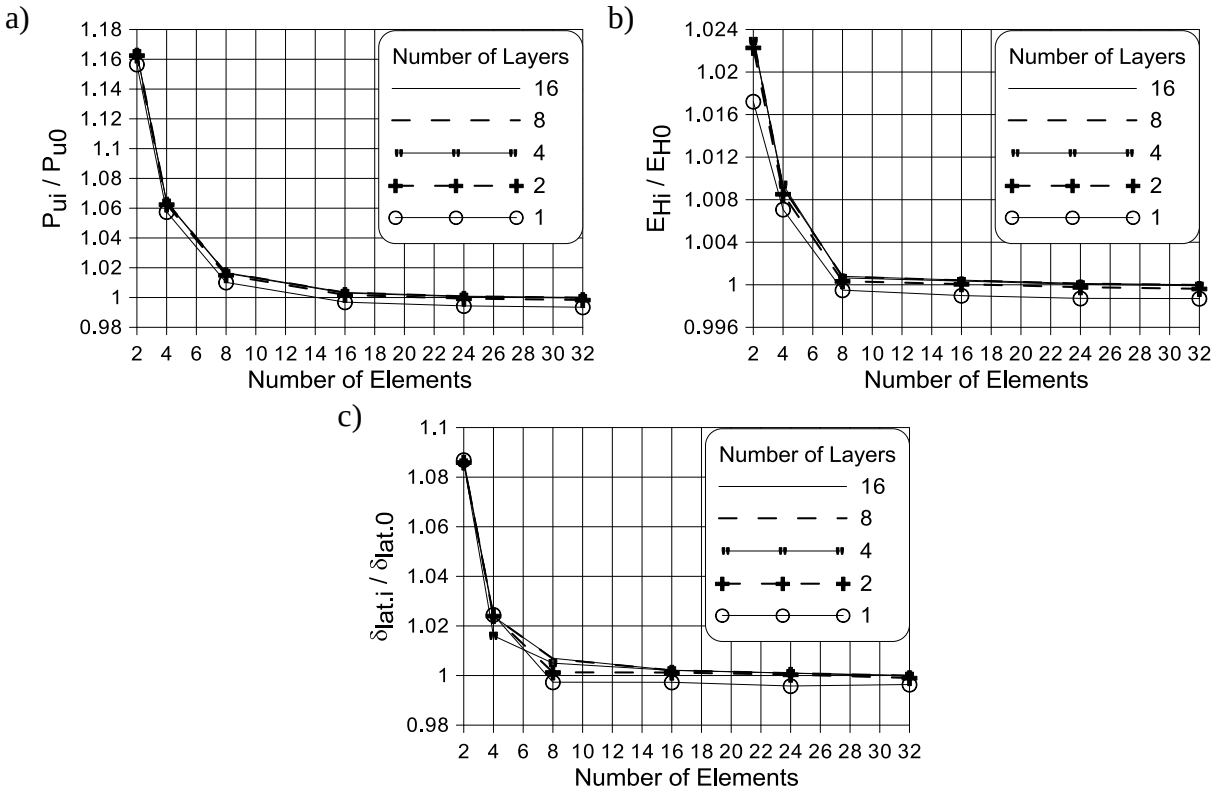

Figure 4.12: Influence of the number of elements and fibre layers across the thickness on the: a) Buckling load; b) Energy dissipation; c) Lateral displacement at brace mid-span

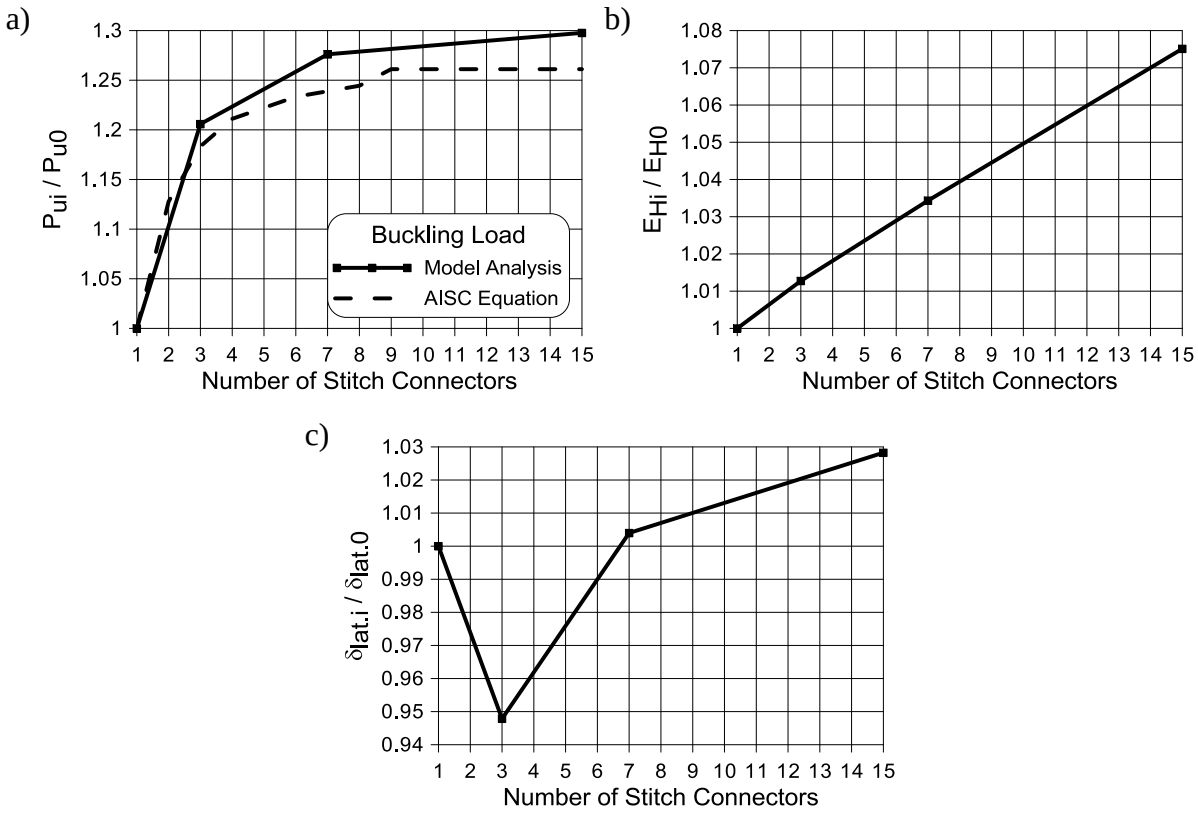

Figure 4.13： Influence of the number of stitch connectors between the two angles on the: a) Buckling load; b) Energy dissipation; and c) Lateral displacement at brace mid-span

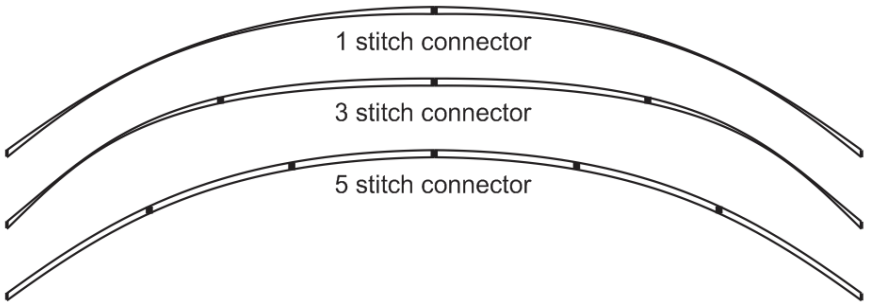

Figure 4.14: Influence of the stitch connectors on the buckling shape of double angle braces

when: $\frac{a}{r_i} \leq 40$

$$\left(\frac{KL}{r}\right)_m = \left(\frac{KL}{r}\right)_o \tag{4.2a}$$

when: $\frac{a}{r_i} \geq 40$

$$\left(\frac{KL}{r}\right)_m = \sqrt{\left(\frac{KL}{r}\right)_o^2 + \left(\frac{K_i a}{r_i}\right)^2} \tag{4.2a}$$

where K_i is 0.50 for angles back-to-back, a is the distance between stitches, r_i is the minimum radius of gyration of individual component.

4.4 Summary

A numerical model has been proposed to study the buckling behaviour of single angle and double angles steel bracing members using the OpenSees computer framework. In the numerical models, the brace is modelled using forced-based beam-column elements with fibre discretization of the cross-section. The Giuffré-Menegotto-Pinto (*Steel02*) material is used with isotropic and kinematic strain hardening properties. Initial out-of-straightness and residual stresses are considered in both models. The single brace model is used to predict the flexural buckling response of a fictitious brace with fixed end conditions. Its accuracy is verified against the predictions from code design equations. In addition, a modified single angle model with appropriately defined connections is validated by using the data from a single angle cyclic test. For the double angle brace model, contact elements are used to simulate the stitch connectors along the length of the bracing member. *ZeroLength* elements with nonlinear axial and flexural responses are used in the double angle member model to simulate the responses of the end connections. The accuracy of the double angle model is verified through comparisons with some cyclic experimental tests. The model is shown to accurately reproduce the measured brace inelastic cyclic response, including the nonlinear behaviour of the end connections. A sensitivity analysis has permitted to determine the required number of integration points, the number of elements, and the number of fibre layers across the angle flange thickness that are required to achieve reliable results. The model is found to adequately predict the benefits of adding stitch connectors on the brace buckling loads. Energy dissipation and lateral displacements are found to also increase when the number of stitch connectors is increased.

CHAPTER 5: BRACED FRAME MODEL AND HYBRID SIMULATION

The double angle brace with connections model is extended to a tension only braced frame model in this chapter. Braced frame model in OpenSees finite element program, OpenFresco middleware, and physical double angle brace with connections work together to carry out hybrid simulation for tension only braced frame in the fictitious building. Difficulties that met during the hybrid simulations are also presented.

5.1 Tension only braced frame modelling

The tension only braced frame model at ground floor is shown in Figure 5.1. Columns of the lateral frame are modelled with the uniaxial Giuffré-Menegotto-Pinto (*Steel02*) steel material and fiber section to reproduce the buckling behaviour that may happen during loading. One elastic leaning column is used to represent the tributary gravity columns in order to simulate the P-delta effect. All columns are pin connected to base plates. To simplify the model, beams are considered as elastic members. The double angle brace with end-connections model is connected to the beam at one end and to the base plate at the other end. The seismic mass and lumped gravity load are applied to the top node of each column of the lateral frame. Lumped gravity load is applied to leaning column as well.

According to the study completed by Liu and Astaneh-Asl (2004), the energy dissipated in beam to column connections due to yielding of shear tabs and crushing of concrete slab under cyclic loading cannot be ignored. Hence, beam-to-column springs (*ZeroLength* element) are defined to simulate the beam-to-column connection. Figure 5.2 shows the three stage of beam-to-column connection behaviour. *Pinching4* material is used in the rotational spring, defined in the *ZeroLength* element, to simulate this behaviour in term of moment-rotation. The hysteretic loop of the *Pinching4* material used in the *ZeroLength* element at the beam-to-column connection is shown in Figure 5.3.

The 4-storey tension only braced frame model of the fictitious building is shown in Figure 5.4. The configuration of each floor is almost the same as that of the ground floor. However, sizes of braces, columns, and beams are those resulted from design, as well as, the seismic mass and lumped gravity load at each floor. In the analysis, only mass proportional damping corresponding to 2% of critical damping is specified in the model.

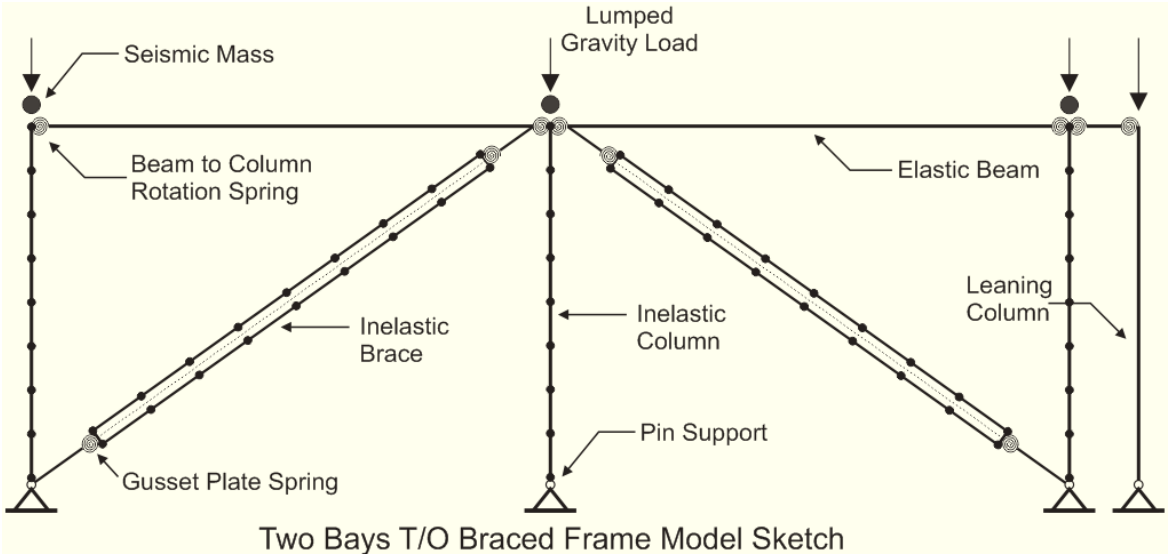

Figure 5.1: Model of the tension only braced frame with leaning columns at ground floor

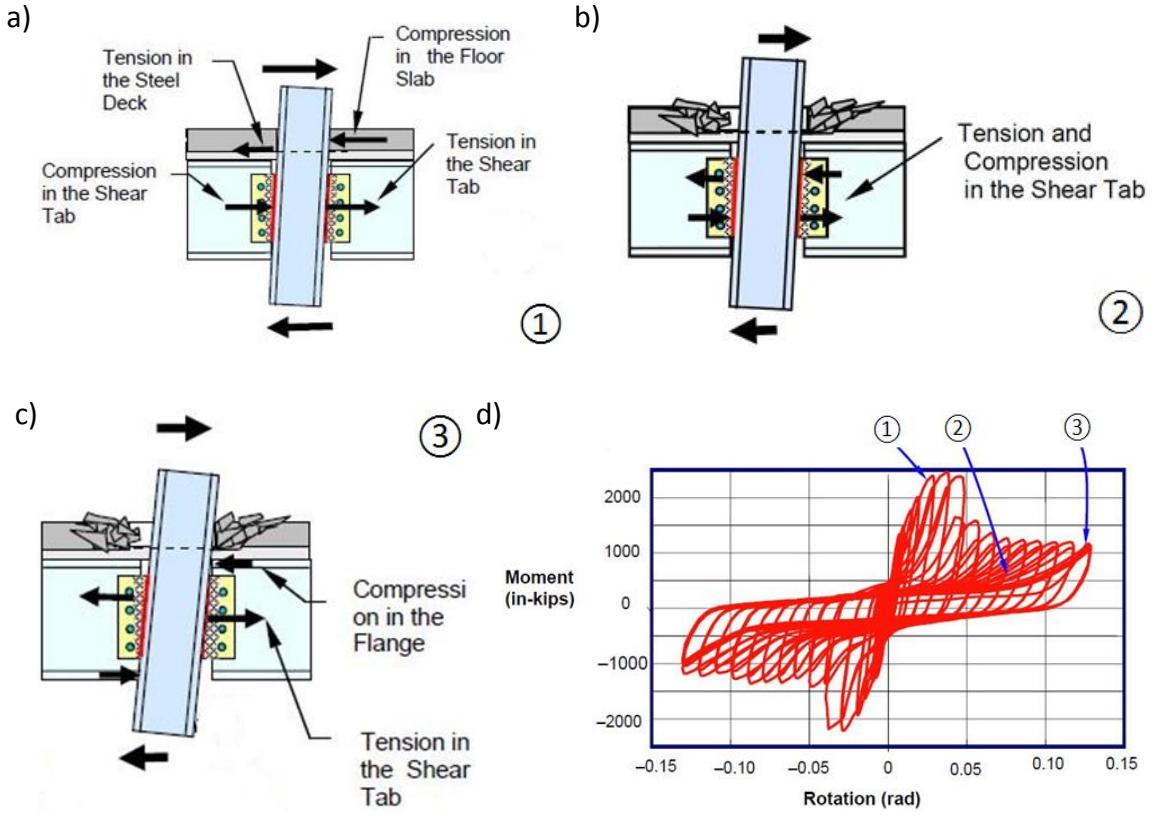

Figure 5.2: Beam-to-column connection behaviour: a) Compression of concrete slab; b) Concrete slab crashed and shear tab is resisting the moment; c) Beam is pressing against the column; d) Moment-rotation hysteretic loops (Liu and Astaneh-Asl, 2004)

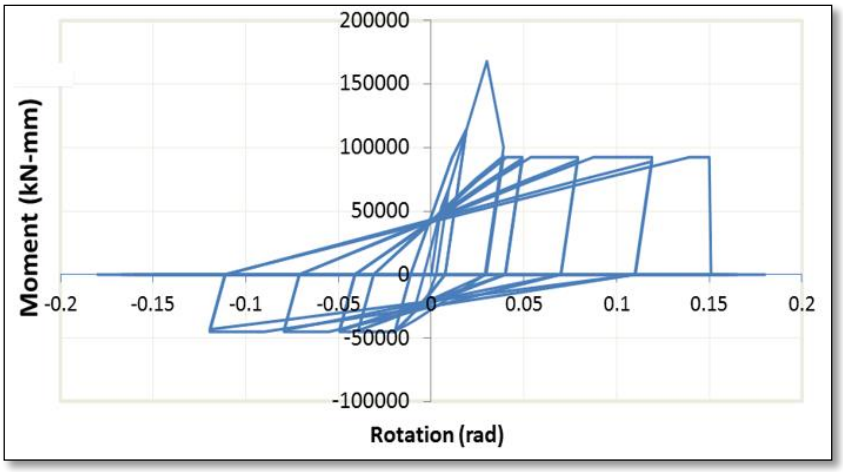

Figure 5.3: Hysteretic loopsof*Pinching4* material simulating the beam-to-column shear tab connection

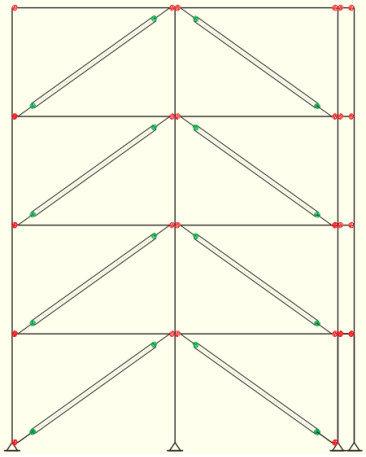

Figure 5.4: Braced frame model for the 4-storey fictitious building

5.2 Hybrid simulation program

In this section, the hybrid test technology, test setup and preparation are described.

5.2.1 Introduction

In hybrid simulation, the middleware OpenFresco (the Open-source Framework for Experimental Setup and Control) software (Schellenberg et al. 2010) is used to link the OpenSees finite element model to the components being physically full-scale modelled in the laboratory, which have been removed from the numerical model. More specifically, the OpenSees model is linked to control and data acquisition system applied to physical specimen (e.g., the brace) through the OpenFresco.

Figure 5.5 shows the hybrid simulation model. The brace member and its end connections in the left side bay (see brace shown in red and its end connections in grey), is physically tested in the 12 MN load frame during the hybrid simulation test. The remaining components of the braced frame structure, which are members shown in blue in Figure 5.5 are numerically modelled. During the hybrid simulation, the force and displacement responses of these physical components are continually fed into the numerical model so that the dynamic time step analysis can be performed. Hence, the purely numerical and the hybrid simulations are identical, except for one brace member.

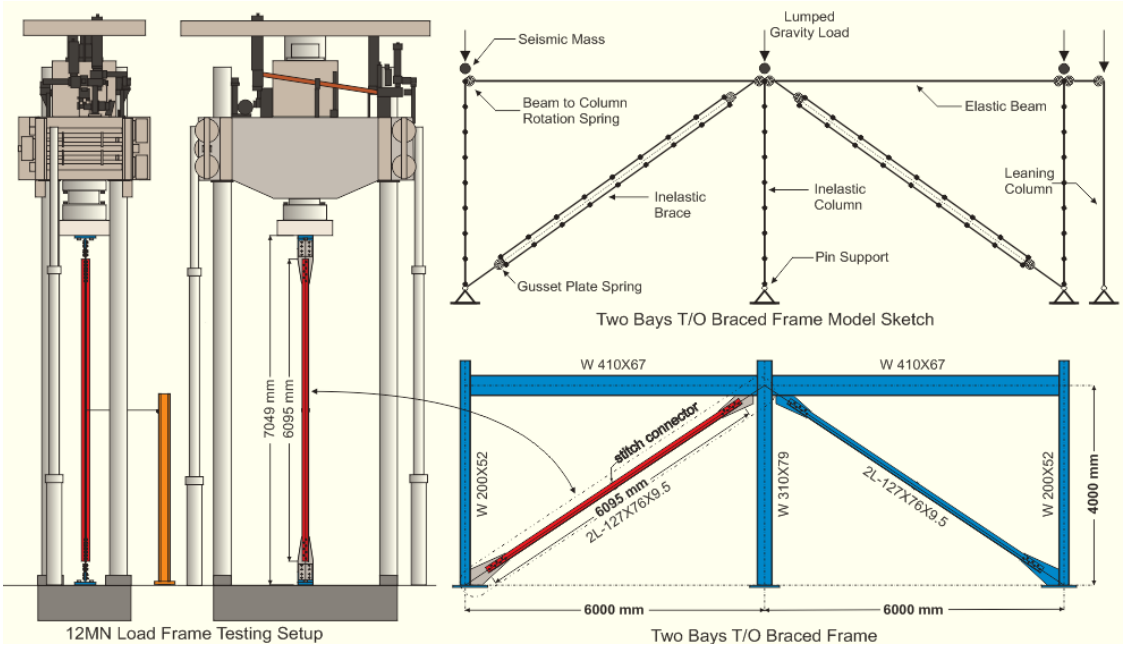

Figure 5.5: Hybrid simulation model

There are some reasons that OpenFresco is selected as the middleware in the hybrid simulation. First, it is one of the most convenient middleware for OpenSees to perform the hybrid simulations of structural systems. Hence, by using OpenFresco and OpenSees the quality of hybrid simulation is assured. Second, OpenFresco and OpenSees were developed by Berkeley. The commands in both programs are similar. Thus, it is not difficult to use OpenFresco, once users knew how to work with OpenSees. Third, the flexibility, extensibility, and re-usability of OpenFresco software can help users to develop and improve their hybrid simulations. Last but not the least, OpenFresco is free to download and free to use.

5.2.2 Test specimen, setup, and instrumentation

Test specimen and instrumentations used in hybrid test are exactly the same as those used in the quasi-static tests performed in the 12 MN load frame. In addition, the test setup is quite similar as well. However, the controlling system and data acquisition system are different from the quasi-static cyclic test. Figure 5.6 shows the architecture of OpenFresco software for local simulation. The numerical model part (client) and physical test part (backend server) communicate each other through the middle tier server that follows the commands received from the OpenFresco package. Herein, the xPCtarget experimental control, *twoNodeLink* experimental element and One Actuator experimental setup are used.

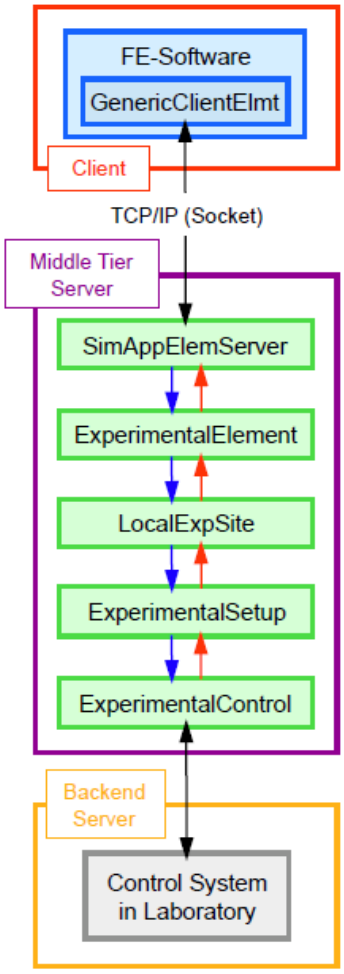

Figure 5.6: OpenFresco software architecture for local simulation. (OpenFresco Command Language Manual, 2009)

The configuration of hybrid test setup used in this research is shown in Figure 5.7. One xPChost (client), one xPCtarget (Middle Tier Server), one MTS server (Backend Server), one MTS controller, and the 12MN load frame are involved in the hybrid simulation. Both, OpenSees model and OpenFresco simulation are running in the xPChost tier during the simulation. A Simulink predictor-corrector is running in the xPCtarget. Although the MTS controller controls the physical test part, data doesn't need to pass through this controller. The MTS server sends commands and feedbacks between the actuator in the 12MN load frame and xPCtarget, while the MTS server also shares real-time data with the MTS controller in order to allow users to control the test. Figure 5.8 shows the photo of hybrid experimental test setup in the structure laboratory of École Polytechnique of Montr éal.

Before test, the predictor-corrector model was loaded from the xPChost to the xPCtarget. Once the simulation started, the OpenFresco received the initial displacement from the OpenSees model and sent it to the predictor-corrector model. The model computed the displacement command, and sent it to the actuator through the MTS server. After the actuator performed the loading of the required step, the OpenFresco sent the force to the OpenSees model for the next analysis step.

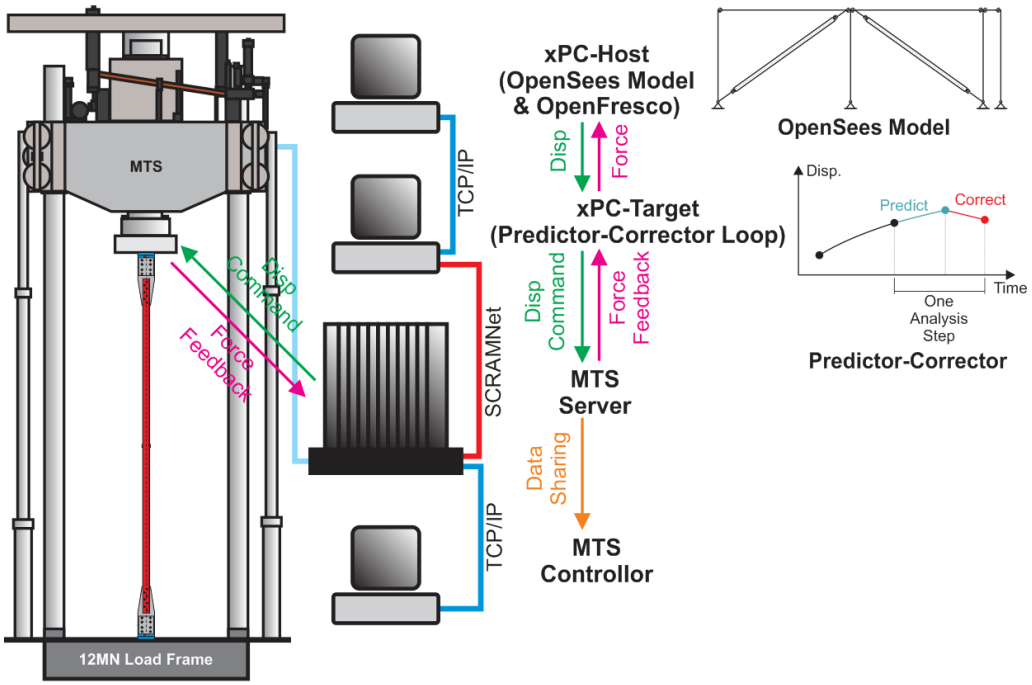

Figure 5.7: Configuration of hybrid test setup

Figure 5.8: Photo of hybrid simulation setup

5.2.3 Ground motion

Nonlinear dynamic time history analysis is carried out under the 90° component of the ground motion recorded at the Castaic Old Ridge Route station during the M6.7, Jan. 17, 1994 Northridge earthquake. The record is scaled by a factor of 0.6 to be compatible with the seismic hazard at the Vancouver site, which is corresponding to the structure design level. Figure 5.9 shows the scaled accelerogram. During the hybrid test, the specimen was loaded with two adjacent ground motions that provided from the same record, scaled with 0.6 and 0.78 scaling factors, while both accelerograms are separated by 10 s of zero acceleration value, as illustrated in Figure 5.10. The ground motion was amplified with 0.78 scale factor in order to obtain the 130% design level. The 10s zero acceleration part is used to allow the amortization of structure displacement that occurred during the application of the first ground motion.

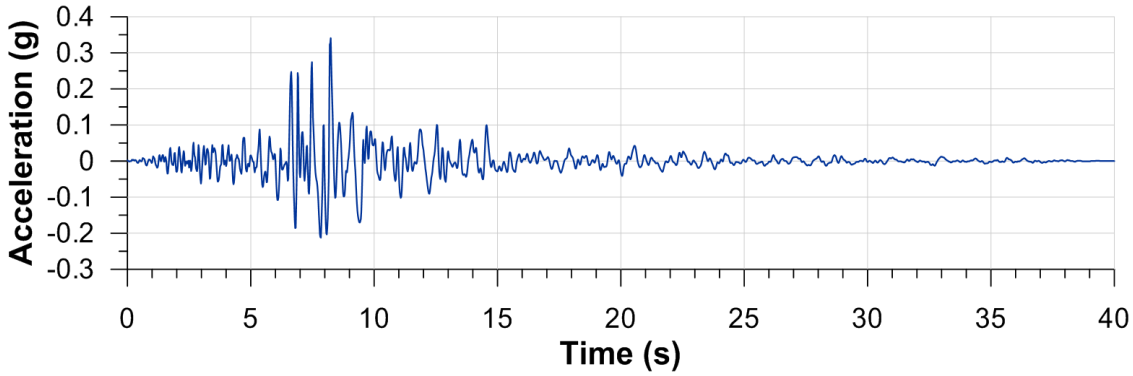

Figure 5.9: Ground motion with 0.6 scale factor

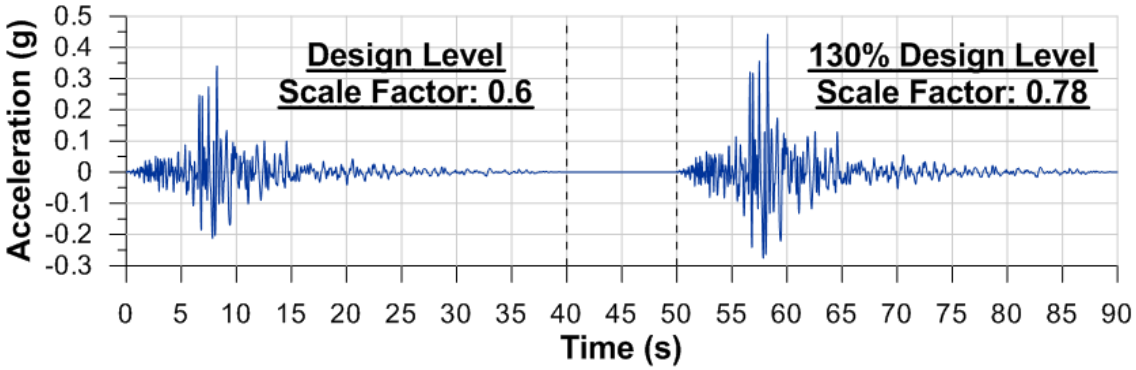

Figure 5.10: Modified ground motion

5.3 Numerical model analysis and hybrid simulation comparison

In order to learn and understand how to use OpenFresco and OpenSees for the hybrid simulation of braced frame system, some simplified models based on the 4-storey tension only braced frame were used. In these simplified models, the first-storey braced frame sub-structure shown in Figure 5.1is considered. For consistency, seismic masses and gravity loads corresponding to the total building seismic weight are assigned at the top of the *fiber* section columns.

Totally, four official hybrid simulation tests were finished and some trial hybrid simulations were tried. Table 5.1 shows the test program for four official hybrid simulations. Two of them: LF-O-H-1 and LF-R1-H-1 were completed successfully, and the rest two were interrupted during the test due to some technical problems.

Table 5.1: Hybrid simulation test program

Order	Name	No. of Storey	Connection type	Ground motion
1	LF-O-H-1	1	Original	S_f (0.6)
2	LF-R1-H-1	1	Retrofitted with slotted holes	S_f (0.6 , 0.78)
3	LF-OM-H-1	1	Modified original	S_f (0.6 , 0.78)
4	LF-O-H-4	4	Original	S_f(0.6 , 0.78)

Hybrid simulation test LF-OM-H-1 was interrupted due to the CPU overloaded problem shown in Figure 5.11. This error message is reading from the xPCtarget and it shows that the CPU of the xPChost was overloaded during the analysis process. The CPU overloaded problem occurred in other three trial hybrid tests as well. It happened occasionally.

Figure 5.11: CPU overloaded problem

The hybrid simulation test LF-O-H-4 was interrupted because of the TCP/IP connection timeout problem, which is shown in Figure 5.12. This connection problem between the xPCtarget and xPChost is abnormal because the physical connection was built successfully. Thus, the data synchronization should be satisfied.

Figure 5.12: Connection timeout problem

Time history dynamic analysis results from the OpenSees model and the hybrid simulation are compared for the two successful hybrid simulation tests. The modified models are also introduced in order to improve the accuracy of numerical model analysis.

5.3.1 Hybrid test 1: LF-O-H-1

This is the first hybrid test using OpenFresco and OpenSees platform for braced frame completed in the Structures laboratory of École Polytechnique of Montréal. The simulation is carried out at lower rate than real time, with a duration of approximately 3.5 hours for the 40 second ground

motion excitation. In addition, some simplifications are applied to the hybrid simulation model. All columns are changed to elastic behaviour, and the beam-to-column connections are simulated as pin connections.

In Figure 5.13a, the time history response of the first-storey lateral displacement obtained from the numerical and hybrid simulations are compared. The brace hysteretic response recorded during the hybrid test is compared to the purely numerical solution in Figure 5.13b. The two responses generally agree well, except that differences are obtained in the lateral displacements experienced by the structure. Examination of the measured response of the physical brace specimen revealed that significant slippage took place in the bolted connections between the gusset plates and the T-shape brackets connected to the test load frame during test. This behaviour is reproduced by modifying the hysteretic axial properties of the *ZeroLength* elements at the ends of the corresponding brace in the purely numerical model. The brace response obtained with these modified properties is compared to that obtained during the hybrid tests in Figure 5.14. Excellent match is obtained when using the corrected model.

a)

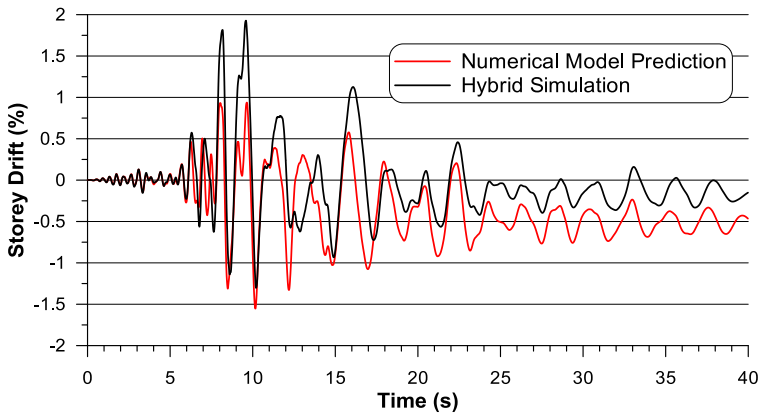

Figure 5.13: Comparison between the original numerical model prediction and hybrid simulation: a) Lateral displacement time history at the first-storey; b) Brace hysteretic response

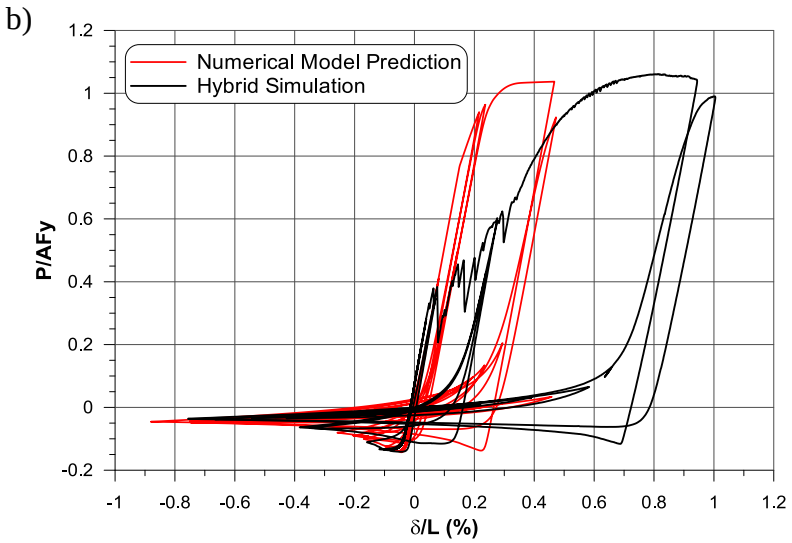

Figure 5.13: Comparison between the original numerical model prediction and hybrid simulation: a) Lateral displacement time history at the first-storey; b) Brace hysteretic response (continued)

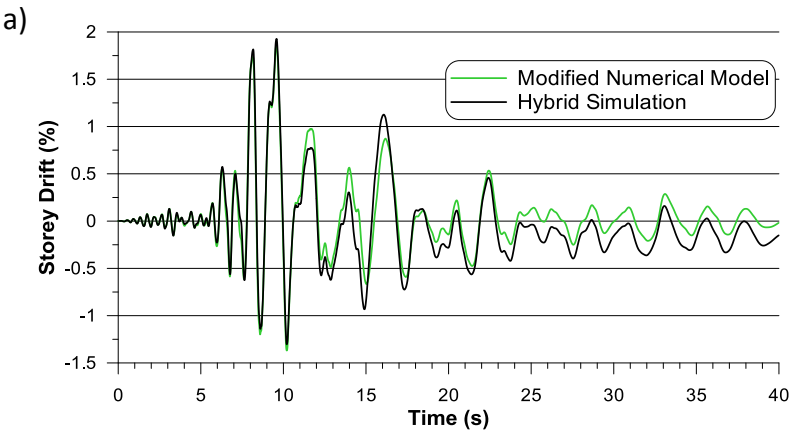

Figure 5.14: Comparison between modified numerical model analysis and hybrid simulation: a) Lateral displacement time history at the first-storey; b) Brace hysteretic response

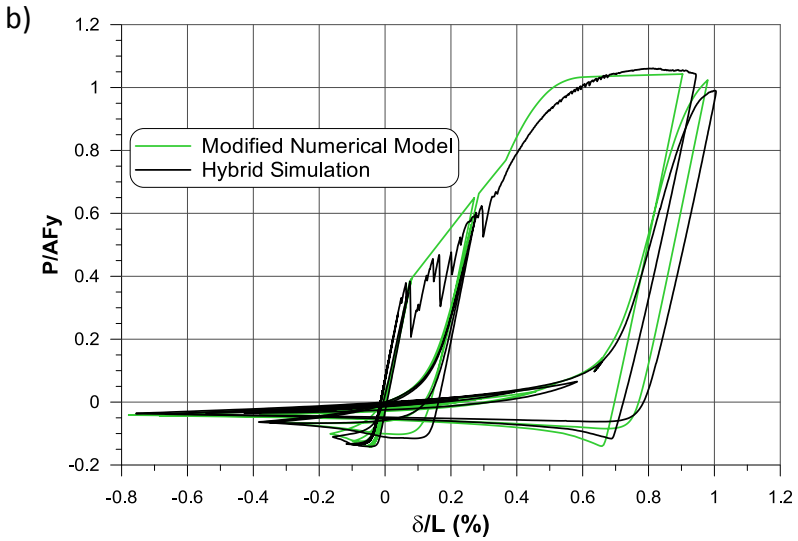

Figure 5.14: Comparison between modified numerical model analysis and hybrid simulation: a) Lateral displacement time history at the first-storey; b) Brace hysteretic response (continued)

These results show that the overall seismic behaviour of a simple braced frame with double angle bracing members can be well predicted with the proposed brace model, even when the inelastic response is shared between the bracing members and the brace connections. Hence, more complicated model can be used in following hybrid tests. It is observed that localized deformations in brace connections can have a significant influence on the overall frame response. Therefore, attention must be paid to connection modelling when assessing the seismic performance of steel structures. In order to get rid of the influence of this situation, slippage in the bolted connections between the gusset plates and the T-shape brackets connected to the test load frame is minimized in following tests.

5.3.2 Hybrid test 2: LF-R1-H-1

In this test, the 15.8 mm slippage which includes the slippage from brace to gusset plate connections and gusset plate to T-shape brackets was removed from the overall brace before the test started. This value is similar to the value of slippage observed in the previous test. The modified ground motion excitation is used in analysis with the aim to fail the retrofitted connections. Duration of this hybrid simulation was about 28 hours for 70 second excitation. Comparing with the duration of the previous hybrid test, the speed of this hybrid simulation is much slower. The

rational of using long test duration was to prevent potential convergence problem due to increasing of non-linearity in the analyzed model.

Figure 5.15a shows the inter-storey drift obtained from numerical model prediction and hybrid simulation. The numerical model predicts the collapse of structure due to connection fracture during the second part of excitation. However, the predicted model is not enough accurate. The numerical model shows that the structure returns to its original position after subjected to the first part of excitation, without exhibiting residual deformations. Nevertheless, this was not the case resulted from the hybrid simulation. The brace hysteretic response shown in Figure 5.15b reveals the origin of this difference. Ductility capacity of the physical connection is higher than what was modeled in the numerical prediction model. The hysteretic properties of *Pinching4* material, which is using in axial direction of the *ZeroLength* elements to replicate brace end connections in purely numerical model. In order to eliminate the difference, the maximum deformation in the hysteretic loop of *Pinching4* material was increased according to the recorded data of connections from the Hybrid test. The comparison between the modified numerical model and hybrid simulation in terms of inter-storey drift and brace hysteresis response is shown in Figure 5.16. The accuracy of residual inter-storey drift resulted after the structure was subjected to the ground motion with 0.6 scale factor was improved. To reproduce the exact behaviour of structure under dynamic lateral loading is not a straightforward task, when the brace connections are almost fractured. It is because the pre-fracture situation in connections is too complicated to model exactly in the hysteretic loop in *Pinching4* materials or OpenSees software.

a)

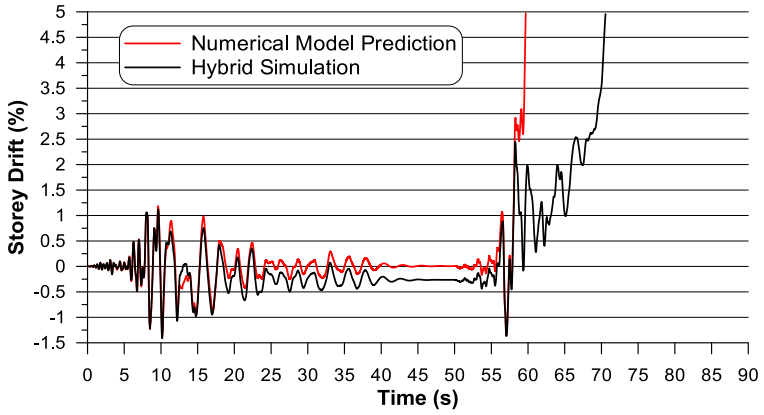

b)

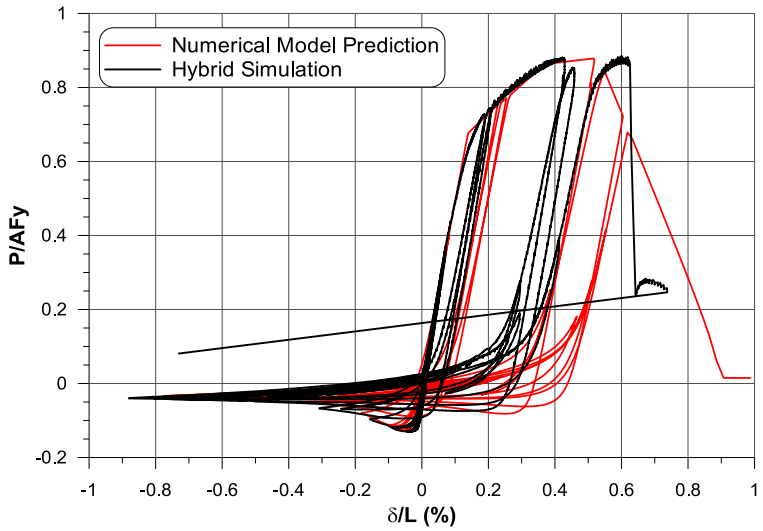

Figure 5.15: Comparison between original numerical model prediction and hybrid simulation: a) Lateral displacement time history at the first-storey; b) Brace hysteretic response

a)

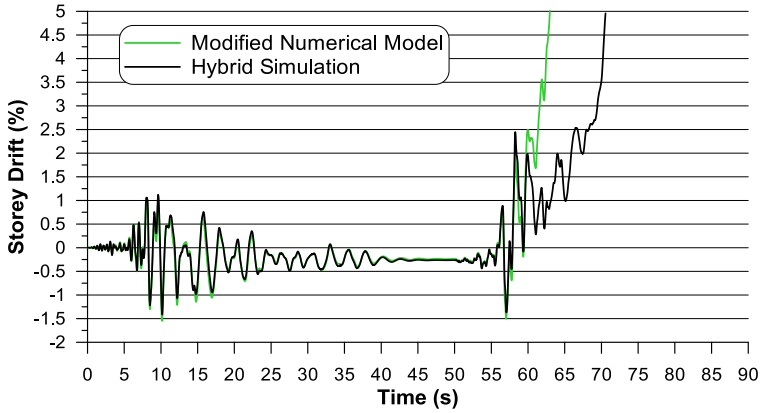

Figure 5.16: Comparison between modified numerical model analysis and hybrid simulation: a) Lateral displacement time history at the first-storey; b) Brace hysteretic response

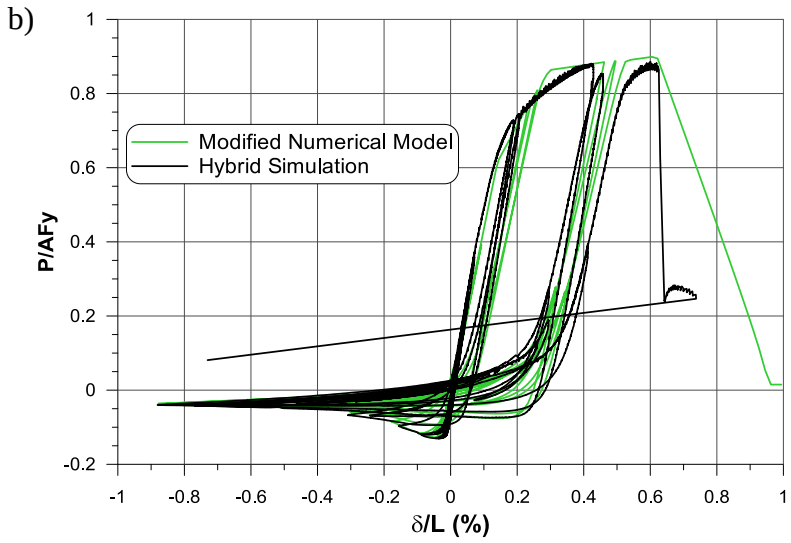

Figure 5.16: Comparison between modified numerical model analysis and hybrid simulation: a) Lateral displacement time history at the first-storey; b) Brace hysteretic response (continued)

The collapse mechanism of structure under earthquake loading was simulated successfully in this hybrid test. It is showed that accurate and robust hybrid simulations can provide reliable assessment of structures response in seismic events.

5.4 Difficulties encountered

Convergence problem is the most critical problem encountered in the OpenSees analysis of braced frame subjected to earthquake loading. Due to large amount of non-linearity and stiffness degradation in the model, the convergence problem is very common and unpredictable. Generally, the convergence problem is likely to happen, when connection hysteretic curve goes to negative slope. Sometimes a small modification that has no impact on the structure response may solve the problem, but this is not always the case. In hybrid simulation, the convergence problem from the numerical model is less critical. There are two reasons: i) the model used in hybrid simulation is based on the prediction numerical model which has no convergence problem and ii) the double angle brace with end connections model is replaced by the physical brace in the hybrid simulation test. Hence, the amount of calculation is reduced during the hybrid simulation.

In hybrid simulation, the two problems that may interrupt the hybrid test were introduced before: the CPU overloaded problem and connection TCP/IP timeout problem. The possible reason for the CPU overloaded problem may be noise in the force feedback signal that causes more analysis

convergence problem. The noise is very significant, when using a powerful load frame to apply a small load to the test specimen. For example, in the performed test, the buckling load of double angle brace was about 0.18 MN, which is only 1.5% of the maximum capacity of 12 MN load frame. In addition, the force is very small when brace connections are nearly disconnected during the collapse stage. At this time, the noise in force feedback from the load frame is large. Another possible reason for CPU overloaded problem is the slow calculation speed of the host PC, which depends on computer hardware. The host PC has 2.8GB single core CPU and 2GB memory. In order to eliminate the influence of performance of the host PC and boost simulation speed, a new host PC with 3.0GB 8 cores processor and 16GB memory will be used in hybrid simulation in the future. At this moment, the connection between the new host PC and the xPCtarget couldn't be built successfully. Moreover, one of the hybrid tests interrupted because of connection TCP/IP timeout problem. This may be the data synchronization problem between PCs. Helps from computer experts are needed to solve this problem.

Another deficiency in the current hybrid simulation is related to the simulation speed or hybrid simulation duration. In the performed hybrid simulations, the simulation speed was controlled by the numerical model and predictor-corrector model. The numerical model defined the number of analysis steps for certain ground motion excitation and the predictor-corrector defined the real analysis time for each analysis steps. Normally, the real analysis time is proportional to the length of time step in the numerical model. For example, a ground motion excitation is 40s. The analysis process for this ground motion is completed in 1000 steps, so the length of time step is 0.04s. If the simulation is running 100 times slower, the real time for each analysis step is 4s, and the simulation duration is 4000s. However, this relationship between the hybrid simulation duration and ground motion duration needs to be improved. The duration for each hybrid simulation was much longer than expected. In addition, in order to prevent potential convergence problem and potential calculation problem during simulation, relatively large number of analysis steps and large real time limitation for each analysis steps are used. Due to these two reasons, the duration of hybrid simulation was magnified and explained the longer time (more than 24 hours) required to carry out the hybrid test LF-R1-H-1. In order to improve the efficiency of hybrid simulation, the relationship between the hybrid simulation duration and ground motion duration needs to be fixed.

5.5 Summary

In this chapter, double angle braces were considered for the tension only braced frame model. The OpenSees numerical model is linked to physical double angle brace specimen through OpenFresco middleware in order to carry out the hybrid simulation. Hybrid simulation technology and the experimental setup are introduced. Analysis results from numerical model prediction, hybrid simulation, and modified model simulation are compared. It shows that detailedOpenSees model analysis can provides accurate predictions. In addition, the hybrid tests can be reproduced accurately using well defined numerical models. Collapse mechanism of structures under earthquake loads can be successfully simulated in hybrid simulations. However, the problems encountered in the pure numerical model analysis and hybrid simulations cannot be ignored. Convergence problem is the most critical problem that happens during numerical model analysis. Moreover, two out of four hybrid tests were completed successfully. The interruption of hybrid tests was due to CPU overloaded and connection TCP/IP timeout problems. Hence, further improvements on OpenSees finite element software and hybrid simulation technology are necessary to solve these revealed drawbacks.

CHAPTER 6: THE 4-STOREY BRACED FRAME MODEL AND TIME-HISTORY ANALYSIS

In this chapter, two CBF building structures were studied: i) the CBF building in the existing condition (original design); and ii) the retrofitted CBF building considering: the retrofit strategy II with slotted holes in the gusset plates applied at floor levels 1 to 3, and the retrofit strategy I with additional cover plates added on the short leg of angles applied at the top floor. The original design was studied considering two values for the steel properties: 1) the probable strength values corresponding to the code specified values, assuming that test data is not available; and 2) strength values obtained from the coupon test. For all cases, a detailed OpenSees model of the 4-storey prototype building was developed based on the simplified 4-storey tension-only braced frame model that was discussed in Chapter 5. This modified model was used to perform nonlinear incremental time-history analyses under 20 selected and scaled ground motions in order to develop the fragility curves and assess the collapse capacity of the prototype building in accordance with the procedure described in FEMA P695 (ATC 2009).

6.1 Description of the three CBF structures studied

The two building models considered for the 4-storey tension-only braced frame are the existing building model and the retrofitted building model. For the existing building model, two cases were retained for the investigation: 1) the CBF_{design} model that represents the original design condition where the strength of the components is based on the probable material resistance values that are available to design engineers in absence of test data, i.e., code specified values; and 2) the same model as in the first case except that the strength of the components is based on data collected from the coupon tests, $CBF_{design+exp.}$. For the retrofit model, the brace connections were retrofitted according to retrofit strategies I and II and the strength of the components was based material properties obtained from test data: $CBF_{retrofit+exp}$.

In the CBF_{design} model, the material yield and tensile strengths of the braces are based on the probable values specified in the current codes and standards: R_yF_y = 385 MPa and R_tF_u = 490 MPa. The same properties are used to determine the strength of the brace connections using the equations provided in the current CSA S16-09 design standard. The deformation capacity of the brace connections is however based on the experimental data obtained in this research, as explained next

when describing the $CBF_{design+exp.}$ model. This model of the building structure would be representative of common engineering practice, when no test is performed to determine the material properties for the steel used in the structure studied, but the design engineer has access to test data on the seismic performance of specific components such as the brace connections. In that case, the probable axial resistance of the brace connections is likely to be used to predict the strength of the connections.

In the $CBF_{design+exp.}$ model, the bracing members and columns were modelled using the steel yield and ultimate tensile strengths measured in the coupon tests performed in this project, assuming that tensile tests would be performed to characterize the steel properties of the structure studied. In that model, the axial force resistance and ductility performance of the brace connections were obtained from the tests performed in this project. In the test program, only the brace connections at the first floor of the prototype building were tested. Hence, at that level, the experimental results could be used directly to define the hysteretic properties of the *Pinching4* material assigned in the *ZeroLength* element that simulate the brace connections to the gusset plates. For the other levels, the strength properties of the connections were obtained by applying the ratio between the nominal and measured connection resistances obtained at level 1. The deformation capacity of the connections at levels 2 to 4 were determined by multiplying the connection length ratio and the measured connection deformation at the first floor.

In the case of the retrofitted structure model, $CBF_{retrofit+exp.}$, the yield strength used in the brace and column models were the same as in the $CBF_{retrofit+exp.}$ model. The retrofit strategy II that consisted in introducing slotted holes in the gusset plates, with the aim of controlling the level of force transferred between the braces and the frame while increasing the ductility performance of the brace connections. This retrofit strategy was applied to the brace connections at levels 1 to 3. For the brace connections at the top floor, retrofit strategy I was applied where the connections were strengthened by adding cover plates to the outstanding leg of double angle brace cross-section. This different strategy at level 4 was adopted because the axial resistance of the existing brace connections at that level was too low compared to the expected seismic demand. In that case, reducing further the strength of the connections by introducing slotted holes would probably have led to excessive inelastic demand at the top level, with the risk of connection failure. For the brace connections retrofitted by performing slotted holes in the gusset plates at levels 1 to 3, the

experimental data obtained from the physical tests conducted on that retrofitted connection was used directly in the model. In the connection model of the strengthened brace connections at level 4, the Equation 2.26 was used to calculate the axial resistance. In these calculations, we used the steel yield and tensile strengths of the brace and gusset plates, as measured in the test programs.

The flexural resistance of the beam-to-column connections was determined as described in Chapter 5. For the CBF_{design} model the material yield and tensile strengths are based on the probable values specified in codes and standards: R_yF_y = 385 MPa and R_tF_u = 490 MPa. For the $CBF_{design+exp.}$ and $CBF_{retrofit+exp.}$ model the material yield and tensile strength are based on the coupons test results cut from angles. The yield strength of the columns members in all three models was set equal to 330 MPa. This value corresponds to 1.1 times the nominal yield value, similar to what was measured in the coupon tests for the angles.

6.1.1 Preliminary assessment of the building retrofit

Before the numerical time-history analyses for the retrofitted building model were carried out, the expected performance of the retrofitted building models to be analyzed was assessed to validate the adequacy of the proposed retrofit model. Capacity design concept was used to evaluate the performance of the proposed retrofit scheme. The braces at level 4 and the brace connections at levels 1 to 3 were selected to be the "fuses" in the braced frame. Hence, the factored resistance of the remaining structural elements should be equal to or exceed the force level corresponding to the likely resistances of the selected brace and brace connection fuses.

At levels 1 to 3, the maximum brace forces are based on the resistance of the slotted brace connection as obtained from physical tests. At the top floor, the strengthened brace connections have grater resistances than the probable yielding resistances of the double angle braces. The gross yielding strength of the braces was treated as the likely maximum brace force. Based on the maximum forces that can develop in the braces, the design loads in other structural members can be determined, as shown in Figure 6.1.

In Chapter 2, it was found that the central column at the first level was critical for this braced frame. Using the proposed retrofit scheme, the force in that column segment reduces by 20%, form 2717 kN as shown in Figure 2.8 to 2255 kN, which represents a significant improvement resulting from the proposed retrofit solution. In Figure 2.8, the column axial load of 2717 kN was obtained

assuming retrofit strategy I at every level. Using retrofit strategy I only where needed (at level 4) in combination with retrofit strategy II at the other levels produced a more effective retrofit solution.

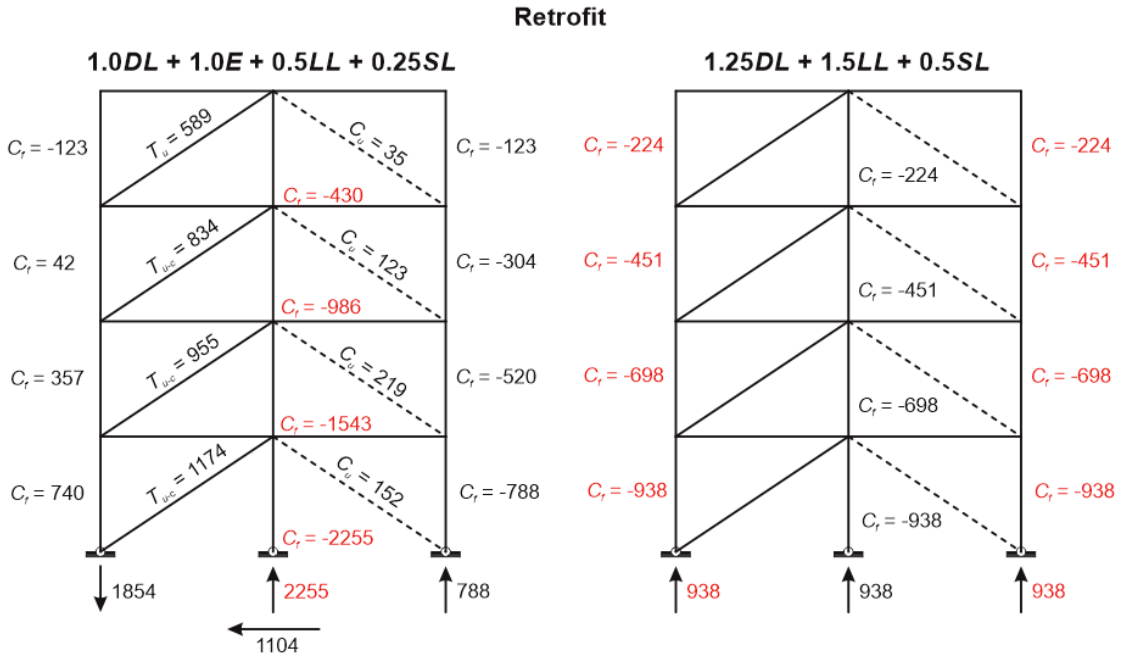

Figure 6.1: Design forces in the retrofitted braced frame

Using these design forces, the beams and columns were checked based on their factored resistance. When the nominal yield strength of 300 MPa is considered for the columns, only the factored compression resistance of the central column at ground floor level (C_r = 2081 kN) is found to be lower (by 8%) than the design force. According to capacity design concept as applied in current codes for new structures. In the context of a retrofit, it is deemed acceptable to use a steel yield strength that more closely reflects the reality, such as the value that would be obtained from coupon tests. When using the steel yield strength equal to 330 MPa, the demand to capacity ratio for this column segment becomes less than 1.0, which is satisfactory. All beam members were also found to be adequate when adopting the same material strength.

Thus, in terms of force demand on members and member resistances, the proposed retrofit scheme is found to reduce the force demand in the braced frame and all column and beam members have sufficient resistance to sustain that demand. However, the ductility performance of this retrofit

scheme must still be evaluated under seismic ground motion demand. This is done in the following sections through numerical model analysis.

6.2 Tension only braced frame model

6.2.1 Introduction to the modelling

Through improvements made in the OpenSees model from the results of the hybrid simulations, an upgraded model of the 4-storey tension-only braced frame was developed for the time-history analyses required to assess the collapse capacity of the structure. The sketch of the model is shown in Figure 6.2. In this model, the lateral frame part in the braced frame model is almost the same as that used in the simplified braced frame model. However, in this upgraded model, the entire gravity load carrying frame system was introduced in order to replace the simplified leaning column used in the hybrid simulations. With this modification, the axial-flexural capacity of each individual gravity columns is considered in the analyses.

As shown in Figure 6.2, due to the building symmetry, only half of the building structure was modeled to investigate the building response. The analysis is performed in the E-W direction and the braced frame study is the two-bay braced frame located on grid line 4. The tributary area of the building assigned to this braced frame is illustrated in the figure. The area includes the 3 columns of the CBF studied, 5.5 gravity columns and 4 columns of the two braced frames acting in the N-S direction in grid lines A and E. At every level, the node at the center of the braced frame studied is defined as the master node. Due to diaphragm action, all other nodes at each level are assumed to experience the same horizontal displacement as the master node in the E-W direction. In the model, these nodes are therefore considered as slave frame nodes that are connected to the master node at each level using the *EqualDOF* command in OpenSees. The lumped seismic masses at each floor are distributed equally to the top of the frame columns. Gravity loads on each column are assigned according to the column tributary area. All columns are pin connected at their bases. As mentioned before, the column size is kept the same over two consecutive floors. Hence, the columns are continuous between the first and the second storeys, and between the third and fourth storeys. Pinned connections are used for the columns between the second and third storeys.

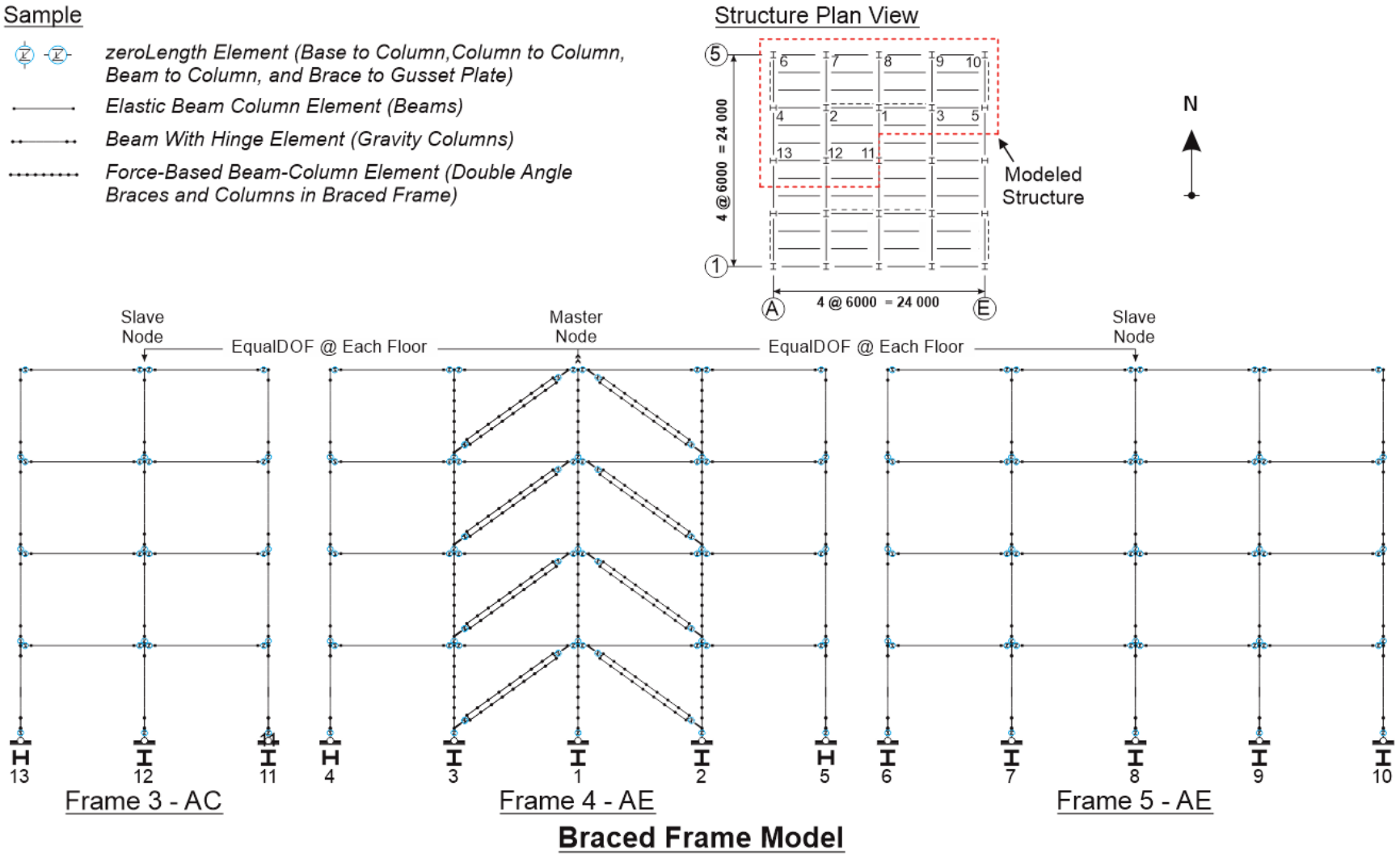

Figure 6.2: 4-storey braced frame model

6.2.2 Lateral frame

The two adjacent bays of the four-storey tension-only braced frame are exactly the same as introduced in Chapter 5, except that the *MinMax* material available in OpenSees is introduced at two locations: i) in parallel to the translational spring assigned in the axial direction of the *ZeroLength* element used to replicate the double angle brace end connections; and ii) in parallel to the in-plane rotational spring assigned in the *ZeroLength* element used to simulate the beam-to-column connections.

6.2.2.1 *MinMax* material

The function of the *MinMax* material is to decouple the pre-defined *Pinching4* material from the model once a predefined level of deformations or rotation is reached in the analysis. According to the definition of the *MinMax* material, this material uses the stress-strain or displacement-force (or moment-rotation) behaviour from another controlled material. When the strain or displacement in the controlled material goes over or fall below the defined limitations in the *MinMax* material, the controlled material is considered to have failed. Zero stress or force value is then returned to the stiffness matrix. In the brace connection model, when the axial deformation in the *Pinching4* material exceeds the maximum deformation defined in the *MinMax* material, the *MinMax* material will decouple the *Pinching4* material from the *ZeroLength* element. In the beam-to-column connection model, the *MinMax* material has the same function. When the rotation angle in the beam-to-column connection exceeds the maximum allowed rotation, the *Pinching4* material in the *ZeroLength* element assigned to simulate the beam-to-column connection is decoupled. After decoupling, it does not provide any in-plane moment resistance.

The advantage of using the *MinMax* material together with the *Pinching4* material is to prevent the *Pinching4* material to introduce negative stiffness slope to the stiffness matrix during the analysis. Introducing this material can improve the stability of the whole model. Although the accuracy of the model is slightly affected, the negative influence is minor and can be omitted when compared to the overall behaviour of the braced frame model.

6.2.3 Gravity frame

Modelling of the beams of the gravity frame is the same as that in the frame model of Chapter 5. The *Elastic beam column* element was used with the flexural and axial stiffness beam properties.

As mentioned, the modelling of the gravity columns was modified compared to the leaning column model used in Chapter 5.

6.2.3.1 Gravity column

As shown in Figure 6.2, the gravity columns are modelled with the *Beam with hinge* element to account for P-Delta effects on the structure when subjected to earthquake induced lateral displacements. With the *beam with hinge* element, plastic hinges may form at the ends of the gravity columns when they undergo large inter-storey displacements. As observed in the hybrid simulations, this situation is likely to happen after failure of the brace connections in this model analysis. The formation of plastic hinges will provide a more realistic representation of the column flexural resistance that can be mobilized when building collapse develops on the form of soft-storey response.

In the *Beam with hinge* element, the middle part is defined to undergo elastic behaviour, while flexural hinges are defined at the element ends, as is shown in Figure 6.3. The definition of the linear elastic part is similar to the definition used for the *elastic beam column* elements. The plastic hinges are pre-defined fiber sections that are similar to the fiber cross-section discretization used in the nonlinear beam column element with spread plasticity that is assigned to the braced frame columns. The length of the plastic hinges is taken equal to the depth of the column cross-section.

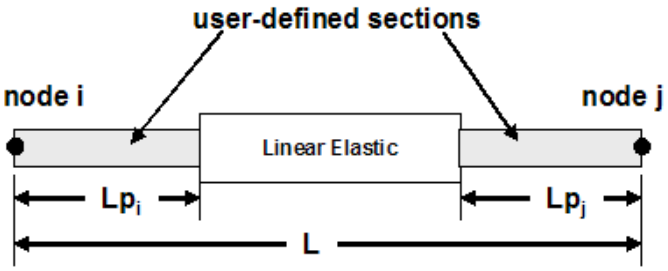

Figure 6.3: Beam with hinge element

6.3 Analysis procedure

6.3.1 Ground motions

The twenty horizontal components of far-field ground motions described in Table 6.1 were selected to perform the nonlinear incremental dynamic time history analysis of the three structure models.

All selected ground motions corresponding to site class C were downloaded from the PEER Strong Ground Motions Database (PEER 2011) These records were scaled to be compatible with the seismic hazard at the building site. The scaling factors (S_f) applied to the ground motions are given in the last column of Table 6.1. The ground motions were scaled to fit or be above the uniform hazard spectrum defined for Vancouver over the period of interest range, 0.5 T_1 to 1.5 T_1, where T_1 is the fundamental period of the structure. For the braced frame studied, this period range is between 0.4 s to 1.2 s. The uniform hazard spectrum for Vancouver defined as per the NBCC 2010 provisions and the scaled spectra for selected records are shown in Figure 6.4.

Table 6.1: Selected ground motion records

No.	NGA	Event	M_w	Station	S_f
1	15	July 21, 1952 Kern County	7.4	Taft Lincoln School	2.0
2	57	Feb. 9, 1971 San Fernando	6.6	Castaic, Old Ridge Route	1.2
3	83	Feb. 9, 1971 San Fernando	6.61	Puddingstone Dam (Abutment)	6.0
4	735	Oct. 18, 1989 Loma Prieta	6.9	APEEL 7 - Pulgas	2.0
5	762	Oct. 18, 1989 Loma Prieta	6.93	Fremont - Mission San Jose	2.5
6	776	Oct. 18, 1989 Loma Prieta	6.9	Hollister - South & Pine	1.2
7	787	Oct. 18, 1989 Loma Prieta	6.9	Palo Alto - SLAC Lab	1.1
8	796	Oct. 18, 1989 Loma Prieta	6.9	SF-Presidio	1.5
9	807	Oct. 18, 1989 Loma Prieta	6.93	Sunol - Forest Fire Station	3.8
10	838	June 28, 1992 Landers	7.3	Barstow	2.0
11	900	June 28, 1992 Landers	7.3	Yermo Fire Station	1.2
12	953	Jan. 17, 1994 Northridge	6.7	Beverly Hills - 14145 Mulhol	0.5
13	963	Jan. 17, 1994 Northridge	6.7	Castaic, Old Ridge Route	0.6
14	975	Jan. 17, 1994 Northridge	6.69	Glendora - N Oakbank	5.0
15	986	Jan. 17, 1994 Northridge	6.7	LA - Brentwood VA Hospital	1.4
16	1005	Jan. 17, 1994 Northridge	6.7	LA - Temple & Hope	1.6
17	1006	Jan. 17, 1994 Northridge	6.7	LA - UCLA Grounds	1.5
18	1049	Jan. 17, 1994 Northridge	6.7	Pacific Palisades-Sunset	1.8
19	1787	Oct. 16, 1999 Hector Mines	7.1	Hector	1.0
20	1794	Oct. 16, 1999 Hector Mines	7.1	Joshua Tree	1.4

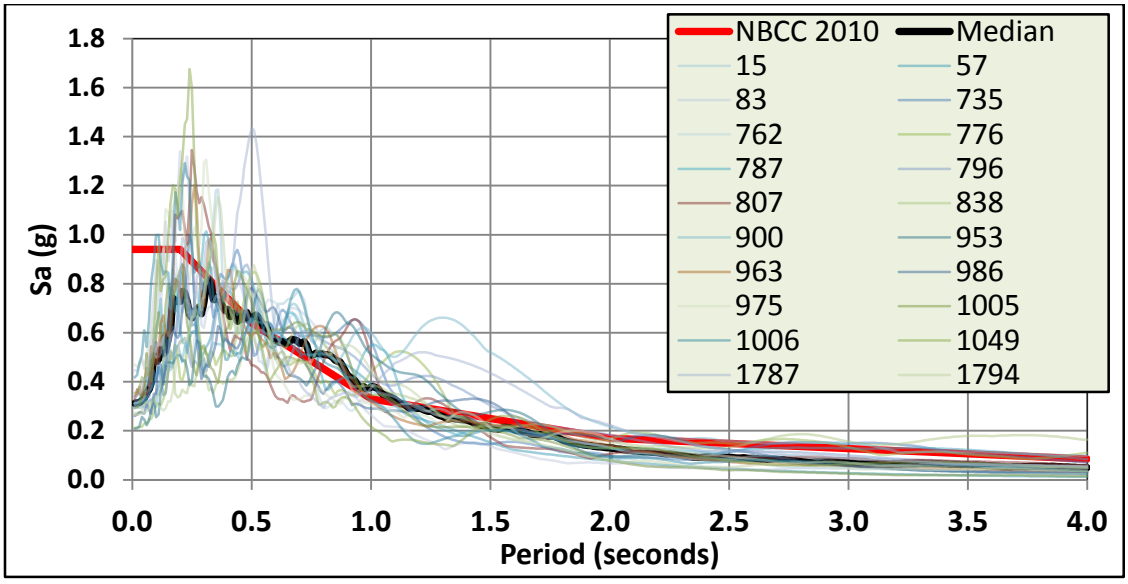

Figure 6.4: Design uniform hazard spectrum and scaled acceleration spectra of selected ground motions

6.3.2 Collapse criteria

In this study, the failure of brace connections is likely to happen. When the braces disconnect from the braced frame because of connection failure, it is likely that large storey drifts develop and a soft-storey response occurs. In the model analysis, it is therefore assumed that the structures reach collapse when a soft-storey phenomenon occurs or the columns of the braced frame have buckled due to large storey drifts. In addition, an inter-storey drift limit is also used as a reference parameter to determine whether collapse has occurred or not. Herein, an inter-storey drift limitation equal to 5% h_s is used to define the collapse of structure.

6.3.3 Analysis steps

The structure models were subjected to an incremental dynamic analysis up to the point where the structure reached the collapse state. In the incremental dynamic analysis, the amplitudes of the ground motions were increased by 10% increments until the structure collapsed. When the structure collapsed under ground motion scaled to the design level, the scaling factor for that ground motion was decreased by 10% until the structure was able to survive. For each of the three models, the incremental time history analysis for this type of structure was halted once the structural collapse had been observed under half of the 20 ground motions, which means 50% probability of collapse.

According to FEMA-P695, the 50% probability of collapse is the median collapse capacity. Data obtained from the analysis up to this point is sufficient to assess the structure collapse capacity.

6.4 Analysis results

In order to visualize the model behaviour, the 2D model display file provided by OpenSees was used. Although the proportions of the structure shown in the resulting 2D view does not reflect the actual dimensions, this file can display in real time a 2D view of the structure behaviour during model analysis, which was found very useful to examin the colapse response and verify if a convergence problem had occurred. Figure 6.5 shows some typical structural collapse patterns obtained from the print screen of the 2D view of the structure at the end of the analysis. These views of the structures could be obtained for different types of structure. Typical soft-storey failure modes are illustrated. In the figure, the red circles show where brace connection failures occured. After a brace connection failure, the inter-storey drift at that location generally increases more than the accepted limit and leads to soft-storey phenomena or buckling of the columns. An example is provided in the following section to illustrate the behaviour of the $CBF_{retrof+exp}$ model under one ground motion.

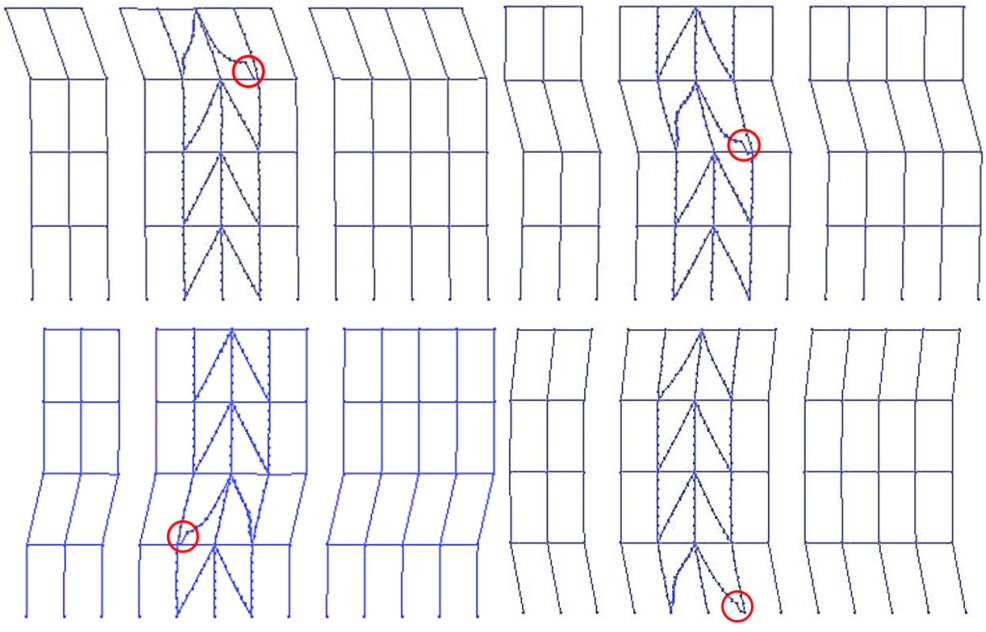

Figure 6.5: Collapsed structure corresponding to different storey failure

6.4.1 Detailed analysis example upon collapse of the $CBF_{retrof+exp.}$ structure

A typical structural collapse response is described herein for the 4-storey $CBF_{retrof+exp.}$ structure under the Joshua Tree ground motion recorded during the M7.1, Oct. 16, 1999 Hector Mines earthquake. A scaling factor of 1.4 was applied to the record to be compatible with the seismic hazard for Vancouver. The scaling factor was further increased by 10% to produce collapse. A print screen at collapse is shown in Figure 6.6. As illustrated, the building reached collapse due to a soft-storey phenomena that occurred at the ground level.

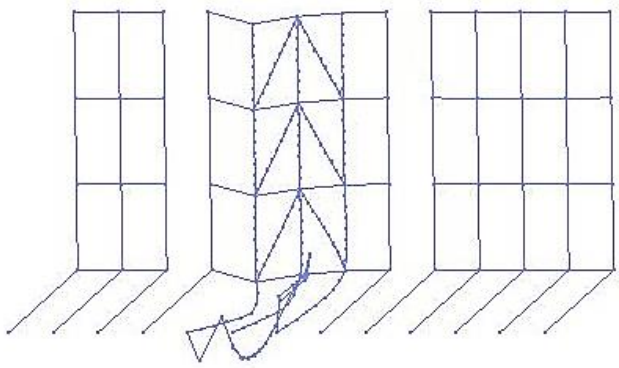

Figure 6.6: 2D view of the $CBF_{retrofit+exp.}$ structure at collapse (obtained from OpenSees)

The portion of the ground motion accelerogram that shook the building up to the collapse at t = 18.2 s is shown in Figure 6.7a. In this case, the building failure occurred just after the peak ground acceleration (PGA) of 0.21 g had been applied at t = 15.4 s. At this time, the structure moved towards the positive direction (to the right on Figures 6.2 and 6.6) and the braces in the left bay of the braced frame were loaded in tension. At t = 15.6 s, the retrofitted brace connection of the left bay brace located at the ground level reached its failure axial load. After the connection had reached its capacity, the *MinMax* material decoupled the *Pinching4* material used to simulate the brace connection and the attached brace was disconnected from the frame. Although the corresponding double angle brace loaded in compression could still provide some lateral resistance to the structure, that resistance was very small and could not prevent the movement of the structure towards the right hand side, and collapse then initiated towards that direction. As shown in Figure 6.7b and 6.7c, the storey displacement and inter-storey drift substantially increased after failure of the brace connection has occurred. At the time of connection failure, the inter-storey drift approximately 1% h_s. Suddenly, the axial compressive load in the middle column dropped (Figure

6.7e) because the first-storey tensile brace that had induced compressive force in the middle column became decoupled due to the connection failure (Figure 6.7d). Then, the inter-storey drift continued to increase and the bending moments at the top end of each column gradually increased. At the end of analysis, the bending moments developed in the two exterior columns of the braced frame (Columns 2 & 3) reached the columns' moment capacities about weak axis (Figure 6.7f).

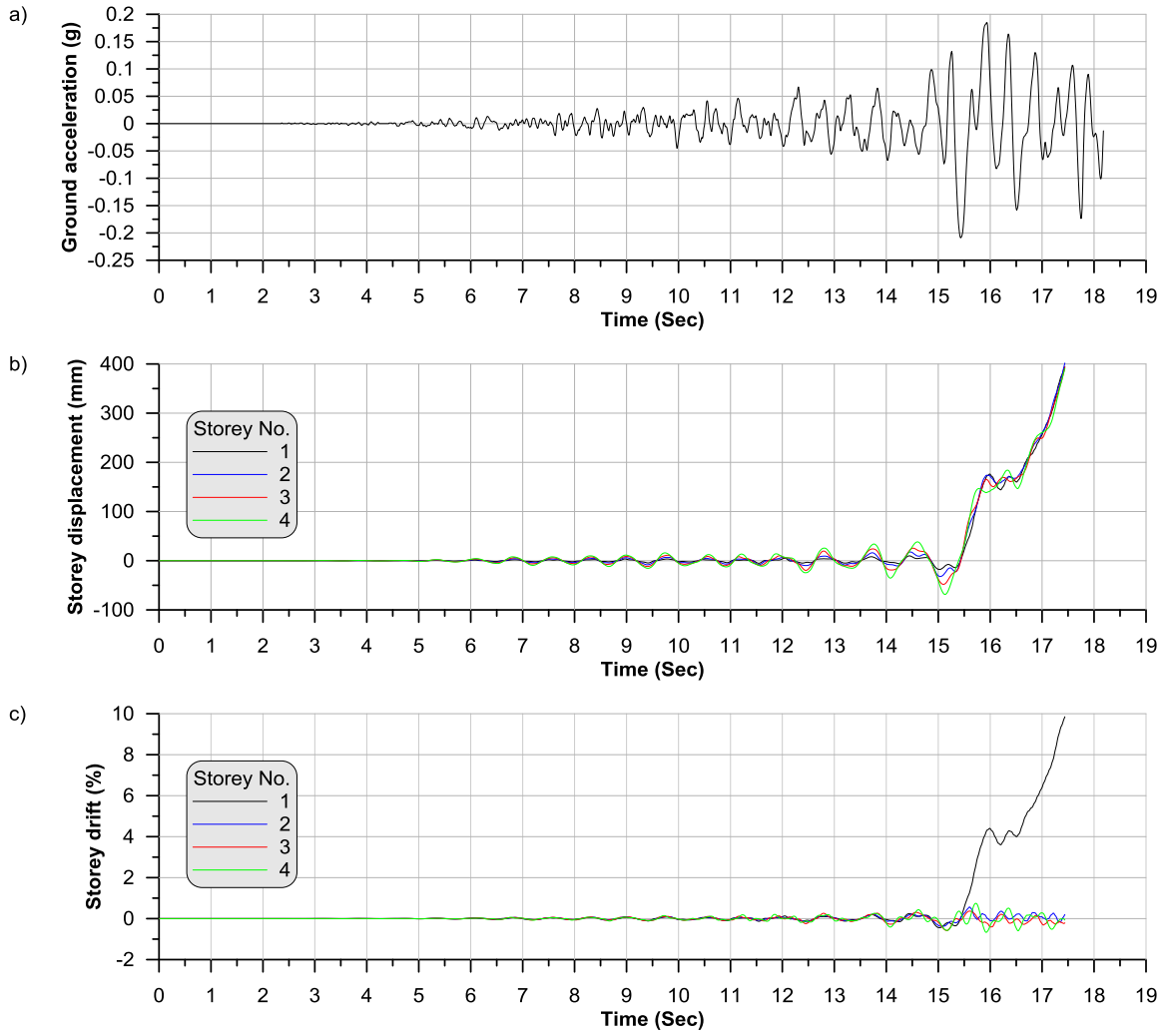

Figure 6.7: Time-history response: a) Ground motion accelerogram; b) Storey lateral displacements; c) Inter-storey drifts; d) Axial force in the braces at ground floor level; e) Axial force in the frame columns at the ground floor level; f) Bending moment at the top of the frame columns at the ground level

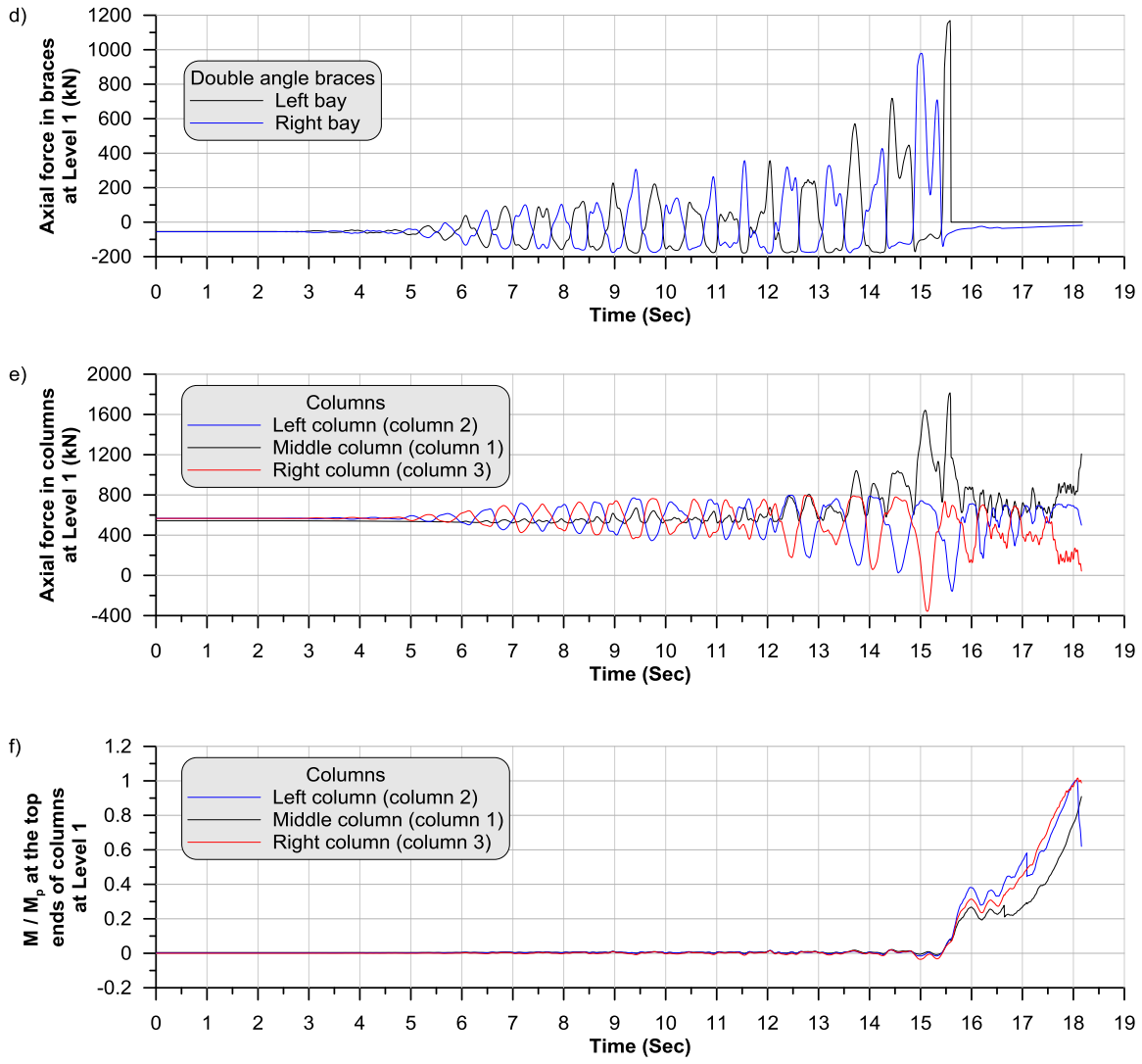

Figure 6.7: Time-history response: a) Ground motion accelerogram; b) Storey lateral displacements; c) Inter-storey drifts; d) Axial force in the braces at ground floor level; e) Axial force in the frame columns at the ground floor level; f) Bending moment at the top of the frame columns at the ground level (continued)

The brace hysteretic behaviour at the ground and 2nd floors are respectively shown in Figures 6.8 and 6.9. In both figures, the horizontal axis in the first plot (Figure 6.8a) is the total elongation of the two end connections; the total brace elongation including connection deformations are given in the second plot (Figures 6.8b). Failure of the brace connection can be seen in Figure 6.8a. Although the brace connections in the left bay at the 2nd level did not fracture during the analysis, they sustained 6 mm plastic deformation at the end of the analyses. This 6 mm deformation was obtained before the failure of brace connections at the first level. The maximum axial deformation of the

brace in the left bay at the 2nd floor level is about 14 mm, which is approximately 35% of the maximum axial deformation of the failed brace at the first level.

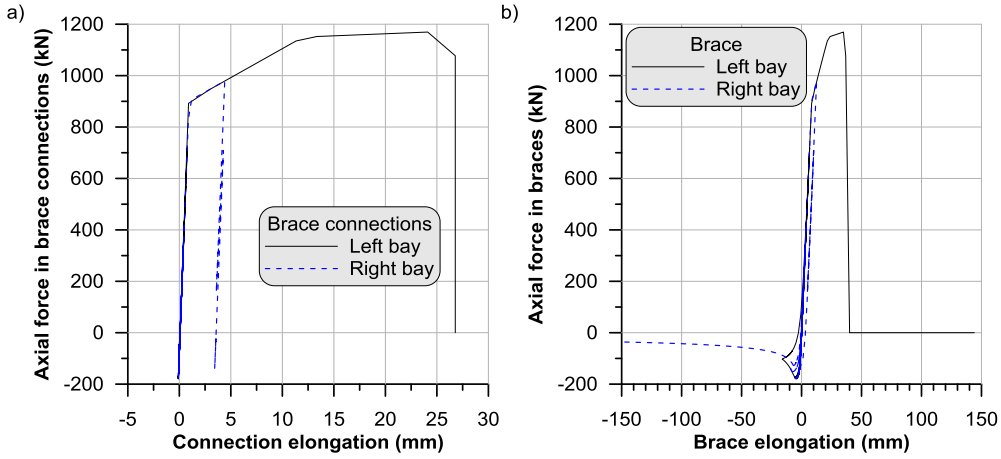

Figure 6.8: Brace hysteretic behaviour at GF level: a) sum of two connections; b) angle brace with connections

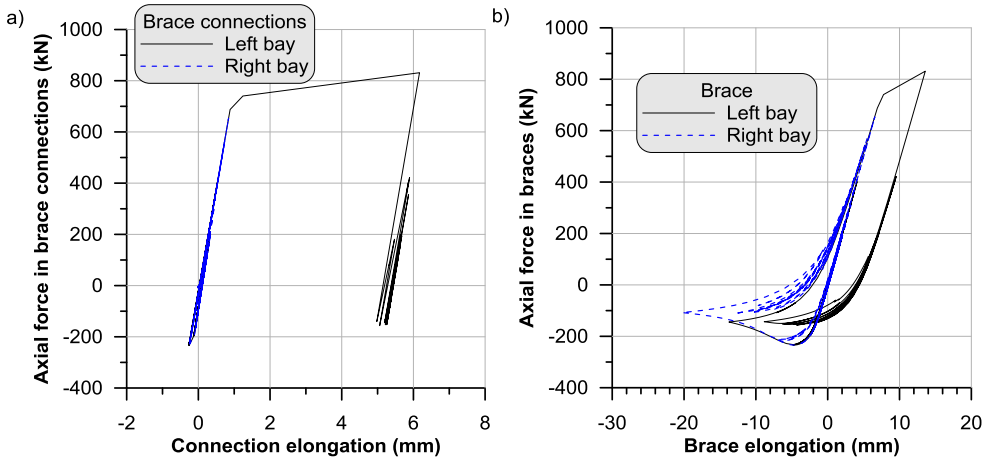

Figure 6.9: Brace hysteretic behaviour at the 2nd floor level: a) sum of two connections; b) angle brace with connections

The axial load and bending interaction diagram for all columns are shown in Figure 6.10. Columns 1 to 3 are the braced frame columns that are modelled with *fiber* cross-section discretization and the *nonlinear beam column elements.* Buckling of these columns can therefore be reproduced during the analysis. Columns 4 to 13 are columns in the gravity frame that were modelled using the *beam with hinges* element. In this last formulation, bending moments and flexural yielding can develop at the plastic hinge locations, but the columns cannot buckle. This is the reason why the gravity columns located at the first level illustrated in Figure 6.6 undergo a linear behaviour with

a nearly straight profile. For columns 1 to 3, the axial force demand from gravity loads was small when the columns were subjected to the maximum axial compression force demand due to brace yielding and buckling. The peak axial compression load demand remained lower than the columns' probable axial compressive resistances and the columns did not buckle. After failure of the brace connection, the storey drift increased at the first level and large bending moments were imposed to the columns. At the end of the analysis, columns 2 and 3 reached their capacities under combined axial force and bending moment, while column 2 reached buckling as shown in Figure 6.6. Because of the low axial load due to gravity loads after brace connection failure, the strength of the columns is essentially governed by flexure. Column 1 followed the same trend and was close to reaching its probable cross-section interaction strength at the end of the analysis. During building collapse due to soft-storey response, a plastic hinge must eventually form at the top of all of the columns. When the analysis was halted, all gravity columns bent about their weak axis (Columns 6 to 12) and exceeded their axial and bending interaction limit (see Figure 6.10). However, gravity columns bent about their strong axis (Column 4, 5 and 13) did not yet reach their capacities and could still provide additional resistance against the P-delta effects.

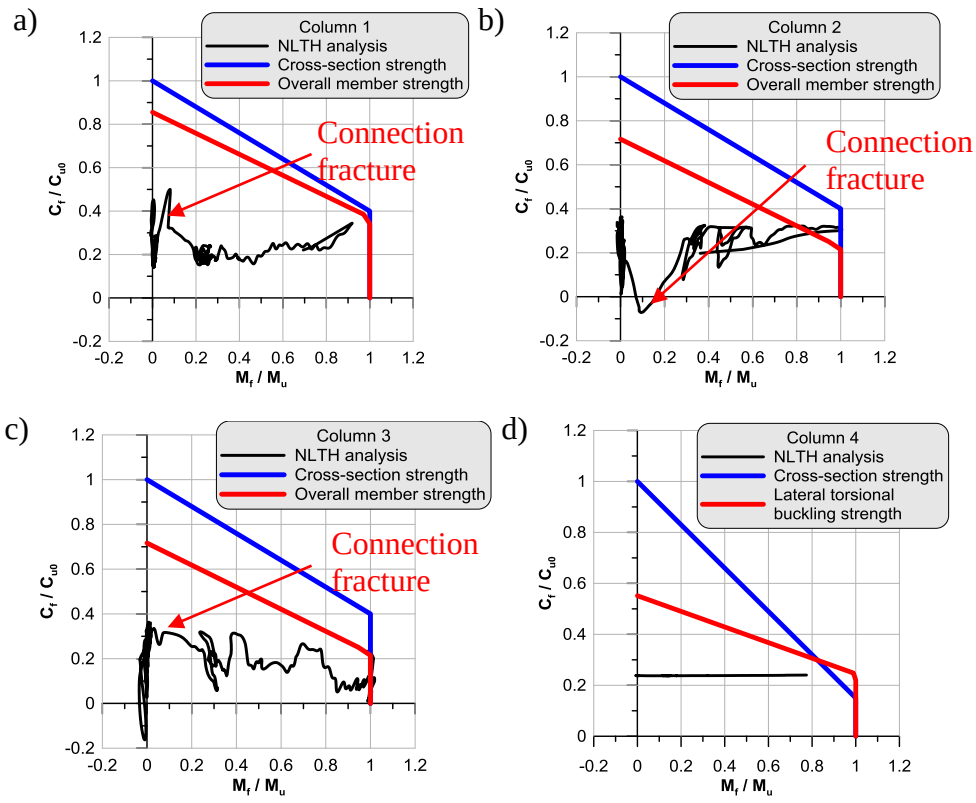

Figure 6.10: Axial force-bending moment interaction diagrams: a) to m) Columns 1 to 13

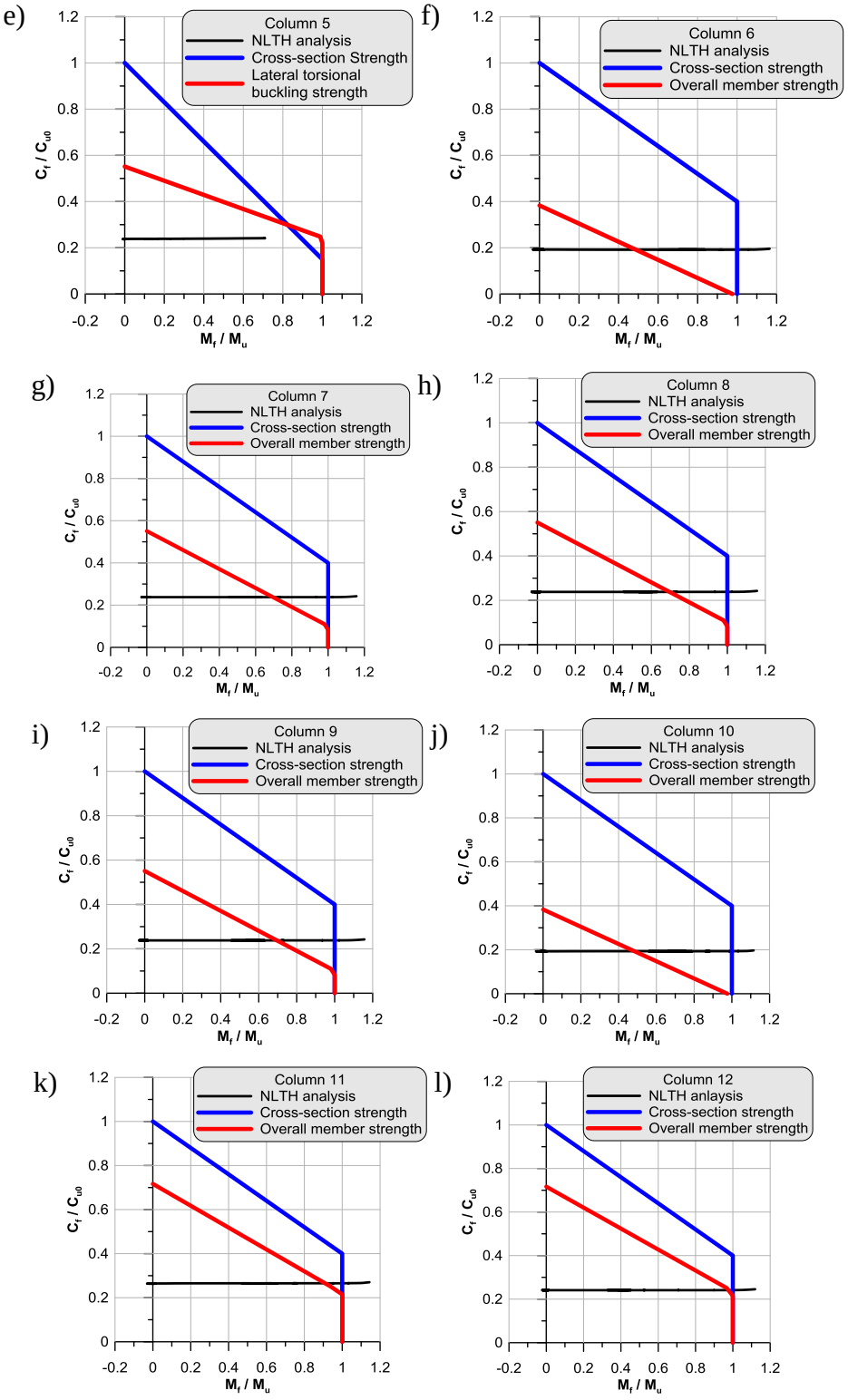

Figure 6.10: Axial force-bending moment interaction diagrams: a) to m) Columns 1 to 13 (continued)

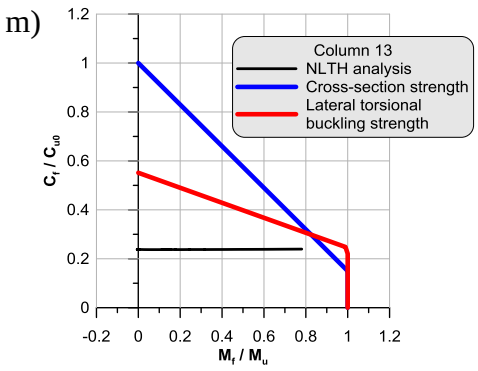

Figure 6.10: Axial force-bending moment interaction diagrams: a) to m) Columns 1 to 13 (continued)

At the end of analysis, the conditions were such that collapse of the building structure was unavoidable, even if some of the columns had not reached their axial-bending moment resistance interaction limit. For instance, in Figure 6.11b, the storey shear at the ground floor level, produced by the overturning moment induced by the gravity loads supported by the frame multiplied by the inter-storey drift ($V_{P\text{-}\Delta} = P\Delta_1 / h_{s1}$), increased rapidly and had largely exceeded the total shear force contributed by the columns (V_c). In this case, the structure had no other means to resist any further increase storey shear due to P-delta effects.

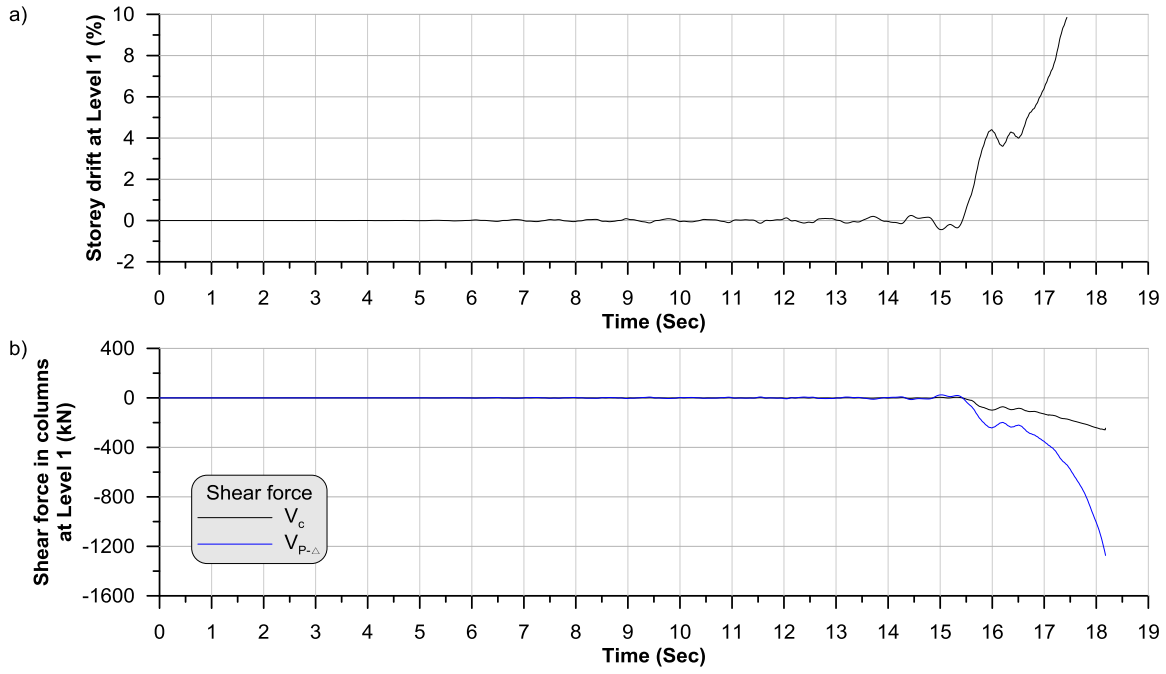

Figure 6.11: Shear force in columns

6.4.2 Analysis results summary

The analysis results obtained from the incremental dynamic time history analyses are summarized in Table 6.2. In the table, F_{sm} is the additional scaling factor required to reach structural collapse (beyond the scaling factor initially applied to match the design spectrum) in the incremental analysis, h_{sm} is the maximum inter-storey drift, in percentage, reached in that analysis, S_{nm} is the floor level where the maximum inter-storey drift occurred, S_{nf} is the floor level where brace connection failure occurred brace. It was found that the brace connections at the top level of the CBF_{design} and $CBF_{design+exp.}$ structures were the weakest point in these two structures. For the CBF_{design} structure, the median collapse capacity was found to correspond to an additional scaling factor (F_{sm}) of 1.10. For the $CBF_{design+exp.}$ structure model, the collapse occurred under 12 selected ground motions at 125% of ground motion level corresponding to the design level. For the retrofitted structure, $CBF_{retrofit+exp.}$, the soft-storey phenomena was shifted from the top floor to other floors, mostly at the ground level. The additional scaling factor for the retrofitted structure is 1.17 corresponding to the median collapse level. Time-history of inter-storey drifts for all collapsed structures are shown in Appendix I.

Table 6.2: Summary for collapsed structure in analysis

No.	NGA	$CBF_{design+exp.}$				CBF_{design}				$CBF_{retrofit+exp.}$			
		F_{sm}	h_{sm} (%)	S_{nm}	S_{nf}	F_{sm}	h_{sm} (%)	S_{nm}	S_{nf}	F_{sm}	h_{sm} (%)	S_{nm}	S_{nf}
1	15	1.2	8.9	4th	4th	1.1	8.6	4th	4th	N.A.			
2	57	1.2	9.7	4th	4th	N.A.				N.A.			
3	83	N.A.				N.A.				N.A.			
4	735	N.A.				1.1	4.4	4th	1st	1.1	5.4	2nd	2nd
5	762	1.25	8.7	4th	4th	N.A				1.2	5.4	2nd	2nd
6	776	1.1	8.9	4th	4th	1.0	8.9	4th	4th	0.8	5.4	2nd	2nd
7	787	N.A.				1.0	10.21	4th	4th	1.1	5.4	1st	1st
8	796	1.0	9.6	4th	4th	0.8	9.7	4th	4th	0.9	7.3	3rd	3rd
9	807	1.2	9.9	4th	4th	1.1	6.5	4th	4th	1.2	5.4	2nd	2nd
10	838	1.0	9.7	4th	4th	1.1	9.0	4th	4th	1.2	5.4	2nd	2nd
11	900	1.0	9.6	4th	4th	1.0	6.6	4th	4th	0.8	6.5	2nd	2nd
12	953	1.25	7.3	4th	1st	0.9	5.2	1st	1st	1.0	5.4	1st	1st
13	963	N.A.				N.A.				N.A.			
14	975	1.1	9.7	4th	4th	N.A.				N.A.			
15	986	N.A.				N.A.				N.A.			
16	1005	1.25	8.8	4th	4th	N.A.				N.A.			
17	1006	1.0	7.3	3rd	3rd	N.A.				N.A.			
18	1049	N.A.				N.A.				N.A.			
19	1787	N.A.				0.9	9.8	4th	4th	1.0	5.1	2nd	2nd
20	1794	N.A.				N.A.				1.1	25	1st	1st

6.4.3 Assessment of the collapse capacity

The primary parameter used to characterize the collapse safety of structures in seismic analysis is the collapse margin ratio (*CMR*). In FEMA P695 procedure, *CMR* is defined as the ratio between the median collapse intensity and the maximum considered earthquake (MCE) intensity. The MCE level is not explicitly defined in the National Building Code of Canada (NBCC). However, the design level in NBCC can be considered as the MCE since collapse prevention is the main design objective in the NBCC. As mentioned, the selected ground motions in this analysis were scaled to the NBCC design level and the median collapse intensity is the ratio with respect to that design intensity. Hence, the additional scaling factor used to reach collapse in the incremental time-history

analysis corresponds to the *CMR*. The *CMR* parameters for all three structure types are given in Table 6.4.

The frequency content (spectral shape) of the ground motions can influence significantly the collapse capacity and the collapse margin ratio. Thus, an adjusted collapse margin ratio parameter, *ACMR*, is used to account for the effects of the spectral shape in the FEMA P695 procedure. By using Equation 6.1, the *CMR* parameter is modified to obtain the *ACMR* parameter that incorporates the spectral shape effects. In Equation 6.1, the spectral shape factor (*SSF*) is a function of the fundamental period, *T*, and the period-based ductility, μ_T. The latter is defined as the ratio of the ultimate roof drift displacement, δ_u, to the effective yield roof drift displacement $\delta_{y,eff}$. There is no period-based ductility defined in the Canadian building code. However, according to its definition, it is very similar to the ductility-related force modification factor, R_d, in NBCC. Hence, R_d is used to replace μ_T in our analysis. For the studied structure, the fundamental period is 0.7s, and R_d is 1.5 for the conventional construction category.

$$ACMR_i = SSF_i \times CMR_i \tag{6.1}$$

In Section 6.2.1 of FEMA P695, *MCE* ground motion intensities are assorted into three ranges of spectral accelerations associated with the seismic design categories (*SDC*) B, C and D. As shown in Figure 6.12, the site location, Vancouver, is between category D_{min} and D_{max}. According to the *SDC*, the *SSF* factor can be obtained from the table provided in FEMA P695, based on the period-based ductility factor, μ_T. In the FEMA procedure, this period-based ductility factor is determined based on the nonlinear static analysis procedure. However, the ductility factor is predefined for each type of seismic force resisting systems in NBCC. For conventional construction, which is our case, it is 1.5 and that value was used to determine the SSF factor. The useful part of the table is re-built in Table 6.3. Thus, the *SSF* factor used in this analysis was selected as 1.08, which is between the 1.06 and 1.11 values shown in the table. The calculated *ACMR* parameter is given in Table 6.4.

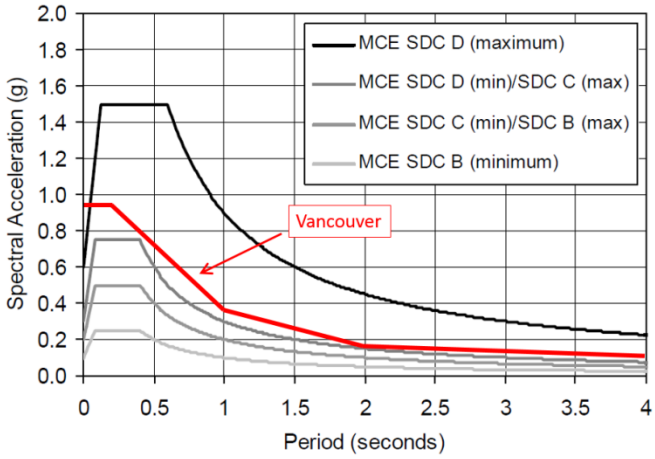

Figure 6.12: MCE response spectra for the corresponding ground motion intensities (FEMA P695)

Table 6.3: Spectral shape factor (FEMA P695)

T (s)	Period-based ductility, μ_T					
	SDC B, C, or D_{min}			*SDC* D_{max}		
	1.0	1.1	1.5	1.0	1.1	1.5
≤ 0.5	1.00	1.02	1.04	1.00	1.05	1.1
0.6	1.00	1.02	1.05	1.00	1.05	1.11
0.7	1.00	1.03	**1.06**	1.00	1.05	**1.11**

Figure 6.13a shows the observed collapse as dots, which lead to the fitted collapse fragility curve for all studied structure models. The fragility curve is defined through a cumulative distribution function. The lognormal collapse fragility function defined in Equation 6.2 was recommended by Baker (2011). Herein, μ and β are the mean and standard deviation of $\ln(S_a)$. Although the spectral acceleration (S_a) is used in the equation as a variable, it may be replaced by other parameters related to the ground motion intensity. Hence, this fragility function also works in the analysis to plot the fragility curve using the modification factor instead of the scaling factor. In our case, μ is the modification factor for the scaling factor corresponding to the median collapse capacity, while β is replaced by β_{RTR}, which is obtained from FEMA P695. The β_{RTR} parameter is the slope of the lognormal distribution reflecting the dispersion in results due to record-to-record (RTR) variability. It has a value between 0.20 and 0.40. The factors used to develop the fragility curve are shown in Table 6.5.

$$P(C|S_a = x) = \Phi\left(\frac{\ln x - \mu}{\beta}\right) \tag{6.2}$$

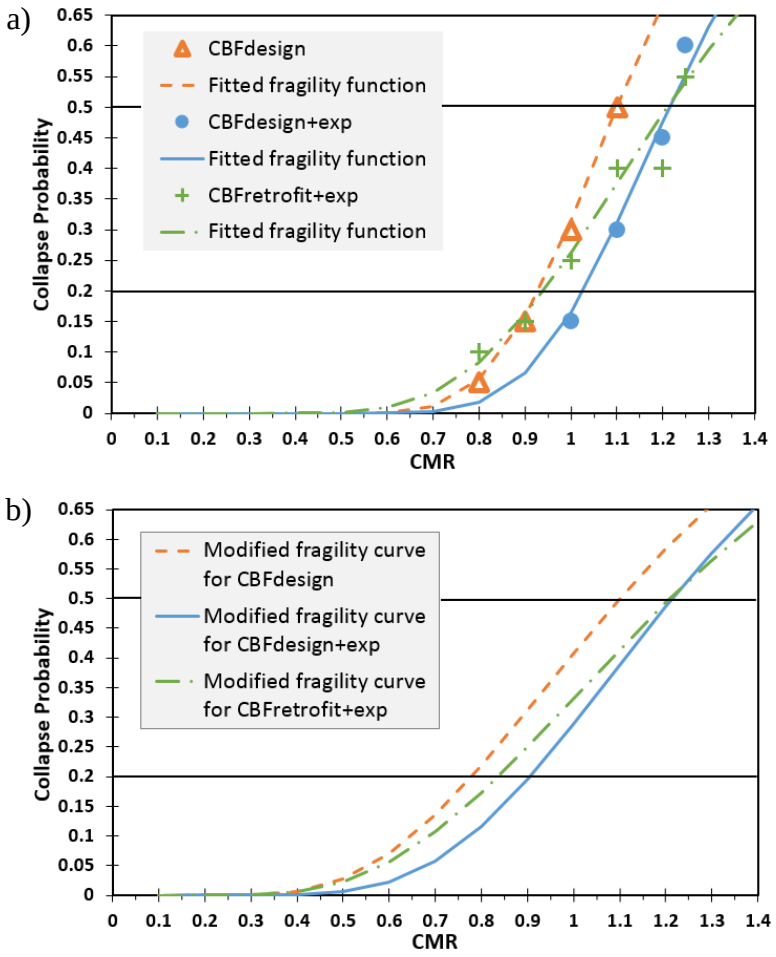

Figure 6.13: The collapse interception and collapse fragility curves of structure models: a) fitted fragility curve by considering β_{RTR}; b) modified fragility curve by considering β_{TOT}

Table 6.4: *CMR* and *ACMR* parameters

Structure type	*CMR*	*ACMR*	*SSF*	$CMR_{20\%}$	$ACMR_{20\%}$	$CMR_{20\%\text{-}m}$	$ACMR_{20\%\text{-}m}$
CBF_{design}	1.1	1.19	1.08	0.91	1.00	0.77	0.83
$CBF_{design+exp.}$	1.22	1.31	1.08	1.02	1.10	0.90	0.97
$CBF_{retrofit+exp.}$	1.21	1.31	1.08	0.93	0.98	0.84	0.91

Table 6.5: Parameters for the fragility function and uncertainty factors

Structure type	μ	β_{RTR}	β_{DR}	β_{TD}	β_{MDL}	β_{TOT}
CBF_{design}	1.1	0.2	0.2	0.15	0.25	0.41
$CBF_{design+exp.}$	1.215	0.2	0.2	0.15	0.15	0.35
$CBF_{retrofit+exp.}$	1.21	0.3	0.2	0.15	0.2	0.44

In the fragility curve corresponding to β_{RTR}, only the record-to-record (*RTR*) collapse uncertainty is considered. Other significant sources of uncertainty in collapse response such as the design requirements uncertainty (*DR*), the test data uncertainty (*TD*), and the modeling uncertainty (*MDL*), are not included. It is important to incorporate the effects of all significant sources of uncertainty in the collapse assessment process. The lognormal standard deviation parameter, β_{TOT}, which contains all significant sources of variability, is used for this purpose. The β_{TOT} factor is given in Equation 6.3, where β_{DR}, β_{TD}, and β_{MDL} vary from 0.10 to 0.50. It is estimated that β_{TOT} is in the range between 0.275 and 0.95.

$$\beta_{TOT} = \sqrt{\beta_{RTR}^2 + \beta_{DR}^2 + \beta_{TD}^2 + \beta_{MDL}^2} \tag{6.3}$$

Tables 6.6 to 6.8, as given by FEMAP695, are used to rate the β_{DR}, β_{TD}, and β_{MDL} factors. It is assumed that the design requirements uncertainty (β_{DR}) for all structure models is the same because all models are similar with the exception of the brace connections. The completeness and robustness of the design requirements are assumed as medium because although the design requirements as per NBCC 1980 and CSA S16-78 provisions were addressed, the model did not consider all possible types of failure mechanism that may occur due to failure of other structural members. The confidence in the basis of the design requirements is high because several of the equations that were used in the design in the 1980's have not been modified substantially or replaced when compared to current design requirements. Hence, β_{DR} is taken equal to 0.20.

Table 6.6: Quality rating of design requirements (FEMA P695)

Completeness and Robustness	Confidence in Basis of Design Requirements		
	High	Medium	Low
High. Extensive safeguards against unanticipated failure modes. All important design and quality assurance issues are addressed.	(A) Superior $\beta_{DR} = 0.10$	(B) Good $\beta_{DR} = 0.20$	(C) Fair $\beta_{DR} = 0.35$
Medium. Reasonable safeguards against unanticipated failure modes. Most of the important design and quality assurance issues are addressed.	(B) Good $\beta_{DR} = 0.20$	(C) Fair $\beta_{DR} = 0.35$	(D) Poor $\beta_{DR} = 0.50$
Low. Questionable safeguards against unanticipated failure modes. Many important design and quality assurance issues are not addressed.	(C) Fair $\beta_{DR} = 0.35$	(D) Poor $\beta_{DR} = 0.50$	--

Test data related to collapse uncertainty is considered to be the same for all types of structure models. In the braced frame models, some data were collected from experimental tests directly such as the axial force capacity and the ductility capacity of the brace connections used in the structure $CBF_{design+exp.}$. Moreover, some data were obtained from tests indirectly, such as the tests that were used to develop and calibrate the equations provided in the design standards. For instance, the axial force resisting capacity of the brace connections used in the CBF_{design} structure was obtained from calculations using current design provisions. Both types of tests were considered as reliable experimental information. Completeness and robustness characteristics are between high and medium as shown in Table 6.7. Hence, β_{TD} is 0.15.

Table 6.7: Quality rating of test data from an experimental investigation program (FEMA P695)

Completeness and Robustness	Confidence in Test Results		
	High	Medium	Low
High. Material, component, connection, assembly, and system behavior well understood and accounted for. All, or nearly all, important testing issues addressed.	(A) Superior $\beta_{TD} = 0.10$	(B) Good $\beta_{TD} = 0.20$	(C) Fair $\beta_{TD} = 0.35$
Medium. Material, component, connection, assembly, and system behavior generally understood and accounted for. Most important testing issues addressed.	(B) Good $\beta_{TD} = 0.20$	(C) Fair $\beta_{TD} = 0.35$	(D) Poor $\beta_{TD} = 0.50$
Low. Material, component, connection, assembly, and system behavior fairly understood and accounted for. Several important testing issues not addressed.	(C) Fair $\beta_{TD} = 0.35$	(D) Poor $\beta_{TD} = 0.50$	--

Quality rating of index archetype model shown in Table 6.8 varies among the different structure models used herein. As discussed before, the only difference between the three types of structure models was the modelling of the brace connections. The structure model includes most of the structural configurations, design parameters and behavioral characteristics that may affect structural collapse. However, the accuracy and robustness of the brace connections are different for the considered structure models. For the $CBF_{design+exp.}$ structure, the accuracy of the brace connection model is between high and medium, which means β_{MDL} equals to 0.15, because the data used to develop the connection model at the ground level is obtained directly from physical tests. At all the remaining floors, the connection resistances were modelled using the proportions found for the tested brace connection. The accuracy and robustness of the retrofitted structure model, $CBF_{retrofit+exp.}$, are medium because the axial force resistance of the strengthened brace connection model at the top floor is based on equations. At all other floor levels, the data collected from physical tests was used to calibrate the connection models. The CBF_{design} structure model is considered to be the less accurate and robust model. Thus, the β_{MDL} factor was assumed to be equal to 0.25 for this model because the axial capacity of the brace connections was based on equations.

Table 6.8: Quality rating of index archetype model (FEMA P695)

Representation of Collapse Characteristics	Accuracy and Robustness of Models		
	High	Medium	Low
High. Index models capture the full range of the archetype design space and structural behavioral effects that contribute to collapse.	(A) Superior $\beta_{MDL} = 0.10$	(B) Good $\beta_{MDL} = 0.20$	(C) Fair $\beta_{MDL} = 0.35$
Medium. Index models are generally comprehensive and representative of the design space and behavioral effects that contribute to collapse.	(B) Good $\beta_{MDL} = 0.20$	(C) Fair $\beta_{MDL} = 0.35$	(D) Poor $\beta_{MDL} = 0.50$
Low. Significant aspects of the design space and/or collapse behavior are not captured in the index models.	(C) Fair $\beta_{MDL} = 0.35$	(D) Poor $\beta_{MDL} = 0.50$	--

For the three types of structure models, the computation of $\beta_{TOT,}$ shown in Table 6.5, was conducted after the parameters β_{DR}, β_{TD}, and β_{MDL} were evaluated. As illustrated in Figure 6.12b, all fitted fragility curves were modified after replacing β_{RTR} with β_{TOT}. The $CMR_{20\%}$ and $CMR_{20\%\text{-}m}$ give the *CMR* value related to 20% probability of collapse in the fitted fragility curve. In addition, $ACMR_{20\%}$ and $ACMR_{20\%\text{-}m}$ were calculated using equation 6.1 for the $CMR_{20\%}$ and $CMR_{20\%\text{-}m}$ values given in Table 6.4. These values are used to check the structure performance.

6.4.4 Acceptable performance

In FEMA P695, acceptable performance is defined for each index archetype by the following two requirements:

- The probability of collapse for *MCE* ground motions is approximately 20%, or less, for each index archetype within a performance group.
- Individual values of the adjusted collapse margin ratio for each index archetype within a performance group exceeds *ACMR20%*. Thus, $ACMR_i \geq ACMR20\%$.

The only structure model that passed the first requirement when only the record-to-record uncertainty was considered is the $CBF_{design+exp.}$. As shown in Figure 6.12a, the collapse probability is about 18% at the design intensity considered as the *MCE*. In our case, the first condition can be

treated as that $CMR_{20\%}$ cannot be less than 1.0. For the CBF_{design} and $CBF_{retrofit+exp.}$, the$CMR_{20\%}$ are 0.91 and 0.93 respectively. When considering total uncertainty (β_{TOT}), none of the structure models has an acceptable performance level.

To evaluate the second condition, acceptable values of the adjusted collapse margin ratio is available in a table illustrated in FEMA P695. The useful part of this table is reproduced in Table 6.9. According to the system collapse uncertainty of each type of structures, the acceptable *AMCR20%* parameter obtained from the table are 1.29, 1.41 and 1.45 for the $CBF_{design+exp.}$, $CBF_{design,}$ and $CBF_{retrofit+exp.}$ structure models, respectively. As shown in Table 6.4, all $AMCR_{20\%}$ and $AMCR_{20\%-m}$ values are less than the acceptable value. According to the assessment results, it is necessary to upgrade the prototype building structure. However, the proposed retrofit strategy is not sufficient to meet the required structure performance.

Table 6.9: Acceptable values of ACMR (FEMA P695)

Total System Collapse Uncertainty (β_{TOT})	Collapse Probability 20% (*ACMR20%*)
0.275	1.26
0.300	1.29
0.325	1.31
0.350	1.34
0.375	1.37
0.400	1.40
0.425	1.43
0.450	1.46

Structure seismic retrofit provisions are presented in the commentary "L" to NBCC 2010. In these guidelines, it is recommended that existing buildings be retrofitted if the shear resistance is less than $0.6V_{design}$, where V_{design} is the minimum design earthquake load specified in NBCC 2010. Hence, 60% of the current design level can be used as a design level to evaluate the necessity to retrofit existing structures. This can be simply done by dividing the previously obtained CMR values by 0.6. Figure 6.14 shows the new fragility curves and the corresponding modified *CMR* and *ACMR* parameters are given in Table 6.10.

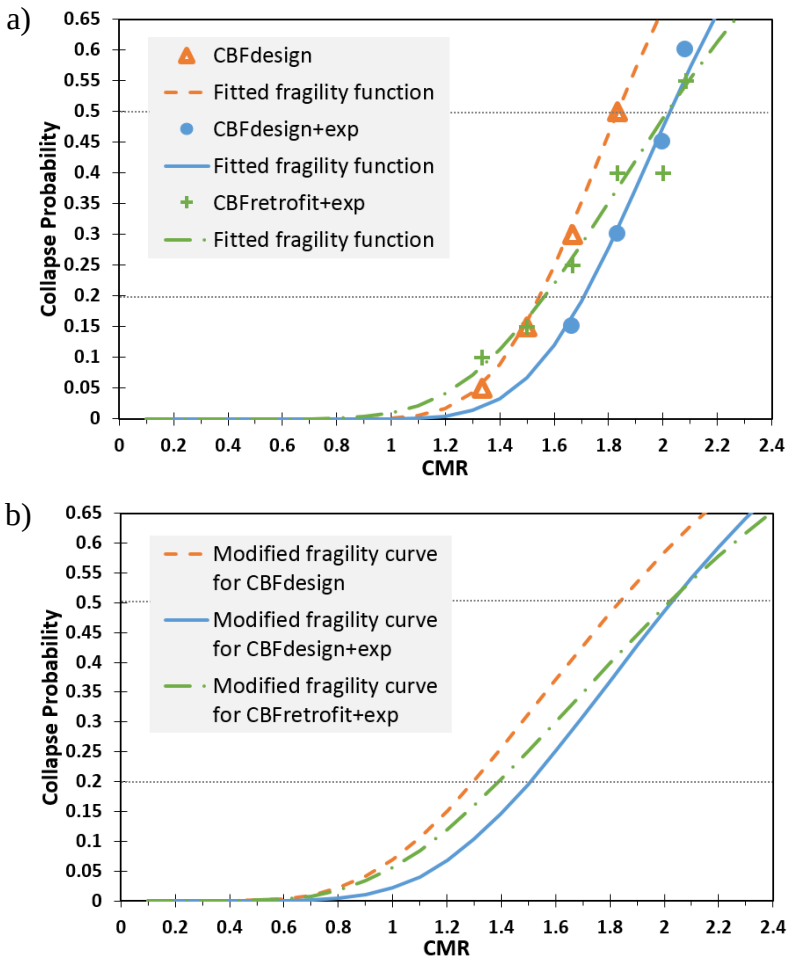

Figure 6.14: Observed collapse and collapse fragility curve for structures under 60%V_{design}, criteria: a) fitted fragility curve only considering β_{RTR}; b) modified fragility curve considering β_{TOT}

Table 6.10: *CMR* and *ACMR* under 60%, V_{design}, criteria

Structure type	*CMR*	*ACMR*	*SSF*	$CMR_{20\%}$	$ACMR_{20\%}$	$CMR_{20\%\text{-}m}$	$ACMR_{20\%\text{-}m}$
CBF_{design}	1.83	1.98	1.08	1.52	1.64	1.29	1.39
$CBF_{design+exp.}$	2.03	2.19	1.08	1.7	1.84	1.5	1.62
$CBF_{retrofit+exp.}$	2.02	2.18	1.08	1.55	1.67	1.38	1.49

After changing the design level criteria, the assessment results are different. When using the provision recommended in the NBCC 2010 commentary "L", seismic upgrading of $CBF_{design+exp.}$ and CBF_{design} structure models is no longer necessary because $CMR_{20\%}$ are 1.7 and 1.52 respectively for these two models, which are larger than 1.0. In addition, $ACMR_{20\%}$ and $ACMR_{20\%\text{-}m}$ value of these two models exceed the acceptable *ACMR20%*. However, for the $CBF_{retrofit+exp.}$ structure

model, it seems that the adopted retrofit scheme applied for the brace connections is the most economical intervention that may be performed in order to improve the ductility of the brace connections and reduce the level of axial forces in the braces. However, the seismic performance of $CBF_{retrofit+exp.}$ structure has no large improvement comparing to $CBF_{design+exp.}$ and CBF_{design} structure.

6.4.5 Discussion about the retrofit scheme

According to the collapse capacity assessment results, the performance of the retrofit building model is not acceptable. Although an increase of the local ductility of the retrofitted connections with slotted holes was observed in the cyclic tests, the assessment of the retrofitted CBF shows that ductility capacity of this retrofitted connection is still not sufficient. As shown in the detailed analysis example in Section 6.3.1, connection failure happened at 1% equivalent storey drift. It is believed that further increasing the local ductility of this retrofitted connection can be achieved conveniently by increasing the length of the slotted holes in the gusset plates. This should be examined in future studies.

In the cyclic tests, the length of the slotted holes was 76.2 mm (3 in.) and the length of the steel segments with reduced cross-section between the slotted holes was 50.8 mm (2 in.). The total connection deformation at failure for the test specimens was 22.8 mm. By calculation, it is found that this 22.8 mm brace connection deformation contributes to about 0.7% equivalent storey drift. If, for example, the length of the steel segments between the slotted holes was doubled to obtain 127 mm (5 in.) long slotted holes, the total deformation capacity of the retrofitted brace connections would likely double as well. The equivalent storey drift capacity would then be equal to 1.7% (0.7% X 2 + 0.3%). The adequacy of this elongated retrofitted connection would need to be validated by applying the FEMA P695 procedure to a model of the retrofitted CBF with this modified connection. Such a detailed verification exceeds the scope of this project and could be performed in future studies on the system. However, it can be foreseen that the structure capacity against collapse could be increased by increasing the length of the slotted holes of the retrofitted connections. Thus, although the proposed retrofit scheme as studied could not provide sufficient ductility, it is believed that it can still represent a good retrofit concept.

6.5 Summary

A detailed 4-storey braced frame model was developed to carry out incremental dynamic time-history analysis for three types of structure models. The differences between the detailed braced frame model and the simplified braced frame model used in the hybrid tests were described. A set of twenty ground motions were selected and scaled to fit the uniform hazard spectrum at the site over the period range of interest. The collapse capacity of the structures was assessed following the FEMA P695 procedure. The study showed that the existing building as designed and built in agreement with the NBCC 1980 and CSA S16-78 provisions would need no seismic upgrade based on Commentary "L" of NBCC 2010. Although the proposed cost-efficient seismic upgrading strategy as studied did not improve the seismic performance to the level required in FEMA P695 procedure, it is believed that the concept is sound and the connection retrofit design could be improved to meet the requirement. This should be studied more in detail in the future.

CHAPTER 7: CONCLUSIONS AND RECOMMENDATIONS

7.1 Conclusions

Existing low-rise steel braced frames designed as seismic force resisting systems before the introduction of seismic design provisions in the 1989 edition of the Steel structure design standard are likely to exhibit seismic deficiencies under earthquake events. In this study, a prototype 4-storey structure was assessed using the current code design provisions and through physical testing to identify potential deficiencies. Retrofit schemes were proposed and studied for deficient brace connections.

The prototype building was a 4-storey steel commercial building with tension-only braces, designed in accordance with the requirements contained in the 1980 NBCC and the CSA S16.1-M78 design standard. The structure was assumed to be located on a firm ground site in Vancouver, British Columbia. Braces were made from back-to-back double angle members with bolted end connections, as per the 1980 engineering practice. The seismic evaluation of the prototype building was performed using the current 2010 NBCC and CSA-S16-09 design standard, assuming the structure would qualify as being of the conventional category (Type CC). The connections of the double angle braces were found to be the most critical components of the seismic force resisting system: the connections have insufficient axial force resistance and are likely to exhibit low-ductility failure modes. This deficiency is typical to the 1980 design philosophy, where member forces were considered instead of capacity design provisions. When failure hierarchy and ductile brace response were not considered in design, concentration of deformations within a floor leading to soft storey response and, eventually, collapse of the building in the case of a strong seismic event was usually encountered.

Four retrofit strategies were proposed for the brace connections. These strategies are based on two different concepts. One concept consists in reinforcing the brace connections in order to trigger braces to yield in their gross section. The other concept consists in increasing the local ductility of the brace connections while controlling the force level in the braced frame.

In order to investigate the behaviour of double angle braces and their connections and to collect data for the development and validation of numerical models, physical quasi-static cyclic tests were carried out on full scale double angle braces with bolted end connections specimens, located at the

ground floor of the prototype building. All specimens were fabricated from the same CSA G40.21-300W steel grade that was specified in the initial design. Coupon tests performed on the brace and gusset plate specimens indicated that these components have a yield strength equal to 1.13 and 0.97 times the minimum specified values respectively. The corresponding tensile strengths were 1.01 and 1.07 times the minimum specified values. The actual yield strength of the bracing member was lower than the expected value considered in the first seismic assessment (385 MPa). These tests also showed that the current equation in CSA S16-09 that accounts for shear lag effect on the net section rupture resistance of angles bolted through one leg only is too conservative. The combined effects of these two findings impacted on the seismic assessment of structure: the brace-connection assembly as originally designed exhibited some ductility through the gross-section yielding of bracing members. Failure in the connections only occurred after strain hardening in braces was developed. The maximum forces triggered in the bracing members may be considered as high; however, they can result in overloading of the other components of braced frames such as the columns.

Retrofit strategy I consisted in strengthening the brace connection with additional plates welded to the outstanding short leg of angles. In retrofit strategy II, the objective was to increase the ductility of brace connection by introducing slotted holes in the gusset plates between the brace ends and the surrounding beams, while limiting the brace forces. These two retrofit schemes performed as expected and the design objectives were reached. The other two retrofit strategies proposed involved the drilling of holes in the gusset plates to promote ductile shear yielding due to bolt bearing and the drilling of additional holes in the braces at their connections to control the brace loads, while developing yielding in the connections. These two approaches did not improve the performance of the brace-connection assemblies and only the retrofit strategy II was considered in further numerical analyses, performed to assess the building collapse capacity.

A numerical model was developed to predict the cyclic inelastic response of back-to-back double angle steel braces using the OpenSees finite element program. The model accounts for residual stress effects, initial out-of-straightness, and stability of the individual and combined angle sections on the buckling response of braces. The inelastic axial deformations, flexural response and failure of brace connections were also included in the model. The *Steel02* material and *fiber* cross-section discretization were used to model angle braces. The *Pinching4* material was used in the connection

model with the aim to reproduce the inelastic deformation and fracture response of connections. The model was validated against the data obtained from physical tests.

The hybrid simulation technology was also used to verify the ability of the model to predict the brace inelastic response including connection failure and its impact on the collapse capacity of braced frame. This was the first implementation of the OpenSees-OpenFresco platform for hybrid stimulation at École Polytechnique of Montréal.

A simplified numerical braced frame model was used for the hybrid simulation. However, only two out of four hybrid tests were completed successfully. The synchronization problem and the simulation speed problem need to be solved. Nevertheless, the two successful tests showed that well defined numerical models can reproduce well the braced frame behaviour, including collapse due to failure of brace connections.

In the last part of this research project, three different building models were examined through nonlinear time-history dynamic analyse: 1) the CBF building as originally designed with component strengths based on code specified probable material resistances, CBF_{design}; 2) the CBF building as originally designed with component strengths based on measured material properties, $CBF_{design+exp.}$; and 3) the retrofit model, $CBF_{retrofit+exp.}$, with component strengths based on measured material properties. These three models were based on a detailed structure numerical model. Twenty selected ground motions were used to perform incremental dynamic analysis in order to evaluate the structure collapse capacity following the FEMA P-695 approach. During the analysis, it was found that the fracture of a brace connection can trigger large inter-storey drifts at the floor level where brace connection fracture occurred. Once the inter-storey drift exceeded a certain level, a soft-storey phenomenon may happen that may lead to complete collapse of the structure. In addition, it was observed that columns of CBFs when modelled as nonlinear beam-columns elements with spread plasticity and fiber cross-section discretization may buckle due to the interaction of the gravity loads and the large bending moments produced by large inter-storey drifts. Either the soft-storey mechanism or buckling of the columns can lead to collapse of the structure. The evaluation showed that CBF structures with brace connections designed as per the 1980 code provisions ($CBF_{design+exp.}$ and CBF_{design}) could not provide the required safety against collapse, regardless of the material properties assumed in the model. The proposed retrofit strategy ($CBF_{retrofit+exp.}$) did not improve the collapse capacity of structures to a satisfactory level. However,

it is believed that the concept has potential and can be considered as a good retrofit scheme due to its ductile behaviour.

7.2 Recommendations for future studies

- Further investigation is needed to better understand the behaviour of seismically deficient brace connections in existing steel braced frame systems designed before the implementation of current seismic design provisions. Various building heights and site locations should be considered to identify the most critical conditions.
- Other retrofit strategies need to be proposed for steel brace connections. Increasing the local ductility of the brace connections while controlling the force level in the brace appears to be a promising direction for this development. Reinforcing the brace connections to promote yielding of the braces is another good approach to increase the ductility performance of structures, provided that this does not lead to overstressing other elements along the lateral load path that may exhibit a brittle failure mode.
- Performing an evaluation and a retrofit study for an actual existing steel building structure would be very useful to accounts for possible problems or limitations that have not been considered in this study.
- A more robust hybrid simulation technique is needed to more easily carry out this type of testing. Although two simulations could be successfully completed in this project, the current hybrid test system was found to be too slow and sensitive to potential communication problems between the different computers. In particular, the test speed needs to be improved for highly nonlinear braced frame models. A more stable and robust connection is also necessary between the xPC-target and xPC-Host to avoid synchronization problems.
- Additional improvements can be made to the OpenSees braced frame model used in this study. Firstly, the gravity columns could be modelled using *Force-Based Beam-Column* elements with *fiber* cross-section discretization such that buckling response can be included for these columns. After brace connection failure, the study showed that the structure is subjected to large storey drifts that may result in column buckling that may lead to earlier building collapse. Secondly, the*Pinching4* material could be replaced by a more stable and precise hysteretic behaviour to reproduce in-plane bending of beam-

to-column connections. Thirdly, the restraint provided at the column bases by the base plates and anchor rods should be included in the numerical model. In many cases, collapse developed at the first floor and it is expected that the building response would be strongly influenced by the boundary conditions at the column base. For steel braced frames, tension failure of the anchor rods may also occur, which would result in rocking of the structure under seismic forces. Lastly, fracture of the beam-to-column connections should be added to the model. When the structure experiences large inter-storey drifts, failure is likely to happen in the beam-to-column joints and this failure mode should be considered in the structure assessment.

REFERENCES

ADLURI, S. M. R., and MADUGULA, M. K. S., (1995) "Residual Stresses and Initial Out-of Straightness of Hot-Rolled Steel Angles" *Proc. 1995 SSRC Annual Technical Meeting*, Kansas City, MO: 115-126.

AGUERO, A., IZVERNARI, C., and TREMBLAY, R., (2006) "Modelling of the Seismic Response of Concentrically Braced Steel Frames using the OpenSees Analysis Environment" *Int. J. of Advanced Steel Construction*, 2(3): 242-274.

AISC, (2005) "ANSI/AISC 341-05" Chicago, IL.

AISC, (1984) "Engineering for Steel Construction: A Source Book on Connections" Chicago, IL.

ASLANI, F., and GOEL, S. C., (1991) "Stitch Spacing and Local Buckling in Seismic-Resistant Double-Angle Braces" *J. Struct. Eng.*, 117: 2442-2463.

ASTANEH-ASL, A., and GOEL, S. C., (1984) "Cyclic In-Plane Buckling of Double Angle Bracing" *J. Struct. Eng.*, 110: 2036-2055.

ASTANEH-ASL, A., GOEL, S. C., and HANSON, R. D., (1985) "Cyclic Out-of-Plane Buckling of Double Angle Bracing" *J. Struct. Eng.*, 111: 1135-1153.

ATC, (2009) "Quantification of Building Seismic Performance Factors" Report No. ATC-P695, Applided Technology Council, Redwood City, California.

BAKER, J. W., (2011) "Fitting Fragility Functions to Structural Analysis Data Using Maximum Likelihood Estimation" http://www.stanford.edu/~bakerjw/fragility_old.html.

CASTONGUAY, P. X., (2009) "Seismic Performance of Concentrically Braced Steel Frames of the Conventional Construction Category" Masters Thesis, École Polytechnique de Montréal, QC.

CHEN, L., (2011) "Innovative Bracing System for Earthquake Resistant Concentrically Braced Frame" Masters Thesis, Concordia University, Montreal, QC.

CSA, (1978) "Limit States Design of Steel Structures, CAN 3 S16.1-M78" Canadian Standards Association, Toronto, ON.

CSA, (1989) “Design of Steel Structures, CSA-S16-89” Canadian Standards Association, Toronto, ON.

CSA, (2009) “Design of Steel Structures, CSA-S16-09” Canadian Standards Association, Toronto, ON.

CSI, (2009) “ETABS - INTEGRATED ANALYSIS DESIGN AND DRAFTING OF BUILDING SYSTEMS, Version 9.0.4 (Computer Program)” Computer & Structures INC., Berkeley, CA.

CSI, (2008) “SAP2000 - INTERGRATED SOFTWARE FOR STRUCTURAL ANALYSIS & DESIGN, Version 12 (Computer Program),” Computer & Structures INC., Berkeley, CA.

FRANCHUK, C. R., DRIVER, R. G., and GRONDIN, G. Y., (2002) “Block Shear Behaviour of Coped Steel Beams” *Structural Engineering Report No. 244*, Department of Civil Engineering, University of Alberta, Edmonton, AL.

HADDAD, M., and TREMBLAY, R., (2006) “Influence of Connection Cesign of the Inelastic Seismic Response of HSS Steel Bracing Members” *WELDING IN THE WORLD-LONDON-*, 50(I):574.

HARTLEY, J., ROGERS, C. A., CASTONGUAY, P. X., and TREMBLAY, R., (2011) “Inelastic seismic performance of brace connections in steel tension-only concentrically braced frames” *Proc. The Seventh International Conference STESSA 2012*, Santiago, Chile: 289-295.

HSIAO, P. C., LEHMAN, D. R., and ROEDER, C. W., (2012) “Improved analytical model for special concentrically braced frames” *Journal of Constructional Steel Research*.

HUNS, B. B. S., GRONDIN, G. Y., and DRIVER, R. G., (2002) “Block Shear Behaviour of Bolted Gusset Plates” *Structural Engineering Report No. 248*, Department of Civil Engineering, University of Alberta, Edmonton, AL.

IZVERNARI, C., (2007) “The Seismic Behaviour of Steel Braces with large Sections” Masters Thesis, École Polytechnique de Montréal, QC.

KULAK, G. L., and GRONDIN, G. Y., (2001) “AISC LRFD Rules for Block Shear in Bolted Connections-A Review” *AISC, Engineering Journal*, 38(4):199-203.

LAMARCHE, C. P., and TREMBLAY, R., (2008) "Accounting for Residual Stresses in the Seismic Stability of Nonlinear Beam-Column Elements With Cross-Section Fiber Discretization" *2008 Annual Stability Conference*, p. 59-78.

LECLERC, M., MOLINARI, M., BOUAANANI, N., TREMBLAY, R., LÉGER, P., and BURSI, O., (2011) "Effective Strategies for Real Time Hybrid Simulation of Near Seismic Collapse Response of Moment Resisting Frames" *Proc. 2011 American Control Conference*, San Francisco, CA., Paper No. 5991145: 3307-3314.

MAZZONI, S., MCKENNA, F., SCOTT, M., FENVES, G. L. et al., (2009) "OpenSees User Manual" Pacific Earthquake Engineering Research Center (PEER), University of California, Berkeley, CA.

MITCHELL, D., PAULTRE, P., TINAWI, R., SAATCIOGLU, M., TREMBLAY, R., ELWOOD, K., ADAMS, J., and DEVALL, R., (2010) "Evolution of seismic design provisions in the National building code of Canada" *Can. J. of Civ. Eng.*, 37(9): 1157-1170.

NRCC, (1980) "National Building Code of Canada 1980" 8th ed., National Research Council of Canada, Ottawa, ON.

NRCC, (2010) "National Building Code of Canada 2010" 13th ed., National Research Council of Canada, Ottawa, ON.

PEER, (2010) "PEER Ground Motion Database" http://peer.berkeley.edu/products/strong_ground_motion_db.html.

SALAWDEH, S., and GOGGINS, J., (2013) "Numerical simulation for steel brace members incorporating a fatigue model" *Engineering Structures*, 46: 332-349.

SCHELLENBERG, A., Kim, H. K., TAKAHASHI, Y., FENVES, G. L., F., and MAHIN, S. A., (2009) "OpenFresco Command Language Manual" Department of Civil and Environmental Engineering, University of California, Berkeley, CA.

SCHELLENBERG, A., YANG, T. Y., MAHIN, S. A., and STOJADINOVIC, B., (2008) "Hybrid Simulation of Structure Collapse" *Proc.14th World Conference on Earthquake Engineering*, Beijing, China, Paper No. S16-02-004.

ST-ONGE, E., (2012) "Étude expérimentale et conception de fusibles ductiles travaillant en traction pour l'amélioration de l'efficacité des contreventements parasismiques en acier" Masters Thesis (In French), École Polytechnique de Montréal, QC.

TREMBLAY, R., (2011) "Evolution of the Canadian Seismic Design Provisions for Steel Structures since 1989" *Proc. CSCE Annual Conf.*, Ottawa, ON.

TREMBLAY, R., BRUNEAU, M., DRIVER, R., METTEN, A., MONTGOMERY, C. J., and ROGERS, C., (2010) "Seismic Design of Steel Structures in accordance with CSA-S16-09" *Proc. 9th US National and 10thCanadian Conference on Earthquake* Engineering, Toronto, ON., Paper No. 1768.

URIZ, P., FILIPPOU, F. C., and MAHIN, S. A., (2008) "Model for Cyclic Inelastic Buckling of Steel Braces" *J. Struct. Eng.*,ASCE, 134(4): 619-628.

URIZ, P., MAHIN, S. A., (2004) "Seismic vulnerability assessment of concerntrically braced steel frams" *International Journal of Steel Structures*, 4(4):239-248.

WANG, T., MOSQUEDA, G., JACOBSEN, A., and CORTES-DELGADO, M., (2012) "Performance evaluation of a distributed hybrid test framework to reproduce the collapse behavior of a structre" *Earthquake Engineering & Structrual Dynamics*, 41(2), 295-313.

WU, Y., and KULAK, G. L., (1993) "Shear Lag in Bolted Single and Double Angle Tension Members" *Structural Engineering Report No. 187*, Department of Civil Engineering, University of Alberta, Edmonton, AL.

YANG, T. Y., STOJADINOVIC, B., and MOEHLE, J., (2006) "Hybrid Simulation Evaluation of Innovative Steel Braced Framing System" *8th US National Conference on Earthquake Engineering*, San Francisco, USA.

APPENDICES

APPENDIX I

Inter-storey drift time-history response for $CBF_{design+exp.}$

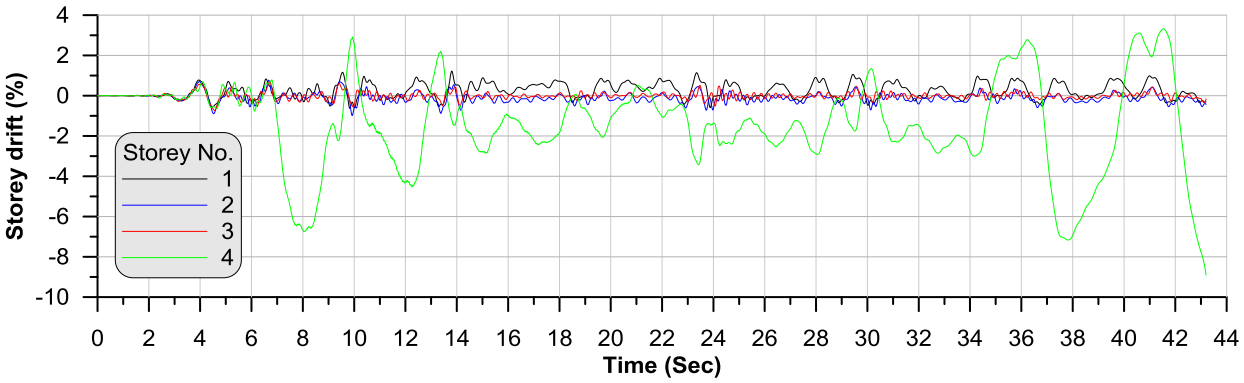

Figure I. 1: Inter-storey drift for $CBF_{design+exp.}$ model under earthquake NGA-15 with F_{sm} 1.2

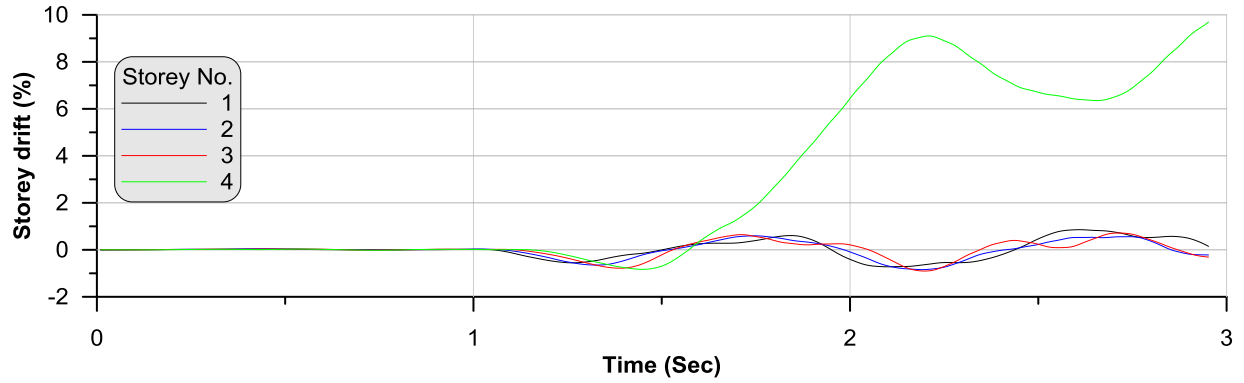

Figure I. 2: Inter-storey drift for $CBF_{design+exp.}$ model under earthquake NGA-57 with F_{sm} 1.2

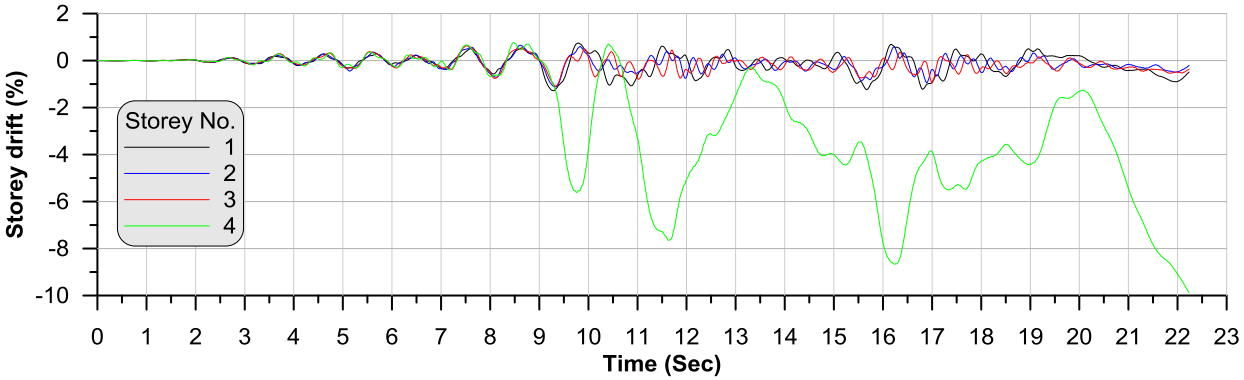

Figure I. 3:Inter-storey drift for $CBF_{design+exp.}$ model under earthquake NGA-762 with F_{sm} 1.25

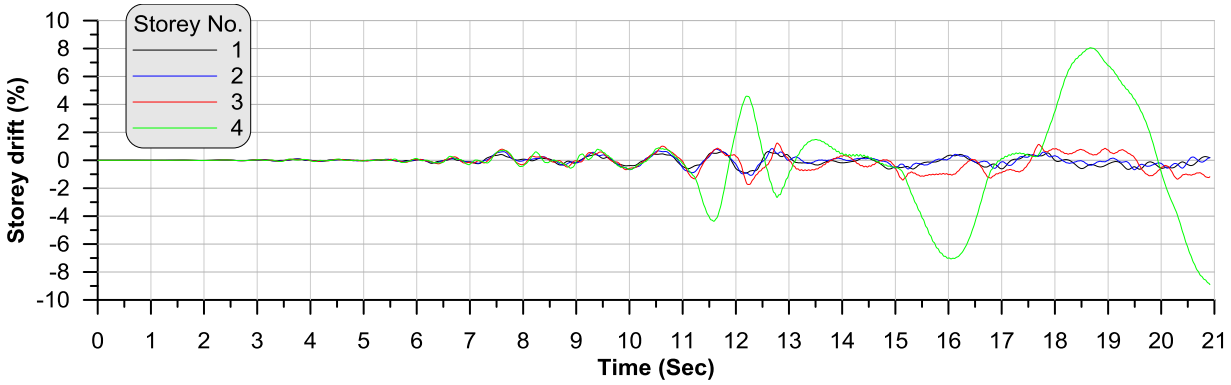

Figure I. 4:Inter-storey drift for $CBF_{design+exp.}$ model under earthquake NGA-776 with F_{sm} 1.1

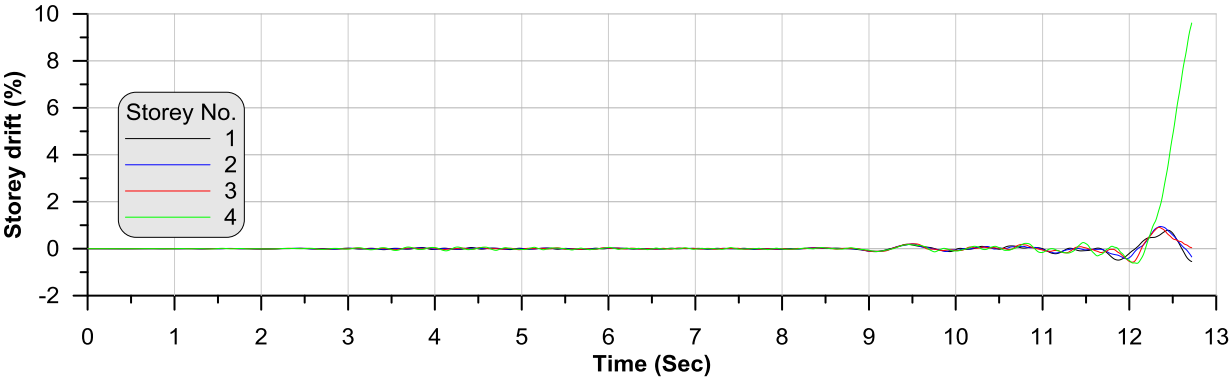

Figure I. 5:Inter-storey drift for $CBF_{design+exp.}$ model under earthquake NGA-796 with F_{sm} 1.0

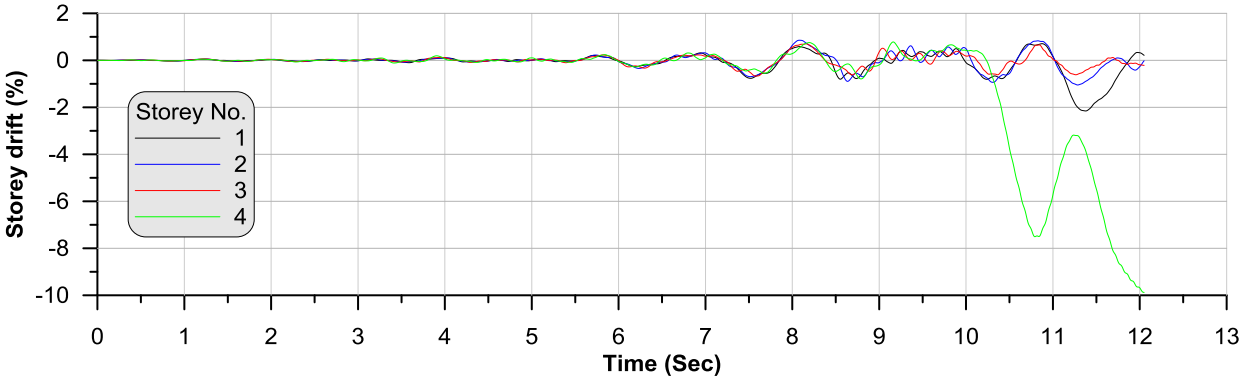

Figure I. 6:Inter-storey drift for $CBF_{design+exp.}$ model under earthquake NGA-807 with F_{sm} 1.2

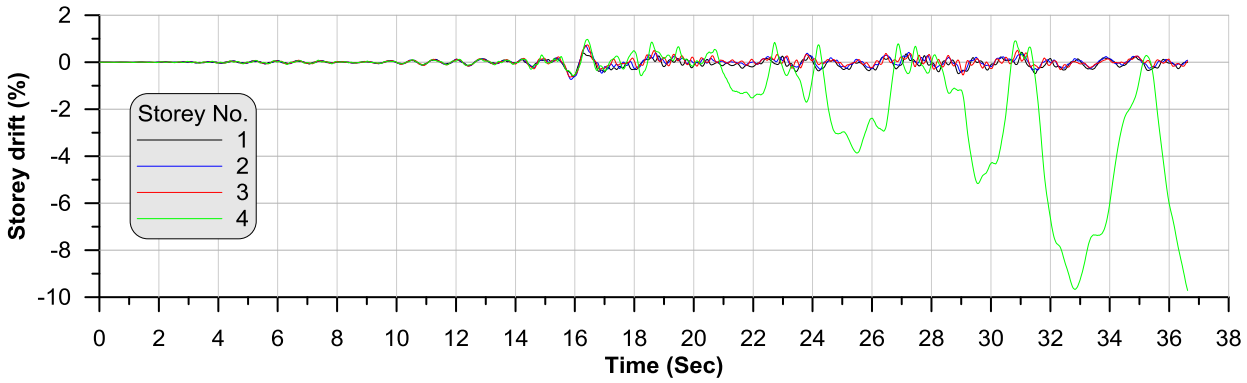

Figure I. 7:Inter-storey drift for $CBF_{design+exp.}$ model under earthquake NGA-838 with F_{sm} 1.0

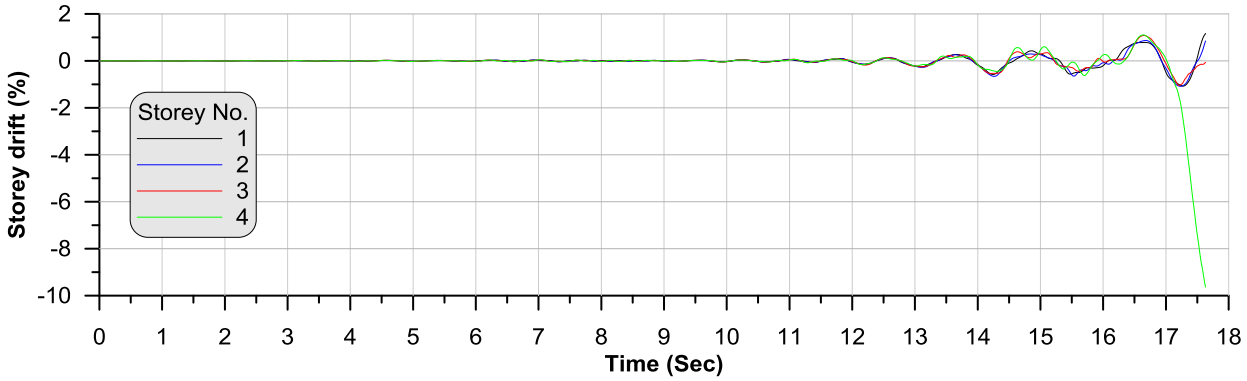

Figure I. 8:Inter-storey drift for $CBF_{design+exp.}$ model under earthquake NGA-900 with F_{sm} 1.0

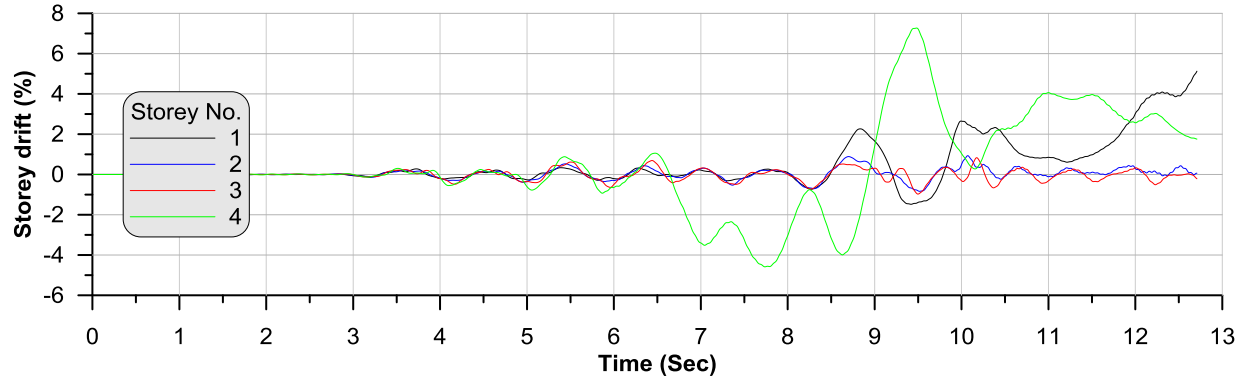

Figure I. 9:Inter-storey drift for $CBF_{design+exp.}$ model under earthquake NGA-935 with F_{sm} 1.25

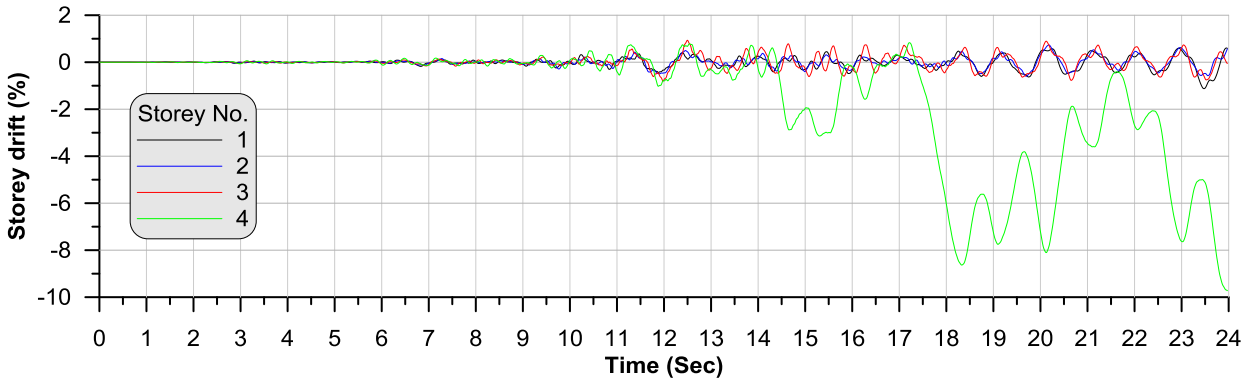

Figure I. 10:Inter-storey drift for $CBF_{design+exp.}$ model under earthquake NGA-975 with F_{sm} 1.1

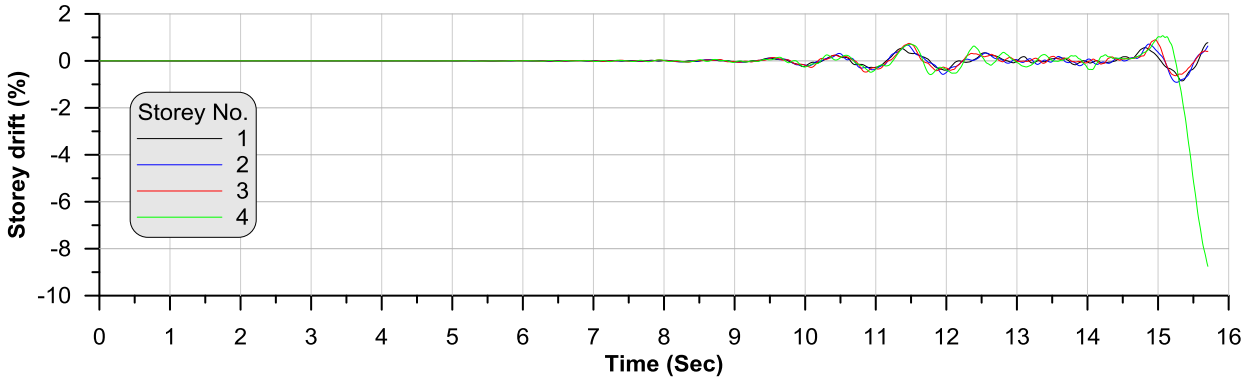

Figure I. 11:Inter-storey drift for $CBF_{design+exp.}$ model under earthquake NGA-1005 with F_{sm} 1.25

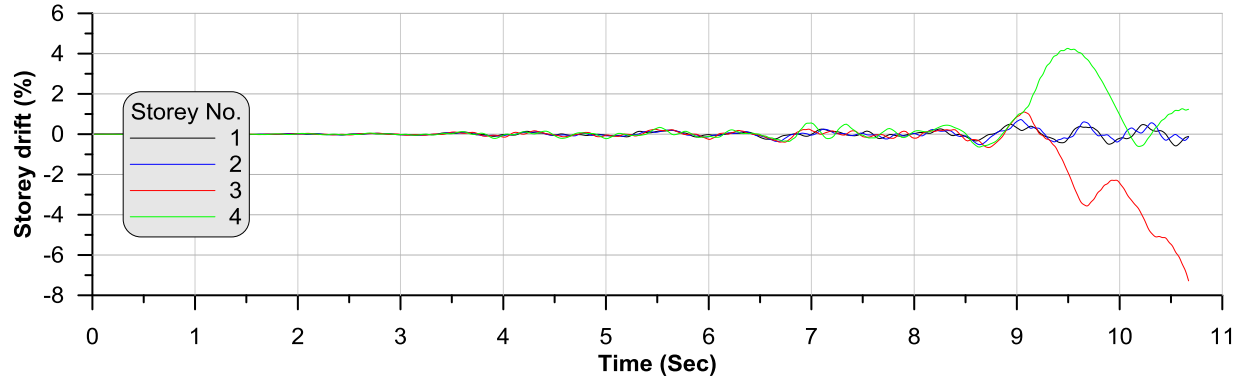

Figure I. 12:Inter-storey drift for $CBF_{design+exp.}$ model under earthquake NGA-1006 with F_{sm} 1.0

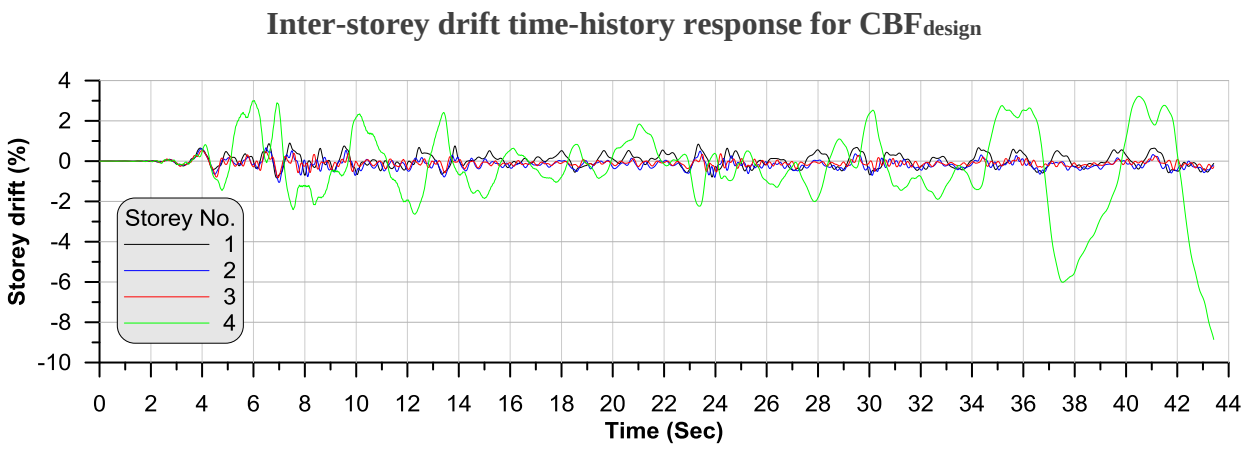

Figure I. 13:Inter-storey drift for CBF_{design} model under earthquake NGA-15 with F_{sm} 1.1

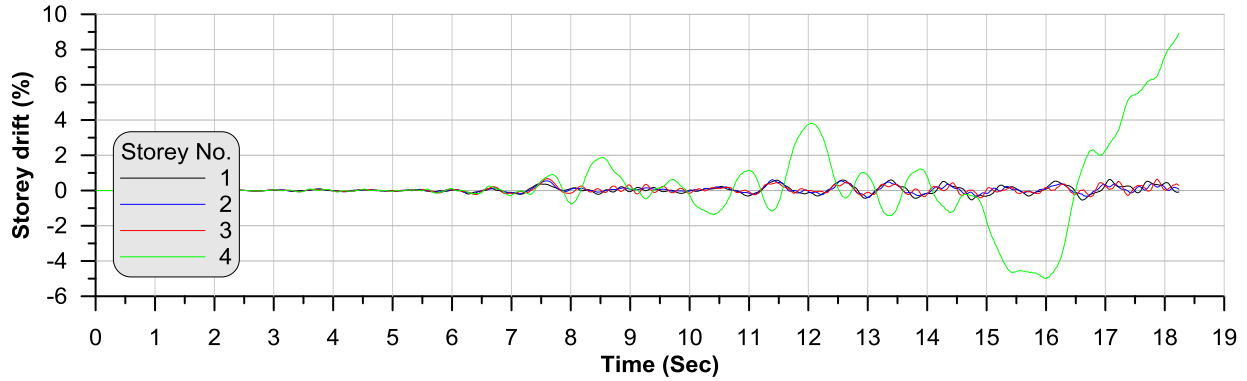

Figure I. 14:Inter-storey drift for CBF_{design} model under earthquake NGA-776 with F_{sm} 1.0

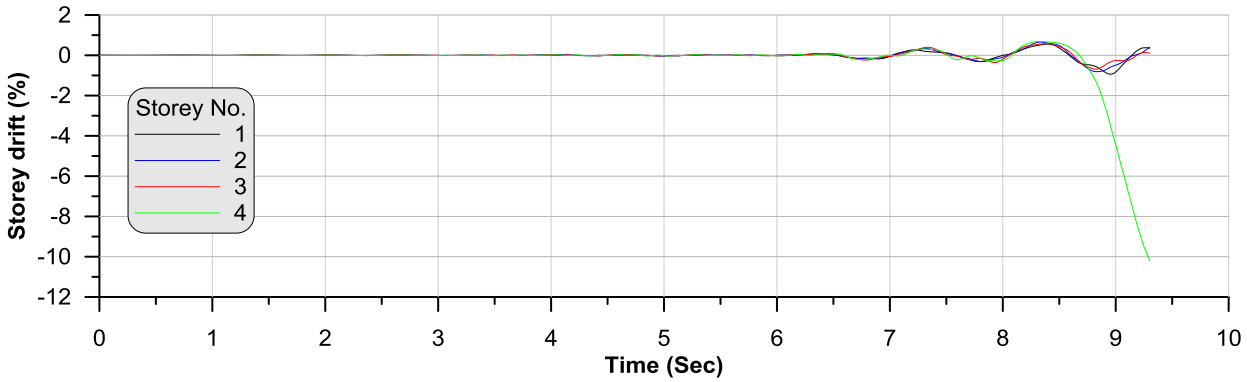

Figure I. 15:Inter-storey drift for CBF_{design} model under earthquake NGA-787 with F_{sm} 1.0

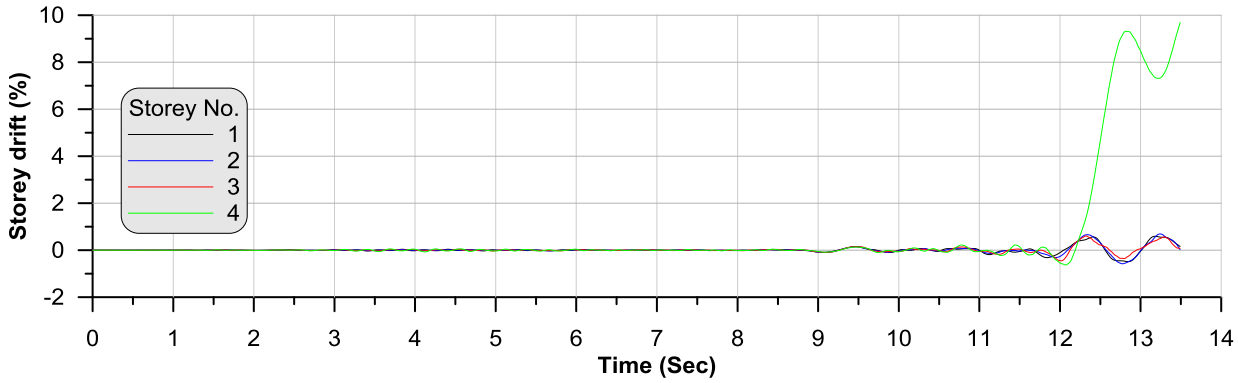

Figure I. 16:Inter-storey drift for CBF_{design} model under earthquake NGA-796 with F_{sm} 0.8

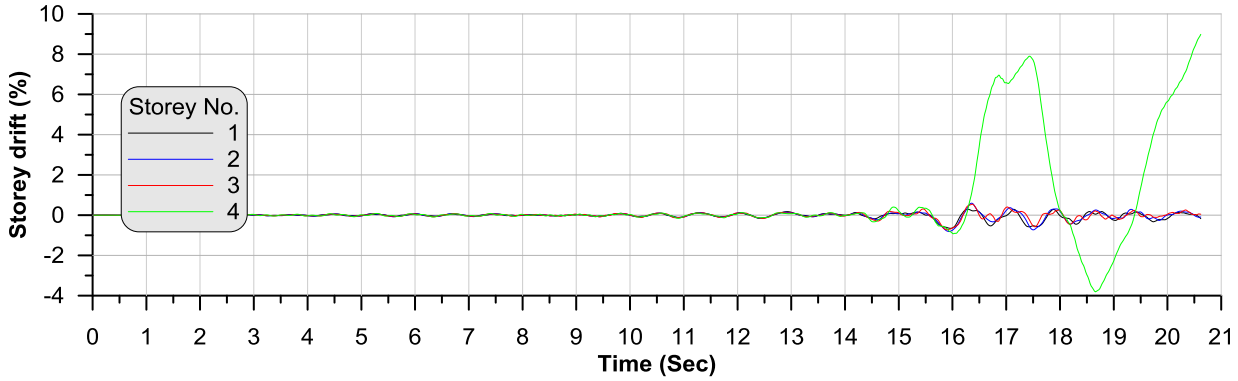

Figure I. 17:Inter-storey drift for CBF_{design} model under earthquake NGA-838 with F_{sm} 1.1

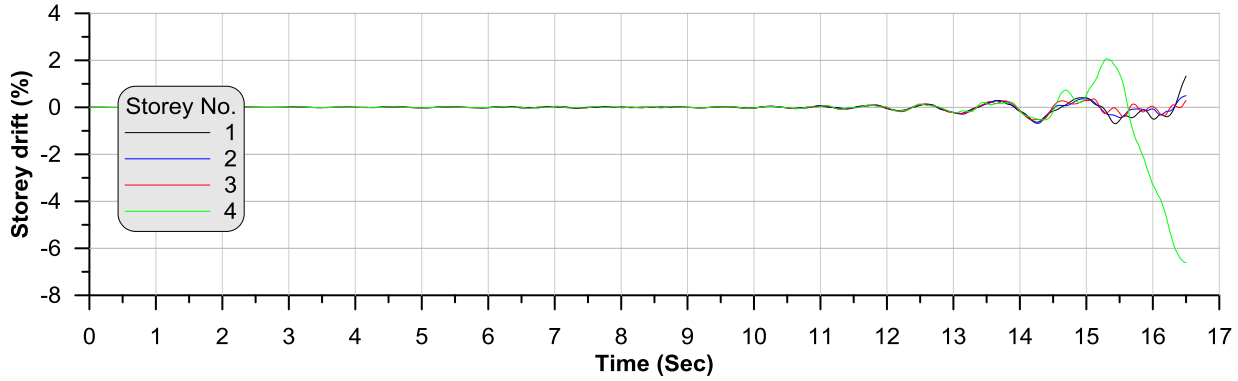

Figure I. 18:Inter-storey drift for CBF_{design} model under earthquake NGA-900 with F_{sm} 1.0

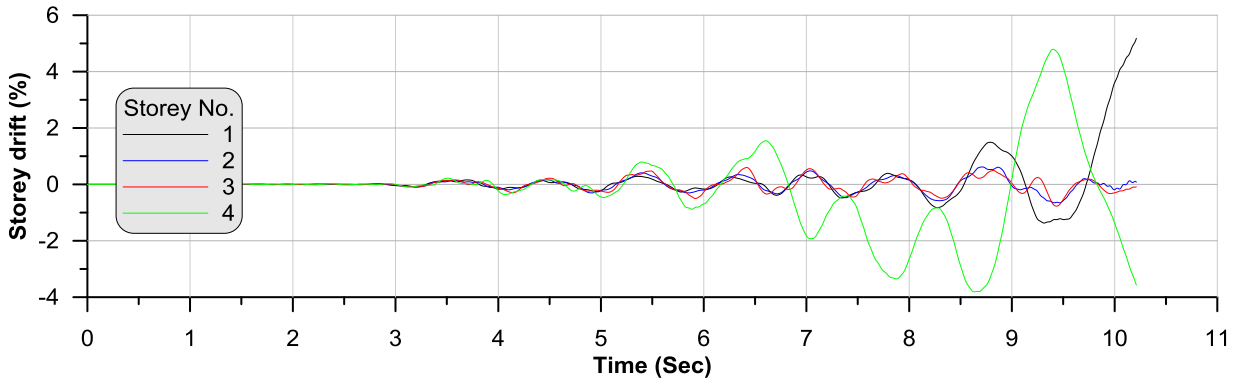

Figure I. 19:Inter-storey drift for CBF_{design} model under earthquake NGA-953 with F_{sm} 0.9

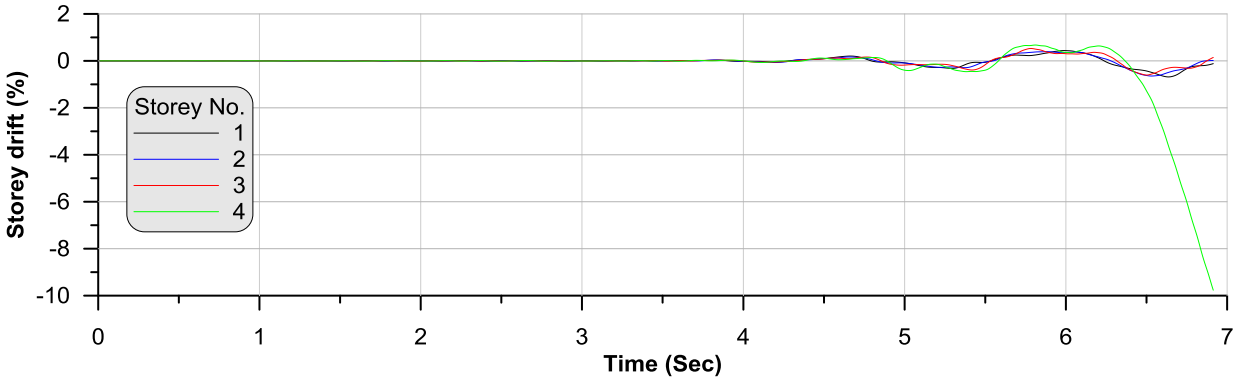

Figure I. 20:Inter-storey drift for CBF_{design} model under earthquake NGA-1787 with F_{sm} 0.9

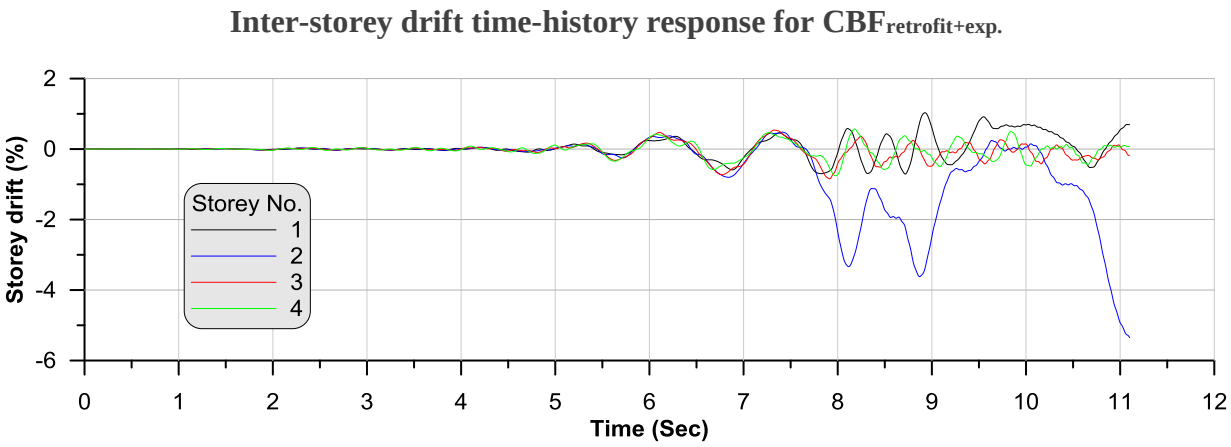

Figure I. 21:Inter-storey drift for $CBF_{retrofit+exp.}$ model under earthquake NGA-735 with F_{sm} 1.1

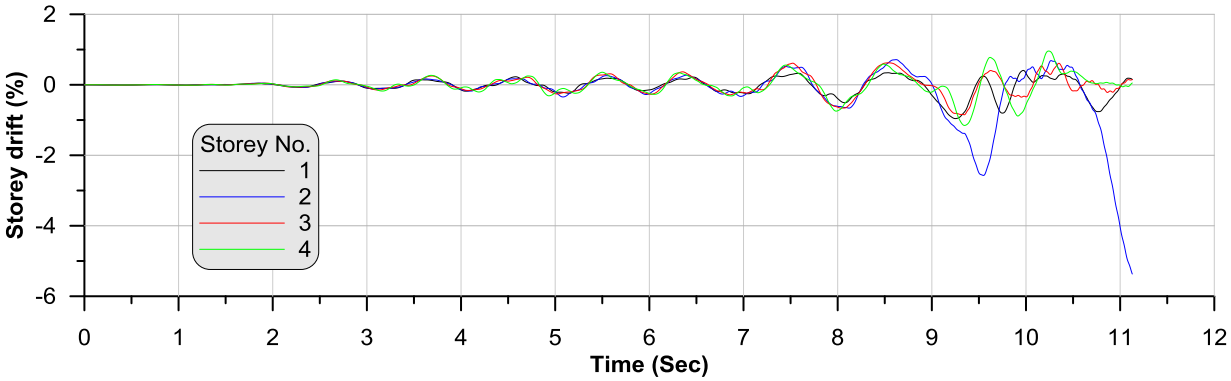

Figure I. 22:Inter-storey drift for $CBF_{retrofit+exp.}$ model under earthquake NGA-762 with F_{sm} 1.2

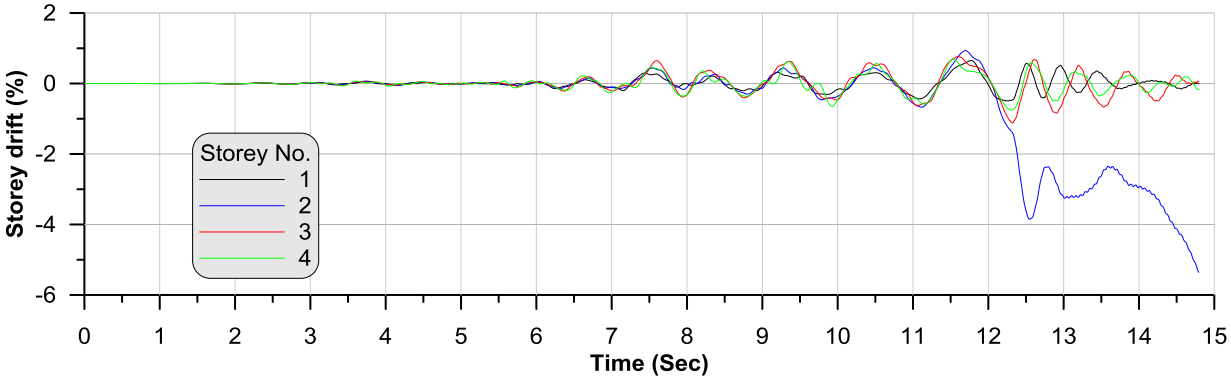

Figure I. 23:Inter-storey drift for $CBF_{retrofit+exp.}$ model under earthquake NGA-776 with F_{sm} 0.8

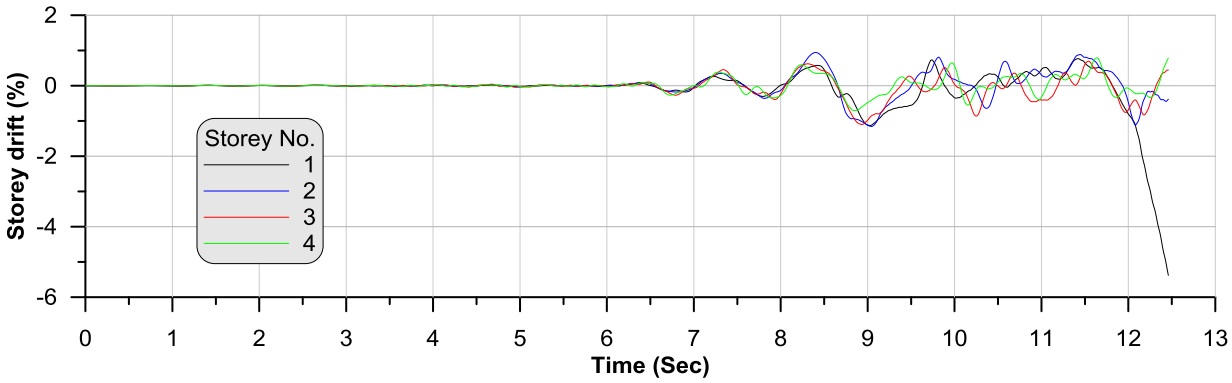

Figure I. 24:Inter-storey drift for $CBF_{retrofit+exp.}$ model under earthquake NGA-787 with F_{sm} 1.1

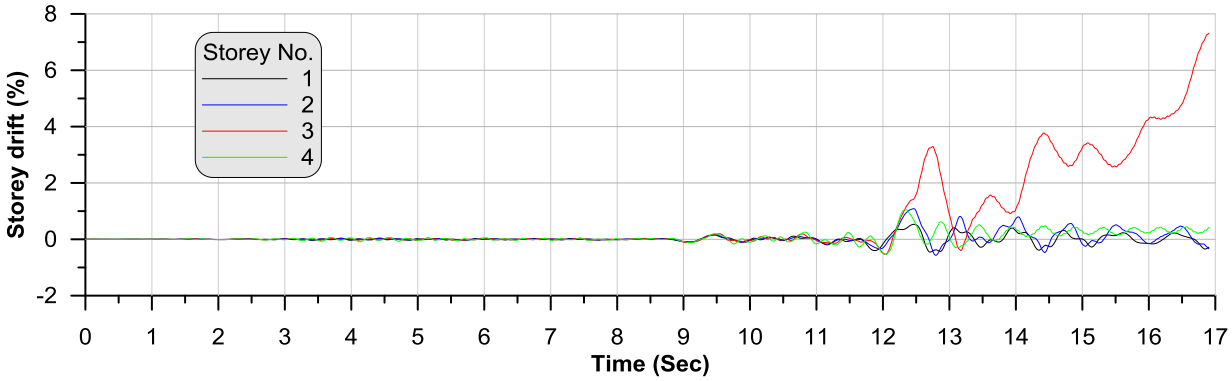

Figure I. 25:Inter-storey drift for $CBF_{retrofit+exp.}$ model under earthquake NGA-796 with F_{sm} 0.9

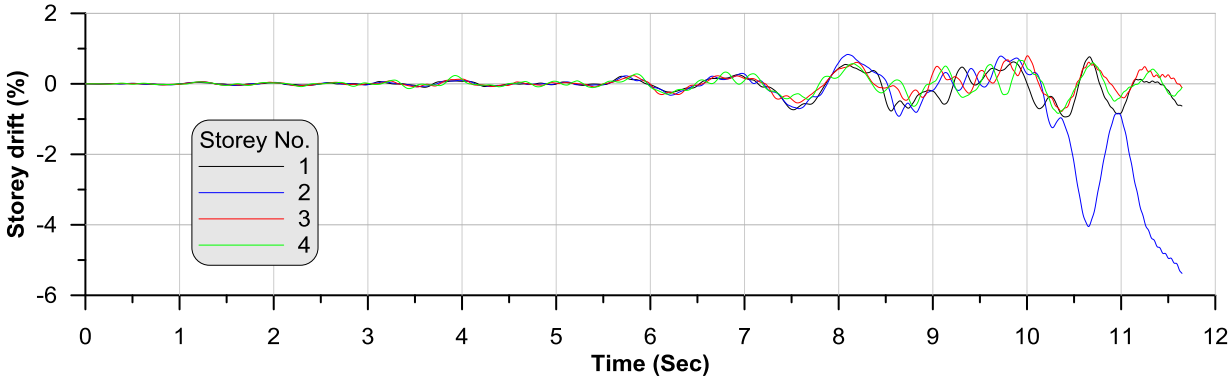

Figure I. 26:Inter-storey drift for $CBF_{retrofit+exp.}$ model under earthquake NGA-807 with F_{sm} 1.2

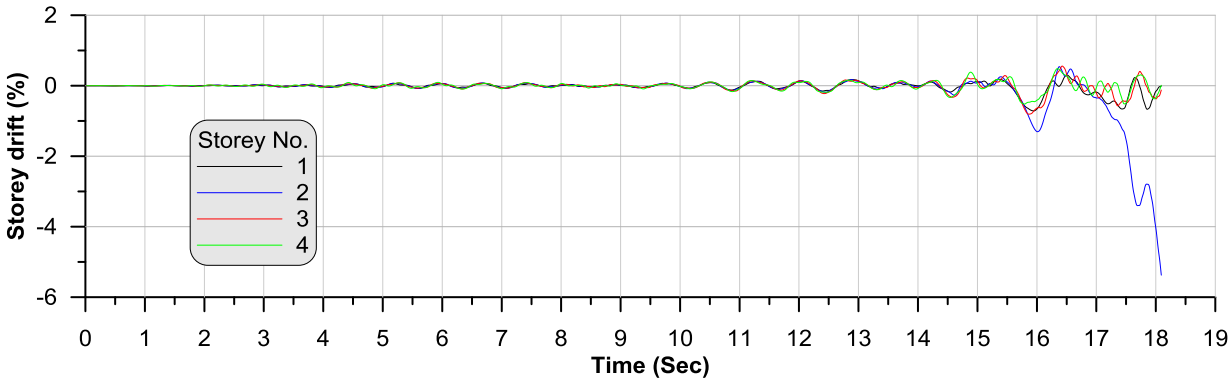

Figure I. 27:Inter-storey drift for $CBF_{retrofit+exp.}$ model under earthquake NGA-838 with F_{sm} 1.2

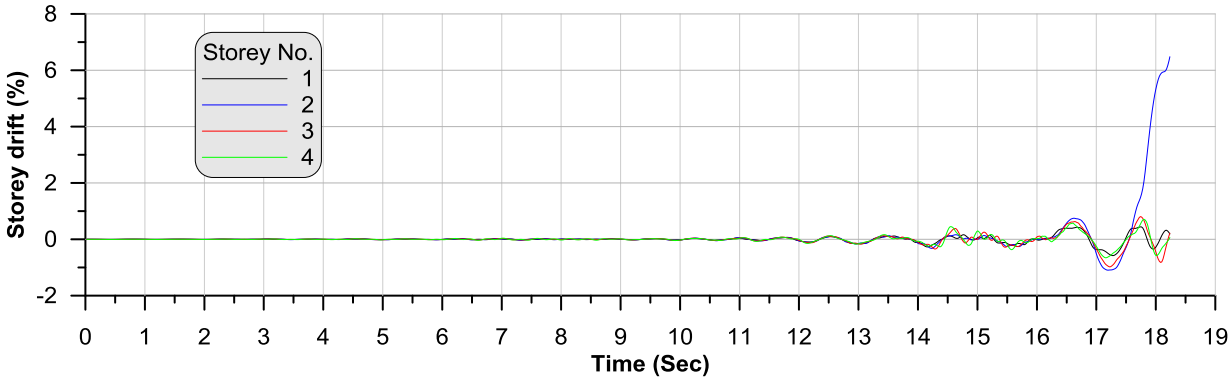

Figure I. 28:Inter-storey drift for $CBF_{retrofit+exp.}$ model under earthquake NGA-900 with F_{sm} 0.8

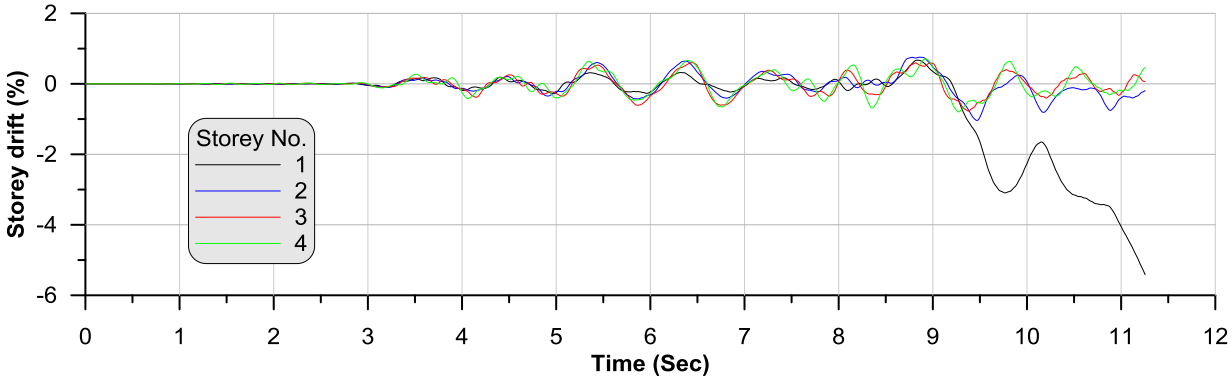

Figure I. 29:Inter-storey drift for $CBF_{retrofit+exp.}$ model under earthquake NGA-935 with F_{sm} 1.0

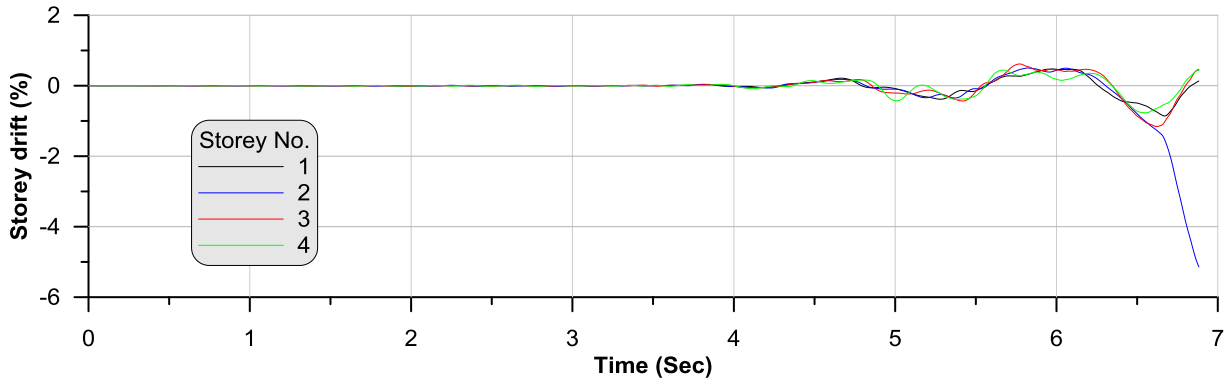

Figure I. 30:Inter-storey drift for $CBF_{retrofit+exp.}$ model under earthquake NGA-1787 with F_{sm} 1.0